Injectable Chitosan Hydrogel as a Delivery System for Cancer Immunotherapy

by

Nicholas CUNNINGHAM

THESIS PRESENTED TO ÉCOLE DE TECHNOLOGIE SUPÉRIEURE IN
PARTIAL FULFILLEMENT FOR THE DEGREE OF
DOCTOR OF PHILOSOPHY
Ph.D.

MONTREAL, 20TH DECEMBER 2022

ÉCOLE DE TECHNOLOGIE SUPÉRIEURE
UNIVERSITÉ DU QUÉBEC

BOARD OF EXAMINERS (THESIS PH.D.)

THIS THESIS HAS BEEN EVALUATED

BY THE FOLLOWING BOARD OF EXAMINERS

Mrs. Sophie Lerouge, Thesis Supervisor
Department of Mechanical Engineering, École de technologie supérieure

Mr. Réjean Lapointe, Thesis Co-supervisor
Department of Medicine, University of Montreal

Mr. Vahé Nerguizian , President of the Board of Examiners
Department of Electrical Engineering, École de technologie supérieure

Mr. Ali Ahmadi, Member of the jury
Department of Mechanical Engineering, École de technologie supérieure

Mr. Guojun Chen, External Evaluator
Department of Biomedical Engineering, McGill University

THIS THESIS WAS PRENSENTED AND DEFENDED

IN THE PRESENCE OF A BOARD OF EXAMINERS AND PUBLIC

20TH DECEMBER 2022

AT ÉCOLE DE TECHNOLOGIE SUPÉRIEURE

ACKNOWLEDGMENT

I would firstly like to thank the members of the jury for evaluating my manuscript and thesis defense.

An enormous thank you to my thesis director Sophie, for your unceasing support during this (longer than expected!) PhD. Looking back, I can see how much I have grown as a scientist and a person under your supervision, and I am truly grateful for both your advice and technological expertise, as well as your compassion and understanding during the many difficult moments that inevitably occur. Without your perseverance and belief in me I don't think I would have made it this far, so thank you for encouraging me to keep going when I wasn't sure if I could. To my co-director Réjean, your expertise has been invaluable throughout my studies, and I appreciate your support and guidance when a more experienced voice has been needed in matters related to immunology. Your achievements and career have been an inspiration, while you remain a humble and welcoming researcher which for me is equally important. It would be with pleasure should our paths cross in the future if I pursue a career in immunology in Quebec.

I cannot thank enough all of my amazing colleagues from LBeV, as much a family as a lab and every one of them brilliant scientists and wonderful people. From my very first day I appreciated the welcome I had from Eve and Melusine, who have both gone on to further successes. I appreciate the knowledge I could gain from more experienced colleagues such as Marion, Yasaman and Fatemeh, always willing to pass on their knowledge. It's been a pleasure to work with and accompany students like Tommy, Thierry and Werner, all highly talented and who have become good friends. To my PhD comrades Capucine, Francesco, Atma and Maedeh, thank you for being there and understanding what we were all going through – the hardest challenges in life can still be overcome as a team and I admire you all greatly as researchers and people. Thanks also to the many interns who have each contributed to my research, some of whom I also had the pleasure of living with or even inviting to my wedding. The 11th floor at large has also been a stimulating and friendly environment for research and

socialising and so I thank my lab neighbours in LIO, LBUM and other labs for much needed coffee breaks and social events.

I have adored my time in Montreal and completely fallen in love with Quebec, but it hasn't always been easy being so far from home. For that reason, I thank my friends here who have become like a second family. From my first housemates Boris and Beryl who put up with my mediocre French to the amazing new people I continue to meet. Thank you to the hikers, snow tubers, to my multiple adventuring parties, soccer and spikeball opponents, swing dancers, or simply fellow microbrewery enthusiasts. A special mention to Jerome, Clarisse, Romain and Thomas who have all been close and valued friends, and who I had the honour to call my groomsmen and bridesmaid at my wedding. Thanks also to dear friends now slightly further away – Montreal & Lyon power couple Sophie and Bastien; Craig, Chiara and the Matts; and all of the YSE. I always look forward to seeing you on a zoom call or as online teammates.

My heartfelt thanks go to my family, larger now than when I started my PhD for multiple, wonderful reasons. Thanks to the Cerisy family for constant encouragement and every warm welcome, now my own family whose name I look forward to officially share. Thanks to my brothers Dan and Callum, people who I know I can always count on and who inspire me every day. I'm so happy and proud to be part of your growing families and can't wait to see what the future holds for you. Mum and Dad, my whole life everything you've done for me has contributed to me being able to complete this PhD, and there's no way I would have made it through without your love and support. I really couldn't hope for better parents and I'm so happy that you got to see me defend my thesis.

Lastly, the most important person to thank, my beloved wife Laure. I can't believe how lucky I have been to find my soulmate here in Canada, and I treasure every moment with you. You more than anyone know the sacrifices necessary for this PhD, some of which you have made yourself and for which I will be eternally grateful. For every late night, stressful day and working holiday, I thank you for your patience, support, kindness and love, and I'm so proud to be your husband. Je t'aime.

Hydrogel de chitosane injectable pour l'immunothérapie du cancer

Nicholas CUNNINGHAM

RESUMÉ

Le transfert adoptif des cellules (Adoptive cell therapy[(ACT]) est un type d'immunothérapie pour traiter le cancer, qui consiste en l'administration intraveineuse de grandes quantités de lymphocytes T qui ciblent et détruisent spécifiquement les cellules cancéreuses du patient. Sous différentes formes, l'ACT a montré du succès contre des cancers difficile à traiter comme le mélanome métastatique et certains cancers du sang. Malgré son succès, il reste des limites à ce traitement, notamment la difficulté à obtenir le nombre important de cellules requis, la perte de cellules aux sites non-tumoraux et les effets secondaires liés aux autres médicaments nécessaires pour l'ACT en clinique.

L'administration locale des lymphocytes T, par exemple avec une matrice, pourrait répondre à ces limites en concentrant les cellules sur le site tumoral, diminuant ainsi le nombre de cellules requis et le dosage des médicaments nécessaire pour un traitement efficace. La matrice idéale doit pouvoir être facilement administrée et mélangée avec les cellules, biodégradable et biocompatible avec les cellules encapsulées pour garantir leurs fonctions anti-cancéreuses. L'hypothèse de ce doctorat est que le traitement localisé permettra d'utiliser moins de cellules pour un traitement plus efficace.

L'hydrogel thermosensible de chitosane que nous avons développé est biocompatible avec les lymphocytes T, biodegradable *in vivo*, et permet la survie, la sortie et le maintien de l'activité anti-cancéreuse des lymphocytes T encapsulées. Avec le modèle murin MC38-OVA, les lymphocytes T anti-OVA (OT-I) encapsulés ont limité la croissance tumorale comparées aux souris non-traitées et traitées avec des OT-I suspendues dans du PBS. Toutefois, le traitement intraveineux était plus efficace que celui avec le gel. Ces résultats démontrent la faisabilité et le potentiel du gel de chitosane pour délivrer localement des OT-1 dans le cadre d'une immunothérapie contre le cancer. Des microbilles ont été développées comme format alternatif pour améliorer l'accès aux nutriments et à l'oxygène pour les cellules encapsulées. Cependant, le processus doit encore être optimisé car il induit une mortalité importante chez les cellules encapsulées dans les microbilles. L'amélioration des microbilles, notamment avec l'ajout des facteurs de croissance et de motifs d'adhésion cellulaire, permettrait d'améliorer l'efficacité du gel pour continuer son développement vers une éventuelle translation clinique.

Mots clés : Adoptive cell therapy, immunothérapie du cancer, chitosane, hydrogel, injectable, études animales, modèles de tumeur, microbilles

Injectable chitosan hydrogel as a delivery system for cancer immunotherapy

Nicholas CUNNINGHAM

ABSTRACT

Adoptive cell therapy (ACT) is a cancer immunotherapy where high quantities of T cells that specifically target cancer cells are administered intravenously to patients, where the delivered cytotoxic CD8+ T cells can directly eliminate cancer cells. In various forms, it has shown success against previously treatment-resistant cancers such as metastatic melanoma and certain blood cancers, though its use is often limited in solid cancers. Despite its success, limitations persist including the difficulty of cultivating the high number of cells required, their dispersal to non-tumour sites and side effects resulting from the drugs necessary in clinical ACT.

Localised delivery of T cells, for example via a scaffold, could address these limitations by concentrating cells at the tumour site, reducing both the initial number of cells and the dosage of associated drugs required for successful treatment. An ideal scaffold for this application should be easily administered and mixed with cells, biodegradable and biocompatible with encapsulated cells, allowing them to perform their anti-cancer function. The hypothesis of this PhD is that localised delivery will allow treatment with fewer cells and greater efficacy than systemic treatment.

The thermosensitive chitosan hydrogel that we have developed was shown to be biocompatible and biodegradable in vivo, and supported the survival, escape and anti-cancer functionality of encapsulated T cells. In the MC38-OVA murine tumour model, gel-encapsulated OT-I limited tumour growth compared to untreated and mice treated with PBS-suspended OT-I, though IV-delivered OT-I were more effective than the gel in limiting tumour growth. This showed the feasibility and potential of the chitosan gel for localised OT-I delivery as a cancer immunotherapy. Microbeads were successfully produced as an alternative gel format to potentially improve oxygen and nutrient access to encapsulated cells, although their fabrication must be optimized due to the currently elevated mortality in microbead-encapsulated cells. Further development of the microbeads, as well as the addition of growth factors and binding motifs, could further improve gel efficacy and continue progress towards eventual clinical translation.

Keywords: Adoptive cell therapy, cancer immunotherapy, chitosan, hydrogel, injectable, biodegradable, animal studies, tumour models, microbeads

TABLE OF CONTENTS

LIST OF TABLES

Page

LIST OF FIGURES

Page

LIST OF ABREVIATIONS

ACT	Adoptive cell therapy
APC	Antigen-presenting cells
BGP	Beta-glycerophosphate
BSA	Bovine serum albumin
CAR	Chimeric antigen receptor
CH	Chitosan
CH-Gel	Chitosan-gelatin
CTLA-4	cytotoxic T lymphocyte antigen-4
CpG ODN	(cytosine-guanine) oligonucleotides
DC	Dendritic cells
DDA	Degree of deacetylation
ECM	Extracellular matrix
EthD-1	Ethidium homodimer
FBS	Foetal bovine serum
GA	Gelling agent
GHPA	gelatin-hydroxyphenyl propionic acid
GM-CSF	granulocyte–macrophage colony-stimulating factor
H&E	hematoxylin and eosin
HPS	hematoxylin phloxine saffron
ICI	Immune checkpoint inhibitors
IFN	Interferon
IL	Interleukin

LCST	Lower citical solution temperature
LVE	Linear viscoelastic [region]
MHC	Major histocompatibility complex
MSR	Mesoporous silica rod
MSM	Mesoporous silica microspheres
NC	Normalised count
NK	Natural killer cells
OV	Oncolytic virus
OVA	Ovalbumin
PAP	Prostatic acid phosphatase
PB	Phosphate buffer
PBMC	peripheral blood mononuclear cells
PCL	polycaprolactone
PD-1	Programmed cell death protein 1
PD-L1	Programmed death-ligand 1
PEI	polyethyleneimine
PEG	poly(ethylene glycol)
PEO–PPO–PEO	poly(ethylene oxide)–b-poly(propylene oxide)–b-poly(ethylene oxide)
PIC	Polyisocyanopeptide
PLGA	poly (lactide-co-glycolide) acid
pMHC	MHC-peptide complex
PNIPAM	Poly(N-isopropylacrylamide)
PPG	poly(propylene glycol)

ROI	Region of interest
ROS	Reactive oxygen species
SEM	Standard error mean
SHC	Sodium hydrocarbonate
STING	Stimulator of Interferon Genes
TIL	Tumour-infiltrating lymphocytes
TLS	Tertiary lymphoid structure
UCST	Upper critical solution temperature

LIST OF SYMBOLS

°C	Degré Celsius
Δ	Phase shift wrt. Strain
ε	Strain
G’	Storage Modulus
G’’	Loss Modulus
G*	Complex Modulus
H	Hertz
kDa	Kilodalton
kPa	Kilopascal
µg	Microgram
mg	Milligram
min	Minute
mL	Millilitre
µL	microlitre
µm	micrometre
mm	Millimetre
M	Moles
MP	Megapixel
MW	Molecular weight
ng	Nanogram
nm	Nanometre
s	Second

σ	Stress

INTRODUCTION

Despite continuous progress in developing and refining clinical treatments, cancer remains a leading cause of death in countries of all income levels (Torre, Siegel, Ward, & Jemal, 2016), not to mention the significant economic and social burdens suffered by patients, caregivers and wider society alike (Bradley, 2019; Wissinger, Griebsch, Lungershausen, Foster, & Pashos, 2014). Surgical resection, chemotherapy and radiotherapy have historically been the first-line therapies in cancer treatment, though these treatments may be of little survival benefit or simply impossible to administer in patients with advanced or metastatic disease. Immunotherapies are a relatively new and successful class of treatment, which utilise and augment the patient's own immune system to generate an anti-tumour response. While not yet applicable to many cancers, immunotherapies have shown great success in treating metastatic melanoma, and are gaining interest in numerous other cancers (Argiris et al., 2017; Domingues, Lopes, Soares, & Populo, 2018; Duma, Santana-Davila, & Molina, 2019; Sitarz et al., 2018). Numerous immunotherapeutic drugs, vaccines and cell therapies have been investigated, for which biomaterials have been investigated to improve treatment delivery and efficacy. Chapter 1 of this thesis will present the background of cancer and immune system biology, as well as the current clinical landscape of immunotherapies and their limitations. It will also review how biomaterials can help improve the efficacy and reduce the toxicity of cancer immunotherapies, with a detailed review of the state of the art of biomaterials used for cancer immunotherapies.

In this PhD we will then concentrate of one specific immunotherapy, namely adoptive cell therapy (ACT), in which tumour-specific cytotoxic T lymphocytes are cultivated and expanded in great numbers in vitro before intravenous administration in patients along with immunostimulatory molecules such as interleukin (IL)-2 (Itzhaki et al., 2011). It has shown impressive results in previously hard to treat cancers, with ACT using tumour infiltrating lymphocytes (TIL) successfully used to treat metastatic melanoma. Furthermore, chimeric antigen receptor (CAR) T cells – genetically modified to target antigens independent of the major histocompatibility complex (MHC) – successful in treating B cell cancers (Waldman, Fritz, & Lenardo, 2020).

Despite this success, several limitations remain which restrict the use of ACT. Billions of T cells must be administered, as only a small fraction reach the tumour after systemic administration. This expansion is costly and difficult for some patients, causing many to lose treatment eligibility. Cells also lack persistence in the immunosuppressive tumour microenvironment (Stephanie L. Goff et al., 2010; Ronnie Shapira-Frommer & Jacob Schachter, 2012; Richard Wu et al., 2012). ACT is also associated with toxicities, with cytokine release syndrome the main toxicity associated with the high-dose IL-2 administered during ACT (J. C. Yang, 2015) and CAR T cells also associated with cytokine release syndrome as well as neurotoxicity (Neelapu et al., 2018). The systemic delivery of ACT, as well as the necessarily high dosages associated with this non-targeted method of delivery, clearly contributes to these observed toxicities. For this reason, biomaterials are of increasing interest as delivery systems for ACT, as well as other cancer immunotherapies (Jie Li et al., 2020).

Our group has previously developed injectable chitosan hydrogels that support T cell survival and proliferation, and the destruction of cancer cells by gel-encapsulated T cells (Monette, Ceccaldi, Assaad, Lerouge, & Lapointe, 2016). The general aim of this Ph.D., presented in chapter 2 with the hypotheses and specific objectives, is to further develop this technology, investigating the in vivo biocompatibility of the gel and its potential for localised T cell delivery as a cancer treatment in murine tumour models. Where possible, we also aimed to improve and optimise the gel and its components.

Chapter 3 lists the methodologies used in this work, with details of experiments performed as well as more general explanations of and justifications for the techniques and instruments used. Chapter 4 presents the results obtained in the course of this Ph.D., while in chapter 5 these results are discussed within the context of our stated objectives and in comparison to other research in the field. Finally, the conclusion summarises the work as well as proposed recommendations and perspectives for future work.

CHAPTER 1

LITERATURE REVIEW

1.1 Cancer and the immune system

Despite continuous progress in detection and treatment, cancer remains one of the leading causes of death worldwide (Sung et al., 2021). Cancer immunotherapy – where cancer treatment is achieved by harnessing and assisting patients' own immune systems – has revolutionized oncology, allowing previously impossible precision in targeting tumour cells compared to conventional treatments and showing impressive results in previously untreatable disease (Farkona, Diamandis, & Blasutig, 2016). Immunotherapy exploits the inherent response of the host immune system, which can detect the foreign antigens created by cancerous cells and recognize and eliminate malignant cells.

Our immune system is constantly attempting to eliminate cancerous cells and cancers at early stages. Cell-mediated immunity is the most relevant part of the immune system in the response to cancer, which in innate immunity consists of polymorphonuclear cells (neutrophils, eosinophils, basophils, and mast cells), phagocytic cells (monocytes, macrophages, and dendritic cells [DC]) and natural killer (NK) cells. B and T lymphocytes (commonly referred to as B and T cells) – of which there are multiple subtypes – are the primary immune cells involved in adaptive immunity. Immunotherapy relies on the interaction of cells such as T cells, B cells, DC, and NK cells with cancers (Anguille et al., 2015; Kennedy & Celis, 2008; Martínez-Lostao, Anel, & Pardo, 2015; Sharonov, Serebrovskaya, Yuzhakova, Britanova, & Chudakov, 2020; Shimasaki, Jain, & Campana, 2020) briefly explained in Figure 1-1.

This process has been described as the cancer immunity cycle, where antigens from necrotic or apoptotic cancer cells are captured by antigen-presenting cells (APC). The APC subsequently stimulate cytotoxic T lymphocytes to specifically target and destroy the associated tumour cells via apoptosis (Chen & Mellman, 2013). Unfortunately, alone, its efficacy is often limited by the inhibitory effect of the tumour microenvironment and hence

the evasion of the immune system by cancer cells. Therefore, several strategies have been proposed to enhance its efficacy. Some are based on drugs enhancing the T cell response such as Interleukin 2 (IL-2), or immunomodulatory drugs targeting immune checkpoint inhibitors (ICI). Some treatments encourage the development of immune cells specialized against the tumour (so-called cancer vaccines, (Shemesh et al., 2021). Oncolytic viruses (OV) can both directly destroy cancer cells and produce immunostimulatory cytokines (A. H. Choi, O'Leary, Fong, & Chen, 2016). Others consist of the injection of cytotoxic T cells, referred to as adoptive cell therapy (ACT) (Itzhaki et al., 2011).

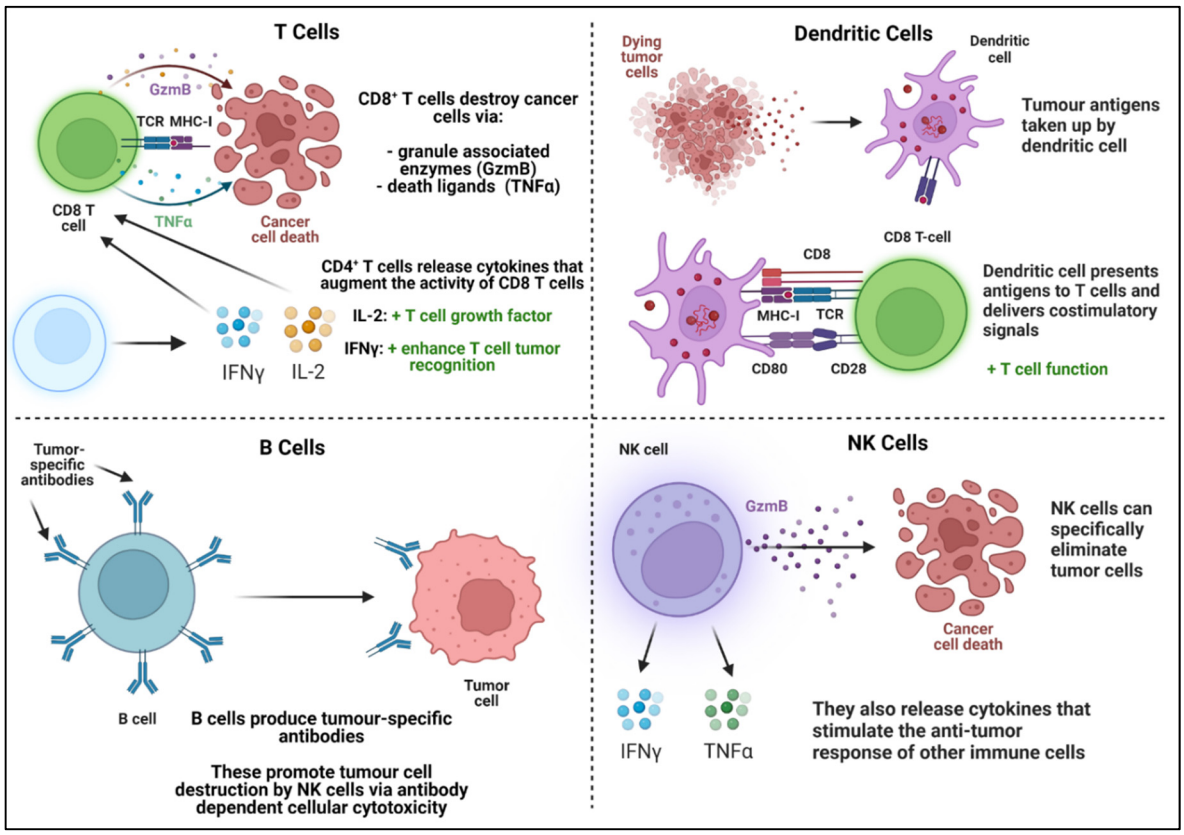

Figure 1-1 Summary of the main immune cell types relevant to cancer immunotherapy and their functions

GzmB: Granzyme B, TNFα: Tumour necrosis factor α, IL-2: Interleukin-2, IFNγ: Interferon γ, TCR: T cell receptor, MHC: Major histocompatibility complex

Numerous immunotherapies have been developed based on this principle of stimulating and augmenting the immune system. There are countless ongoing clinical trials, of which it is not

possible (and not the aim of this review) to summarize here. Selected FDA-approved immunotherapies are highlighted in Figure 1-2 and are explained in greater detail where relevant in section 1.2.

Despite promising results and numerous clinical studies, the efficacy of these strategies is still limited, due to diverse factors which will be later summarized. A current trend is to combine multiple therapies, particularly a combination of anti-programmed cell death protein 1 (PD-1) & anti-cytotoxic T lymphocyte antigen-4 (CTLA-4) (Larkin et al., 2015) or more recently PD-1 and the newly approved ICI Lymphocyte-activation gene 3 (LAG-3) (Tawbi et al., 2022), or the combination of these checkpoint inhibitors with ACT for melanoma and ovarian cancers (Kverneland et al., 2020; Mullinax et al., 2018). These combinations are a major focus for current clinical trials with the goal of establishing best practice, and it seems likely that future gold-standard treatments will comprise multiple immunotherapies, perhaps alongside conventional treatments, as combination therapies.

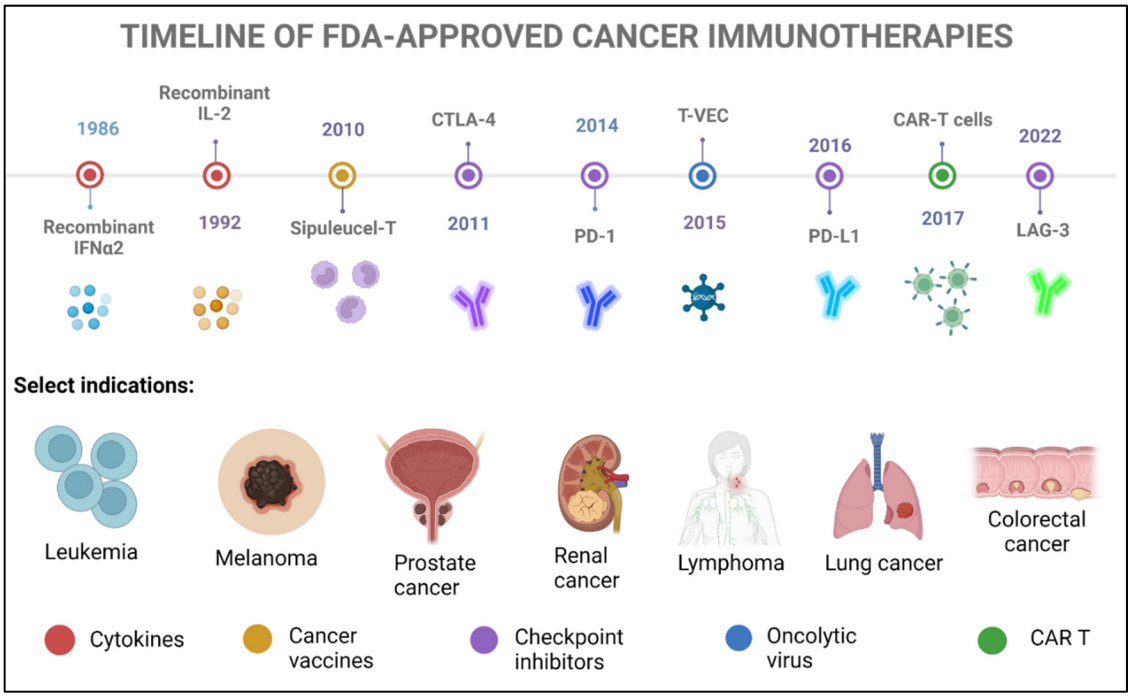

Figure 1-2 Timeline of selected FDA-approved cancer immunotherapies
Adapted from Cancer Research Institute (2022)

Another trend is the increasing use of biomaterials to improve the efficiency of immunotherapies and decrease their toxic effects. This review will focus on the potential of biomaterials (as cell scaffolds or controlled delivery systems for antibodies or tumour antigens) to further enhance the efficacy and decrease the toxicity of immunotherapy.

1.2 Biomaterials in immunotherapy

1.2.1 Introduction and rationale

Biomaterials, defined as "materials designed to take a form that can direct, through interactions with living systems, the course of any therapeutic or diagnostic procedure" (Ghasemi-Mobarakeh, Kolahreez, Ramakrishna, & Williams, 2019) have long been widely studied in numerous biomedical applications (O'Brien, 2011). We can differentiate biomaterials by their source (natural or synthetic), their class (metals, ceramics or polymers) and their stability (permanent or biodegradable). Biomaterials have been used in several oncology treatments, for example for local administration of chemotherapy in urothelial carcinoma (Matin Surena et al., 2022) or the embolization of blood vessels for palliative treatment of hepatic cancers (Raoul et al., 2019), to name just a few. In the present review we will limit ourselves to immunotherapies. While only comparatively recently have developments in immunotherapy supported their use in oncology, biomaterials offer numerous possibilities to augment the efficacy of immunotherapies or limit their harmful side effects, as summarized in Figure 3. In brief, they can achieve this through controlled spatial and temporal release of the cells and immunotherapeutic agents, which can result in dose-dependent and off-target toxicities in current immunotherapies (Koshy & Mooney, 2016). They can also create a 'niche' for the activation of endogenous or exogenous APC, with potential additional anti-tumour efficacy coming from the biomaterial itself such as their pro-inflammatory effects or reactive oxygen species (ROS) generation (Cai, Li, Akinade, Zhu, & Leong, 2021).

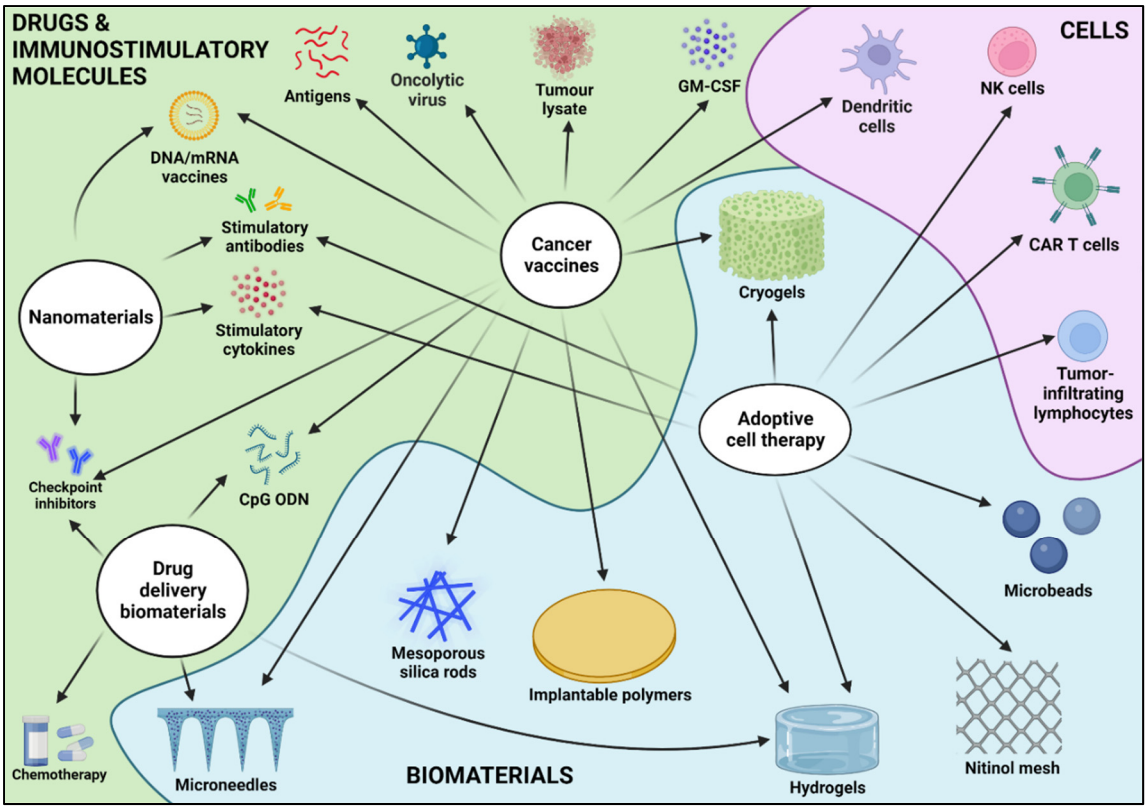

Figure 1.3 Summary of immunotherapies and the potential role of biomaterials

Due to the interlinked nature of the immune system, there is extensive crossover in the components and mechanisms of action of immunotherapeutic biomaterials. However, two broad categories that can be proposed are cell-delivery biomaterials, directly incorporating cells such as lymphocytes and DC as localized immunotherapies (Leach, Young, & Hartgerink, 2019), and cell-free biomaterials, which can incorporate a combination of immune adjuvants, antigens and even additional cancer therapeutics such as chemotherapeutic agents alongside the inherent immunomodulatory effects of certain biomaterials (Cai et al., 2021; H. Wang & Mooney, 2018). This following section will focus on biomaterials in these categories with a particular focus on lymphocytes as antitumoral agents, either through direct administration and stimulation of lymphocytes or by their indirect stimulation by other cells or immunomodulatory components.

1.2.2 Cell-free biomaterials

The aim of cell-free scaffolds for immunotherapies is to provide, either through their own chemical composition or through attached or encapsulated biological factors, cellular cues to direct and encourage a favourable immune response towards a given stimulus, or alternatively to locally deliver anti-cancer drugs. In the case of a biomaterial for cancer immunotherapy, this would implicate either the inclusion of immune agonists and/or immunotherapeutic drugs, within a material matrix suitable for the administration and controlled delivery of these factors, such that a strong anti-cancer response is achieved, and/or the utilization of the inherent immune response to a particular matrix to recruit and activate APC.

These systems should be composed of a biocompatible material, which according to the definition of biocompatibility must not elicit adverse biological effects (cytotoxicity, carcinogenicity, hypersensitivity etc.), but should promote an "appropriate host response in a specific application" (Ghasemi-Mobarakeh, Kolahreez, Ramakrishna, & Williams, 2019), namely here help recruit and activate the APC or be at least immunologically inert to allow the function of its immunomodulatory components. Indeed, in this particular case as detailed below, provoking some immune response is deemed beneficial in the anti-cancer response and some inflammation could even be encouraged.

Such a material should also be:

- Injectable through a small needle to enable minimally invasive procedures.
- Persistent over the necessary timescale for maximum efficacy of its drug or molecule of choice and ideally be degraded afterwards.
- For drug delivery, the release rate must be well controlled by the scaffold properties and degradation rate.
- The use of simple materials, potentially already used in FDA-approved medical devices or therapies, is generally desired for easier regulatory approval.

The sections below detail the principles and review the cases of biomaterials used for cancer vaccines and controlled release of OV or immunotherapeutic drugs.

1.2.2.1 Biomaterials for cancer vaccines

Cancer vaccines can include dead tumor cells or lysate, DC, antigens, or nucleic acids such as mRNA, with DC the most widely studied form of cancer vaccine to date (Riley, June, Langer, & Mitchell, 2019). Whatever their component, the vaccines - generally administered subcutaneously, intramuscularly, or intravenously – act to supplement or improve tumour-specific lymphocyte activity via improved antigen presentation, lymphocyte activation and localization of the immune response to the tumour (Shemesh et al., 2021). A summary of cancer vaccine mechanisms is shown in Figure 1-3.

Exogenous cells can be added to the antigens injected, to ensure the formation of activated DC. This is the case of Sipuleucel-T (Provenge®) the first immune cell therapy approved by the FDA as a cancer treatment (Madan et al., 2020). Sipuleucel T improved antitumour $CD8^+$ cell response and survival in a clinical trial in patients with castration-resistant prostate cancer (Antonarakis et al., 2018). Despite this initial success, limited progress has since been made in the clinical use of cancer vaccines, with other candidate vaccines failing to demonstrate clinical efficacy and leaving Sipuleucel-T as still the only FDA-approved cancer vaccine (Antonarelli et al., 2021). Nevertheless, research continues with recent developments such as neoantigen vaccines, which target patient specific antigens rather than tumour associated antigens that are common between patients and associated with higher immune tolerance.

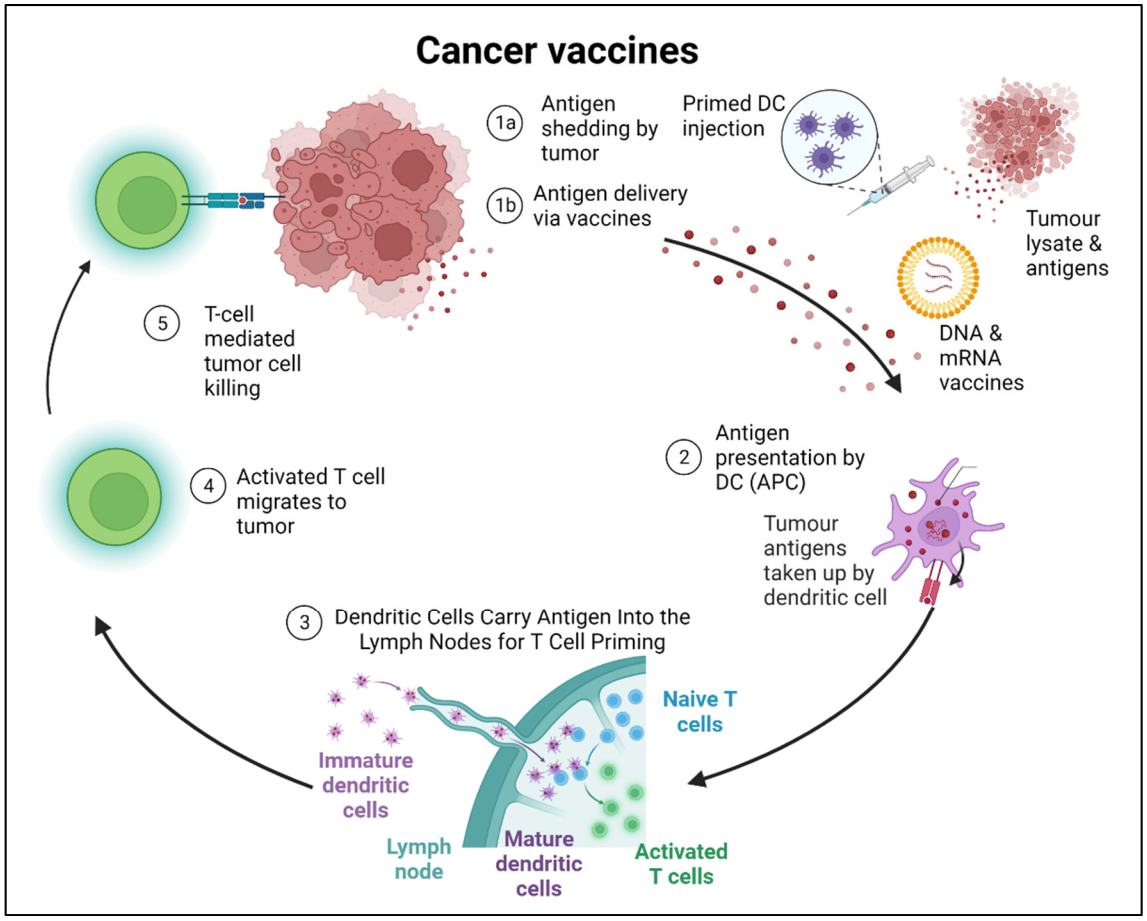

Figure 1-3 Cancer vaccine mechanisms
Tumour antigens from tumour cell death or administered vaccines are taken up by dendritic cells for priming of tumour-specific T cells, which can then specifically eliminate cancer cells, continuing the cycle

To be effective, cancer vaccines must have two main properties. First, they must stimulate the appropriate specific immune responses against the correct target. Second, the immune responses must be powerful enough to overcome the barriers that cancer cells use to protect themselves. Therefore, sustained delivery (to avoid rapid clearance) and an appropriate structure for the APC to interface with the vaccine component is key.

Biomaterials have thus been used to create a physical structure loaded with vaccine components which stimulate APC cells *in situ*. These will then disperse to lymph nodes and activate resident T cells which then travel to the tumour site and eliminate malignant cells.

Various approaches are summarised in Figure 1-4. In brief, we can distinguish between implantable and injectable scaffolds.

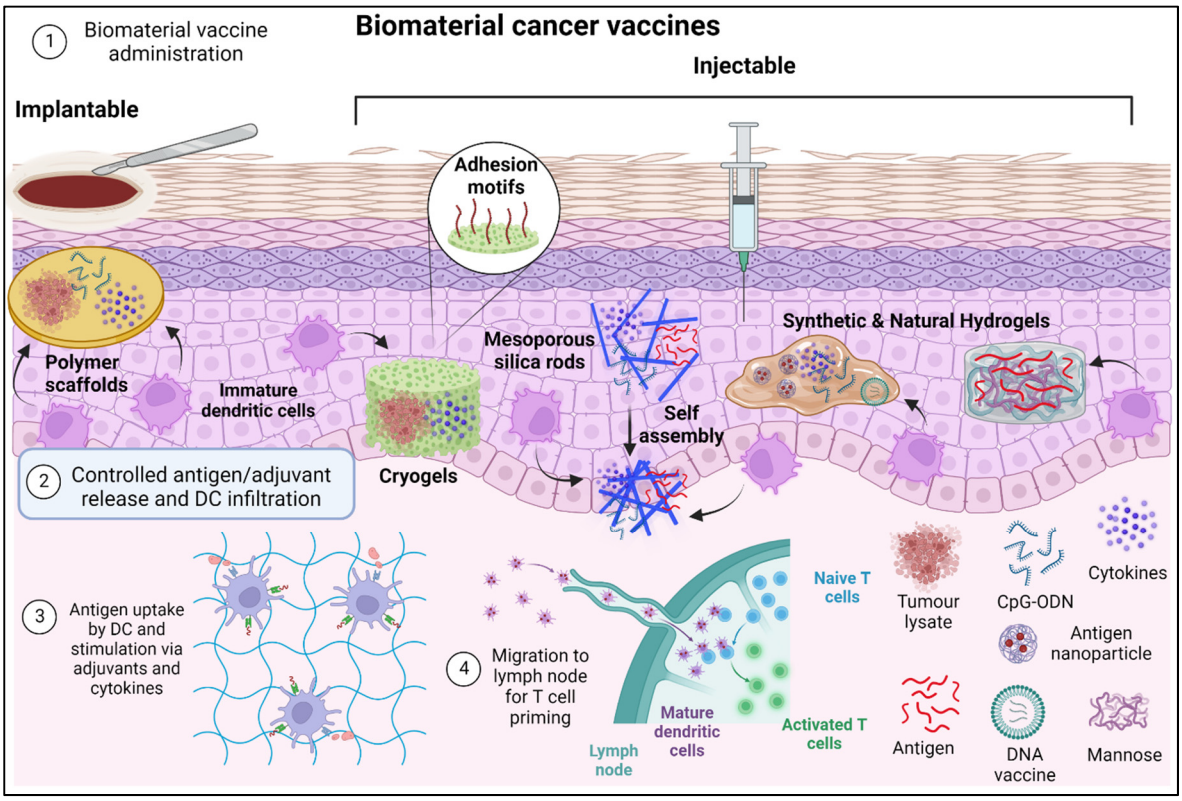

Figure 1-4 Principles of biomaterial vaccines
Biomaterials containing tumour lysates, antigens, cytokines, and adjuvants are implanted or injected. Antigens and adjuvants are released in a controlled manner and DC infiltrate the biomaterial niche where antigen uptake can occur. DC then migrate to lymph nodes where T cell priming occurs

Biomaterial vaccines were among the first biomaterial-delivered immunotherapies to be researched, with the pioneering and impressive work from Mooney's group being essential in this field and influential in its development.

They first developed an implantable poly (lactide-co-glycolide) acid (PLGA) scaffold incorporating tumour lysate antigens (from destroyed cancer cells), GM-CSF as a stimulatory cytokine for DC and (cytosine-guanine) oligonucleotides (CpG ODN) a Toll-like receptor9 agonist which also activates DC (Ali, Huebsch, Cao, Dranoff, & Mooney, 2009). The interconnected pores in the scaffold create an environment in which infiltrating DC are

activated and process the tumour lysate antigens before migrating to lymph nodes where they can prime antigen-specific T cells. The scaffold also regulates the release of antigens and adjuvants to encourage a persistent immune response. This biomaterial-based vaccine paved the way for future developments in biomaterial immunotherapies and has the distinction of being the first such biomaterial to enter clinical trials, where the above vaccine is being tested in a phase I clinical trial to determine its safety, feasibility and confirm its biological activity when used to treat metastatic melanoma ("Dendritic Cell Activating Scaffold in Melanoma,"). The study completion date is in 2022. Mooney's group has further developed the scaffold, showing that the vaccine is even more effective in combination with checkpoint inhibitors (Ali, Lewin, Dranoff, & Mooney, 2016). Furthermore, alternative vaccine adjuvants such as monophosphoryl lipid A, and polyinosinic:polycytidylic acid, also preventively and therapeutically reduced tumour growth in mouse melanoma models (Ali et al., 2014).

Later, the team developed a methacrylated alginate (MA-alginate) "cryogel" scaffold functionalised with RGD binding sites and using the same immunomodulatory factors, which demonstrated both therapeutic and preventative effects in mice melanoma models, with a further benefit of injectability as opposed to the previous PLGA scaffold (Bencherif et al., 2015). However, this requires quite large diameter needles (16G). According to *in vitro* tests, approximately 80% of the encapsulated vaccine compounds (GM-CSF and CpG ODN) were released within the first 4 days, followed by slow and sustained release over the next month. The interconnected macroporous structure allowed cellular infiltration and immune cell trafficking *in situ.* Further work interestingly showed that the vaccine maintained its efficacy regardless of whether the injection site was adjacent or distal to the tumour and draining lymph nodes (Najibi, Shih, & Mooney, 2022). This group also developed a similar cryogel using a combination of MA-alginate and PEG to eradicate established acute myeloid leukaemia in mice (Shah et al., 2020). Another relatively similar cryogel which incorporates tumour cell lysates during hydrogel preparation was used by Deng's group and significantly reduced the growth of a secondary tumour after surgical resection of the primary tumour (Y. Lu et al., 2022).

All these 3D biomaterials are however fabricated *ex vivo* and require either surgical placement in the body or large invasive needles for implantation. Moreover they are not biodegradable and their preformed structures could limit the capability of host cells to organize themselves (Jaeyun Kim et al., 2015).

To solve this issue, Mooney's team proposed self-assembling mesoporous silica rods (MSR) that are more easily injectable (18G needle), biodegradable and create more macroporous 3D structures for better interaction with immune cells. The MSRs are injected with a needle and spontaneously assemble *in vivo*, degrading over time and allowing a slow release of vaccine antigens and adjuvants (Jaeyun Kim et al., 2015). These self-assembled MSR scaffolds increased the number of recruited cells compared to previously reported preformed macro-porous polymer scaffolds, with 20M cells in the MSR vaccine after 5 days in vivo versus only 6M in the MA-alginate cryogel vaccine after 6 days. In later work the MSR vaccine was coated with polyethyleneimine (PEI) to enhance the effect of neoantigen peptides (A. W. Li et al., 2018). MSR–PEI vaccines significantly enriched the DC population, roughly doubling the number of recruited DC, and enhanced host DC activation and T-cell responses compared to the existing MSR vaccine. The MSR vaccines eradicated established E7-OVA tumours in 80% of mice and showed efficacy in reducing tumour growth in melanoma & carcinoma cell lines, with an additive effect when combined with CTLA-4 injection, demonstrating the potential of biomaterials-based vaccines to function alongside other immunotherapies such as checkpoint inhibitors (A. W. Li et al., 2018). Further work using MSR vaccines has applied the same principle for alternative peptide antigens such as gonadotropin-releasing hormone (GnRH) and HER2/neu, implicated in multiple cancers including breast cancer (Dellacherie et al., 2020).

Other groups have developed biomaterial vaccines with similar stimulatory molecules, using other commonly used biomaterials such as chitosan, polycaprolactone (PCL) and even bovine serum albumin (BSA). For example, an injectable thermosensitive PCL–PEG–PCL hydrogel encapsulated GM-CSF and chitosan-coated ovalbumin (OVA) nanoparticles to create the immune cell niche for DC activation (Z. Sun et al., 2018), where the chitosan itself may induce DC maturation via the Stimulator of Interferon Genes (STING) signalling pathway (Carroll et

al., 2016). STING is a transmembrane protein that interacts with cyclic dinucleotides (CDNs) produced in response to cytosolic double-stranded DNA, resulting in the production of IFN-β and other cytokines which promote the *in vivo* anti-tumour T cell response (Corrales et al., 2015). In another study, BSA was crosslinked with a similar PCL-PEG-PCL hydrogel to deliver a DNA vaccine against the amyloid-β Alzheimer antigen (Giang Phan et al., 2019). Both PCL-PEG-PCL hydrogel vaccines induced strong immune responses and improved DC recruitment.

Chitosan seems to be gaining popularity for use in cancer vaccines, with an injectable gel formed by a Schiff base reaction between CpG-modified carboxymethyl chitosan and partially oxidized mannan increasing DC infiltration and maturation and significantly reducing tumour growth in a B16-F10 mouse melanoma model (Liang et al., 2021). Furthermore, though not tested in tumour models, an OVA-antigen-containing "nanosheet" was formed through the simple mixing of catechol-modified chitosan, PBS and $CaCl_2$ (Pei et al., 2019). The nanosheet significantly increased DC activation and antigen presentation compared to free antigen and so could be another promising future carrier of antigens as a cancer vaccine. Carroll *et al.* showed that chitosan, a cationic polymer, can engage the cGAS-STING pathway to mediate the selective production of type I IFN and interferon-stimulated genes, which were then responsible for mediating the activation of DC and induction of cellular immunity (Carroll et al., 2016). More generally, these studies show that the choice of the biomaterial composition and porosity of the scaffold is key to induce successful recruitment and activation of DC. Moreover, hydrogels have the advantage of being injectable and can play the dual role of being a vaccine carrier with sustained release and a platform for recruiting DCs.

While clinical results are still absent, all these results suggest that biomaterials will play a key role in the development of cancer vaccines and that, alongside other immunotherapies, vaccines will have a role to play in therapeutic cancer treatment. Furthermore, while still at an early stage, the prophylactic vaccination of cancers with known antigens such as human epidermal growth factor receptor-2-positive breast cancers is an intriguing possibility (Palladini et al., 2018). Prophylactic vaccination could be targeted to genetically high-risk

populations, or alternatively used to prevent cancer recurrence and metastases (Crews, Dombroski, & King, 2021). Cancer vaccines may also be pioneering precursor technologies, demonstrating the benefit of antigens, adjuvants and DC which can then be included as additional components of other immunotherapies.

1.2.2.2 Oncolytic viruses

OV are genetically modified in order to infect and lyse only cancer cells which sacrifice their normal antiviral defenses in order to grow more rapidly. (A. H. Choi et al., 2016). OV can thus selectively infect and kill cancer cells, while leaving surrounding non-cancerous cells unharmed. While the precise mechanisms of their anti-tumour effect remain to be defined, they include direct tumour cell lysis, recruitment of APC and tumour infiltrating lymphocytes, as well as the release of pro-inflammatory cytokines from lysed tumour cells (Figure 1-5). In addition, some OV have been genetically modified to express these cytokines in order to augment their anti-tumour activity (Zeng et al., 2021). They are a somewhat niche area of cancer immunotherapy, with only one OV to date approved by the FDA: T-VEC, a herpes simplex virus that showed a significant clinical response in the treatment of unresectable melanoma, with the virus modified to also express granulocyte–macrophage colony-stimulating factor (GM-CSF) (Raman, Hecht, & Chan, 2019). Recent work has proposed the use of biomaterials in the form of nanofibers (Badrinath et al., 2018) or nanoparticles (J.-j. Lee et al., 2017) for targeted delivery of OV.

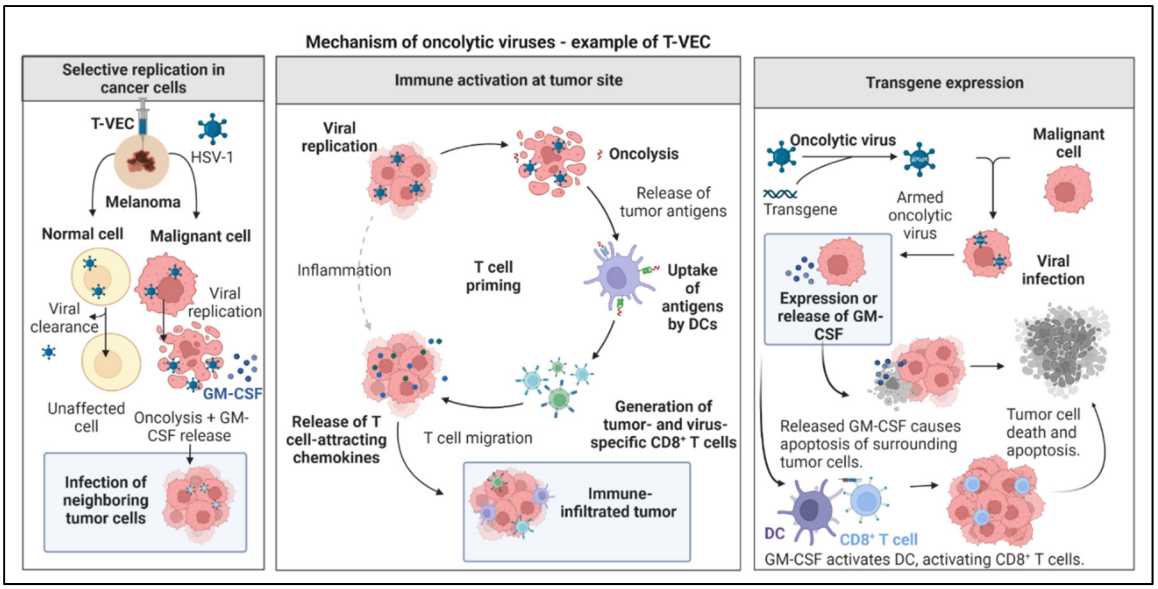

Figure 1-5 Oncolytic virus mechanisms
Oncolytic viruses such as T-VEC are selectively replicated in cancer cells, eliminating tumour cells via oncolysis and stimulating the immune system via the antigen release of destroyed tumour cells and expressed transgene products such as GM-CSF

There are several examples of bulk biomaterials which have been investigated for the delivery of OV, with Choi's group one of the first, showing that OV encapsulated in an alginate gel doubled their accumulation in the tumour and reduced tumour growth by half compared to non-encapsulated OV in mouse xenograft models of human C33A (cervical) and U343 (glioma) cancer cell lines. Gel encapsulation also reduced OV accumulation in off target tissues (J. W. Choi et al., 2013).

Other groups have shown similar improvements in OV efficacy, with a gelatin-hydroxyphenyl propionic acid (GHPA) hydrogel also showing a two-fold increase in anti-tumour efficacy, reduced accumulation in off target tissues and a reduced anti-OV immune response in hamster models with the HaP-T1 hamster pancreatic carcinoma cell line (B.-K. Jung et al., 2017). In murine xenograft models of localised OV delivery, both a recombinant silk elastin-like hydrogel in a head and neck cancer model and a polyurethane-sulfamethazine injectable hydrogel in a lung cancer model also reduced tumour growth by around half compared to non-

encapsulated OV. Histological analysis also demonstrated greater persistence of the OV at the tumour site in these cases (S.-H. Jung et al., 2014; Le et al., 2019).

Clearly biomaterials have the potential to improve OV retention in tumours, protect them from elimination by the immune system, and hence improve their efficacy. Clinical trials of locally delivered OV will no doubt be awaited with interest as this immunotherapy experiences a resurgence.

1.2.2.3 Drug delivery biomaterials

Biomaterials for simple local delivery of anti-cancer drugs have also been investigated, as with numerous other medical domains (Jianyu Li & Mooney, 2016). Drug delivery scaffolds and the principles underlying the design of hydrogel drug delivery systems, focusing on the physical and chemical properties of the hydrogel network and the hydrogel–drug interactions have been reviewed previously and won't be detailed here (Ahsan et al., 2018; Correa et al., 2021; Eskandari, Guerin, Toth, & Stephenson, 2017; Fenton, Olafson, Pillai, Mitchell, & Langer, 2018; Sponchioni, Capasso Palmiero, & Moscatelli, 2019). Biomaterial scaffolds allow local and controlled release of drugs and molecules, therefore allowing lower doses for equivalent efficacy and limiting dose-related toxicities. Spatial control also has the double benefit of increasing the payload of the drug or molecule at the relevant site, while ensuring a minimum is lost to non-tumour sites where it would be ineffective or even potentially cause off-target toxicity.

Whatever drugs and molecules are being delivered, the drug dosage, mechanism of release and ease of administration of the biomaterial are of greater importance. Here the ability to chemically conjugate molecules of interest to the material, and easier administration such as with an injectable material, would be highly desirable.

In terms of immunotherapeutic drugs, immune checkpoint inhibitors (ICI) are among the most popular for local drug delivery, often combined with other drugs. ICI are monoclonal

antibodies targeted towards so-called “immune checkpoints” – inhibitory immune pathways which downregulate T cell activation when their receptors on immune cells are activated that aim to maintain organism self-tolerance and avoid autoimmunity. Cancer cells themselves can develop the ability to activate these receptors and hence escape the downregulated immune system, for example Programmed death-ligand 1 (PD-L1) expressed on tumour cells (see Figure 1-6). The most commonly targeted ICI are CTLA-4, which competes with CD28 to bind CD80/CD86 and hence downregulates T cells (Hodi et al., 2010), PD-1, which has an inhibitory effect on T cell activation while stimulating Treg cells, which suppress the anti-tumoral immune response, and the ligand of PD-1, PD-L1, which can be found on the surface of tumour cells as well as endogenous epithelial and immune cells and contributes to the downregulating of T cells in the tumour microenvironment. LAG-3, a new addition to the ICI portfolio, is a cell surface protein expressed on immune cells that downregulates T cell proliferation and function (Workman & Vignali, 2005).

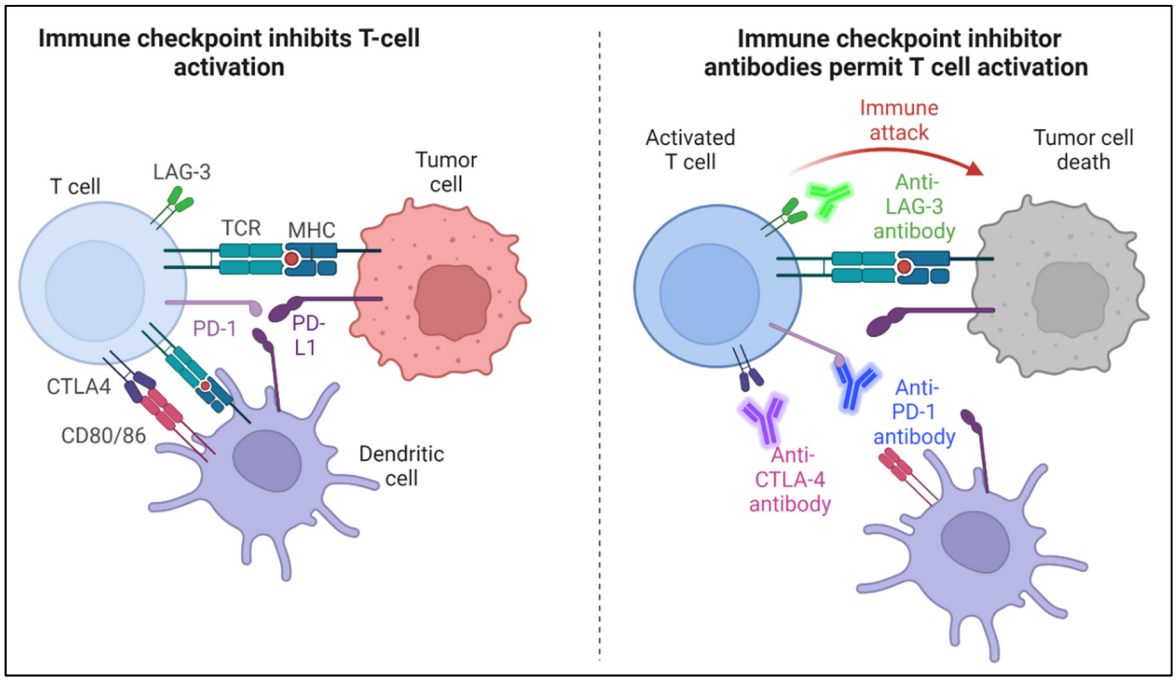

Figure 1-6 Mechanism of checkpoint blockade
Antibodies inhibit binding of immune checkpoint pathway receptors such as PD-1, CTLA-4 and LAG-3, preventing T cell inhibition and hence allowing tumour attack by activated T cells

ICI have become one of the most successful immunotherapies and dominate among FDA-approved immunotherapies and immunotherapy clinical trials, with Ipilimumab the first commercially approved ICI, targeting CTLA-4. Nivolumab, targeting PD-1, followed. Both treatments demonstrated improved survival over chemotherapeutic agents as treatments for metastatic melanoma patients, especially PD-1 which has the advantage of reduced toxicity compared to CTLA-4 (Haanen, Thienen, & Blank, 2015). ICI have had a revolutionary impact in oncology, although durable responses to ICI remain limited for certain cancers, and their associated toxicities remain a limitation to be addressed (Wilky, 2019).

Dosage and localization clearly contribute to the limitations associated with ICI, with ICI autoimmunity resulting from the systemic delivery of the treatment. For this reason, localized delivery of the drugs could result in more widely usable and safer treatments. However, the rapid and variable release of drugs in conventional delivery means that carriers such as biomaterial scaffolds are required for the controlled release and sustained delivery of therapeutics (Fenton et al., 2018).

For example, an alginate hydrogel incorporating anti-PD-1 and the anti-inflammatory drug Celecoxib reduced tumour growth by 90% compared to a blank hydrogel in a mouse B16-F10 melanoma model (Y. Li et al., 2015). The sustained co-delivery of Celecoxib and PD-1 enhanced their effects in a synergistic manner, where PD-1 augmented the inhibition of tumour angiogenesis provoked by Celecoxib, whereas the anti-inflammatory effect of Celecoxib downregulates inflammatory genes which may otherwise interfere with the therapeutic effect of PD-1. Another interesting example consisted of a poly(vinyl alcohol) hydrogel, crosslinked with a compound that can be oxidized and hydrolyzed in the presence of ROS such as H_2O_2 in the tumour microenvironment (C. Wang et al., 2018). This led to gel degradation at the tumour site where ROS are highly prevalent, and the subsequent controlled release of the chemotherapy drug gemcitabine and anti-PD-L1 antibodies. The local release of this drug combination resulted in over 60-day mouse survival in a B16-F10 melanoma model, where no mice in any untreated or single-treatment control groups survived after two months. As well

as controlling drug release, the hydrogel acts as a ROS scavenger which may limit the ROS-induced differentiation of macrophages to the tumorigenic “M” phenotype.

An example of biomaterials gaining popularity for immunotherapeutic drug delivery is multidomain peptide (MDP) hydrogels. One example consists of an amphiphilic core of amino acids, which self-assemble into nanofibers, and gels upon interaction with a negatively charged multivalent (Aulisa, Dong, & Hartgerink, 2009). This hydrogel was used to locally deliver anti-PD-1 in a sustained and controlled manner, which was significantly more effective and durable than systemic anti-PD-1 in preventing oral carcinomas in mice, with 20% of hydrogel-treated mice showing high-grade lesions 5 weeks after treatment compared to 60% of control mice (Shi et al., 2021). The same group further developed this gel with the addition of CDN as a STING agonist, as well as synthesizing another MDP that included an inhibitor of the pro-tumorigenic enzyme inducible nitric oxide synthase (Leach et al., 2021). The cationic gel further slowed and controlled CDN release for longer drug persistence compared to the previous MDP and resulted in the greatest tumour size reduction and survival among treatment groups.

Alternative biomaterial formats for immunotherapeutic drug delivery have also been developed. For example, Sun’s group developed a sprayable fibrin gel containing doxorubicin (DOX)-loaded platelet-derived extracellular vesicles (which preferentially target circulating tumour cells) and anti-PD-L1 (Zhao et al., 2022). The gel permitted sustained and controlled release of the two therapies at the tumour site in a murine B16-F10 model, permitting their synergistic effect which greatly decreased tumour growth and increased survival compared to single treatments. Furthermore, tumour growth was also limited in a distal tumour, showing the abscopal effect of the treatment.

Tong’s group developed an implantable optical fiber device that could simultaneously deliver ICI locally and measure tumour growth in real time by measuring tumour impedance (Chin et al., 2021). The device included photodynamic therapy as a combination therapy, where an administered photosensitiser will create ROS that can both damage tumour cells and

vasculature in response to light and improve intratumoral drug retention. Its combination with repeated ICI delivery directed by impedance measurements resulted in a durable anti-tumour response in a range of mouse melanoma and breast cancer models, and though the device is relatively invasive its real-time tumour growth monitoring to direct treatment is advantageous and it could be seen as analogous to routine medical devices such as insulin-delivery pumps (Kesavadev, Saboo, Krishna, & Krishnan, 2020).

Another relatively novel biomaterial drug delivery method is the use of microneedles, micron sized needles which are associated with faster action, increased efficacy and better patient compliance compared to transdermal injection (Waghule et al., 2019). Wu's group demonstrated microneedle patches composed of a polyvinyl alcohol core containing the melanoma drug 1-methyl-D,L-tryptophan, surrounded by a chitosan needle shell that contained anti-PD-L1 (Peipei Yang et al., 2020). The microneedle patch showed greater anti-PD-L1 retention at the administration site, as well as decreased tumour growth and greater survival compared to untreated mice and mice with intra-tumour drug delivery using conventional needles. The group further developed this work by also incorporating indocyanine green, a photosensitizer used in photothermal therapy where light interaction with the photosensitizer ablates the tumour to release antigens and further stimulate the anti-tumour immune response (P. Yang et al., 2021). These microneedles had an even greater anti-tumour effect and a further survival increase compared to the previous microneedles.

These results demonstrate the still unexplored potential of novel drug delivery systems in immunotherapy, which will only become more necessary as these treatments improve and are approved for other malignancies.

1.2.3 Nano-scale biomaterials

While their mechanisms differ from localized bulk biomaterials, nanoparticles have seen interest in both cancer vaccine and tumour drug delivery, due to their ability to act systemically but in a highly targeted manner (Riley et al., 2019). With targets and functions similar to certain

bulk biomaterials used for cancer immunotherapy, nanoparticles represent an alternative material form and perhaps an intermediate treatment classified somewhere between systemic therapies and localized biomaterials for cancer immunotherapy. Below are a few examples of the use of nanoparticles in immunotherapy, either as drug or OV delivery system or means to activate the immune response.

In work by Irvine's group, liposomic nanoparticles conjugated to stimulatory factors such as IL15/IL21 allowed complete tumour elimination, compared to limited survival increase with ACT and systemic stimulatory factors without nanoparticles (M. T. Stephan, Moon, Um, Bershteyn, & Irvine, 2010). PEG-PLGA nanoparticle-conjugated PD-1, combined with antitumour necrosis factor receptor superfamily member 4, ensured simultaneous binding to the two molecules and showed a tumour-free survival rate of 30% after biomaterial treatment, compared to 10% after treatment with a mix of NP-conjugated and free drugs in a murine B16F10 melanoma tumour model (Mi et al., 2018). Nanoparticles also offer interesting possibilities for different methods of drug delivery, as shown by Chen's group who developed inhaled chitosan nanoparticles conjugated to anti-PD-L1 (Jin et al., 2021). The cationic chitosan nanoparticles were able to adhere to the lung mucus layer to prolong anti-PD-L1 retention as well as act as an immune adjuvant due to the inherent immunostimulatory qualities of chitosan. Increased mouse survival and fewer metastases were seen in a mouse model of B16-F10 lung metastases as compared to free drugs or nanoparticles alone.

Nanoparticles have been utilized as synthetic APCs, such as work by Schneck *et al*. where iron-dextran & quantum dot nanoparticles were conjugated to CD28 and major histocompatibility complex (MHC)-peptide complexes to form synthetic APC, leading to significant reduction in tumour growth in mice (Perica et al., 2014).

Some groups have conjugated nanoparticles with OV, to prolong their circulation time and improve their antitumour efficacy. An OV conjugated with PEGylated oligopeptide-modified poly(β-aminoester)s showed a 3-fold increased circulation time, reduced immune neutralization of OV and significantly reduced tumour growth in murine xenograft models

compared to unconjugated OV using the human pancreatic cell lines PANC-1 or MIA PaCa-2 (Brugada-Vilà et al., 2020).

Methoxy poly(ethylene glycol)-b-poly{N-[N-(2-aminoethyl)-2-aminoethyl]-l-glutamate and PEG grafted to the OV increased accumulation in the tumour and reduced OV accumulation in off-target tissues. Tumour growth was also reduced 2-3 fold compared to unconjugated OV in murine xenograft models using HT1080 human fibrosarcoma and A549 lung cancer cell lines (Jaesung Kim, Li, Kim, Lee, & Yun, 2013).

Kasala 2017 – OV + paclitaxel conjugated with PEG and a polymeric micelle demonstrated higher viral replication in tumour, 12-fold increased blood retention and 2.5 fold increased anti-tumour efficacy compared to unconjugated OV in murine xenograft models using the human breast cancer cell line MCF-7 compared to free OV + PTX (Kasala et al., 2017).
Chitosan PEG folate nanoparticles greatly increased blood circulation time And showed a 2-fold reduced tumour growth compared to unconjugated OV in murine xenograft models using the KB human epithelial carcinoma cell line (Kwon, Kang, Choi, Kim, & Yun, 2013).

Nanoparticles have also been used in cancer vaccines, interestingly including mRNA delivery as the vaccine technology. Work using a lipid nanoparticle for mRNA vaccine delivery showed potent anti-tumour effects in mice and some success in clinical trials to treat melanoma (Kranz et al., 2016). In this case, mRNA coding for cancer antigens was encapsulated in negatively charged lipid nanoparticles, which protect the mRNA from elimination by the immune system and efficiently transport the mRNA to APC in the spleen. The mRNA expression appears to mimic infection with RNA viruses where free DNA and RNA are sensed by APC via receptors such as TLR7, which in turn stimulates the production of IFN-α that activates DC, NK, B and T cells. Furthermore, the RNA is internalised and translated by DC resident in the spleen, producing antigens which are then presented by the DC to activate and stimulate the proliferation of antigen-specific T cells. This technology was also one of the precursors to the revolutionary and now ubiquitous mRNA vaccines developed by Pfizer and Moderna against COVID-19 (Patel, Kaki, Potluri, Kahar, & Khanna, 2022).

1.2.4 Scaffolds for immune cell delivery

1.2.4.1 Principles of ACT

Another therapeutic strategy for which biomaterials could bring strong benefit is ACT. Conventional ACT consists of the intravenous administration of immune cells, mostly of T lymphocytes, which are expanded *ex vivo* and implanted into the patient to harness their specific anti-tumour effects. Presently, there are two main types of ACT treatment, depending on the sources of immune cells: tumour infiltrating lymphocytes (TIL) and genetically-modified T cells with chimeric antigen receptors (CAR) or with tumour-specific TCRs.

TIL used are obtained from the patient tumour, due to their well-established, inherent tumour specific response, considerably more abundant than peripheral lymphocytes. Since its first adoption in 1988 by the team of Rosenberg et al., TIL-ACT has shown great promise in the treatment of metastatic melanoma. In this treatment, TIL must be isolated from the tumour and expanded *in vitro* to reach 1-20 billion cells, before being intravenously reinjected in the patient. IL-2 is an essential growth factor for T cell proliferation, though other growth factors such as 4-1BB and TGF-β1 have been proposed as additional factors to improve cell growth and the anti-tumour response (Chacon, Pilon-Thomas, Sarnaik, & Radvanyi, 2013; S. Liu et al., 2010). Current ACT with TIL also uses a rapid expansion protocol, where minimally cultured and non-selected “young” TIL have been shown to be more effective than TIL cultured over a longer time period and selected *in vitro* based on antigenic stimulation (Itzhaki et al., 2011), though a limited number of treatment centres are able to both rapidly culture “young” TIL and select them for tumour specificity through the identification of unique tumour mutations via whole exome sequencing (Y.-C. Lu et al., 2018). Lymphodepletion via a combination of chemotherapy and total body radiation, prior to T cell injection, is also considered to have a beneficial effect on the anti-tumour activity. High dose IL-2 is also administered in order to maintain T cell activation *in vivo*, which is a source of the toxicity and

negative side effects of current ACT (Atkins et al., 1999). The main steps of ACT are summarized in Figure 1-7.

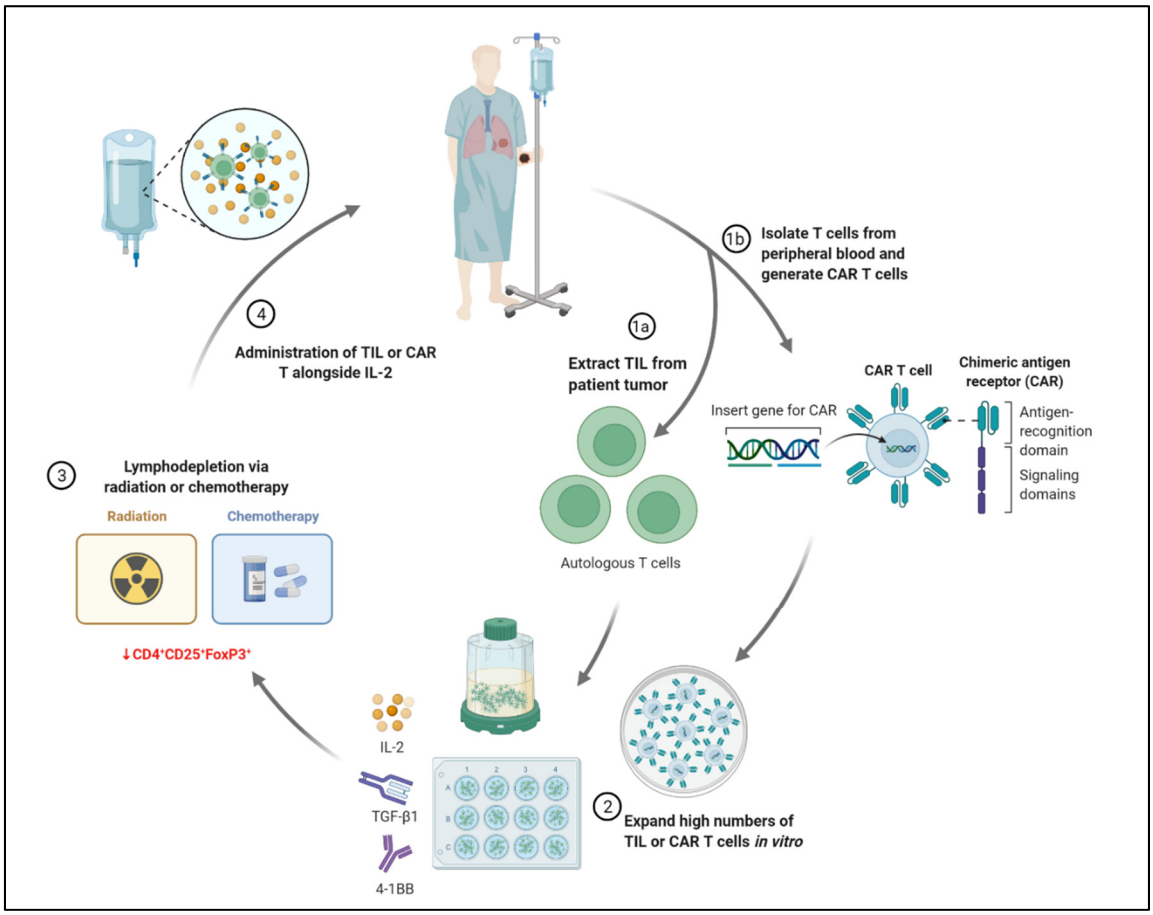

Figure 1-7 Typical phases of in clinical ACT
TIL or CAR are obtained and expanded in vitro, before lymphodepletion and re-administration alongside growth factors such as high or low-dose IL-2. CD4+CD25+FoxPE+ cells are immunosuppressive regulatory T cells that downregulated the activity of cytotoxic T lymphocytes in ACT

Another large area of interest is in so-called CAR-T cells, where T cells are genetically modified to express CARs in addition to the native T cell receptors. Their advantage lies in the fact that their recognition is not MHC-dependent, and they can recognize a wider variety of antigens than T cell receptors (which are limited to short peptides). Several pitfalls, however, keep these promising treatments from becoming mainstream.

One significant limitation of ACT is the large numbers of T cells that must be obtained, as many are lost to non-cancerous sites of inflammation during systemic administration and only a small fraction is reaching the tumour. This expansion can be lengthy, expensive, and difficult to achieve for some patients, causing many to lose treatment eligibility because of their deteriorating condition. Cells can also struggle to persist and survive in the immunosuppressive tumour microenvironment (S. L. Goff et al., 2010; R. Shapira-Frommer & J. Schachter, 2012; R. Wu et al., 2012). Even CAR-T cells, despite their success, show similar problems to ACT with TIL, including toxicities such as cytokine release syndrome and neurotoxicity, as well as limited efficacy in solid tumours (Neelapu et al., 2018).

These limitations call for reduced dosage and local cell delivery, in order to reduce the number of cells needed and avoid IL-2 associated toxicity, resulting in safer treatments. Simple cell injection around tumours is not sufficient, due to rapid cell loss due to dispersion, inflammation and anoikis (Roche et al., 2014). Biomaterial scaffolds could increase the number of cells at the target tumour site, while decreasing the overall doses and numbers required (Fenton et al., 2018). Furthermore, the inclusion of drugs or molecules to improve T cell persistence and anti-tumour activity, as well as the improved physical retention of T cells at the tumour site when delivered via a biomaterial, could improve cell persistence and functionality as well.

1.2.4.2 Design criteria for immune cell scaffolds

Cell-delivery scaffolds refer to biomaterials used as structures with defined architecture and composition, used for the delivery, retention and support of cells, possibly combined with therapeutic molecules. Only recently have been cell-delivery scaffolds proposed to enhance

the efficacy and overcome the limitations of immunotherapies. In terms of the requirements for an immune cell delivery scaffold, the scaffold should satisfy several criteria (Guyot & Lerouge, 2018; O'Brien, 2011):

1. Ease of administration – the scaffold must ideally be capable of minimally invasive implantation, via either a catheter or injection of the scaffold through a needle, to avoid the complications of surgical insertion and reach any location within the body.
2. Easy and simple homogenous mixing with cells, with a matrix capable of cell protection from applied shear stress during injection through standard needles or catheters.
3. Rapid stability in vivo – after minimally invasive implantation the scaffold must form a mechanically stable structure, stationary in the location it has been put in the body to ensure cell retention close to the target site.
4. Cell compatibility – In addition to general biocompatibility of the scaffold, it must support cell encapsulation. Once in situ the scaffold must support the survival, growth, anticancer function and escape of immune cells over a timeframe sufficient for cancer treatment.
5. Porosity – the scaffold must have a porosity that allows access to nutrients and waste removal for encapsulated cells, as well as allows immune cells to escape and perform their anti-cancer functionality, eliminating cancerous cells while other immune cells such as DC and B cells could colonise scaffolds to form protective tertiary lymphoid tissue.
6. Biodegradability – the scaffold should biodegrade into non-toxic, metabolizable products. In the case of cancer immunotherapy, degradability such that when the tumour is eliminated the biomaterial will also degrade and disappear would be desirable.
7. Formulation – the scaffold should ideally be chemically simple to formulate and avoid toxic chemical processes, to ease fabrication and approval by regulatory bodies such as the FDA in the USA or the EMA in Europe.

8. Sterilizability - the biomaterial should be capable of sterilization using standard methods such as autoclaving, ethylene oxide or gamma radiation prior to cell mixing and injection.

Table 1.1 gives a summary of recent or current studies of cell delivery scaffolds for cancer immunotherapy, which run from simple in vitro studies to preclinical murine models and use lymphocytes, dendritic cells and even in one case NK cells. These are detailed further in the following sections and a selection are shown in Figure 1-8.

Table 1.1 Cell-delivery biomaterial scaffolds for immunotherapies

Materials	Cells	Therapeutic agents	Injectable?	Immunotherapy model and outcomes	Ref
Chitosan-PEG	Human PBMC	None	Yes	In vitro glioblastoma cells	**(Tsao et al., 2014)**
Chitosan-PEG	Human CAR T cells	Self-expression of IL-15	Yes	Human retinoblastoma Elimination of tumours and 100% survival with gel-delivered IL-15 expressing CAR	**(K. Wang et al., 2020)**

Materials	PCL-PEG-PPG copolymer	PEG-heparin	PEG	Chitosan	Polyisocyanopeptide (PIC) + GRGDS peptide
Cells	Human CD4+ T cells	Human CD4+ T cells	Human CD3+ T cells	Human PBMC and TIL	Human T cells, DC and NK, mouse T cells
Therapeutic agents	None	CCL21	None	None	
Injectable?	Yes	Yes	Yes	Yes	Yes
Immunotherapy model and outcomes	Human CD4+ T cell survival over 5 days	Increased human CD4+ T cell proliferation	Proliferation upon restimulation of escaped T cells	In vitro renal cancer, breast cancer and melanoma	Migration in mice in vivo without tumours
Ref	**(Brewer, Gundsambu**	**(Pérez del Río et al.,**	**(Yan et al., 2022)**	**(Monette et al., 2016)**	**(Weiden et al., 2018)**

Materials	Hyaluronic acid	Alginate + GFOGER collagen-like peptide	Alginate + GFOGER collagen-like peptide	Fibrin-coated Nitinol
Cells	Human CAR T cells	Human CAR T cells	Human CAR T cells	Human CAR T cells
Therapeutic agents	None	IL-15 agonist, CD137, CD28,	IL-15 agonist, CD137, CD28, CD3, STING agonist	IL-15 agonist, CD137, CD28, CD3
Injectable?	Yes	No	No	No
Immunotherapy model and outcomes	In vitro glioma cell line	Mouse breast cancer resection model: regression in 60% of treated mice vs 0% survival in untreated mice	Mouse pancreatic cancer and melanoma models: complete pancreatic tumour elimination in 40% of treated mice, with persistent immunity on tumour rechallenge.	Mouse ovarian cancer model 2.7-fold survival increase with CAR T-loaded Nitinol film vs untreated mice
Ref	**(Atik et al., 2018)**	**(S. B. Stephan et al., 2015)**	**(Smith et al., 2017)**	**(Coon, Stephan, Gupta, Kealey, & Stephan,**

Materials	Fibrin	RADA16 Peptide	α-CD/PEG
Cells	Murine DC	Murine DC	Murine DC
Therapeutic agents	None	Tumour antigens, anti-PD-1	DOX, CpG, B16 tumour cells
Injectable?	Yes	No	Yes
Immunotherapy model and outcomes	Mouse lung cancer model Single encapsulated DC treatment more effective than multiple non-encapsulated	Mouse lymphoma model Significant survival improvement with gel-encapsulated DC vs untreated mice	Mouse melanoma model Significant survival improvement with gel-encapsulated DC with CpG + B16 vs single treatments
Ref	**(Verma et al., 2016)**	**(Pengxiang Yang et al., 2018)**	**(A. Yang, Y. Bai, et al., 2021; A. Yang, X. Dong, et al., 2021)**

Materials	gelatin-hydroxyphenyl propionic acid (GHPA)	Hyaluronic acid	Alginate microspheres
Cells	Murine DC	Human CAR NK cells	Human CAR T cells
Therapeutic agents	Oncolytic virus	None	IL-15, Hemoglobin
Injectable?	Yes	Yes	Yes
Immunotherapy model and outcomes	Mouse lung cancer model Significantly increased survival compared to single treatments of DC/OV	Mouse leukaemia and breast cancer models Significant survival improvement with gel-encapsulated CAR NK vs non-encapsulated NK	Mouse renal and ovarian cancer models Greatly improved mouse survival with alginate-encapsulated CAR T cells compared to untreated mice
Ref	**(Oh et al., 2017)**	**(Ahn et al., 2020)**	**(Zuyuan Luo et al., 2020)**

Materials	Fibrin	Methacrylated hyaluronic acid
Cells	Human CAR T cells	Human CAR T cells
Therapeutic agents		IL-15 nanoparticles, anti-PD-L1 platelets
Injectable?	No	No
Immunotherapy model and outcomes	Mouse lymphoma and glioma models Significantly improved mouse survival with fibrin-encapsulated CAR T cells compared to mice treated with non-encapsulated CAR	Mouse model of human melanoma Extensive tumour elimination with CAR + IL-15 + anti-PD-L1
Ref	**Ogunnaike Edikan et al.**	**(Q. Hu et al., 2021)**

Materials	Alginate
Cells	Monocytes
Therapeutic agents	Tumour antigens, anti-PD-1
Injectable?	Yes
Immunotherapy model and outcomes	Mouse breast cancer model Significant preventative and therapeutic anti-tumour effects
Ref	**(Tian et al., 2021)**

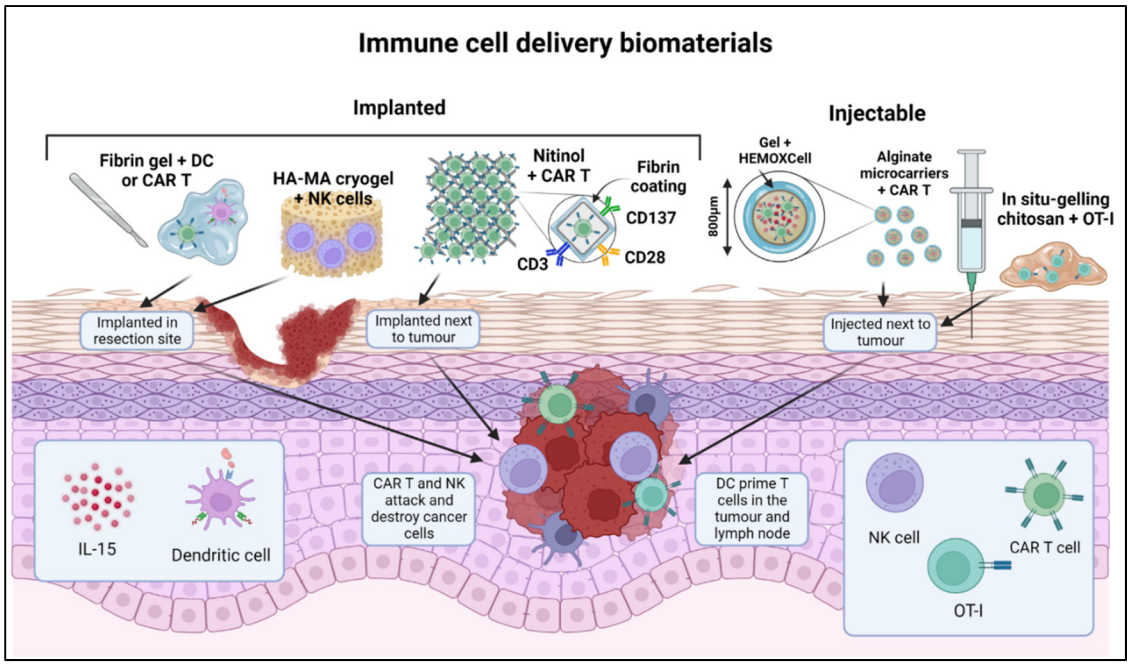

Figure 1-8 Selected biomaterials for immune cell delivery
Implantable or injectable gels, meshes and microcarriers are loaded with dendritic cells, NK cells or CAR T cells to improve cell delivery and persistence in and around the tumour. Cells progressively escape from the scaffolds towards the tumour and immune system, while the biomaterials and additions such as stimulatory antibodies or cytokines augment treatment efficacy

1.2.4.3 T lymphocyte scaffolds

Cell-delivery scaffolds offer improvements to systemic cell delivery using inherent biomaterial advantages such as localisation and the incorporation of immunostimulatory factors. T cell-delivery scaffolds have been the most studied approach, with a range of both implantable and injectable materials been investigated with varying progress from in vitro work to in vivo models.

Implantable scaffolds

Stephan's group, prominent in this area and at the forefront of biomaterial immune cell therapies, developed oxidised (and therefore biodegradable) alginate gels grafted with a collagen-mimetic peptide to locally deliver CAR-T cells (S. B. Stephan et al., 2015). In vitro studies demonstrated the benefit of this adhesive peptide which increased lymphocyte

migration within the gel and lymphocyte escape into a surrounding collagen gel, as well as increasing cell viability compared to unmodified alginate, Lipid-coated mesoporous silica microspheres incorporating an IL-15 agonist, as well as the immunostimulatory antibodies CD3, CD28 & CD137, similar to those present in the Dynabeads Human T-Activator commonly used for in vitro T cell expansion, were also included and the scaffold was lyophilized to create an implantable porous matrix which was seeded with T cells immediately before implantation. The scaffold led to very promising in vitro and in vivo results in mice models. In a breast cancer resection model, it reduced tumour relapse compared to conventional intravenous or peritoneal treatments and supported tumour-targeting T cells throughout resection beds and associated lymph nodes, while it triggered much stronger regression in a multifocal ovarian cancer model resulting in greater mouse survival than locally delivered cells without the scaffold.

The same group further developed this model in 2017, adding cyclic di–GMP as a STING agonist, again loaded into the mesoporous silica microspheres, to activate DC and further enhance the immune response. (Smith et al., 2017) .The combination showed increased efficacy in treating solid pancreatic cancer and melanoma tumours in mice, with the STING agonist addition resulting in complete tumour remission in some cases The authors conclude that the codelivery of STING agonists can stimulate the immune responses to eliminate tumour cells that are not recognized by the adoptively transferred lymphocytes and thus increase the CAR T cell therapy and help protect against the emergence of escape variants.

However, the scaffold is not injectable and its numerous complicated fabrication steps were a strong limitation towards clinical transfer. More importantly it lacks a well-controlled porosity to favor T cell survival and proliferation.

More recently, Stephan’s group adapted similar modifications to a fibrin-coated nickel-titanium alloy (nitinol) porous mesh with well controlled porosity, that can be placed on tumour lesions and release and functionally support tumour targeted T cells (Coon et al., 2019). These micropatterned thin films (approximately 10μm), formed via magnetron sputtering, were

designed to improve oxygen and nutrient transfer to the T cells which was a limiting factor in their previous alginate gels. Nitinol is inherently bioinert due to the thin layer of titanium oxide formed on its surface, though in this work the nitinol was functionalised through fibrin coating which allowed lymphocyte adhesion and migration, as well as coupling to the CD3, CD28 and CD137 antibodies. The system elicited robust proliferation of the seeded T cells in vitro and in vivo, leading to a huge increase of T cell on the site compared to intravenous and locally injected cells. The authors also showed impressively enhanced tumour elimination compared to locally or intravenously injected CAR T cells.

The necessity to implant this scaffold is still a potential limitation compared to injectable cell delivery scaffolds for immunotherapy. However, the mesh can be incorporated into a variety of implant configurations such as an endovascular stent for non-invasive administration. Applicability to human patients may depend on tumour location and the feasibility of surgical or minimally-invasive implantation. Moreover, the practical constraints for producing and manipulating sterile nitinol films, and their subsequent seeding with T cells followed by implantation or catheter administration may be limiting for clinical use.

Another interesting work to mention is Gu's group developed a methacrylated hyaluronic acid hydrogel for CAR T cell encapsulation, using freeze-drying to create implantable porous hydrogels with a similar method to the previously described cryogel vaccines (Q. Hu et al., 2021). The gel also incorporated IL-15 loaded PLGA nanoparticles, and platelets conjugated to anti-PD-L1 as a concurrent ICB therapy. While the effect of the CAR T loaded hydrogel was quite limited, almost complete tumour elimination was achieved with the group with co-encapsulated CAR, IL-15 and PD-L1 in a mouse model using human melanoma WM115 cells (Figure 1-9b). They also demonstrate by bioluminescence the persistence and growth of T cells in vivo. The scaffold also triggered an abscopal effect inhibiting distant tumour growth.

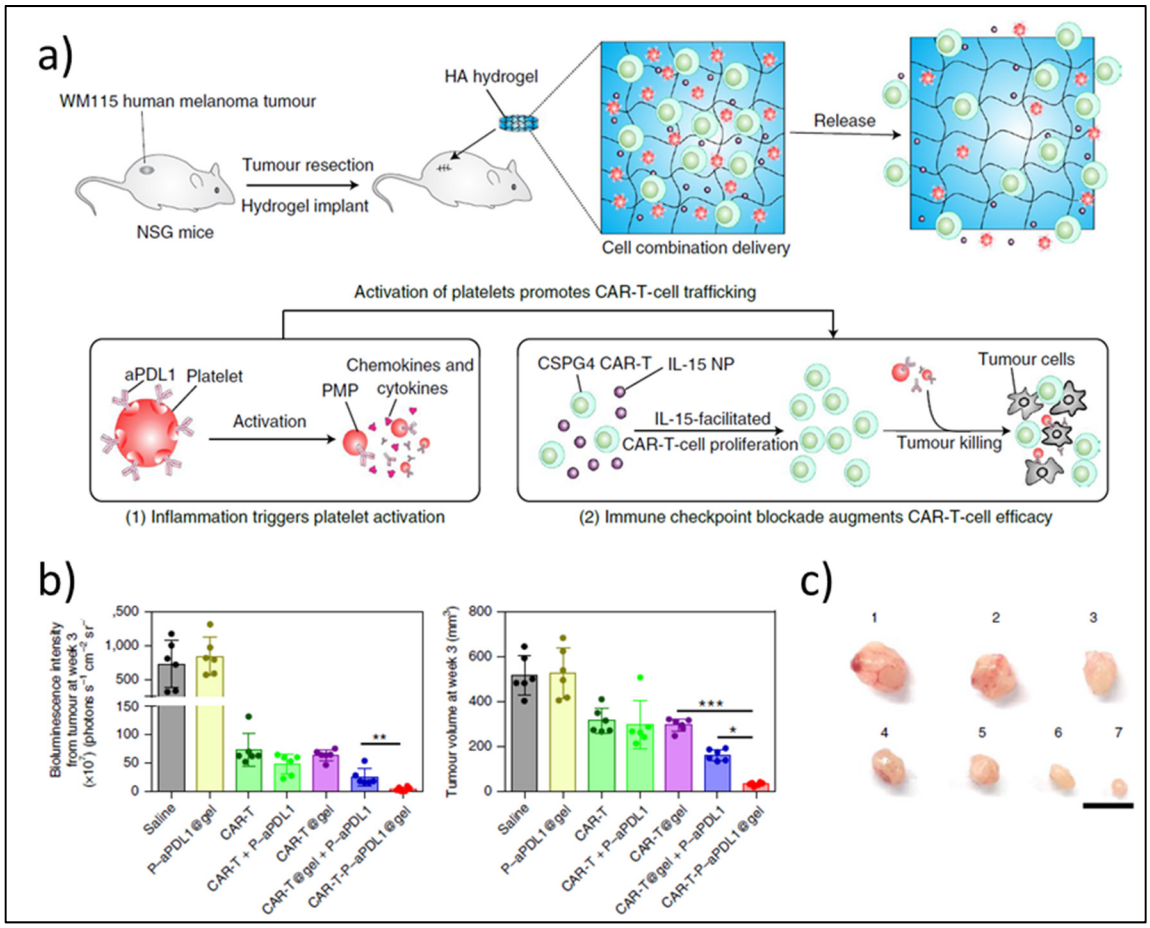

Figure 1-9 Cryogel for CAR T cell delivery
a) Schema of the tumour model and cryogel; b)Tumour bioluminescence (left) and volume (right) 3 weeks after treatment (mean ± SD, n = 6 mice per group). Statistical analysis was performed using one-way ANOVA followed by Tukey's HSD post hoc test. c) Representative photos of tumours at three weeks. Groups: 1, saline; 2, P–aPDL1@gel; 3, CAR-T; 4, CAR-T + P–aPDL1; 5,CAR-T@gel; 6, CAR-T@gel + P–aPDL1; and 7, CAR-T-P–aPDL1. Scale bar, 1 cm. PMP: platelet-derived microparticles, P–aPDL1: PDL1 antibody covalently conjugated to the cell surface of human platelets
Taken from Q. Hu et al. (2021)

Injectable scaffolds

Several efforts have also been made to create injectable T lymphocyte delivery scaffolds. Tsao et al created a thermosensitive chitosan-PEG hydrogel, by alkylation of chitosan followed by Schiff base formation. The gel showed successful loading, survival, escape and anti-cancer activity of T lymphocytes in vitro against a glioblastoma cell line (Tsao et al., 2014). However,

the scaffold had a gelation time of 8-12 min at 37°C, which is quite long to avoid cell dispersion at the time of in vivo injection. Despite this concern, the same gel was later applied to CAR T cells targeted against GD2, an antigen overexpressed in retinoblastoma (K. Wang et al., 2020). The gel prolonged CAR persistence within the tumour and gel-encapsulated CAR significantly reduced tumour growth. Impressively, further modification of the CAR to induce self-expression of IL-15 resulted in tumour elimination and a 100% survival rate.

Other groups have investigated other PEG-containing lymphocyte scaffolds in vitro, with Guasch's group developing a PEG-heparin hydrogel (Pérez del Río et al., 2020), where heparin allowed the conjugation of the cytokine CCL21 which is present in the lymph nodes and is known to enhance T cell proliferation and migration (Flanagan, Moroziewicz, Kwak, Hörig, & Kaufman, 2004). The hydrogels increased CD4+ T cell proliferation, though were demonstrated primarily as T cell culture scaffolds rather than a delivery platform. A PCL-PEG-poly(propylene glycol) (PPG) copolymer has also been demonstrated for T cell encapsulation, though only survival over 5 days and not proliferation was demonstrated in this case (Brewer et al., 2020). Another group demonstrated a PEG hydrogel formed via Diels–Alder cycloaddition of fulvene and maleimide functionalised PEG precursors, which has tunable stiffness and degradation (Yan et al., 2022). However, the gel showed relatively slow gelation (>15min) and limited cell viability after several days even with RGD functionalisation, though cells that escaped from the gel were capable of proliferation after recovery and re-stimulation.

Figdor's group investigated RGD grafted polyisocyanopeptide (PIC) gels to culture human T cells and observe the in vivo escape of murine T cells (Weiden et al., 2018). PIC, a relatively new class of hydrogel, are synthetic hydrogels formed through nickel(II)-catalysed polymerisation of the two monomers - triethylene glycol functionalized isocyano-(D)-alanyl-(L)-alanine (monomer 1) and monomer 2, an azide-appended version of monomer 1. This water-soluble polymer exhibits thermosensitive gelation, remaining liquid below 16°C and forming soft hydrogels in a matter of minutes above this temperature (Das, Gocheva, Hammink, Zouani, & Rowan, 2016). Interestingly its mechanical properties can be tuned to reach similar mechanical properties and stress-stiffening behaviour to biological polymers

such as collagen (Zimoch et al., 2018). The authors showed that GRGDS (RGD) peptides grafting allowed greater T cell migration within the gel compared to unmodified gel and in vitro viability & proliferation up to 72h (Weiden et al., 2018). Scaffold–encapsulated T cells migrated out of the gels over 3-4 weeks in mice, though with the majority of T cells escaping the gel in the first week after injection. The study was performed simply to demonstrate T cell escape from the gel in mice without tumours and so has not demonstrated efficacy in a mouse tumour model. Another group developed a proprietary, low-viscosity HA and gelatin-based gel as a substrate to deliver CAR T for glioblastoma using Convection Enhanced Delivery, in which an intracranial catheter is placed into the tumour that infuses the agent with positive-pressure over time (Atik et al., 2018). The encapsulated CAR T cells migrate from the gel & carry out their cytotoxic function in vitro. The gel itself showed no toxicity when injected in mice, though again this was performed in mice without tumours and so has not demonstrated anti-tumour efficacy.

Other groups are also beginning to investigate alternative materials and biomaterial formats for ACT delivery. For example, Ogunnaike et al. used fibrin gel–mediated CAR-T cell delivery for glioblastoma by inoculating fibrin solution with CAR-T cells in the cavity followed by immediate addition of thrombin solution. However such a method does not ensure complete encapsulation due to cell dispersion prior to gel formation and fibrin gel is known to degrade very rapidly (Ogunnaike Edikan et al.).

The main challenge with injectable scaffolds is to create macroporous structures which allow good access to oxygen and nutrients and the possibility for the cells to escape the scaffold. Several studies including Stephan's work with nitinol films have shown that the small physical size of microscaffolds is beneficial for nutrient supply and cell migration. Another alternative is to encapsulate T cells in small microspheres which allow better diffusion of Oxygen and nutrient, and potential vascularisation in between the microspheres (Alinejad et al., 2020). Luo et al (2020) created an injectable hydrogel-encapsulated porous immune-microchip system (i-G/MC) with the capabilities of enhancing CAR T cell survival and proliferation (Zuyuan Luo et al., 2020). Interestingly, they incorporated the HEMOXCell molecule in their alginate

microspheres, a marine hemoglobin with a high oxygen storage capacity, to counteract the hypoxic effect of the tumour microenvironment. However, the long and complex preparation steps required (including multiple lyophilisations and several days' immersion in PBS) may prevent the use of such systems in clinical trials.

1.2.4.4 Scaffolds for other immune cells

Biomaterials have also shown promise to assist DC-based immunotherapies, with DC probably the most commonly delivered immune cell via biomaterial scaffolds after T cells. Such DC loaded scaffolds can overcome the lack of recruitment of host DCs to create more efficient vaccine-like immune cell niches. DC can be stimulated prior to their addition in the gel or injected in combination with the tumour antigen, and eventually other drugs, as detailed below. Tumour antigen-stimulated DCs in a fibrin gel showed significantly reduced tumour growth in mice with the cell scaffold construct compared to injected DC alone (Verma et al., 2016).

Another group delivered DC in an injectable self-assembled peptide hydrogel (Pengxiang Yang et al., 2018), based on RADA16, a synthetic peptide consisting of 16 alternating hydrophobic and hydrophilic amino acids which self-assembles into a nanofibrous, nanoporous hydrogel in the presence of neutral pH solution (Cormier, Ruiz-Orta, Alamo, & Paravastu, 2012). DC and antigens were mixed with the hydrogel on ice before injection. The gel was biocompatible with DC, did not activate DC by itself (being non-immunogenic) and when containing DC and antigens it improved both therapeutic and prophylactic efficacy in reducing tumour growth in a mouse lymphoma model, compared to intravenous and subcutaneous injection, with even greater efficacy observed in conjunction with an anti-PD-1 checkpoint inhibitor. As well as anti-PD-1, one group showed that the chemotherapeutic DOX in the form of nanoparticles, also potentially conjugated to the immune adjuvant CpG, could be incorporated in an injectable α-cyclodextrin/PEG hydrogel along with DC. The gel significantly reduced tumour growth in a B16 melanoma mouse model compared to single treatment or control groups when treated with the full complement of DC, DOX and CpG-loaded gel (A. Yang, X. Dong, et al., 2021). Subsequent work by this group also showed the

further beneficial effect of including dying B16 tumour cells into the DC scaffold vaccine (A. Yang, Y. Bai, et al., 2021). A similar trend was also observed with monocytes encapsulated in alginate droplets using a microfluidic system (Tian et al., 2021).

One group incorporated IL-12 and GM-CSF-expressing OV with DC delivered using a gelatin-hydroxyphenyl propionic acid hydrogel, enzymatically cross-linked via horseradish peroxidase (HRP) and hydrogen peroxide (H_2O_2). Gel-encapsulated OV + DC significantly increased survival in a murine Lewis lung carcinoma model compared to single treatments of a DC/OV combination without gel, with impressive 100% survival in mice treated with Gel OV + DC. All this work indicates the range of materials and drugs beneficial for monocyte and DC delivery, as with T cell ACT.

Another interesting recent development is a hyaluronic acid-based scaffold which was used for the delivery of NK cells as a cancer immunotherapy. The scaffold was formed from a blend of methacrylate-modified HA and methacrylate-modified oxidized HA, where the methacrylate-modified oxidized HA acted as a highly-degradable sacrificial component to create greater porosity and allow NK cell clustering which improves cell activation and viability (M. Kim, Kim, Kim, Doh, & Lee, 2017). The scaffold upregulated NK cell proliferation and tumour killing activity *in vitro*, and resulted in fewer metastases and increased mouse survival; *in vivo* (Ahn et al., 2020). This work may well be the first of many investigations into NK cell-carrier biomaterials as cancer immunotherapies, though the scaffold is non-injectable and must be implanted so it would be interesting to examine some of the above injectable scaffolds as NK cell carriers.

Altogether, despite impressive developments and a variety of approaches, and very promising results in mice models, there is presently no ideal scaffold for T cell delivery which would combine well controlled porosity and injectability and clinically feasible manufacturing processes. In the following sections we will explore how our group's hydrogel could be a suitable material for this application.

1.3 Hydrogels

1.3.1 Hydrogels in biomedical applications

Hydrogels are, by definition, materials consisting of "*3D polymer networks which are capable of absorbing very high quantities of water while retaining a stable structure"* (Hoffman, 2002). This highly aqueous composition means hydrogels often bear similarities to the water-containing soft tissues in the body, making hydrogels highly suitable for biomedical applications where soft tissues must be supported or replaced (Ruel-Gariépy & Leroux, 2004). There are numerous ways to classify and divide hydrogels, based on a range of criteria. A comprehensive review (Ahmed, 2015) listed polymeric composition – homopolymeric or copolymeric, crystallinity, natural vs synthetic origin, physical or chemical crosslinking and electrical charge as some of the many ways to classify gels.

Figure 1-10 highlights the general structure of gels as classified between chemical and physical gels and the various groups related to physical gels.

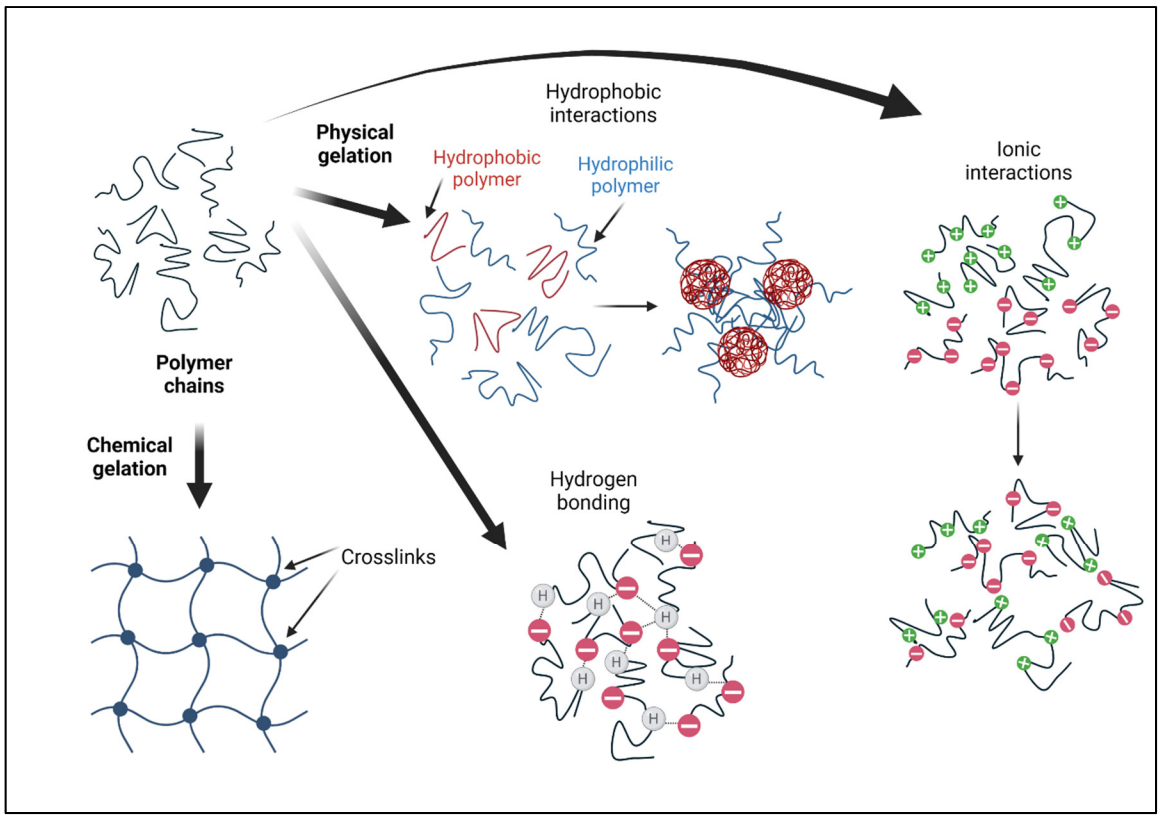

Figure 1-10 Structure and interactions of chemical and physical hydrogels
Original illustration, inspired by Akther, Little, Li, Nguyen, et Ta (2020)

Chemically crosslinked hydrogels possess irreversible covalent bonds between the polymer chains which make up the polymer network of the hydrogel. The crosslinkers used can often be toxic and require a purification step for their removal during the production of the hydrogel, meaning physical hydrogels may possess an advantage in areas such as biocompatibility (Berger, Reist, Mayer, Felt, Peppas, et al., 2004).

Physical hydrogels are formed through potentially reversible links between the polymer chains, which can be through molecular entanglement, ionic interactions, hydrogen-bonding or hydrophobic forces, or a combination of these mechanisms (Berger, Reist, Mayer, Felt, & Gurny, 2004). Clusters of these features can create inhomogeneities, with a common

disadvantage of physical crosslinking being that the gels are unstable and can disintegrate rapidly and unpredictably (Garcia, Aguilar, & San Roman, 2010).

Many hydrogels can undergo reversible volume phase transitions or sol-gel phase transitions in response to external physical or chemical stimuli, such as temperature, pH, ionic strength, light and electromagnetic radiation - called stimuli-sensitive or intelligent hydrogels. Hydrogels formed by stimuli-induced sol-gel phase transitions are called in-situ forming hydrogels, and many of these types of hydrogels offer great potential in applications such as drug delivery, due to their innate ability to respond to physical stimuli (Sung Lee & He, 2010). In this way a hydrogel responding to temperature as a stimulus, for example, could remain as a liquid at an ambient temperature to allow homogenous cell distribution and ease of implantation via injection but gel at body temperature in order to retain a stable structure at the desired site of implantation. These kinds of thermoresponsive hydrogels exist, and their temperature sensitive gelation makes them very suitable candidates for a TIL delivery system.

Hydrogels using polymers such as gelatin (Bozec & Odlyha, 2011) and alginate have been explored (Bidarra, Barrias, & Granja, 2014), however, chitosan is another natural polymer popular for use in hydrogels for cell encapsulation, with certain chitosan hydrogels possibly offering solutions to some of the problems encountered with other materials. The following section will examine chitosan hydrogels in more detail.

1.3.2 Chitosan and its use in thermoresponsive hydrogels

Chitosan is a partially deacetylated derivative of chitin, an abundantly available component of the exoskeleton of invertebrates such as crabs and insects (Kumar, Muzzarelli, Muzzarelli, Sashiwa, & Domb, 2004). It takes the form of a polysaccharide comprised of glucosamine and N-acetylglucosamine residues, as demonstrated in Figure 1-11.

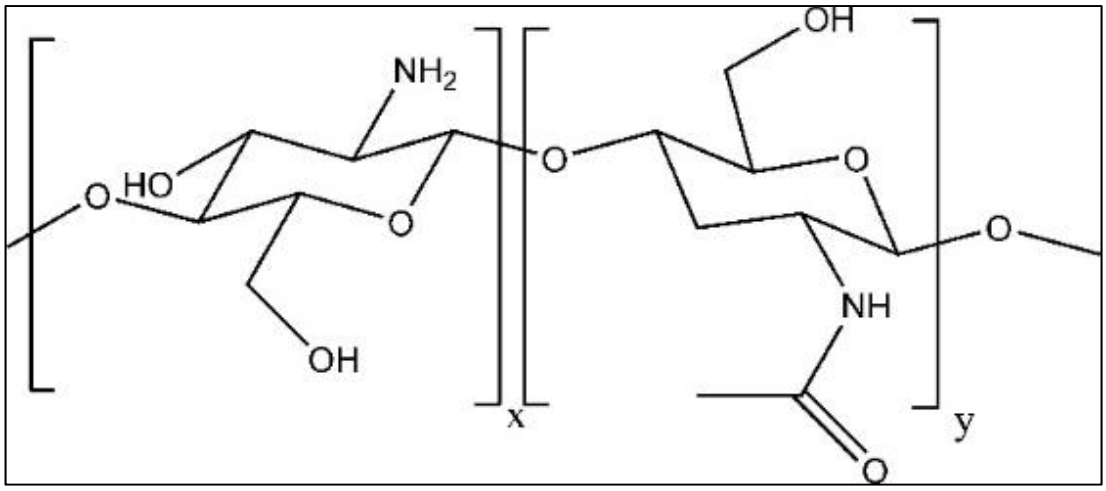

Figure 1-11 Chemical structure of chitosan
x is the deacetylated glucosamine and y is the acetyleated N-acetylglucosamine residue
Taken from Van Vlierberghe, Dubruel, et Schacht (2011)

Its non-toxicity, stability, biodegradability and ability to be sterilized have made it a popular biomaterial in a wide range of applications, including in thermoresponsive hydrogels (Bhattarai, Gunn, & Zhang, 2010). It has been used in conjunction with typical synthetic polymers such as PNIPAM and PEG to produce thermoresponsive gels (Ganji & Abdekhodaie, 2008; Recillas et al., 2009), though taking into account the limitations of these polymers, the formation of thermoresponsive physical chitosan hydrogels with the addition of β-glycerophosphate (BGP) by Chenite et al. in 2000 initiated research into a highly promising alternative type of chitosan hydrogels (Chenite et al., 2000).

Chitosan is soluble only in acidic solutions up to about pH 6.2, due to its pKa at roughly the same value (~6.3) (Pillai, Paul, & Sharma, 2009). However thermally sensitive neutral solutions based on chitosan/polyol salt combinations were discovered which exhibited a physiological pH, were liquid at room temperature and formed monolothic gels at body temperature (Chenite, Buschmann, Wang, Chaput, & Kandani, 2001; Chenite et al., 2000). Hydrogen bonding, electrostatic interactions and hydrophobic interactions have all been hypothesised to be physical mechanisms for the gelation (H. Y. Zhou, Jiang, Cao, Li, & Chen, 2015).

Recent work has shown that, at least in part, gelation occurs through a heat-induced proton transfer between the chitosan and BGP, reducing the repulsion between the amino groups on the chitosan and allowing hydrogen bonding and hydrophobic interactions between the chitosan chains (Lavertu, Filion, & Buschmann, 2008). Other work has built upon this theory, showing that the protective water sheaths (formed via interactions between BGP polyol moieties and water) around the chitosan are removed upon heating, allowing the interaction of the chitosan chains through both hydrophobic interactions and hydrogen bonds (Aliaghaie, Mirzadeh, Dashtimoghadam, & Taranejoo, 2012; Supper et al., 2013). Similar to the proton transfer, this allows greater chitosan chain interaction and hence gel formation. Furthermore, work from Buschmann's group specifically challenged the hypothesis that electrostatic interactions between chitosan and BGP form part of the gelation mechanism, demonstrating that BGP could be completely removed from the gel via diffusion and as such was not electrostatically linked to chitosan molecules (Filion & Buschmann, 2013).

Alternatives to chitosan-BGP gels have also been investigated – such as a novel gel using sodium hydrocarbonate (SHC) as the weak base which is in sol state in certain conditions and gellifies after heating (L. Liu, Tang, Wang, & Guo, 2011). Other weak bases including ammonium hydrogen phosphate (Nair, Starnes, Ko, & Laurencin, 2007) and sodium phosphate dibasic (X. Li et al., 2011) have also been investigated, showing a similar ability to form physically crosslinked hydrogels when combined with chitosan in acidic solution. This would seem to indicate that a multitude of weak bases would be potentially suitable for use in physically crosslinked chitosan gels.

Despite their continued development, none of the above gels has been shown to both gel rapidly and have high mechanical resistance. The weak mechanical properties of BGP gels make them unsuitable for both drug delivery and tissue engineering or embolization as biomedical applications.

To address this, chitosan hydrogels combining SHC with either BGP or phosphate buffer (PB) as the bases used for neutralizing the chitosan were developed by our group. This improved

their mechanical properties dramatically without modifying the chitosan and showed good biocompatibility with L929 cells due to their reduced osmolality compared to BGP only gels which require a high, cytotoxic BGP concentration for fast gelation (Assaad, Maire, & Lerouge, 2015). Further optimisation has resulted in gel formulations with physiological osmolality, rapid gelation at 37°C, strong mechanical properties and demonstrable cell survival (Ceccaldi et al., 2017). The exact mechanism of gelation using multiple bases of either PB with SHC or BGP with SHC has yet to be fully understood, though is thought to be similar to the proton transfer and subsequent chitosan self-association observed in chitosan-BGP gels. PB and BGP respectively may increase the extent and rate of this proton transfer and thus gelation speed, with their competition with SHC carbonate ions possibly explaining their effect on mechanical properties compare to gels with SHC alone.

Because of this, for gels combining PB and SHC a trade-off exists between speed of gelation, increased by increasing the PB concentration, and compression strength which decreases with increasing PB concentration. For this reason the formulation – concentrations of the two gelling agents respectively – is very much dependent on the application. The gel format can also be modified as will be shown in the following section.

1.3.3 Hydrogel microbeads

An interesting development as an alternative to bulk hydrogels is microencapsulation, where cells and other molecules are encapsulated in microscale spheres, in theory < 1mm in diameter but generally accepted to be in the range of 100-1500µm. The goal of this alternative gel format is to exploit the greater surface area/volume ratio of microspheres as compared to bulk macroscale polymers, in turn improving the diffusion of therapeutic molecules and cytokines, encapsulated cells, nutrients and oxygen and the removal of cellular waste products as shown in Figure 1-12.

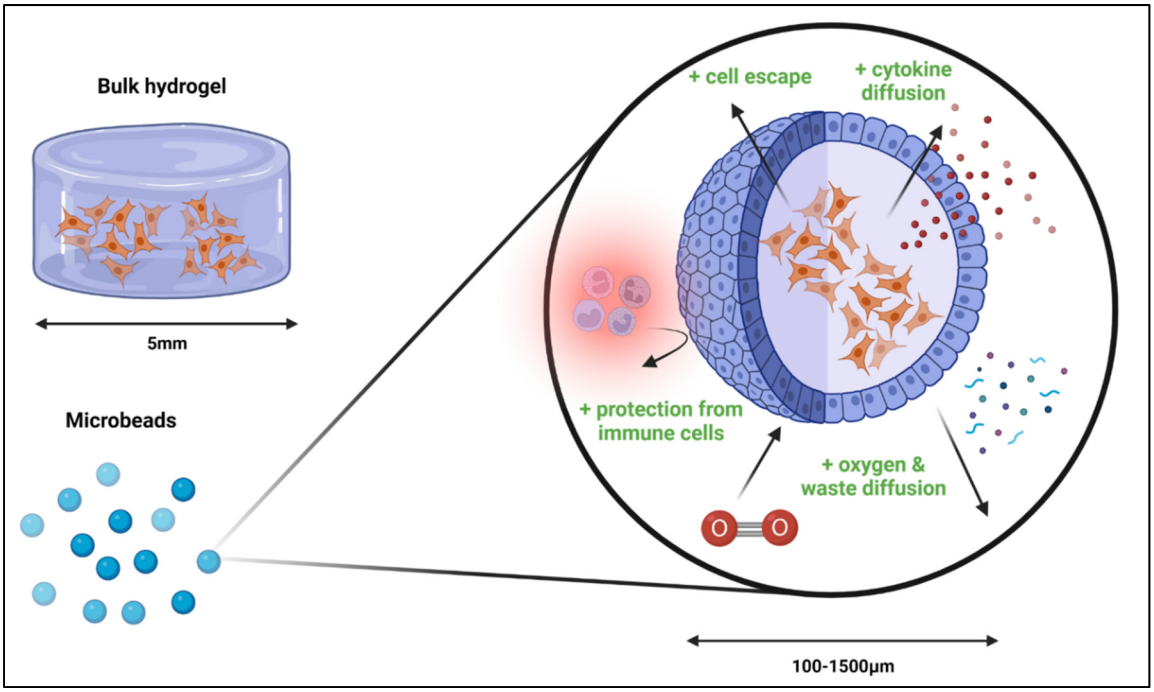

Figure 1-12 Advantages of microencapsulation in bulk hydrogels

Due to these potential benefits, microencapsulation is experiencing growing interest in a range of applications and using a variety of materials, though its mainstream origin was the encapsulation of pancreatic islet cells for the treatment of diabetes (Strand, Coron, & Skjak-Braek, 2017). Work in this area has allowed key aspects of microencapsulation to be evaluated, one of which is the microsphere size which in turn affects permeability and nutrient diffusion. The reduction of microsphere diameter from 1000µm to 400µm has been associated with improved islet function (Canaple, Rehor, & Hunkeler, 2002), though the importance of microsphere size is debated, with some groups suggesting that graft site may be of greater importance and that in vivo demonstration of increased efficacy with smaller microspheres is limited (Calafiore, 2018).

There are numerous methods for the production of microspheres, including electrostatic extrusion, emulsion, lithography, microfluidic systems and bioprinting (S.-Y. Lee et al., 2021). All have their respective advantages and disadvantages but here we will focus on emulsion, as

this is a method optimised by our collaborators in Hoesli's group for the aforementioned application of encapsulating islet cells in alginate microspheres (Hoesli et al., 2017).

This method consists of a water-in-oil emulsion where alginate hydrogel droplets are dispersed in mineral oil before subsequent gelation. Cells are encapsulated in the alginate solution, in addition to a calcium carbonate solution, before this mixture is added to oil under agitation in a spinner flask. The oil is acidified via the addition of acetic acid, which reduces the pH so that the calcium carbonate is solubilised and releases Ca^{2+} ions that are able to form ionic crosslinks between the alginate chains. The beads can be recovered via centrifugation to separate the oil and water phases, with filtration and washing the final steps in bead recovery. This technique has the advantages of relative simplicity, rapidity (beads can be produced in around 20 minutes) and potential for scale up, with higher throughput than methods like extrusion.

Furthermore, our group has demonstrated the feasibility of water-in-oil emulsion for the production of microspheres using our thermosensitive chitosan hydrogel (Alinejad et al., 2020). This is an important development, as alginate microspheres have been developed with a view to block cells from interaction with the immune system, to prevent islet allograft rejection. For a scaffold for lymphocyte microencapsulation, the gel would need to be biocompatible with lymphocytes and allow cell escape. Chitosan microbeads are therefore an interesting potential development in hydrogel scaffolds for immune cell delivery.

Our group tested the developed thermosensitive porous chitosan bulk gel for T cell delivery, demonstrating significantly faster gelation at 37°C than the chitosan-PEG gel and human PBMC viability and growth over 2 weeks. Encapsulated PBMC and TIL were shown to cumulatively escape from the gel for over 3 weeks, with increasing numbers of TIL escaping the gel in the presence of corresponding tumour fragments in transwell assays. Further transwell assays demonstrated the ability of encapsulated antigen-specific T cells to migrate towards and destroy their corresponding cancer cells. Finally, a demonstration of the in vivo injection and recovery after 10 minutes of the gel was performed (Monette et al., 2016). This

study showed the promise of our gel for localised T cell delivery, and the clear next step was to validate its use in vivo.

CHAPTER 2

OBJECTIVES

As shown in the literature review, local immune cell delivery is a promising way to improve ACT safety and efficacy but no ideal T cell delivery scaffold exists. Despite the many challenges, the injectable chitosan scaffold developed by our group demonstrated many desirable qualities for use in this context, including injectability, compatibility with immune cells, and a simple formulation using sterilisable materials already approved for medical use in biomaterials.

The general objective of this Ph.D. is to demonstrate the safety and efficacy in vivo of this promising candidate for T cell delivery, in order to establish a proof-of-concept of its use as a localised form of ACT immunotherapy.

The general hypothesis is that the hydrogel will allow the delivery, escape and anti-cancer activity of delivered T cells, leading to reduced tumour growth at least similar to the systemic intravenous ACT treatment, despite using a lower cell number. This may in turn address current ACT limitations by increasing the number of T cells that can access the tumour while reducing the overall cell number that is administered. Furthermore, this could potentially increase treatment efficacy versus systemic ACT due to increased tumour access for the delivered T cells. A representative diagram of this hypothesis is shown in Figure 2-1.

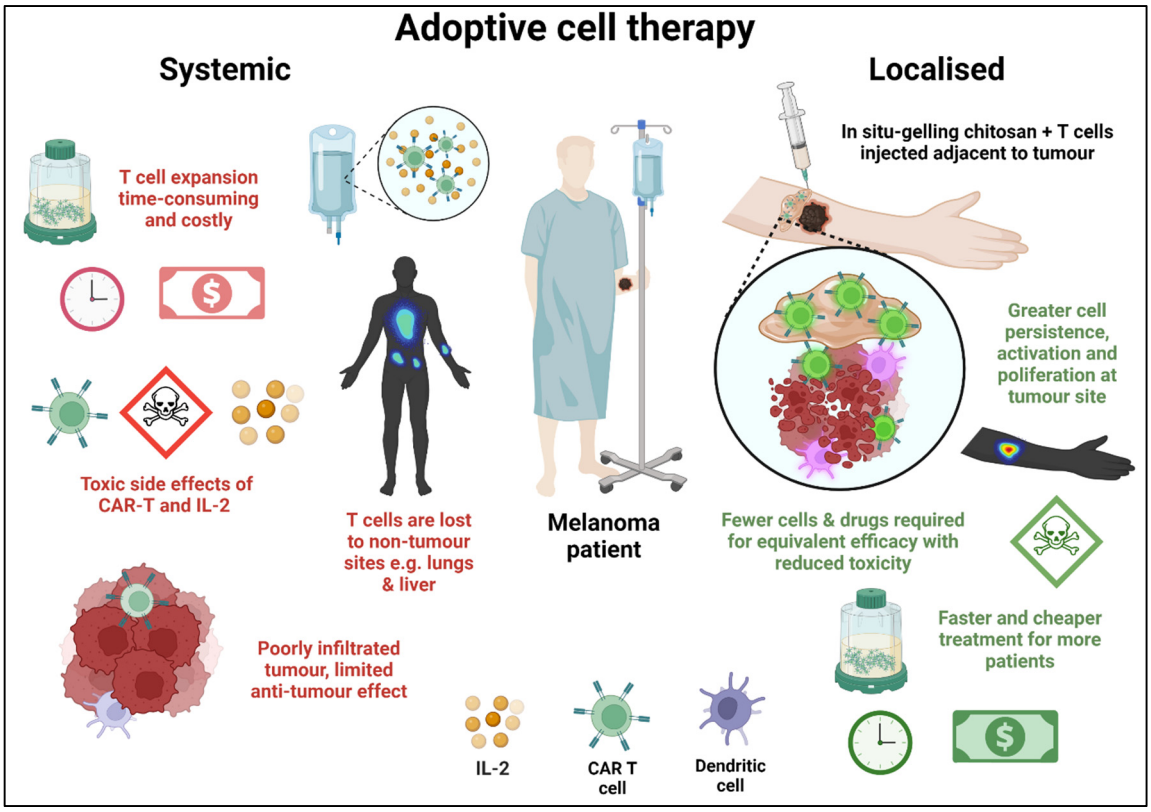

Figure 2-1 Explanatory diagram indicating the general hypothesis of this project, using a melanoma patient as an example

Objective 1: The first objective of this work is to confirm the feasibility of this chitosan hydrogel scaffold for use with in vivo tumour models. The hydrogel had never been implanted long-term in vivo, and so prior to use in these models the injectability, biodegradability and lack of toxicity of the gel must be demonstrated. Furthermore, the immune cells used for in vivo models must show survival in the gel after encapsulation, to supplement previous work showing human T cell survival and proliferation in the gel.

Here our hypothesis was that the gel would be biodegradable and non-toxic, as found in previous investigations of other chitosan biomaterials. Furthermore, we hypothesised that the immune cells appropriate for in vivo models would survive within the hydrogel, as with human T cells.

Objective 2: The second objective is to demonstrate the efficacy of the chitosan hydrogel as a T cell delivery system for localised immunotherapy in vivo. This will be achieved by localised injection of the chitosan hydrogel, in which T cells specifically targeted against the tumours induced in mice have been encapsulated. Tumour growth will be followed to measure the treatment effect as compared to either untreated or systemic ACT-treated controls. Our hypothesis is that localised delivery will reduce tumour growth compared to untreated mice, while using fewer cells than the systemic ACT for a similar effect. Localised treatment may potentially also show greater efficacy and greater persistence of the treatment effect.

One sub objective is to localise and track administered cells to observe and evaluate cell persistence and migration to the tumour, in order to study the mechanism and the limitations of the scaffolds. We hypothesise that localised delivery will result in greater persistence of administered T cells and infiltration of the tumour in greater numbers.

Objective 3: The third objective is to optimise the system, via modifications or additions to the hydrogel in order to maximise its anti-tumour effect. In particular, we hypothesize that scaffold in the form of microbeads can improve nutrient access, improve T cell survival and escape and hence treatment efficacy. Moreover, the addition of binding motifs for T cells, through the inclusion of bioactive materials (e.g. gelatin or collagen) could also improve cell survival and proliferation in the gel, as well as migration from the gel to the tumour. The effect of these changes on the gel efficacy in vitro and in vivo was assessed.

CHAPTER 3

MATERIALS AND METHODS

3.1 T cell loaded scaffold fabrication

Several chitosan-based hydrogels were prepared for this study. The principal gel is chitosan hydrogel, but chitosan gelatin, chitosan-collagen and alginate were also used as a comparison. Details of preparation and characterisation are explained below.

3.1.1 Hydrogel preparation

3.1.1.1 Chitosan hydrogel

Chitosan (CH) purchased from Primex (Iceland) was used, with two different batches used over the course of the project – a 2017 batch (P17) and a 2018 batch (P18). Due to the inherent variability of chitosan as a material, preliminary tests using NMR spectroscopy were performed to verify that the intrinsic material properties were close to that of the original chitosan (Table 3.1). Here multiple measures of degree of deacetylation (DDA) and Mw are presented that were obtained throughout the project as new chitosan sources became necessary. The variability between the batches according to our own measurements must be noted, as well as the discrepancy with the official supplier data.

Table 3.1 Summary of chitosan and suppliers
DDA calculated using NMR spectroscopy and Mw determined via gel permeation chromatography

Supplier	Product name	Common name	Supplier DDA (%)	Supplier Mw (kDa)	Meas. DDA (%)	Meas. Mw (Da)
Marinard Biotech	Kitomer chitosan	Kitomer	94	N/A	90%	290,833±1,716
Primex	ChitoClear HQG 110 (43010) Batch TM4854	P17	95	150-250	89%	255,400±2,524
Primex	ChitoClear HQG 110 (43010) Batch TM4737	P18	95	150-250	74%	159,467±929

The cell-loaded hydrogels were formed by simple mixing of two solutions, namely an acidic solution of chitosan (a) and a gelling agent solution (b), followed by further mixing with the cell suspension.

Solution a : P17 chitosan solution was purified as previously described by filtration then heating to 96C and mixing precipitated chitosan with sodium dodecyl sulphate before multiple rinses and subsequent freeze drying (Assaad et al., 2015) then solubilised in HCl (0.09M) at 3.33% (w/v), sterilized by autoclaving (20 minutes, 121°C) and stored in closed vials at 4°C. P18 chitosan was used unpurified and solubilized with 0.1M HCl due to other work showing that the long and potentially variable purification step was not necessary for chitosan solubilisation, otherwise its processing was identical to P17 chitosan. The chitosan used is noted for each experiment in the results section in figure legends.

Solution b: Phosphate buffer at pH8 was prepared by mixing dibasic and monobasic sodium phosphate purchased from Sigma Aldrich (Canada) at a ratio of 0.06 w/w in milli-Q water. The gelling agent (GA) consisted of a solution containing phosphate buffer and SHC (MP

Biomedicals, USA) at concentrations of between 0 and 0.25M and 0.375M, respectively. When used in cell experiments the GA was sterilised using a 0.22um filter. The gel was prepared by mixing the CH acidic solution with the GA solution at a 3:1 volume ratio using syringes connected by female-to female luer-lock syringe connectors. The CH-GA mixture was then mixed with the content of a third syringe containing cell suspension in complete culture media for cell experiments, or media with varying foetal bovine serum (FBS) or bovine serum albumin (BSA) when performing microbead optimisation as described in the microbead results section. CH-GA was mixed with media or cell suspension at a 4:1 volume ratio, so that the final concentrations in the gel were 2% chitosan, 0 to 0.05M PB and 0.075M SHC.The gel mixing process is shown in Figure 3-1 below.

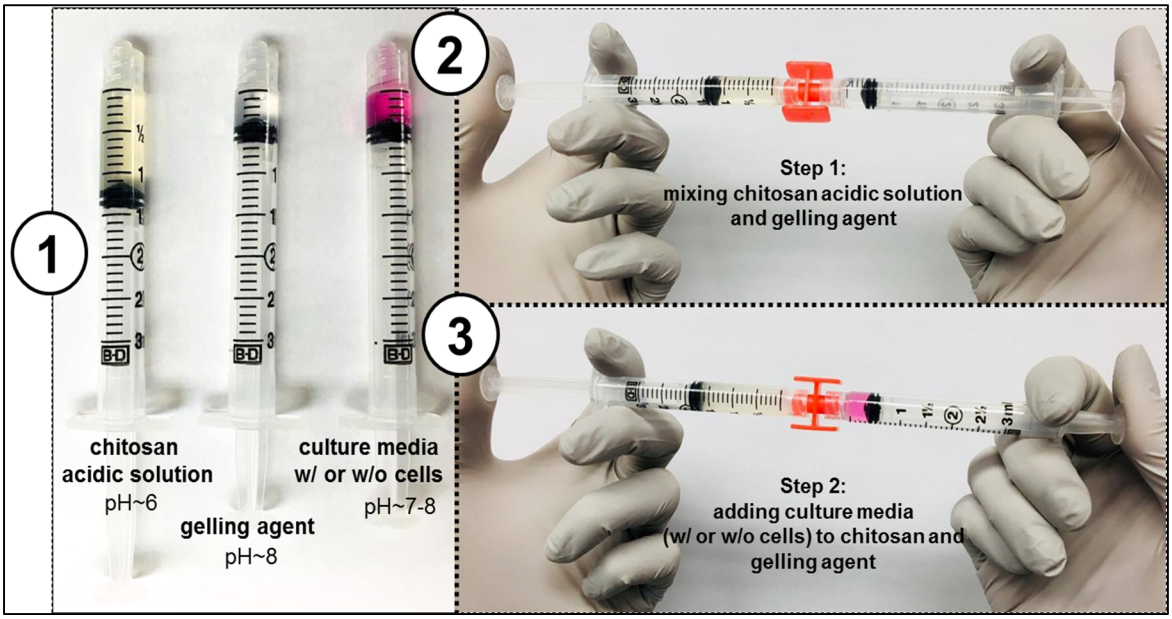

Figure 3-1 The gel mixing process
Taken from Monette et al. (2016)

The hydrogel was prepared in two different formats: a) macrogel, a bulk hydrogel with the entire gel solution forming a single continuous structure; b) microspheres, where the same gel formulation was produced in the form of small gel beads of several hundred microns in diameter.

For the volumic macrogel, the solution was mixed prior to use and deposited or injected as appropriate in each experiment. For in vitro studies, the macrogel was left to gel for at least 5 minutes at 37°C before adding any solution, unless otherwise stated.

3.1.1.2 Chitosan-gelatin hydrogel

The chitosan-gelatin hydrogel was prepared in the same way as the chitosan hydrogel, with only the addition of type A gelatin derived from porcine skin (Sigma-Aldrich, USA, G1890-110G) solubilised at 1% w/v in the chitosan solution at the same time as chitosan solubilisation.

3.1.1.3 Chitosan collagen hydrogel

Chitosan-collagen hydrogel consisted of a 75:25 ratio of 75% chitosan gel with 25% Collagen solution (PureCol EZ gel, solution 5mg/mL, Advanced BioMatrix). The final gel therefore contained 1.5% chitosan and 0.125% type I bovine collagen. The collagen solution replaced the cell culture media in the gel and hence cells were suspended in the PureCol before mixing with the CH-GA solution.

3.1.1.4 Alginate hydrogel

Alginate powder (W201502, Sigma Aldrich, Canada) was solubilized overnight in HEPES buffered saline solution (10 mM HEPES and 170mM NaCl (Sigma Aldrich, Canada), pH 7.4) 2.2% (w/v) and sterilized by autoclaving (20 min, 121 °C). To make the gel, 0.9 volume ratio of the alginate solution was added to 0.05 volume ratio of 0.5M calcium carbonate ($CaCO_3$) and 0.05 volume ratio of complete culture media or cell suspension for a 2% final alginate concentration (Alinejad et al., 2020). $CaCO_3$ solutions were also sterilized by autoclaving (20 min, 121 °C).

3.2 Scaffold characterisation

3.2.1 Rheology

Rheological studies were performed to ensure that the hydrogel is injectable and gel rapidly enough to avoid dispersion into the tissues at injection.

Basics of rheology

Rheology is the study of flow and deformation of materials under an applied stress, and is particularly relevant in the characterisation of viscoelastic materials – hydrogels for example. In a Hookean solid, material deformation is proportional to the applied stress and remains for the duration of the applied stress, defined as elasticity. Conversely, an ideal Newtonian liquid will persistently flow while stress is applied, with stress proportional to the flow rate – this can be referred to as the viscous response. In reality, many materials, especially hydrogels, are viscoelastic, i.e. their mechanical behaviour is a combination of both.

Small amplitude oscillatory shear rheology is the preferred technique for measuring the viscoelastic properties of biological materials and hydrogels, and can also be applied to the measurement of a hydrogel gelation kinetic such as our hydrogel's gelification at various temperatures and with varying gelling agents. In this kind of system, stress σ and strain ε are defined by the following equations:

$$\varepsilon(t) = \varepsilon_0 \, sin\, \omega t \tag{3.1}$$

$$\sigma(t) = \sigma_0 \sin\, (\omega t + \delta) \tag{3.2}$$

where ε_0 is the amplitude of deformation, ω is the applied angular frequency (2πν were ν is the frequency in Hz), σ_0 is the amplitude of the applied stress and δ is the phase shift of the stress with respect to the strain, between 0° and 90°. This phase shift relates to the elastic and viscous contributions to the overall stress-strain relationship (also considered as the solid and liquid contributions). For an ideal elastic solid, δ = 0° and for an ideal Newtonian liquid δ = 90°, and for a viscoelastic material δ is in between. The viscoelastic stress-strain relationship can be expressed as follows: $\sigma(t) = \varepsilon_0(G' \sin \omega t + G'' \cos \omega t)$

G’ is referred to as the elastic or storage modulus as it corresponds to the energy stored in the material under elastic deformation, whereas G’’ is referred to as the loss modulus as it corresponds to the energy loss due to the viscous response to deformation. As with the phase shift, these values correspond to the solid/liquid behaviour of the material, where in an ideal elastic solid, G’ = G (the elastic shear modulus) and G’’ = 0, and for an ideal Newtonian liquid G’’ = ωη, where η is the viscosity, and G’ = 0.

The storage modulus G’, representing the elastic behaviour in the complex modulus and the loss modulus G’’, representing the viscous behaviour in the complex modulus can be calculated using this raw data as follows:

$$G'' = G^* \sin\delta \tag{3.3}$$

$$G'' = G^* \cos\delta \tag{3.4}$$

$$\frac{G''}{G'} = \tan\delta \tag{3.5}$$

This data must be collected in the linear viscoelastic region: the range of frequency and strain where the equilibrium modulus is within 10% of its starting value. Strain and frequency sweeps were used to find these ranges, after which a time sweep can be performed where the evolution of G’ and G’’ at a set temperature is observed over time to measure gel’s gelation kinetic.
These two moduli contribute to the complex modulus G*, a complex number defined below and demonstrated in Figure 3-2.

$$G^* = G' + iG'' \tag{3.6}$$

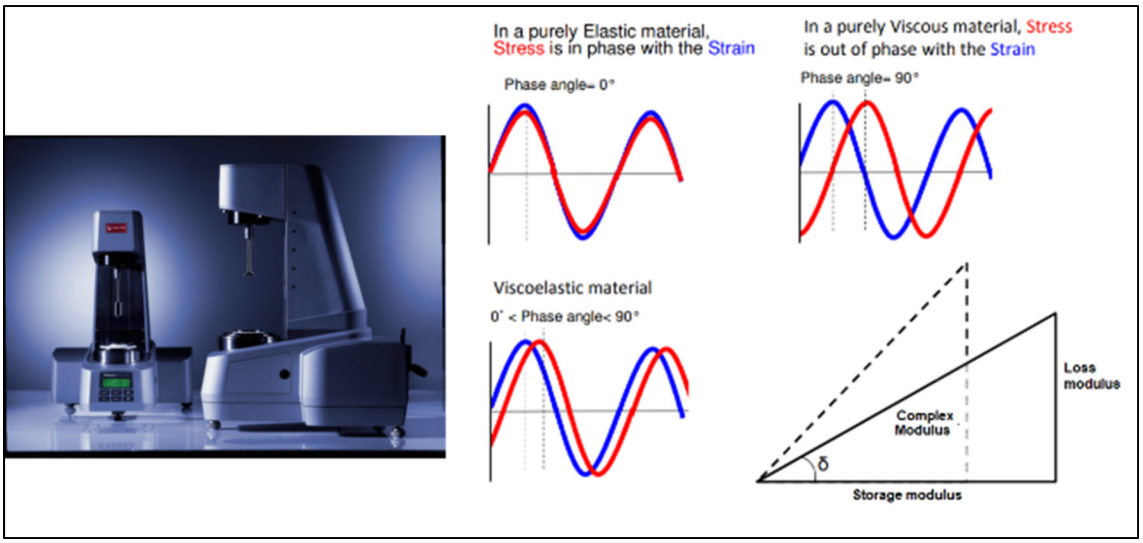

Figure 3-2 Anton Paar system and typical data
(Left) A Physica MCR 301 Anton Paar rheometer and (Right) a representation of the Storage and Loss moduli as components of the Complex modulus
Taken from Anton Paar (2021) and TA Instruments (2016)

Rheology is often used to follow sol-gel transition such as our hydrogel's gelification at various temperatures and with varying gelling agents. The technique dates from original experiments by (Winter, 1986) where the gelation point of PDMS (and subsequently the sol-to-gel transition for hydrogels in general) was demonstrated to occur when G' = G''. A material is considered to have principally elastic and hence solid behaviour when G' > G''.

Methodology

Rheological tests were performed using an Anton Paar rheometer (Physica MCR 301, Germany) using the coaxial cylinder geometry (CC10/T200). In this technique, a small sample is placed in a coaxial cylinder geometry, with a small-amplitude torsional oscillation causing a shear stress in the sample. The raw data collected by the rheometer with this technique consists of the torque – from which the complex modulus G* can be calculated – and the angle δ, corresponding to the phase difference between the oscillating stress and strain waves. Time sweeps were performed at 5% strain (later 1% after later LVE strain and frequency sweeps advised us to reduce this value) and 1Hz. The evolution of the storage and loss moduli (G' & G'') were measured for 30 minutes at 37°C immediately after mixing at room temperature. Gelation time was defined as the point where G' = G'' and therefore $\tan\delta = 1$ so this

technique can measure the speed of gelation (Zuidema, Rivet, Gilbert, & Morrison, 2014). For rheological study, the hydrogel was prepared using a two-syringe method with gelling agents at half the concentration and double the volume compared to those used in cell encapsulation.

3.2.2 Compression

As a complementary method to rheological testing, the gels were also characterised under unconfined compression, as this allowed us to compare final material rigidity after gelation and hence its ability to withstand mechanical forces during its utilisation in vivo. Unconfined compression was performed using the MACH-1 apparatus (Figure 3.3a) (Biomomentum, Canada) on cylindrical hydrogel samples (14mm diameter, 20mm height) incubated at 37°C for 24h. A strain rate of 100% min^{-1} was applied. Since the stress-strain curve is non-linear, the rigidity was defined as the secant modulus E at a certain percentage of deformation and was calculated as the slope of the straight line between the origin and the stress at a given strain as shown in Figure 3.3b.

$$E = \frac{\sigma}{\varepsilon} \tag{3.7}$$

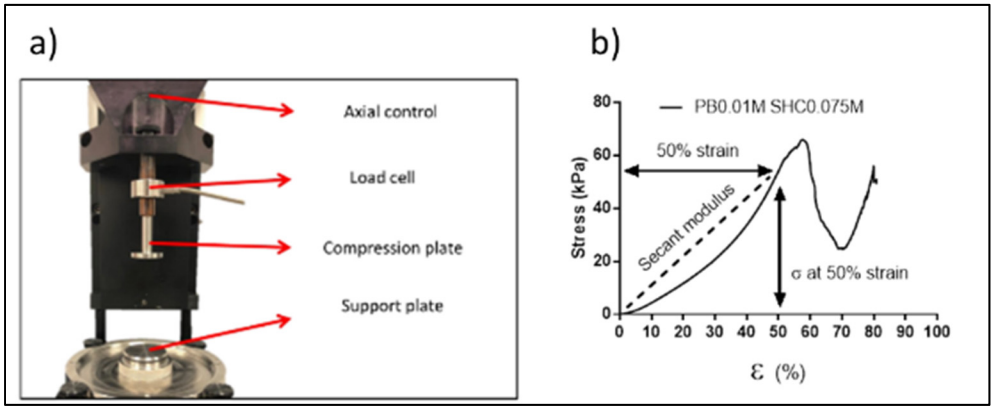

Figure 3-3 MACH-1 system and typical data
a) The MACH-1 system from Biomomentum and b) an example stress-strain curve showing the calculation of the Secant modulus

3.3 Microbead fabrication

Chitosan microbeads were investigated as an alternative gel format to improve cell viability and migration through greater nutrient access and encapsulation closer to the gel surface. Stirred emulsification was used to fabricate chitosan microbeads, according to the method developed by Hoesli et al. (Alinejad et al., 2020). The method is described in greater detail in the literature review section, but in brief it consists of a water-in-oil emulsion, where the hydrogel acts as the water phase in a mineral oil. The gel can be prepared as with the macrogel, with the pre-gel solution then introduced into the agitated oil, before gelation via a method appropriate to the material (e.g., pH dependent ionic crosslinking for alginate gels or temperature increase for chitosan hydrogels).

3.3.1 Alginate microbeads

To prepare alginate microbeads, first 20 mL light mineral oil at room temperature was introduced into a spinner flask. The stirring speed was set to 300 rpm, then a volume of alginate pre-hydrogel solution, prepared as previously described, was added dropwise using a 23G needle. After 1-minute, acidified oil consisting of 45µl of 1N acetic acid in 11ml of mineral oil was added to the flask. This lowers the pH below the pKa of $CaCO_3$ (9.0), so that Ca^{2+} ions are released which in turn crosslink the alginate beads. In the presence of water the acetic acid dissociates, with the released H^+ ions exchanging with the Ca^{2+} ions of the $CaCO_3$. The Ca^{2+} ions then ionically crosslink the alginate beads.

$$\begin{gathered} \mathrm{C}H_3\mathrm{COOH} \rightarrow \mathrm{C}H_3COO^- + H^+ \\ 2H^+ + CaCO_3 + 2\,alginate - COO^- \leftrightarrow H_2CO_3 + Ca\text{-}alginate \end{gathered} \tag{3.8}$$

At 9 min, 37 °C-warm HEPES-buffered saline solution was added to the flask. Spinning was stopped at 10 min and the emulsion was centrifuged (1500 rpm, 1 min, RT) followed by oil-layer removal by suction and filtration using a 100µm nylon cell strainer (BD Biosciences, USA). The microbeads were washed with HEPES-buffered saline solution to remove oil and transferred with a spatula to the desired suspension solution.

3.3.2 Chitosan microbeads

To prepare chitosan microbeads, the method is similar with some small changes. The 20 mL light mineral oil was pre-warmed to 37°C and placed in a water bath at 37°C as the chitosan hydrogel gelation is temperature-dependent. The stirring speed was set to 1100 rpm, then a volume of chitosan pre-hydrogel solution, prepared as previously described, was added dropwise using a 23G needle into 20ml of mineral oil (Figure 3-4). Stirring speed was reduced to 200rpm after 1 minute and beads were left to gel for a further 7 minutes, followed by one minute after 30ml of HEPES buffer was added.

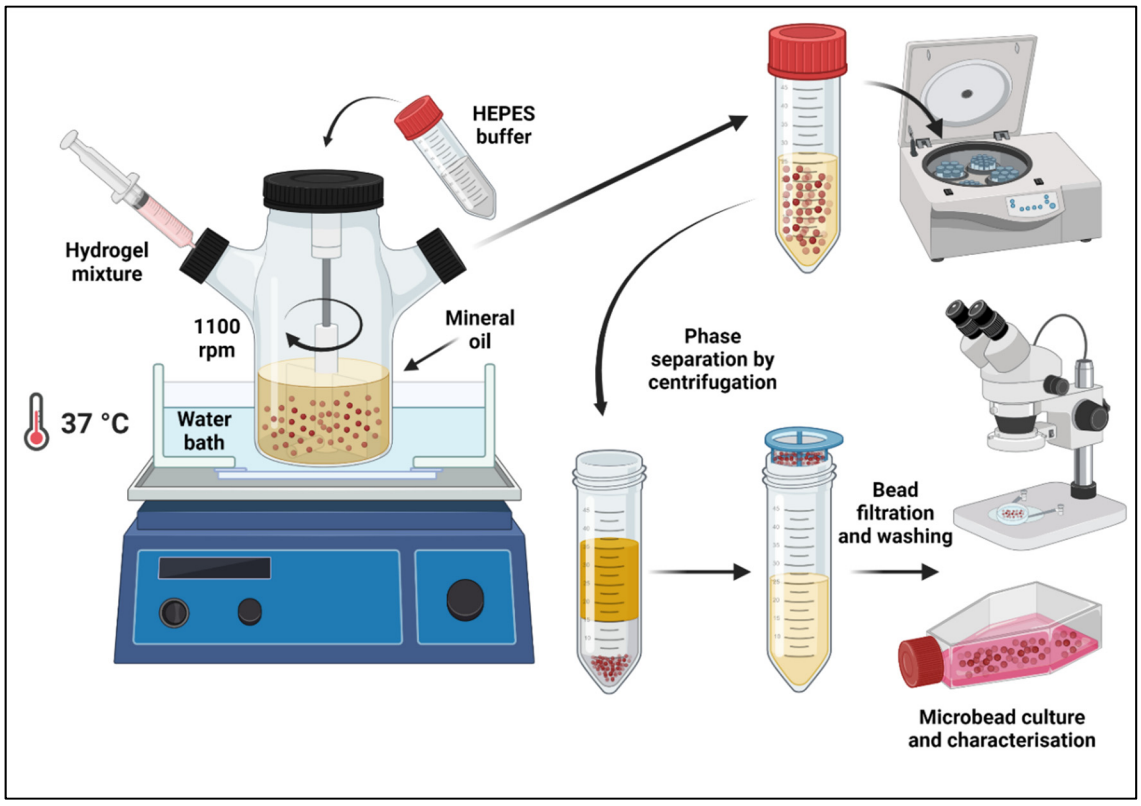

Figure 3-4 Schema of microbead production
Inspired by Alinejad et al. (2020) and Hoesli et al. (2011)

In later experiments, beads were produced with lower concentrations of FBS, as well as with BSA as a replacement for FBS, as the use of animal serum such as FBS is undesirable in vivo and in future clinical applications due to its immunogenicity and potential for pathogen

transfer. The effect of this change on bead size while keeping stirring speed and duration constant was studied.

3.4 Microbead characterisation

It is important to characterise the produced microbeads, to verify the repeatability of this process, as well as the size distribution of microbeads.

To characterise the diameter distribution of the beads, they were stained in eosine solution at room temperature overnight, placed on a gentle mechanical shaker to homogenise the staining solution. Beads were then imaged using a 12 MP camera connected to an OLYMPUS SZX10 stereomicroscope (OLYMPUS, Canada). These images were analysed using the Cell Profiler software (cellprofiler.org).

Cell Profiler allows the determination of each microbead's diameter, through the calculation of its area assuming its form to be spherical. In addition to the mean + SD, the diameter distribution can be plotted as the frequency of microbeads occurring within a given diameter range, allowing an assessment of bead size and variability. Similarly, a volume distribution can be visualised using the same data, to account for the fact that larger beads will form a significantly larger proportion of the total volume (and therefore contain more cells) relative to their proportion in the diameter distribution. This verifies their potential for use in certain applications – for example what proportion of beads (and indeed what proportion of bead volume) will be injectable though a 21G needle (514µm inner diameter). The volumetric median diameter is a measure of this property, calculated as $\frac{\sum D^4}{\sum D^3}$ where D is the bead diameters in a sample, corresponding to the diameter of which half of a total droplet volume in a volume mix is bigger or smaller than the given diameter. Furthermore, bead diameter must also correspond to optimal O_2 and nutrient diffusion.

The circularity was also calculated using the equation 4π x diameter/perimeter^2.

The precision of the data is of course related to the image resolution and the precision with which the microbead area is well delimited. In the present work, the resolution was of 68.5 pixels/mm with the OLYMPUS microscope used at 0.63X magnification.

3.5 Gel in vivo degradation response

Rationale: Another important step for a possible clinical translation of such a T cell delivery scaffold is to establish the biocompatibility and degradability of the scaffold. Biodegradation assays were therefore performed on the scaffold **without** cells, to investigate the acute and chronic in vivo response to the gel, to establish a lack of toxicity or unknown side effects, as well as assess the inflammatory response to gel implantation and its progressive degradation. This is a precursor to eventually using gels with encapsulated immune cells for in vivo tumour models.

Method: 200 µl gel was subcutaneously injected through a 23G needle in both the left and right flanks of 6–8-week-old C57/Bl6 mice, which were followed up over an 8-week period before sacrifice (Figure 3-5). Mice were followed up over an 8-week period before sacrifice (Figure 3-5). Mice activity and condition e.g., weight/hair loss was observed to ensure no adverse effect of the gel. Degradation of the gels was estimated by recording the gel area (calculated as an ellipse using two perpendicular measures) and weight of the gels at sacrifice at predetermined time points: 1, 7, 14, 28 and 56 days, with 3 mice per timepoint and 3 untreated mice as a control. In addition, gel and surrounding tissues were analyzed after measurement and weighing via hematoxylin phloxine saffron (HPS) histology staining after fixation in 10% formalin.

HPS is a variant of the more commonly used hematoxylin and eosin (H&E) staining, where hematoxylin will stain cell nuclei a blue/purple colour, whereas eosin will stain cell cytoplasm and extracellular matrix a pink colour. HPS is similar in using hematoxylin and eosin but substitutes one eosin component for saffron, which will stain collagen yellow. This can be beneficial in more precisely marking collagenous tissue, for example the fibrous layer that may form around the gel due to fibrous encapsulation.

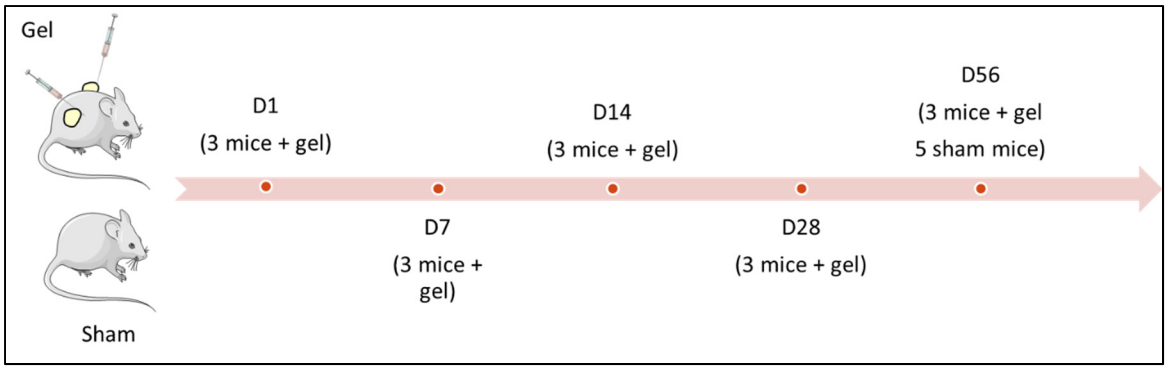

Figure 3-5 Schema of mice treatment in gel degradation experiment

3.6 In vitro efficacy evaluation

Due to the change in chitosan source and slight changes in gel formulation in this project, gels were re-tested for their biocompatibility and ability to support immune cell survival and growth as in previous work by our group (Monette et al., 2016). Furthermore, to study the behaviour of encapsulated T cells and their potential escape from the scaffold (and hence indirectly their anti-tumour killing potential), two in vitro assays – transwell assays and a 3D tumour model, described below – were designed to evaluate and compare the scaffolds for their ability of encapsulated OT-I to migrate towards and kill cancer cells.

3.6.1 Cell sources and culture

Both human immune and mice cell types were used during this thesis to study the scaffold compatibility with encapsulated T cells

1) Human T lymphocytes (Jurkat cell lines and peripheral blood mononuclear cells from human donors (PBMC)) were used to test in vitro gel biocompatibility with these model human cells

2) CD8+ Mouse T lymphocytes called OT-I that specifically recognize and attack the OVA protein were also used in vitro and later in animal models with OVA-expressing tumour cell lines.

The following lines indicate how the cells were harvested and cultured to get active CD8+ T cells in sufficient numbers for the assays.

3.6.1.1 JURKAT cells and Human PBMC

JURKAT cells are an immortalised human CD4+ T lymphocyte cell line, used as a basic proof-of-concept for lymphocyte culture in biomaterials, as they are resilient and easy to culture. JURKAT cells were cultivated in in complete RPMI 1640 medium containing 10% foetal bovine serum (FBS) and 1% penicillin/streptomycin (P/S) (Gibco, USA) in T75 flasks at 500K-1M cells/ml until use in experiments. The JURKAT cell line was kindly provided by the lab of Prof. Réjean Lapointe (CRCHUM).

Peripheral blood mononuclear cells (PBMC) were obtained from healthy donors and expanded for three days in complete medium (IMDM supplemented with 7.5% human AB serum (Sigma Aldrich, Canada), 2mM L-glutamine (Gibco, USA) and 1% penicillin/streptomycin), supplemented with human anti-CD3 human anti-CD3 (0.5mg/ml, OKT3, eBioscience) and human IL-2 (300U/ml, Proleukin). This expansion medium encourages the growth of T lymphocytes, favouring CD8+ cytotoxic T lymphocytes over CD4+ T helper cells– the relevant cytotoxic T lymphocytes for ACT. After expansion, cells were recovered and resuspended in complete medium supplemented with human IL-2 only. PBMC were kindly provided by the lab of Prof. Réjean Lapointe (CRCHUM).

3.6.1.2 Mouse OT-I

OT-I cells were recovered from the spleens of OT-I mice (C57BL/6-Tg(TcraTcrb)1100Mjb/Crl) whose CD8+ T cells (OT-I) express a transgenic, MHC class I-restricted T cell receptor specific for ovalbumin peptide ($OVA_{257-264}$), were bred in the CRCHUM animal facility, and isolated using CD8+ T cell magnetic isolation beads (Miltenyi Biotec). For cell stimulation, 6-well plates were coated with PBS with 0.5µg/ml mouse anti-CD3 (Bioxcell) and 5µg/ml mouse anti-CD28 (Bioxcell) and washed twice with PBS before

seeding. Cells were seeded at 1M cells/ml in complete RPMI 1640 medium containing 10% FBS, l-glutamine (2 mM), 1% penicillin/streptomycin (P/S) , 2-mercaptoethanol (50 µM), 0.1 mM non-essential amino acids (Gibco, USA), 1 mM sodium pyruvate (Sigma Aldrich, Canada) and 1% insulin-transferrin-selenium (ITS) (Gibco, USA). Cells were cultured for 4 days (37°C & 5% CO2), with cells counted and resuspended at 2 and 3 days at 1M cells/ml in fresh medium. In later experiments this was shortened to 3 days (Figure 3-6). Mouse IL-7 and IL-2 added at final concentrations of 0.5 ng/ml and 30 U/ml respectively from 24h culture onwards. OT-I stimulation times are noted in figure captions.

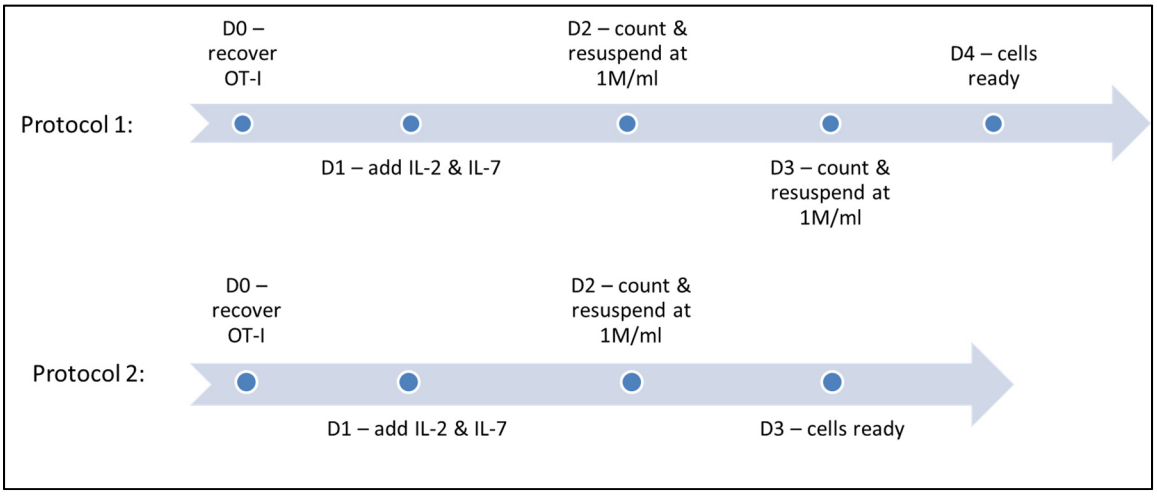

Figure 3-6 Schema of OT-I culture protocols used

3.6.2 Cell viability in vitro

Alamar Blue assays : metabolic activity was measured using the Alamar blue assay at 1, 7 and 14 days (for PBMC only) after encapsulation. Cell culture medium was removed and replaced with medium containing Alamar blue solution (10% v/v, Resazurin Cell Viability Assay Kit, Biotium, USA) and incubated for three hours before measurement with a a microplate fluorescence reader (λex 560 nm, λem 590 nm, BioTek Instruments Inc., Synergy 4, USA). In this assay, resazurin (blue coloured) is converted to its reduced form resorufin (bright pink coloured) by viable cells and hence can give an indication of cell metabolic activity.

LIVE/DEAD assay : two fluorescent dyes – calcein AM and ethidium homodimer (EthD-1) are used simultaneously to stain live and dead cells respectively. Calcein-AM is an esterase substrate that can enter live cells and become enzymatically cleaved, leaving the free calcein fluorophore retained in live cells. This dye emits strong green fluorescence peaking at roughly 525nm when excited at 485nm. EthD-1 is a polar nucleic acid stain that can penetrate dead but not live cell membranes, which on contact with nucleic acids exhibits strong red fluorescence at around 625nm when excited at around 525nm. Cells can then be imaged using fluorescence microscopy to see the ratio between live and dead cells as a measure of the toxicity or support for proliferation of the hydrogel.

For the LIVE/DEAD assay, hydrogels were incubated with calcein-AM and ethidium homodimer-1 (Life technologies, USA) for 45 minutes, then observed using fluorescence microscopy (Leica DM IRB).

3.7 T cell function and migration outside the scaffold

3.7.1 Transwell model

In our transwell model (Figure 3-7), 500K MC38 or MC38-OVA were seeded in 24-well plates, before the addition of 100 µL of gel or microbeads with 8M/ml OT-I deposited onto transwell inserts with an 8µm porous membrane. A further condition without cancerous cells to observe passive cell escape was also included. Cells were cultured for 3 days in complete RPMI with IL-2 and IL-7, before the lower portion of the transwell was analysed via flow cytometry (explained below) to identify OT-I that migrated out of the gel towards the MC38, quantifying their proportion compared to MC38 and their activation via CD25 expression.

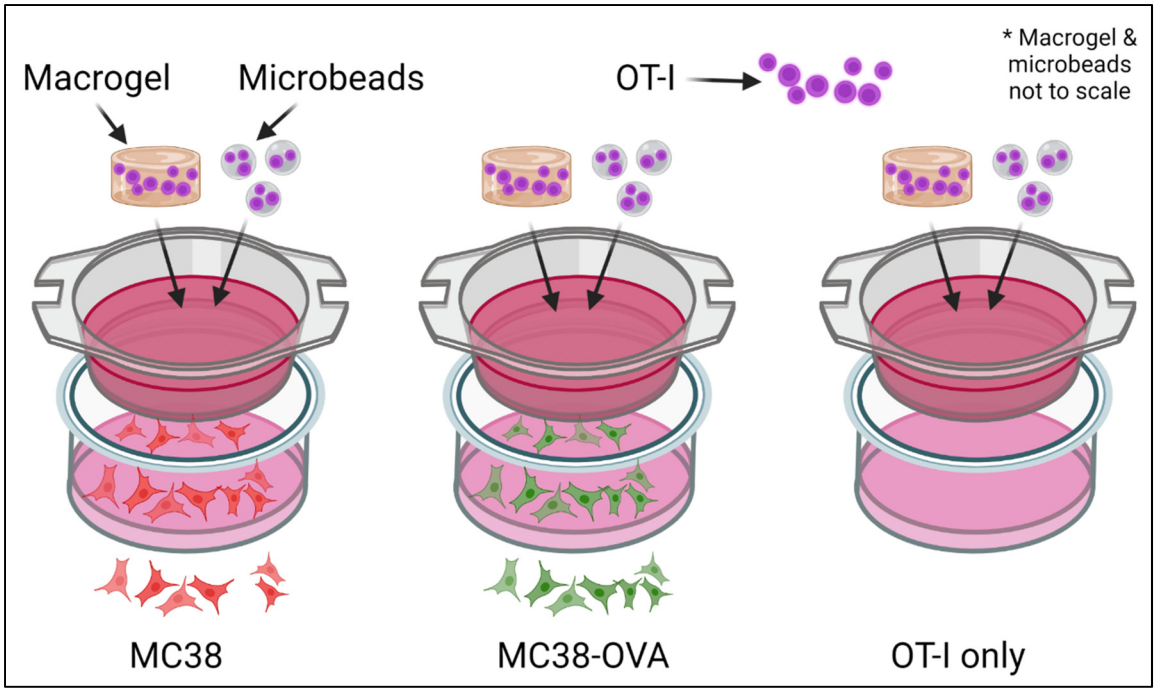

Figure 3-7 Schema of transwell model
MC38 cells will not be targeted by OT-I; MC38-OVA (MC38 linked to the OVA peptide) will interact with migrating OT-I; the OT-I only condition will observe passive OT-I escape where OT-I will be identified via FACS analysis of the lower transwell

Flow cytometry principles

Flow cytometry is a technique that allows high-throughput testing of suspended cells based on morphological differences, as well as fluorescent markers and compounds that can be linked to biological components. A focalised light source in conjunction with detectors will analyse cell compositions, allowing the characterisation of a cell population. Light dispersion by the cells is what differentiates cells morphologically (Figure 3.8).

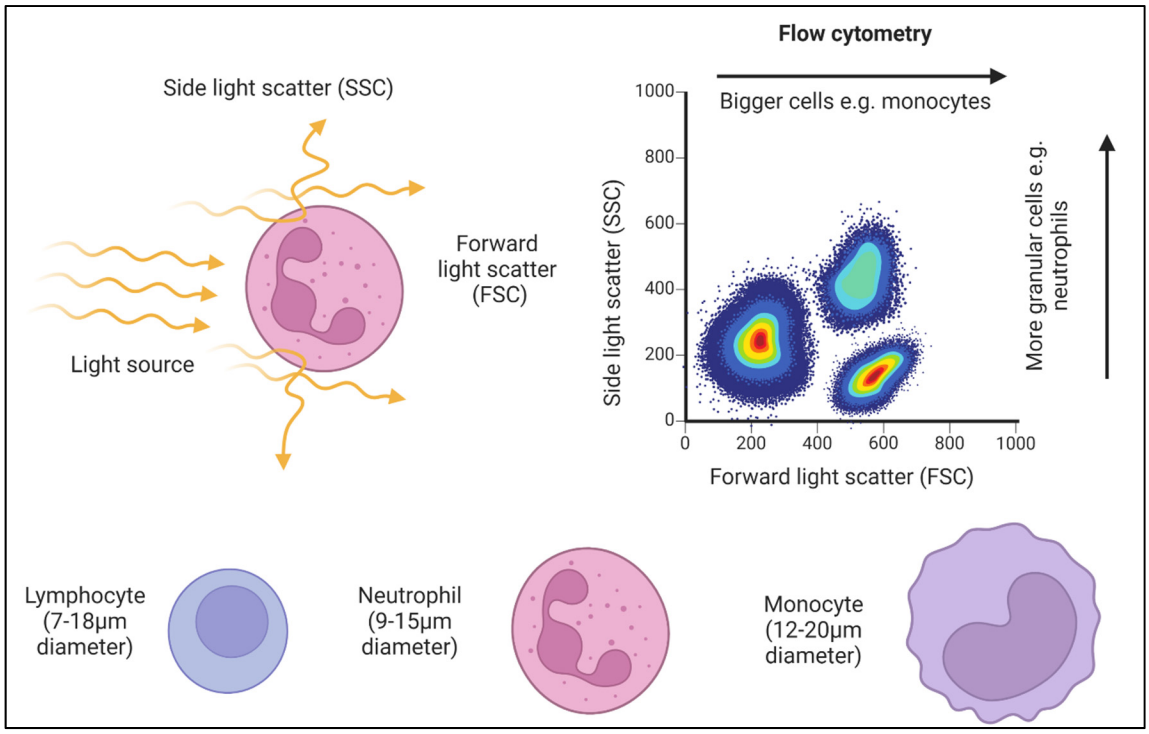

Figure 3-8 Principles of FACS
Diagram of the relationship between light scattering and cell morphology in flow cytometry analysis

Flow cytometry data is presented in scatter plots where cells appear on a grid based on these parameters, as in Figure 3.8. In this way, cells of interest can be identified, as for example CD8 as a marker to identify OT-I in our application. In the transwell model, cell morphology based on lymphocyte SSC and FSC values, as well as Live/Dead Aqua (1:200) (kit LIVE / DEAD Viability / Cytotoxicity, Life Technologies, ON,CA) which is only expressed in dead cells, was used to identify potential live lymphocytes in the lower transwells (selecting for lymphocyte morphology and negative Live/Dead aqua signal. The antibodies CD25 BV786 (1:100) and CD8 BV605 (1:100) (BD Biosciences) were used to identify and characterise the OT-I, where CD8 expression identified OT-I (already selected for CD8 during isolation and culture) and CD25 demonstrated OT-I activation, as it is a high-affinity IL-2 receptor. The proportion of $CD8^{+}CD25^{+}$ cells in this population (which could be contaminated with smaller MC38 or cell debris, hence not all cells were $CD8^{+}$) correlated with OT-I migration, where greater migration results in a greater proportion of OT-I in this sub-group. Data was collected

using the LSRFortessa flow cytometer with the FACSDiva software (BD Biosciences) and data was analysed using the FlowJo V10 software (TreeStar Inc).

3.7.2 3D model

To better mimic the in vivo tumour structure and microenvironment, a 3D model was developed in collaboration with a Masters student, Tommy Malaret. The methodology will be only briefly presented here since it is detailed in great detail in Malaret's masters report (Malaret, 2022). In brief, the developed 3D model has an inner gel containing cancerous cells (MC38 or MC38-OVA) supported on matrigel. Once the core is stable, an outer ring of OT-I-containing hydrogel is added, representing the localised treatment delivered in vivo.
The steps to prepare the model can be seen in Figure 3-9a, and a schema of the model in Figure 3-9b.

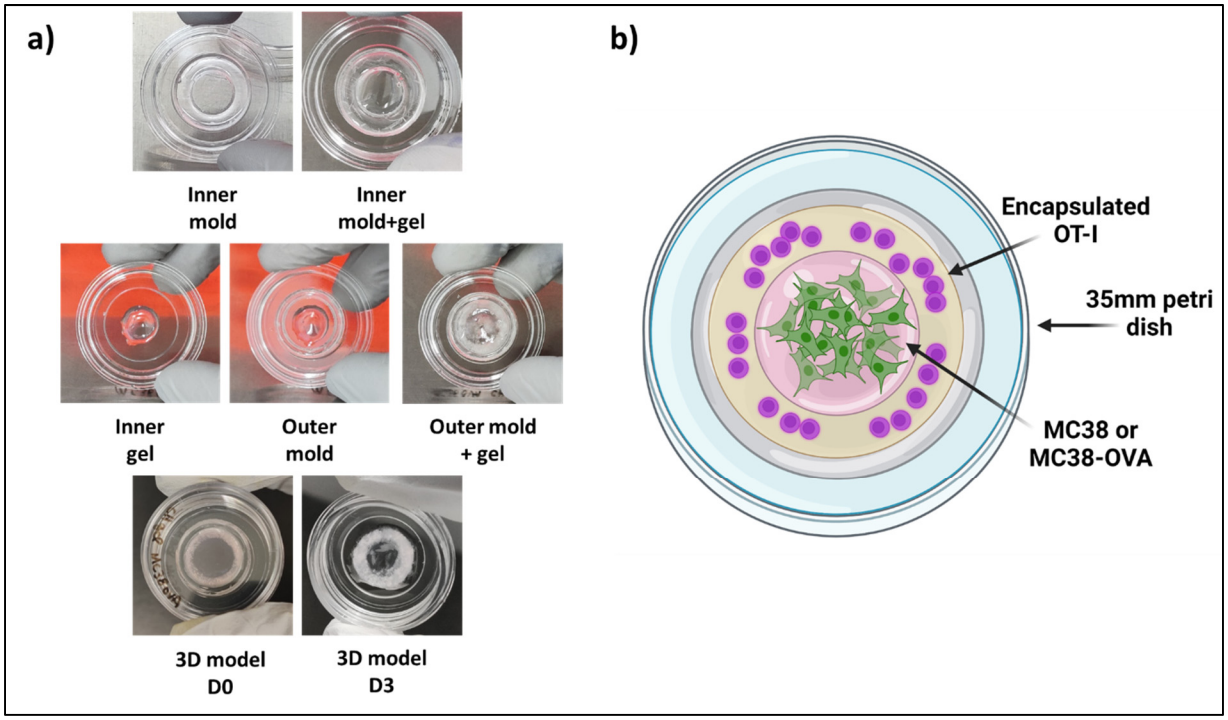

Figure 3-9 3D in vitro tumour model
a) Preparation of the 3D model, b) 3D model schema

Before encapsulation, OT-I were fluorescently labelled in violet with 5µM CellTracker™ Deep Red Dye (ThermoFisher Scientific Inc, MA, USA) for 45min at 37°C 5% CO_2 in the dark. Cancerous cells were stained in green with CFSE (10µM in PBS 1X) (ThermoFisher Scientific Inc, MA, USA) for 15min at 37°C 5% CO_2 in the dark.

The 3D model was imaged at 10X magnification using a spinning disk confocal microscope (Zeiss Axio Observer) with the Zen system software (Zeiss). The model was imaged at days 0, 1 and 3 to observe and count OT-I present in the outer gel, inner gel and gel interface. To track OT-I displacement, live-imaging was performed every 30 seconds over a 30-minute time period on day 1, with data analysed using the Imaris 9.8 software (Oxford Instruments). The primary data from this experiment was the number of OT-I observed in each defined gel section (hence quantifying OT-I migration to the tumour cells and estimating cell growth and survival in the scaffold over 3 days,), as well as a quantification of OT-I displacement speed in the various gel matrices. Flow cytometry was also performed on the digested inner and outer gels to measure OT-I migration and activation and MC38 apoptosis, though difficulties in sample preparation meant that these results were unconvincing and hence not included here.

3.8 Mouse ACT models

After testing in vitro gel biocompatibility and its degradation in vivo, and confirming cell survival in the gel, the gel could be tested against its objective – localised tumour treatment in vivo. Murine models are very commonly used in research due to their relative immunological similarity to the human immune system, as well as their well-established use and management in research settings. For an ACT model, a specificity for the desired antigen is needed between the lymphocytes given as treatment and the tumours treated in mice – hence our use of OT-I cells to recognise OVA-linked tumour cell lines.

The efficacy of the T cell-loaded gel in vivo was initially tested in an EG7-OVA mouse lymphoma model, where OVA expressing tumour cells are injected in mice to develop

tumours, which can be specifically recognized and killed by OT-I lymphocytes, administered intravenously or otherwise.

However, due to difficulties in the treatment and reliability of the EG7 model (see results section), an alternative cell line MC38, was used. MC38 is an adenocarcinoma cell line also commonly used in research, which can also be linked to OVA to create OT-I reactive MC38-OVA cells. This cell line is less immunogenic than EG7, and as such can create reliable tumour models with consistent growth that also react to treatment with OT-I. MC38 and MC38-OVA cells, kindly provided by the lab of Prof. John Stagg (CRCHUM, Canada) were expanded until use for experiments in complete DMEM supplemented with 10% FBS and 1% P/S.

Tumour induction: 6-8-week-old female C57/Bl6 mice were purchased from Charles River Laboratories and identified within their cages via ear punch. 1M MC38-OVA cells suspended in 100µl of PBS were injected in the left flank of the mice using a 1ml syringe with a 26G needle. The MC38-OVA cell suspension was kept in ice during cell injection. Around one week after MC38-OVA cell injection, once tumour diameter was between 4-6mm, mice were randomly allocated to their treatment groups based on the following principle: the average product of tumour diameters had to be statistically similar between groups within the experiment. Tumour growth was measured with callipers 3 times a week (product of the two largest perpendicular diameters measured with calipers, as used by other groups to allow comparison with their results, even if this does not represent true tumour area (Stagg et al., 2011; J. Zhou et al., 2018).

Mice follow-up : The primary endpoint of the study was the tumour growth with time as a function of the treatment group. For that purpose, tumour growth was measured until mice sacrifice 21 days after the treatment or when the average tumour diameter exceeded 15mm. Tumour measurements were performed blind where possible. A secondary endpoint was to qualitatively assess the T cell distribution in the mice after each treatment and quantify the number of T cell reaching the tumour as a function of time. Therefore, intravital microscopy (Optix MX2, see Optix methodology section) was performed to follow T cell distribution and

density in the tumour area at 24h and 7 days. In addition, at sacrifice, the tumours and gel were recovered and fixed in 10% formalin solution for at least 24h before histological and immunopathological analysis.

Experimental groups:

The experimental groups are summarised in Figure 3-10. In brief, the OT-I cell loaded gel was always compared to the negative and positive controls, namely untreated mice and mice treated with the conventional treatment (intravenous injection), respectively. After this first proof of concept, depending on the experiment, other controls were added, such as OT-I in saline, or the gel without cells, to better assess the benefit and role of the gel itself. Later, OT-I loaded microbeads were also studied. These groups are summarized below with methodological details. For technical reasons, it was not possible to test all groups in parallel in the same experiment.

- Untreated mice, with no treatment given
- IV-treated mice, with intravenous injection of 5M OT-1 suspended in 100µl of PBS and injected using a 1ml syringe with a 26G needle in the tail-vein
- Gel-treated mice, with 1.6M OT-I encapsulated in 200µl of gel immediately before injection, then injected adjacent to the tumour using a 1ml syringe with a 23G needle. OT-I in the gel were suspended in PBS.
- Gel only-treated mice, where 200µl of cell-free gel was injected adjacent to the tumour using a 1ml syringe with a 23G needle.
- Saline-treated mice, with 1.6M OT-I suspended in 100µl of PBS then injected adjacent to the tumour using a 1ml syringe with a 23G needle
- Microbead-treated mice, with 1.6M OT-I encapsulated in 200µl of microbeads immediately before injection and suspended in 200µl PBS to allow for microsphere loading in a syringe, with the full 400µl of beads and PBS injected using a 1ml syringe through a 21G needle adjacent to the tumour as with the macrogel. OT-I in the gel were suspended in RPMI with 2% FBS.

Prior to injection or encapsulation, OT-I were stimulated with CD3, CD28, IL-2 and IL-7 as presented earlier (first with the 4-day and then the 3-day stimulation protocol as detailed previously). In addition, OT-I were stained with 1mM Vybrant™ DiD dye (Thermofisher Scientific, Canada). To reduce cell mortality, OT-I cell suspensions were kept on ice until injection or encapsulation.

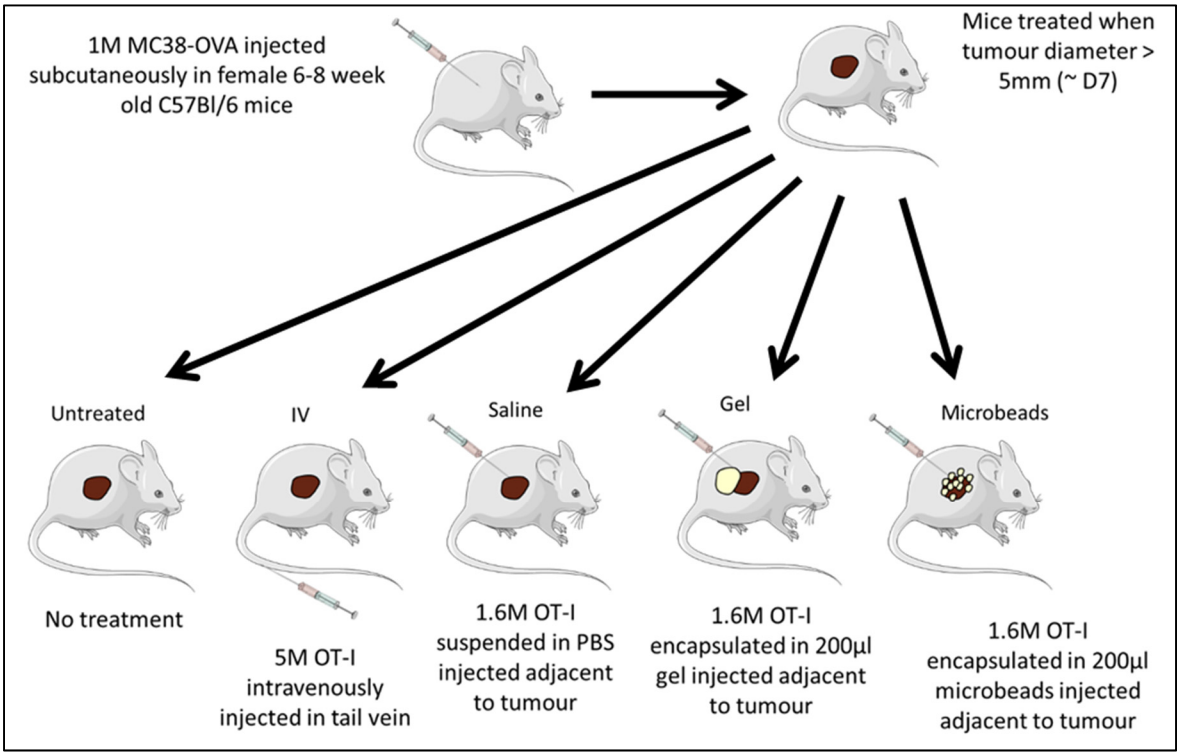

Figure 3-10 Schematic of mouse tumour model and treatment groups

3.9 Optix imaging

In the in vivo tumour models, we were interested in not only the response to treatment but also the migration and localisation of administered OT-I. This would involve tracking the cells to determine the fate of intravenously administered OT-I, the possible gel-escape of encapsulated OT-I and the potentially increased OT-I concentration at the tumour site. For this reason, in vivo fluorescence imaging was performed on the whole mouse, to track fluorescently labelled OT-I using the eXplore Optix MX2 system (ART, Canada).

Briefly, the system functions where a pulsed diode laser excites the sample, with a filter to select the excitation wavelength. Fluorescent light is then detected through an imaging relay, again with a corresponding filter to the excitation wavelength. A photomultiplier tube relays the detected signal to a photon counter, with the outputted Optix data corresponding to this raw photon count of the detected signal.

OT-I were stained with the cell membrane dye Vybrant™ DiD (ThermoFisher Scientific) prior to injection. During imaging, mouse fur around the imaging site was removed, and mice were kept anesthetised with 1-3% isofluorance while in the Optix system. The Cy5.5 laser was used for Vybrant™ DiD (λex 670 nm, λem 693 nm) and various regions of interest (ROI) could be measured within the scanned area (resolution: 1-1.5mm^2). Fluorescence intensity is measured in normalized counts (NC), the photon count per unit laser excitation exposure time, to allow comparison between samples. The method was used to measure average signal at the centre of the tumour (the average accounts for differences in tumour area). A standardised, circular 9mm^2 area created in the Optiview software (ART Inc., Canada) and replicated for each sample to ensure a consistent ROI was analysed for comparison between groups, where the average Optix signal in this area was compared (

Figure 3-11).

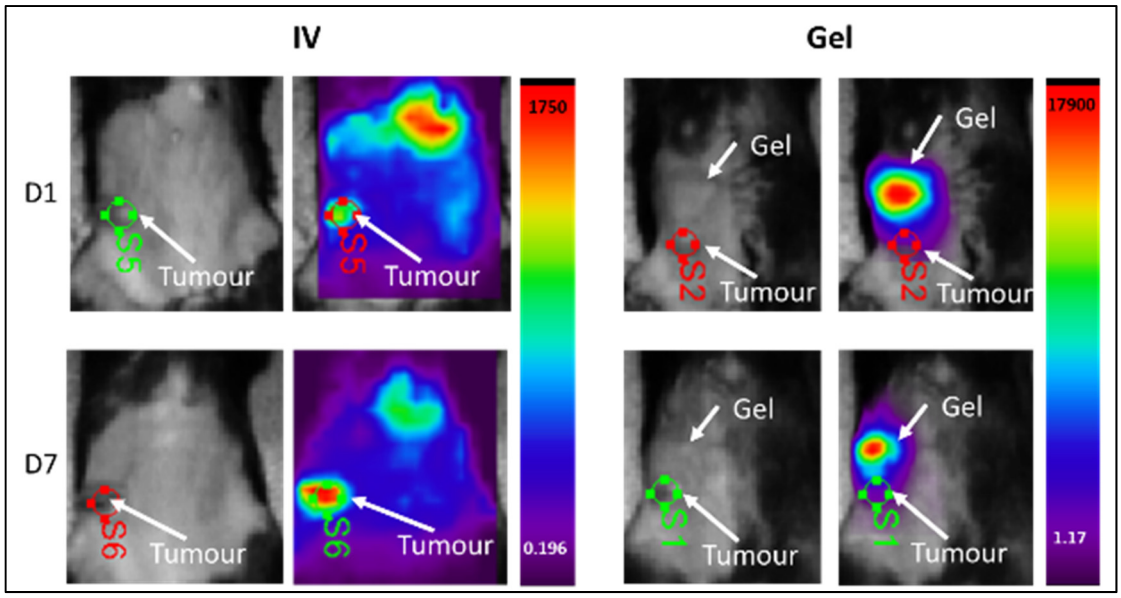

Figure 3-11 Typical Optix images and ROI
ROI selection of a standardised, circular, 9mm^2 area for comparison between groups, with tumours shown for both IV and gel-treated groups

3.10 Histology and Immunohistochemistry

Alongside the observed tumour growth and intravital imaging, histological analysis was performed to analyse the gel and tumour morphology, immune reaction, and more importantly the extent of T cell growth and survival in the gel and their migration towards the tumour as well as the cell types present, in much greater detail and at a much higher resolution than for example the Optix imaging. For this reason, sections of tumours and gels recovered at sacrifice were stained with H&E as well as antibodies to identify lymphocytes such as CD8.

Alcohol dehydration, xylene clearing, embedding in paraffin, microtome cutting and H&E staining were all performed by the CRCHUM molecular pathology platform.

3.10.1 Short term animal experiments

Due to the diminished anti-tumour response over time, we hypothesised that treatment effects occur early, and hence could be observed via histology in mice sacrificed at shorter timepoints.

In addition, it was important to be able to observe and quantify encapsulated cell behaviour in the gel at short term – i.e. do the OT-I survive, proliferate and migrate out of the gel?

Therefore additional animal experiments were performed, with the same groups as MC38-OVA in vivo experiments: untreated, IV, Gel, Saline and Beads. The only difference was in the timepoints where mice were sacrificed on days 1 and 7, and the number of mice, with 4 mice/ timepoint for IV and untreated mice, 6/timepoint for Gel and Saline-treated mice, and 3 mice/timepoint for Bead-treated mice (1 repetition only). Furthermore, C57BL/6-Ly5.1 (Jackson, USA) mice were used as recipient mice for treatment, as their CD8+ T lymphocytes ae of a different phenotype (CD45.1) to OT-I cells (CD45.2). Our hope was that exogenous OT-I could be identified using immunofluorescent histological staining. Unfortunately, despite our attempts in using C57BL/6-Ly5.1 mice to specifically identify OT-I with their CD45.2 phenotype against the CD45.1 phenotype of CD8 endogenous to these mice, successful staining was not achieved (see appendix) and so these samples were simply analysed based on H&E histology and CD8 staining.

3.11 Statistics

To ensure repeatability of obtained data, experiments were repeated 3 times, unless practical reasons prevented doing so (for example gel degradation in vivo). Regardless of the number of experiments, all experiments were performed with at least 3 samples (n = 3). Where appropriate, results are presented as means with standard deviation (SD) shown, with the exception of tumour growth curves where the standard error mean (SEM) is used instead of SD due to variability between animals and the large number of samples.

In experiments with more than two groups for comparison, One-way ANOVA with Tukey's multiple comparisons test was used to assess significant differences between three or more groups e.g. tumour growth in mice. For comparisons of two or more groups, a student's t-test with Welch's correction to account for different standard deviations between groups was used. All statistical analysis was performed using GraphPad Prism 6.0 (GraphPad Software, USA).

P-values lower than 0.05 were deemed significant and are indicated on graphs where appropriate. For graphs of correlation, an r^2 value of above 0.5 indicates that some correlation is present, as taken from (Yadav, 2018).

CHAPTER 4

RESULTS

4.1 Chitosan hydrogel preparation and in vitro characterization

The first step of this PhD was to design the thermosensitive hydrogel scaffold. Following the switch to another chitosan source, work was performed to readjust the HCl concentration and gelling agents, for complete chitosan dissolution and reproduction of the gelation kinetic and mechanical properties in compression observed with the previous chitosan source (Kitomer). This work was performed for the two batches of chitosan (P17 and P18) due to possible batch variability. For both batches, we were able to obtain full dissolution of the chitosan with HCl concentrations even lower than Kitomer chitosan, down to a limit of 0.09M, which with respective pH values of 6.17 (P17) and 6.16 (P18) was well within the acceptable pH range of 6.0-6.3. Rheological and compression test were then performed to find the formulation with the closest gelation kinetic and mechanical properties.

4.1.1 Rheology and compression tests – P17 chitosan

Figure 4-1a shows the evolution of the storage modulus G' over time at 37 °C for P17 gels with SHC 0.075 and increasing PB concentrations. As observed previously (Monette et al., 2016), the gelation kinetic increases with the PB concentration, The PB 0.1M formulation is closest to the Kitomer chitosan but some chitosan precipitation was noticed. PB0.05 shows slower but still acceptable gelation kinetic, with G' greater than G'' after <15s (see insert of Figure 4-1a), while PB0 was discarded due to very slow gelation.

Figure 4-1b shows the PB 0.05M gel has the most similar properties in unconfined compression to the Kitomer gel (secant modulus of 101 ± 8kPa and 100 ± 22 kPa respectively at 50% strain). Based on these results, PB 0.05M SHC 0.075M was chosen as the formulation to use for the P17 chitosan.

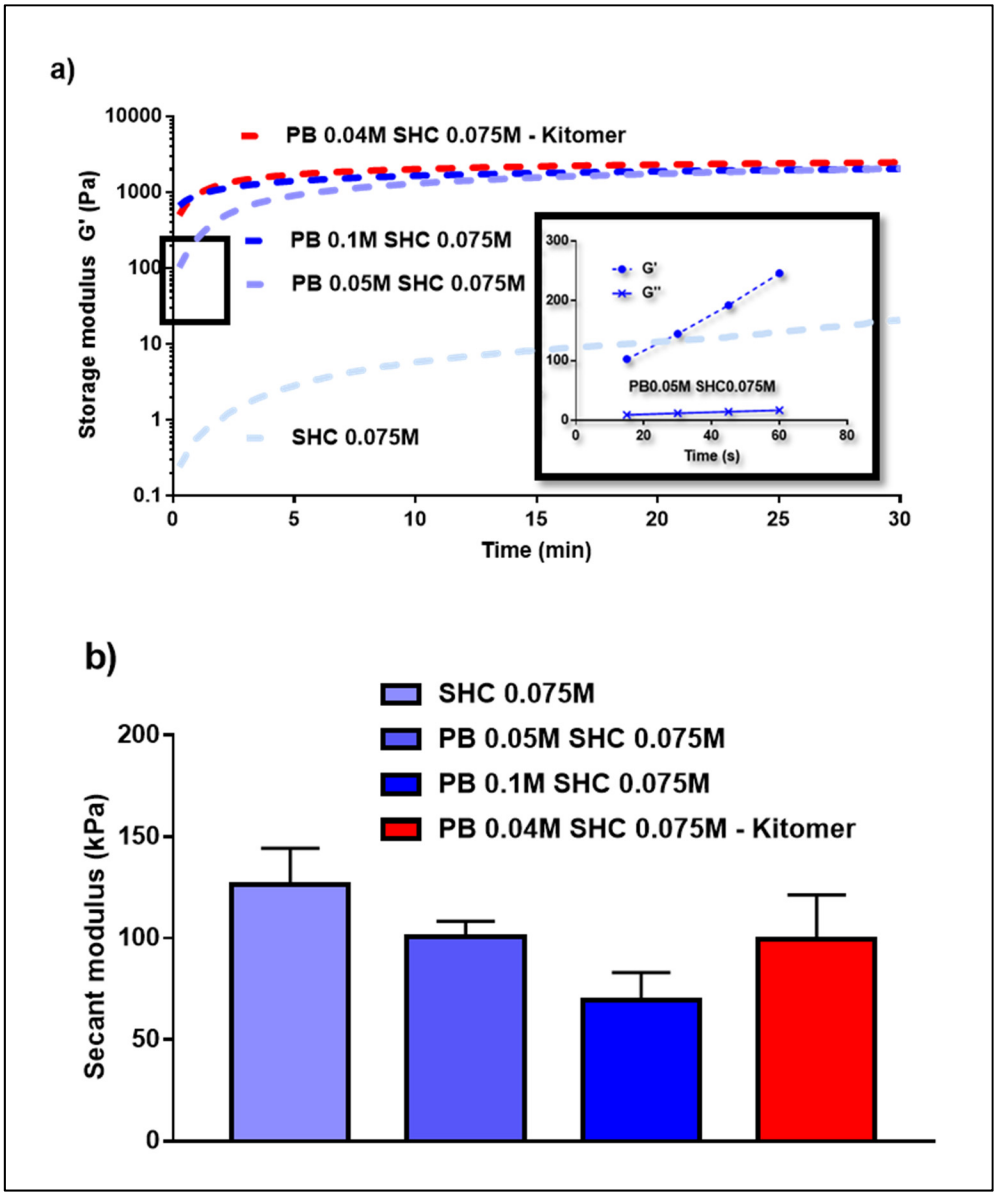

Figure 4-1 Rheology and compression data for P17 chitosan
a) Evolution of the storage modulus G' for P17 chitosan gels with varying PB concentrations, compared to Kitomer chitosan. Insert shows G' greater than G'' at all timepoints. Time sweep experiments were performed at 37°C, 5% strain, 1Hz, using the coaxial cylinder CC10/T200 geometry of a Physica MCR 301 Anton Paar rheometer. Data shown is the average of three independent experiments N = 3; n = 4-6. b) Secant moduli of P17 gels and Kitomer reference value as measured via unconfined compression at 50% strain using the Physica MCR 301 Anton Paar rheometer. Data is the mean ± SD of three independent experiments (N = 3, n = 9)

Similar tests were performed with the other chitosan batch (Figure A I-1 in APPENDIX I). PB0.01M SHC0.075M presented slower gelation compared to the P17 chitosan, but gelation was still considered rapid enough (G' greater than G'' after <15s) and its secant modulus was the closest to the Kitomer chitosan. PB0.01M was therefore chosen as a compromise for P18 chitosan.

4.1.2 In vitro cell experiments

4.1.2.1 JURKAT and PBMC cells

In vitro T cell survival and growth: Figure 4-2A shows good metabolic activity of encapsulated JURKAT cells at day 1 (fluorescence units) which significantly increased over 1 week of culture ($p<0.001$). These results were confirmed by Live Dead assays performed at days 1 and 7 (Figure 4-2B) which clearly show the increase in live cell number of JURKAT cells (in green) within the hydrogel over 1 week, and very limited cell death (in red). Similar results were obtained with the P18 chitosan hydrogel (Figure A I-2 in APPENDIX I).

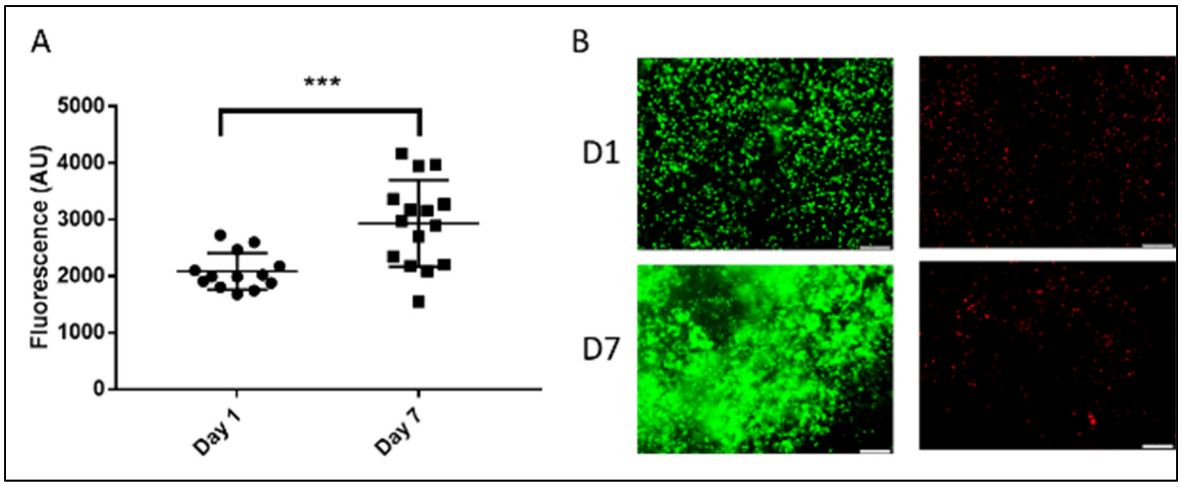

Figure 4-2 JURKAT cell viability
A) Metabolic activity measured via Alamar Blue assay after 1 and 7 days of JURKAT cells encapsulated at 8M cells/ml in P17 chitosan hydrogel. (***p<0,001 determined by t test with Welch's correction, N = 3 n ≥ 13) B) Representative Live Dead images of JURKAT cells (live cells in green, dead cells in red) at days 1 and 7 of culture in PB 0.05 SHC 0.075 P17 chitosan hydrogel (N = 2, n = 4) Scale bars = 200µm

Similar tests were then made with PBMC from human donors. These cells are more representative of the lymphocytes used in ACT than JURKAT (which are an immortalised cell line so do not exhibit the same growth profile and functions of true human immune cells as with PBMC). The metabolic activity of PBMC within the gel was assessed in the presence of two IL2 concentrations since this cytokine is well known to influence their proliferation and could lead to exhaustion. Figure 4-5 shows significantly increased metabolic activity of encapsulated cells at both 7 and 14 days of culture compared to 24 hours with 300U/ml IL-2 ($P > 0.0001$), though with no significant difference between 7 and 14 days. Conversely, metabolic activity decreased over 14 days of culture with 1800U/ml of IL-2, indicating that the high IL-2 concentration does indeed negatively impact the proliferation of PBMC in the gel.

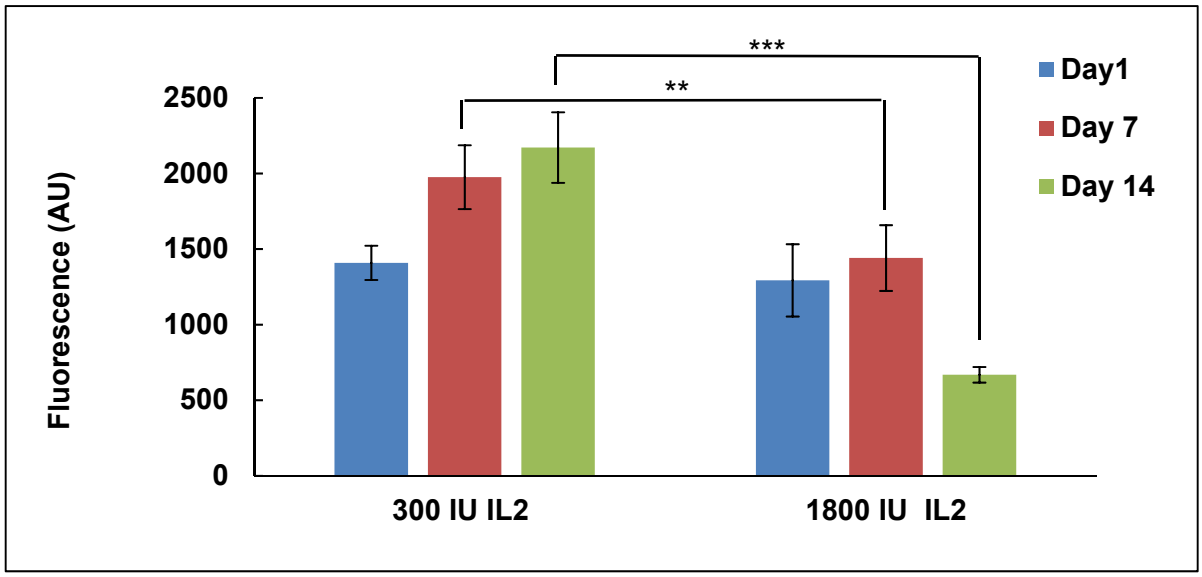

Figure 4-3 Metabolic activity of encapsulated PBMC
Metabolic activity via Alamar blue assay after 1, 7 and 14 days of human PBMC with 300 or 1800U/ml IL-2 in culture (mean ± SD ***p<0,005, **p<0,05, determined by t test with Welch's correction, N = 3 n = 9) in P17 hydrogel

LIVE/DEAD imaging at concurrent timepoints supports these results, where high cell viability, clustering, and proliferation can be observed for PBMC culture with 300U/ml IL-2 (Figure 4-4) in contrast to the higher number of live cells at 24h but progressive reduction in live cell number for PBMC cultured with 1800U/ml IL-2. A number of dead cells are visible at day 7, though at day 14 300U/ml IL-2 shows many more live than dead cells.

These results support the hypothesis that while a high IL-2 concentration can initially 'boost' T cell growth, this high IL-2 concentration is detrimental to T cell proliferation in the medium to long term. Therefore, a concentration of 300U/ml IL-2 was chosen for future experiments. Furthermore, **this demonstration of the compatibility of the new chitosan gel for T lymphocyte encapsulation allowed us to move forward with the project – the next step being validation of in vivo biodegradation and biocompatibility of the gel in mice.**

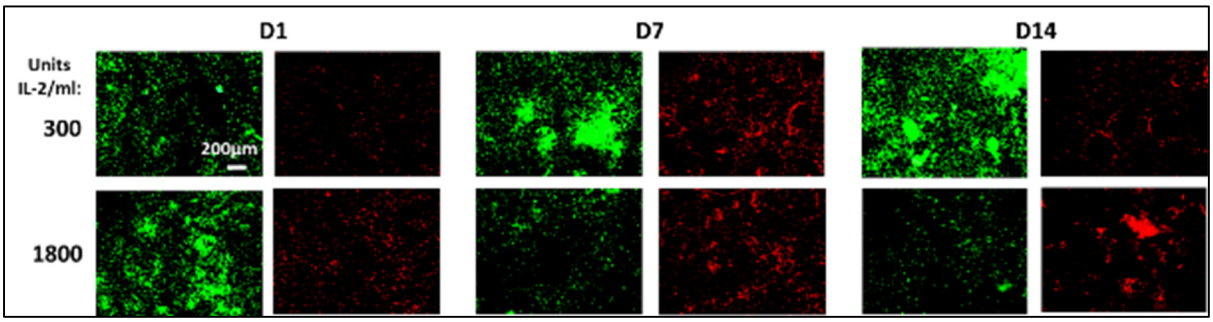

Figure 4-4 Viability of encapsulated PBMC
Representative Live Dead images of human PBMC from healthy donors (live cells in green, dead cells in red) at days 1, 7 and 14 of culture at 8M cells/ml in PB 0.05 SHC 0.075 P17 chitosan hydrogel (N = 3, n = 6)

These assays were later repeated with the new batch of chitosan (P18), to make sure that the change of chitosan did not negatively impact the cytocompatibility of the hydrogel (Figure A I-3 in APPENDIX I). In addition, cell encapsulation in Kitomer hydrogels was added as a control.

4.1.2.2 OT-I cells

One of the main objectives of this PhD was to confirm the efficacy of the technology to decrease tumour burden in vivo in mice. The OVA/OT-I system was chosen, where OVA—expressing tumours are targeted by OT-I T lymphocytes, recovered from genetically modified mice which specifically recognize and attack them. Therefore, the survival of OT-I cells within the gel was also verified in vitro by LIVE/DEAD assays, up to 3 days only due to the more limited culture potential of OT-I cells compared to human lymphocytes. The survival,

proliferation and clustering of encapsulated OT-I cells is clearly shown in representative LIVE/DEAD images over 3 days of culture in the chitosan gel in Figure 4-5.

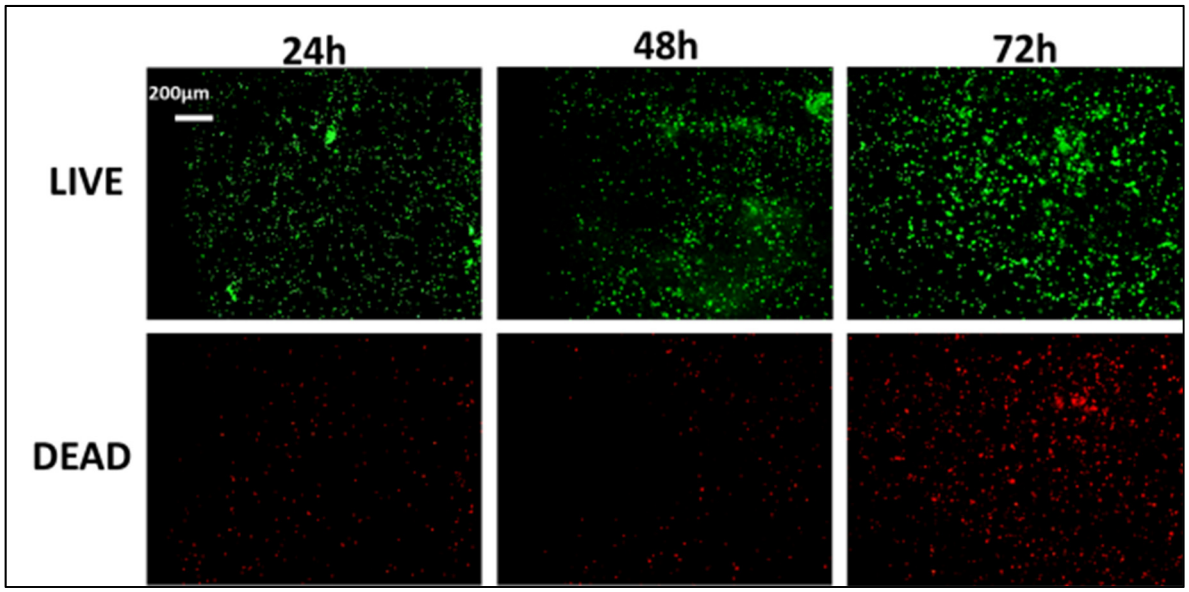

Figure 4-5 OT-I viability
Representative images of OT-I survival in chitosan macrogel (8M/ml) demonstrated over 3 days with Live Dead assay in macrogel. (N=2, n = 4 results with P17 chitosan PB0.05 SHC0.075)

OT-I survival was also confirmed with the new batch of chitosan (P18) (Figure A I-4 in APPENDIX I)**.** However, OT-I mortality appears slightly greater at day 1, and the increase in live cell number over time is less obvious than with the P17 gel.

4.2 Gel biocompatibility and degradation in vivo

Having shown T cell survival within the gel, the next necessary step was to show that the gel is injectable, is biocompatible (does not induce negative effects in vivo) and is biodegradable. Therefore, 200µl of cell-free gel was subcutaneously injected through a 23G needle in the left and right flanks of 6–8-week-old C57 Bl/6 mice. The weight and behavior of mice was studied over a 8-week treatment period, 3 mice being sacrificed at different timepoints to retrieve and weigh the gel. Six untreated mice were included up to 8 weeks as a control group.

Compared to untreated control mice, mice injected with chitosan hydrogel demonstrated no significant difference in their weight (Figure 4-6) or condition over the 8-week treatment period, and no adverse effects were observed throughout the experiment. Mean gel area at sacrifice (calculated as the area of an ellipse, πab where a and b are the two largest perpendicular gel radii measured by calipers) decreased from 84 ± 17 mm^2 at day 1 to 19 ± 1 mm^2 at 8 weeks (Figure 4-6B), indicating progressive biodegradability of the gel, which is also visible in histology (Figure 4.7). It must be mentioned that the mean size at 8 weeks is probably overestimated since only 3 out of 6 gels were identified. It is unclear whether the missing gels were simply not identified and hence not recovered, or if they had completely degraded.

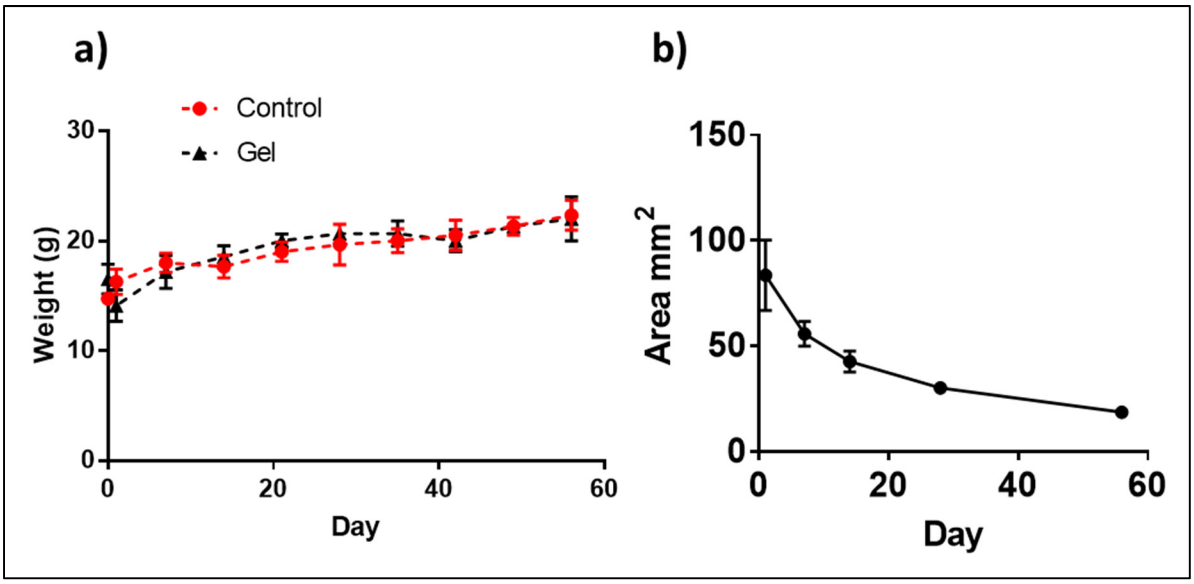

Figure 4-6 Gel biocompatibility and degradation in vivo
a) Weight of 8-week-old female C57 Bl/6 mice with 200µl blank P17 hydrogel injected in each flank (Gel) compared to sham mice (control). All mice weights remained within the expected healthy range throughout the experiment. b) Mean area ± SD of gels recovered from sacrificed mice at specified timepoints after subcutaneous injection of P17 hydrogel in C57/Bl6 mice (n = 3-6)

In addition to measurements, recovered gels were analysed using HPS histology staining to observe gel structure and progressive degradation as well as the biological response around the gel. Representative examples of HPS stained histological slides at the various timepoints tested

(days 1, 7, 28 and 56) are presented in Figure 4.7. While gels were generally cohesive, some porosity and inhomogeneity could be seen, with progressive degradation from the outside to the inside visible over the 8 weeks. There are signs of acute inflammation observed at 24h and slightly increased at one week, characterized by the accumulation of polymorphonuclear cells – particularly neutrophils – at the gel surface and which infiltrate the gel, which increase from minimal to moderate at 1 week. The moderate immune response appears to diminish between 4 and 8 weeks after injection, though some chronic inflammatory cells remain (lymphocytes and macrophages) and the formation of a thin fibrous tissue layer of about 200µm is observed from 2 weeks onwards. While such collagenous tissue formation around the gel is the typical final step of a foreign body response to an implanted material, it might be a limitation for our project since it might limit the migration of T cells out of the scaffold over time.

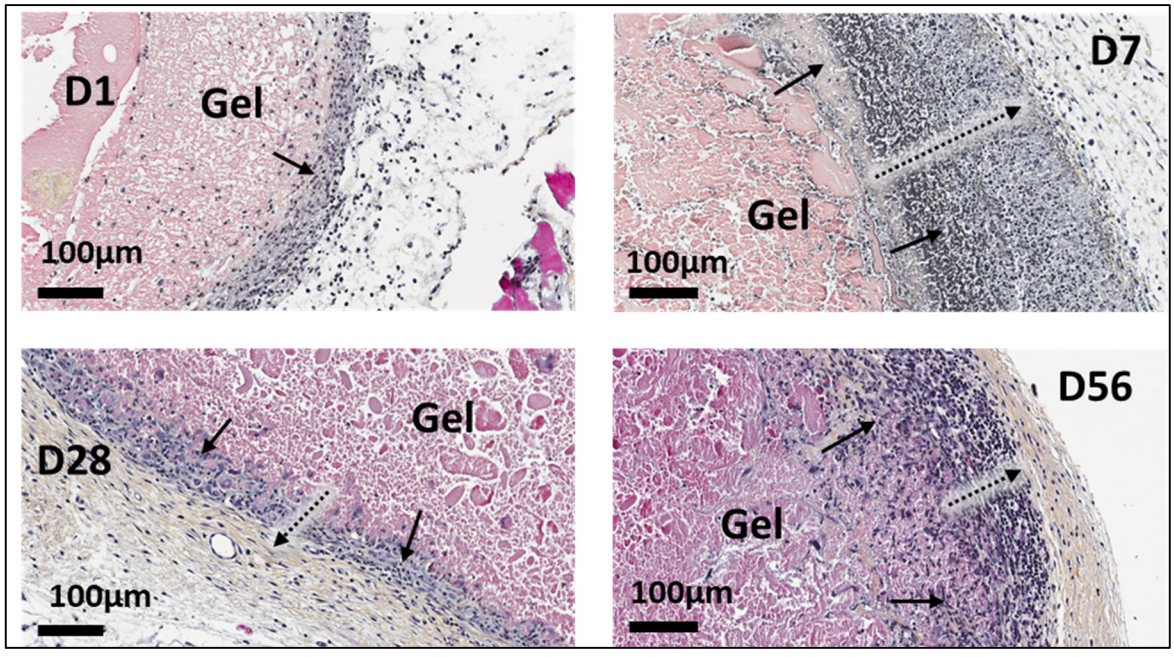

Figure 4-7 HPS staining of hydrogel degradation
HPS staining of the P17 gel and surrounding tissues at day 1, 7, 28 and 56. The acute inflammation (neutrophils) noted in D1 and D7 (solid black arrows) is slowly replaced by chronic inflammation (lymphocytes and macrophages) in D28 and D56 (solid black arrows). The gel, where a mild inflammatory response (solid black arrows) and is progressively encapsulated of by fibrous encapsulation tissue (dotted arrows) can be observed (HPS staining) N = 1 n = 3

4.3 In vivo tumour models

4.3.1 EG7 model

The technology was first tested in the EG7 tumour model. EG7 is a derivative of the EL4 lymphoma cell line that has been conjugated to the OVA peptide, and is often chosen in immunological studies due to its high immunogenicity and hence strong OT-I response. This can act as an initial model to validate the general principles of the system, before optimisation or progress to more stringent models that better mimic clinical ACT. However, we observed a large variability of tumour growth in the untreated group (APPENDIX II), as well as cases of tumour rejections in all groups, treated or otherwise. This indicated the variable growth of EG7 tumours and as such an unsuitability as a valid model to assess our cancer immunotherapy. Due to these issues with the EG7 model, we passed to another in vivo tumour model, as will be subsequently described.

4.3.2 MC38 model

Another murine tumour model was used, using OVA expressing adenocarcinoma tumour cells (MC38-OVA), also specifically recognized by anti-OVA OT-I lymphocytes. This model is relatively well established without problematic autoimmunity nor aggressive tumour growth or difficulty in treatment as seen in the EG7 model. The effect of OT-I loaded gel on MC38 tumour growth in mice was compared to intravenous injections (systemic treatment, as a positive control), and untreated mice (as a negative control).

In brief, 1M MC38 cells were injected in each flank of 8-week-old female Bl6 mice and when tumours were greater 4-6 mm in diameter, they were treated by intravenous injection, (IV, 5M OT-I injected into the tail vein), T cell-loaded gel (Gel, 1.6M OT-I encapsulated in 200µl of gel, injected by needle adjacent to the tumour) or kept untreated (control). Initial experiments demonstrated the treatment effect of both gel and IV treatment.

Pooled data of two initial experiments is presented in Figure 4-8. The mean average tumour area as a function of time after treatment is shown normalised as a % of tumour area at treatment, with each individual replicate also shown.

In both experiments, the untreated group (negative control) showed very consistent tumour growth, suggesting better reproducibility of this model compared to the EG7 model.
Both treatment with gel-encapsulated OT-I cells and systemic injection of OT-I resulted in a significant decrease in subcutaneous MC38-OVA tumour growth. The suppression of tumour growth is, however, less durable in gel-treated mice (significant difference during 11 days after treatment) than in systemically treated mice (during 14 days).

At day 11, tumour size was 251 ± 13%; 168 ± 24% and 143 ± 22% for the untreated, Gel and IV conditions respectively. These results demonstrated the potential of the local treatment in reducing tumour growth, despite using over 3 times fewer cells than the IV treatment. However, the variability of treatment response between the two experiments (APPENDIX III) raises questions of the treatment's reproducibility.

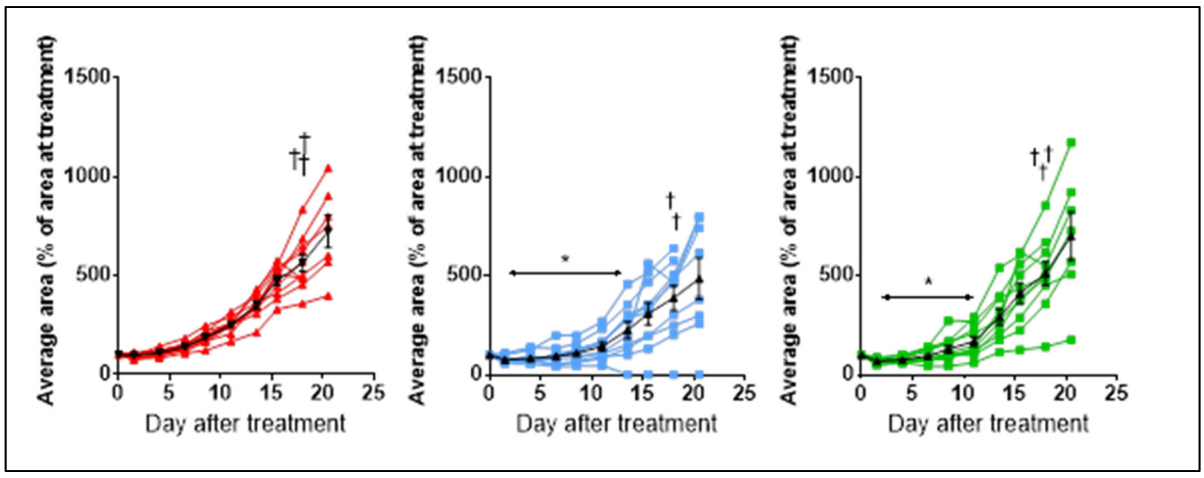

Figure 4-8 Tumour growth curves in MC38-OVA mouse tumour model
Individual tumour growth curves are shown up to 21 days after treatment in subcutaneous MC38-OVA tumours. Each individual tumour as well as the mean ± SEM (black curves) is shown. Red = untreated mice, blue = IV-treated mice, green = P17 gel-treated mice. † indicates mouse sacrifice. * $p < 0.05$ based on two-way ANOVA with Tukey's post-test, arrows indicate duration of significantly different growth compared to untreated mice. OT-I stimulated for 96h (n = 10)

Further experiments were performed to continue to investigate other conditions and reproducibility. Since in vitro flow cytometry data showed improved stimulation without a loss of cell expansion (Figure 4.33) we changed the stimulation protocol from 4 to 3 days stimulation, recovering expanded OT-I one day earlier for use in experiments. We also wanted to compare T cell encapsulation in the hydrogel to simple saline injection close to the tumour. The saline condition acted as a gel-free control to determine if simply the local injection of OT-I results in a beneficial effect, or if encapsulation within the gel itself has a positive impact on the treatment efficacy. The test was performed in duplicate (experiments 3 and 4). A further control condition – Gel only – where 200µl of hydrogel was injected locally alone, without encapsulated OT-I, was also included in the first experiment to confirm that it is the OT-I that result in the treatment effect. By mistake this condition was not, however, repeated.

Figure 4-9 presents the results of experiment 3. The mean average tumour area as a function of time after treatment is shown normalised as a % of tumour area at treatment, with each individual replicate also shown.- Once again, IV treatment led to a significant decrease of tumour growth, up to 14 days, compared to the untreated group. Tumour growth was also significantly reduced for the gel and saline groups at days 11 and 9 respectively compared to untreated mice, while not with Gel only. Interestingly, from day 4 to day 9, both IV and Gel-treated mice showed significantly reduced tumour growth compared to Gel-only treated mice (values at day 9: Gel-only: 197 ± 27%; IV: 101 ± 8%, $p < 0.01$; Gel: 115 ± 17%, $p < 0.05$). This supports the hypothesis of the effect of OT-I. However, the difference is quite small and at least a repetition of the experiment would be required to further demonstrate the specific role of the OT-I. Saline-treated mice showed no significant difference in tumour growth compared to the Gel-only control.

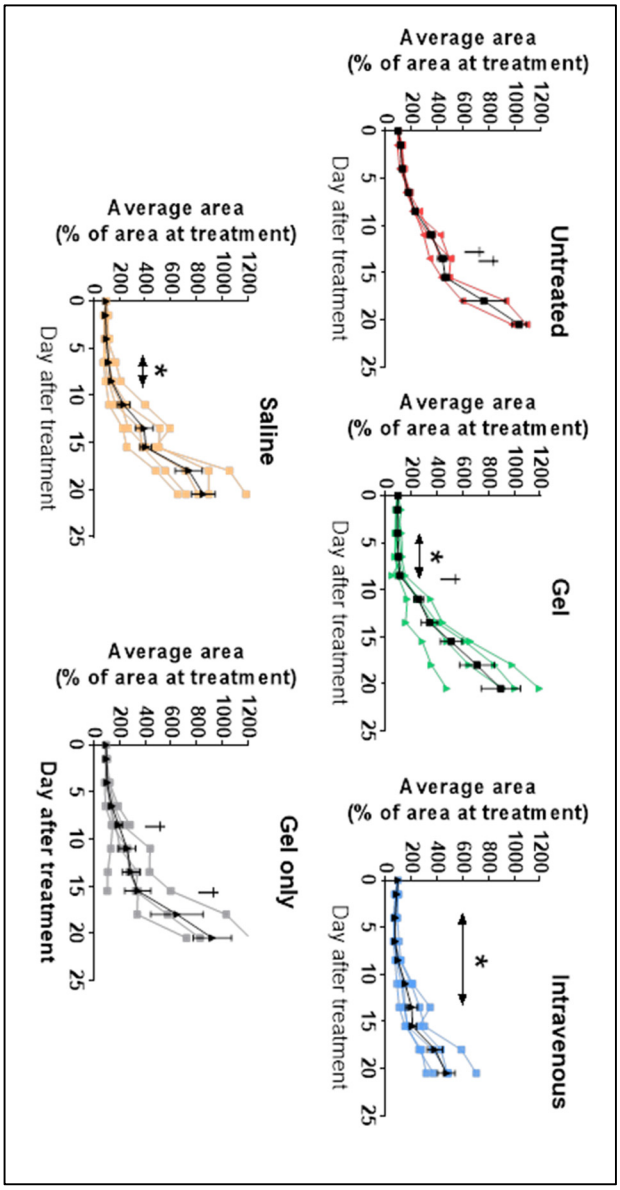

Figure 4-9 Tumour growth curves– saline and gel-only group and shortened stimulation.

Tumour growth curves are shown up to 21 days after treatment in subcutaneous MC38-OVA tumours (mean ± SEM in black, individual curves shown). Red = untreated mice, blue = IV-treated mice, green = P18 gel-treated mice, yellow = saline-treated mice, grey = gel-only-treated mice. * $p < 0.05$ based on two-way ANOVA with Tukey's post-test, arrows indicate duration of significantly different growth compared to untreated mice. OT-I stimulated for 72h; (n = 4-5) † indicates mouse sacrifice

The experiment was repeated and the pooled experiments (experiments 3 and 4) show significantly reduced tumour growth for all treated conditions (Figure 4-10, Figure 4-11a). IV-treated mice showed significantly reduced tumour growth from Day 4 to Day 14 after treatment (D14: untreated: 375 ± 32%; IV: 187 ± 27%, $p < 0.05$). Gel-treated mice showed significantly reduced tumour growth from Day 4 to Day 11 after treatment (D11: untreated: 304 ± 26%; Gel: 180 ± 31%, $p < 0.05$) and saline-treated mice showed significantly reduced tumour growth from Day 4 to Day 9 after treatment (D9: untreated: 221 ± 9%; Saline: 137 ± 12%, $p < 0.0001$), all results which support the efficacy of the gel in reducing tumour growth. These differences are highlighted in Figure 4-11b. The difference between the gel and saline groups indicates a small benefit of the gel itself, perhaps due to cell retention. Overall the results support the hypothesis that localised treatment can have an anti-tumour effect, though with the caveat of inconsistent results, especially in the control groups. Figure 4-11b presents a comparison of the percentage of tumour growth at D9, 11 and 14 for each condition tested.

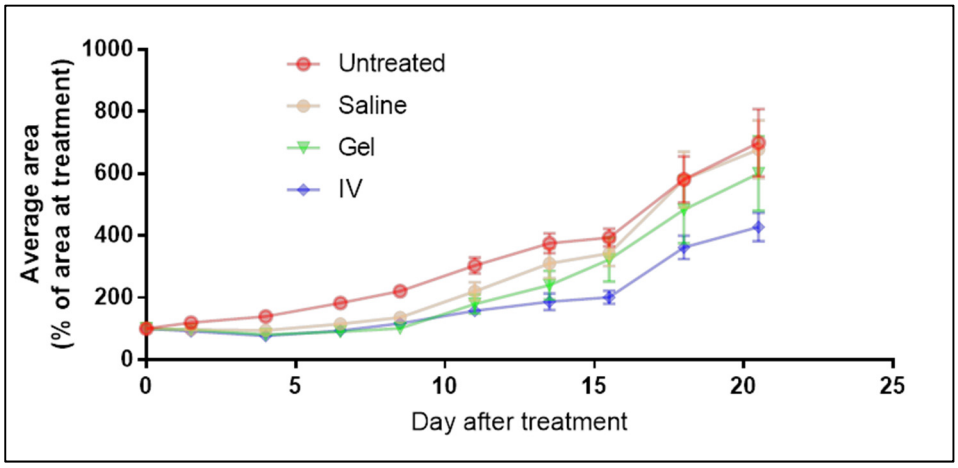

Figure 4-10 Tumour growth comparison - saline and shortened stimulation
The average curves of pooled data from experiments 3 and 4 for each group in Figure 4-11 are shown. (Mean ± SEM, red = untreated mice, blue = IV-treated mice, green = P18 gel-treated mice, yellow = saline-treated mice).

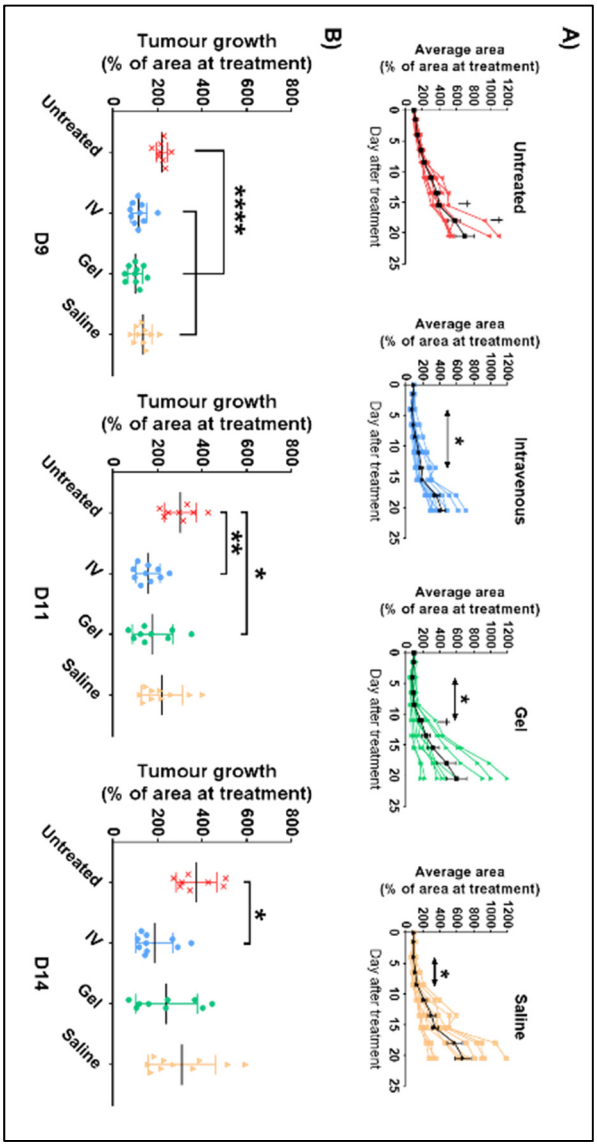

Figure 4-11 Pooled data of experiments 3 and 4 in MC38-OVA model

A) Tumour growth curves are shown up to 21 days after treatment in subcutaneous MC38-OVA tumours (mean ± SEM in black, individual curves shown and compared directly in bottom-right graph). Red = untreated mice, blue = IV-treated mice, green = P18 gel-treated mice, yellow = saline-treated mice, grey = gel-only-treated mice. * $p < 0.05$ based on two-way ANOVA with Tukey's post-test, arrows indicate duration of significantly different growth compared to untreated mice. OT-I stimulated for 72h, (n = 8-10). B) Normalised tumour growth scatter graphs are shown at days 9, 11 and 14, timepoints with reduced tumour growth compared to untreated mice (mean ± SD) * $p < 0.05$, ** $p < 0.01$, **** $p < 0.0001$ based on two-way ANOVA with Tukey's post-test, compared to untreated mice (n = 8-10)

4.3.3 Intravital microscopy for OT-I localisation

Intravital microscopy was also performed at days 1 and 7 to observe cell distribution in the mice, as the OT-I could be localised having previously been marked with Vybrant DiD. As expected, IV-injected OT-I are observed at multiple sites within the animal, for example the lungs and spleen as well as the tumour (Figure 4-12). IV injected cells seem first to congregate mainly around the lungs at 24h, with a sub-population moving into the tumour over the first week after treatment. This confirms that the IV administered OT-I, at least in part, can access the tumour via the bloodstream. In contrast, the signal from gel-encapsulated OT-I remains concentrated to the site of injection adjacent to the tumour. Unfortunately, the resolution of the system is low (1-1.5mm^2) and did not allow us to determine whether cells did enter the tumour and to what extent. The images however suggest that despite the strong Gel signal, it mainly remains within the Gel and does not colonise the entire rounded tumour.

It was therefore much more relevant to compare the number of OT-I reaching the tumour in both groups. A standardised circular 9mm^2 area centered on the tumour was chosen for analysis (Figure 4-12). This figure suggests that OT-I indeed congregate at the tumour site in IV-treated mice, and that despite the strong Gel signal the majority of the signal remains within the Gel rather than migrating towards the tumour. It also highlights the cell retention of the gel, indicated by the larger signal area and higher signal values in Gel-treated mice as compared to saline-treated mice.

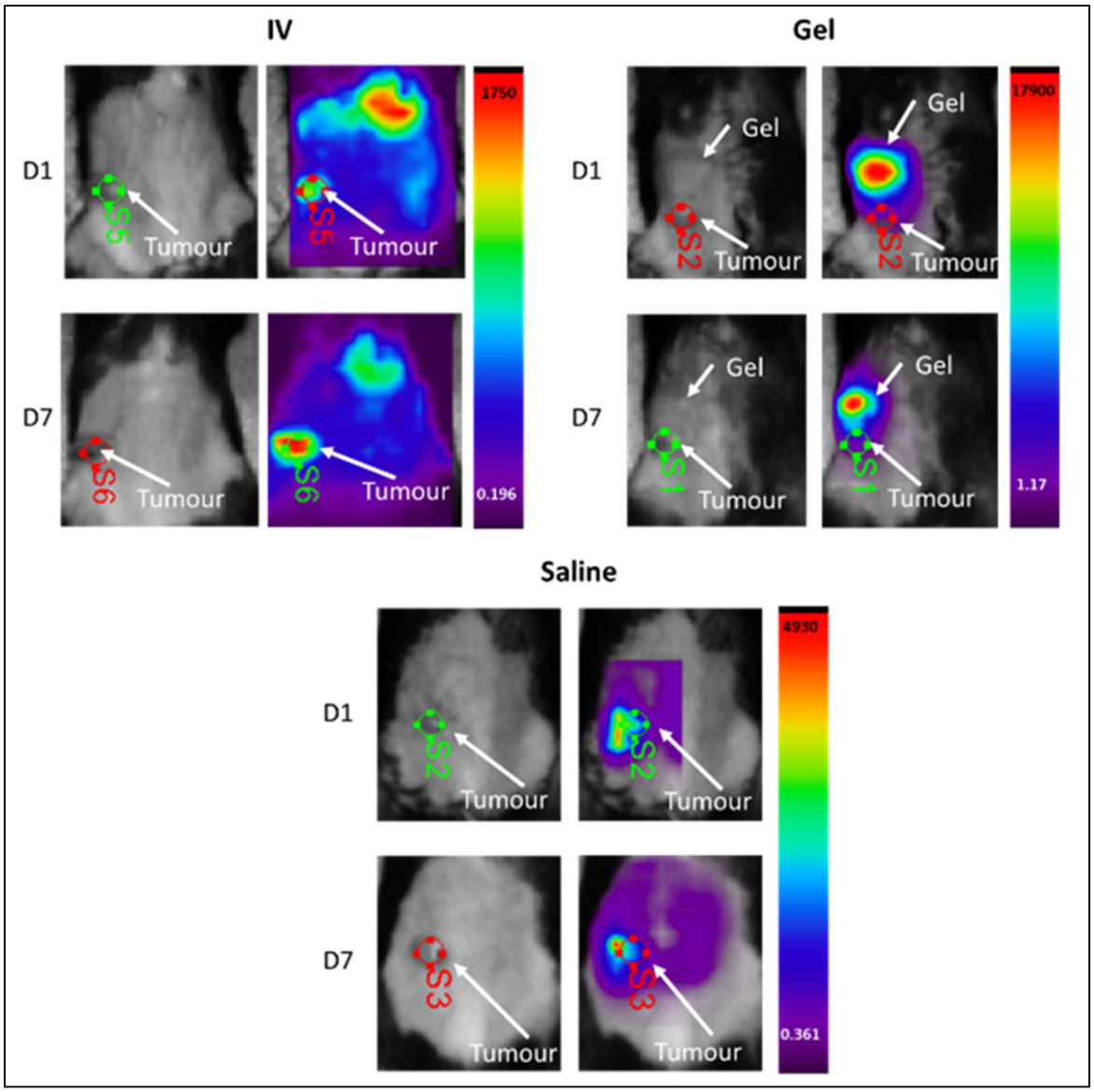

Figure 4-12 Localisation of OT-I cells by intravital microscopy
Region of interest (ROI) for standardised Optix quantification. Representative images of IV, Gel and saline-treated mouse tumours, followed by the placement of a standardised 9mm^2 ROI are shown. Images with the standardised ROI are shown both with and without signal (note the differing scales)

Signal intensity in the tumour region at day 1 and 7 for the IV, Gel and saline groups are presented in Figure 4-13. The local Gel signal was significantly higher (roughly 8 times) than that of IV at both timepoints (D1 $p < 0.05$; D7 $p < 0.01$) than that of IV at both timepoints. The local Saline signal is also significantly higher (roughly 5 times) than that of IV at day 1 ($p < 0.05$), though not at day 7. The fluorescence intensity of the saline-injected OT-I shows greater variation compared to gel-encapsulated OT-I. This probably explains why no significant difference was found between saline-treated mice or gel-treated mice, at both timepoints. This may also be indicative of the variability of cell location and retention without the aid of the gel.

Due to the low resolution of the system, this data must however be considered with caution, especially for the Gel and saline group, since the limit of the tumour area (versus gel area) is very difficult to determine externally before sacrifice. Moreover, one must consider that the signal comes from a single transverse plane at the level of the gel and tumour. It is probable that there is a more dispersed cell location in terms in height for IV than while concentrated in a layer for saline and gel.

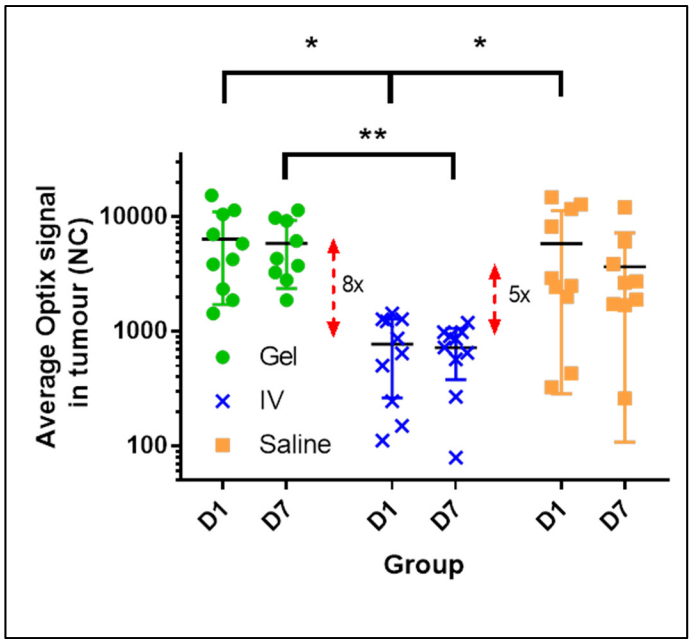

Figure 4-13 OT-I cell signal in intravital microscopy
Average Optix signal intensity of a 9mm2 region of the tumour for IV, P18 gel and saline-treated mice (mean ± SD, n = 10, * $p < 0.05$, ** $p < 0.01$ based on one-way ANOVA with Tukey's post-test)

Surprisingly, despite higher signal intensity in the gel group, the tumour growth tended to be higher than in the IV group. In each group, we searched for possible inverse correlation between the intensity of the signal in the tumour region at day 1 or 7 and the extent of tumour growth at day 7. Figure 4.14 presents the data for the Optix signal at day 7. In both cases, no trend could be observed (very low r^2 values).

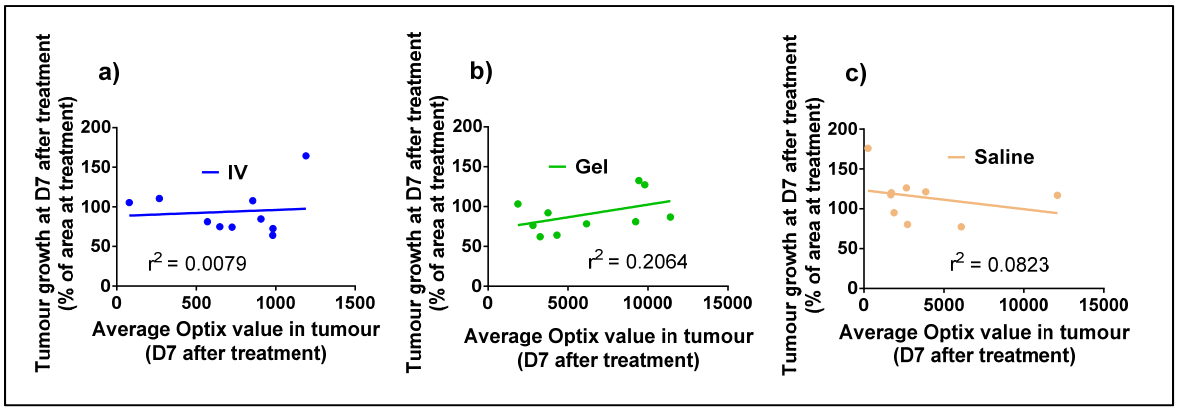

Figure 4-14 Correlation between Optix signal and tumour growth
Correlation is shown between the Optix signal and tumour growth at Day7 after treatment. a) IV-treatment. b) Gel-treatment; c) Saline-treatment. (n = 10 each)

Therefore, further analysis is needed to better assess the access of encapsulated OT-I to the tumour area. Histological analysis was performed after sacrifice of the mice. Moreover, animal experiments were repeated with a much shorter duration (day 1 and 7 as well as some at D0) to better assess the short-term behaviour of encapsulated and non-encapsulated OT-I cells. These results are presented later in section 4.5.

4.4 Scaffolds in microbead format

4.4.1 Rationale

Despite the success of the macrogel in reducing tumour growth, tumour regrowth showed that further improvements to the scaffold were required for optimal anti-cancer activity. One hypothesis of the present work was therefore that OT-I cell encapsulation in small microspheres instead of macrovolumic gel could further enhance the efficacy of the system, thanks to improved nutrient and O_2 transfer (Gonzalez-Pujana, Santos, Orive, Pedraz, & Hernandez, 2017) (leading to enhanced cell survival and hence anti-cancer activity). For this application, the smaller distance needed for cells to move to escape the gel could also aid OT-I migration into the tumour. For optimal results, it is hypothesized that microspheres should have a diameter of 400 µm or less, so that all encapsulated cells are less than 200 µm away for the gel surface.

4.4.2 Microbead fabrication and characterization

Microbeads were first fabricated according to the emulsification protocol developed by our group (Alinejad et al., 2020) using cells suspended in 10% FBS, leading to microbeads with a mean diameter of 441 ± 232µm. While the presence of FBS could help microbead formation by acting as a surfactant, fetal bovine serum should generally be avoided in vivo due to the strong inflammatory and immune response it can generate. We therefore studied the influence of FBS and bovine serum albumin (BSA, APPENDIX IV) concentration on bead formation, while keeping other fabrication parameters constant, such as the stirring rate (1100 rpm, already considered as close to the maximum).

4.4.2.1 Effect of FBS concentration

Figure 4-15 presents typical images of the beads as a function of FBS concentration in the cell media from 10 to 0% v/v (2 to 0% final concentration in the microbeads), while Figure 4-16 presents the mean diameter value for these microbead groups. For decreasing FBS concentration, we found that bead mean size significantly increases at each interval, from 334 ± 168 µm with 2% final FBS concentration to 403 ± 153, 456 ± 202 and 693 ± 257 µm with 1%, 0.4% and 0% FBS respectively, with each group significantly different to each other group ($P < 0.0001$ using one way ANOVA). For decreasing BSA concentration, bead size also increases similarly at each interval (Figure 4-16). The values are quite similar to those obtained with FBS, which suggest that albumin could be used in replacement of serum, to reduce the risk of in vivo immune response without negative effect on microbead morphology. For this proof of concept, we used bovine albumin, but it could be replaced by human albumin for clinical applications.

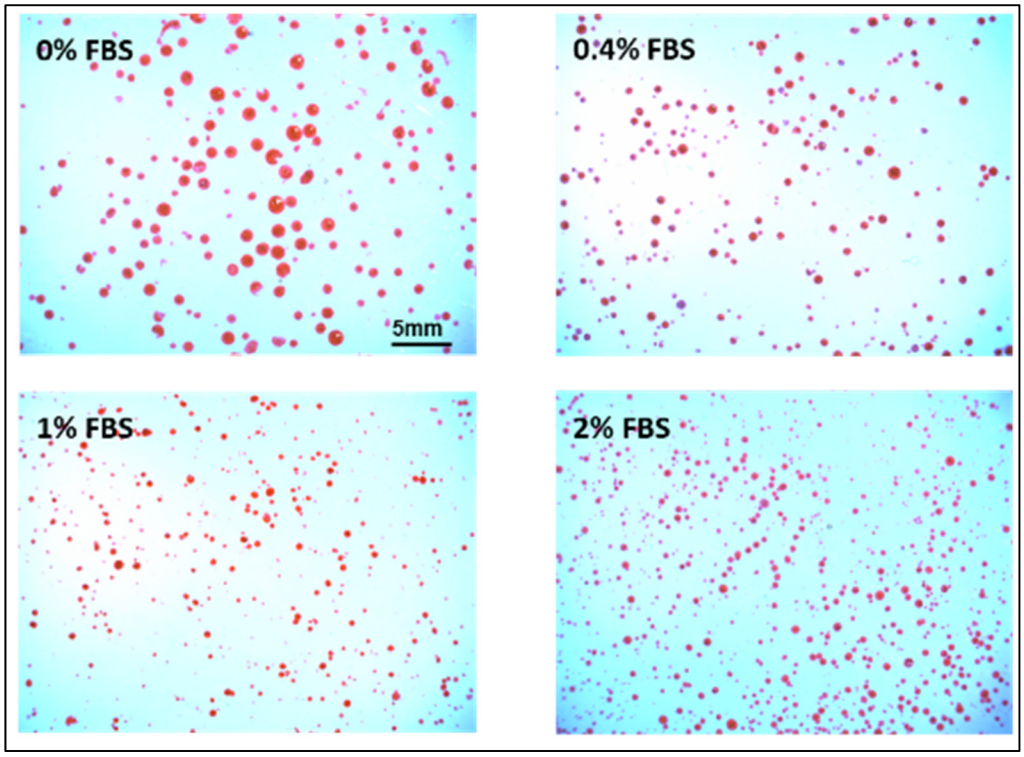

Figure 4-15 Microbead appearance – eosin staining
Pictures of microbeads fabricated with media containing 0, 2, 5 and 10% FBS (0, 0.4, 1 and 2% final FBS concentration in the microbeads)

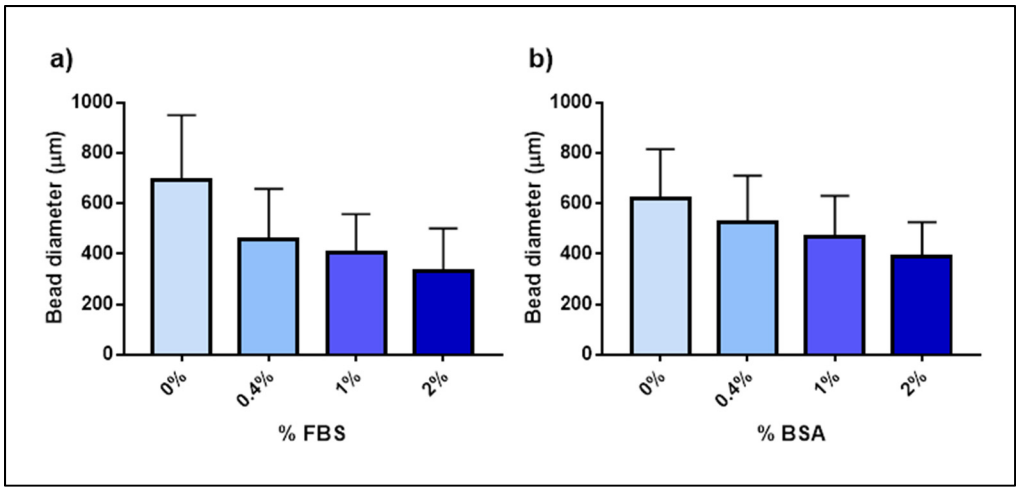

Figure 4-16 FBS effect on bead diameter
Mean diameters ± SD of chitosan microbeads fabricated with media containing a) 0, 0.4, 1 and 2% final FBS concentration in the microbeads, N = 3, n number of beads analyzed > 200 per condition. (Chitosan P18 SHC0.075M PB0.01M); b) 0, 0.4, 1 and 2% final BSA concentration in the microbeads, N = 2, n number of beads analyzed > 1099 per condition. As calculated using Cell Profiler software

Figure 4-17 shows the size distribution of the microbeads. The percentage of beads with a diameter smaller than the 21G needle inner diameter (514µm) used for injection in mice was respectively 25%, 62%, 74% and 82% when containing 0, 0.4, 1 and 2% of FBS. However, this doesn't represent well the percentage of microbead volume (therefore cell %) that would pass through the needle without damage or deformation during injection. We therefore estimated the percentage of bead volume corresponding to the beads bigger than 514 µm for all FBS concentrations.

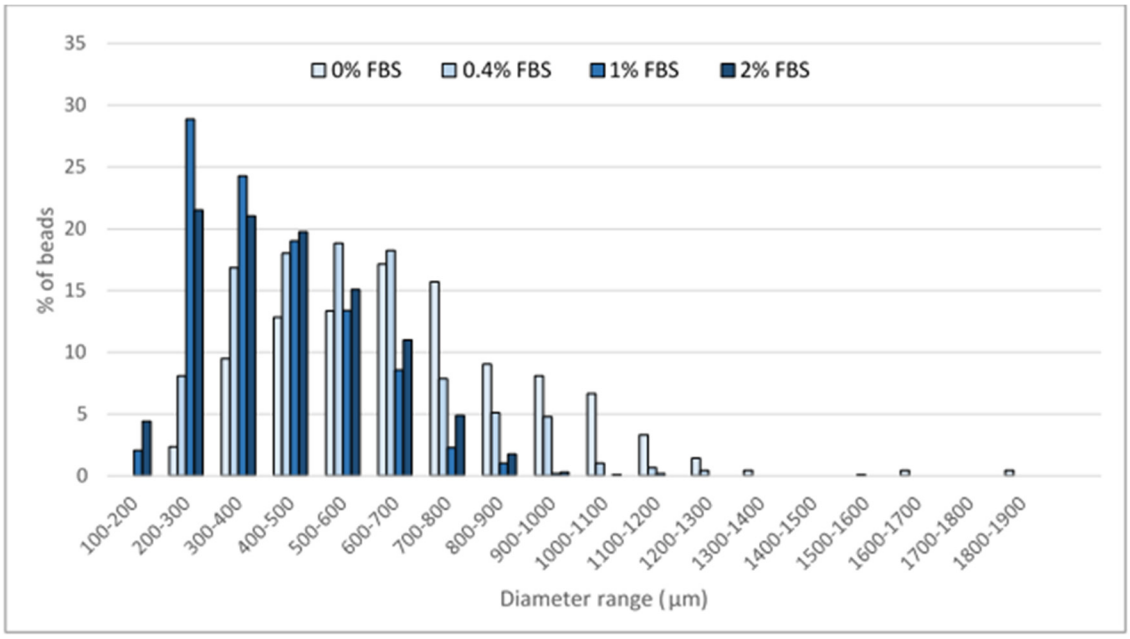

Figure 4-17 FBS effect on size distribution
Effect of final FBS concentration on chitosan microbead diameter size distribution as calculated using Cell Profiler software (chitosan P18 SHC0.075M PB0.01M; N = 3, n number of beads analyzed > 200 per condition

Figure 4-18 shows the volume distribution of the microbeads, where the volume of beads smaller than 514 µm is 4%, 21%, 38% and 42% for 0, 0.4, 1 and 2% FBS respectively as a percentage of total bead volume. As is logical, larger beads form a greater proportion of total volume and hence cell percentage, so fewer larger beads still represent a significant proportion

of encapsulated cells in beads that may be deformed or broken during injection. It is still unclear if this high proportion of potentially deformed/broken beads is problematic.

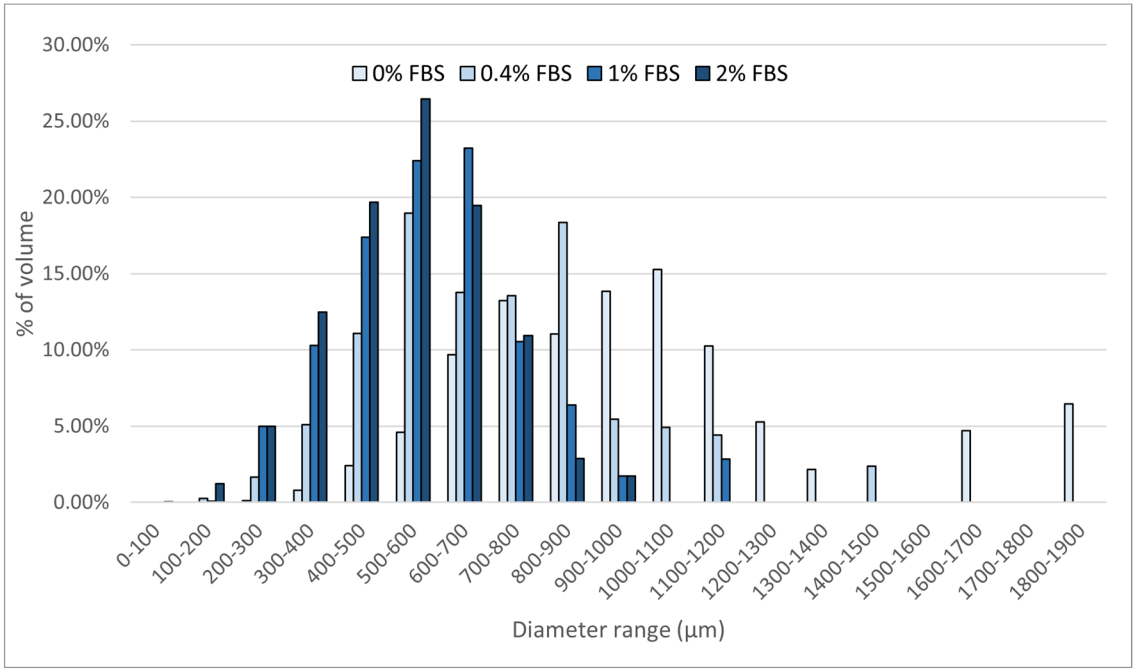

Figure 4-18 FBS effect on volume distribution
Effect of final FBS concentration on chitosan microbead volume distribution as calculated using Cell Profiler software (chitosan P18 SHC0.075M PB0.01M; N = 3, n number of beads analyzed > 200 per condition

A similar study was performed with microbeads fabricated with BSA. Trends were very similar. Results are presented in APPENDIX IV. Alginate microbeads were also fabricated in comparison as a microencapsulation method at a much lower speed and hence with less stress applied to encapsulated cells. Results are presented in Figure 4-40.

4.4.2.2 Effect of encapsulated cells

The effect of cell addition on the diameter of the microbeads was also studied as shown in Figure 4-19. The average diameter of microbeads made with 2% FBS diameter is significantly

increased, from 334 ± 168 to 481 ± 214 μm ($P<0.0001$), when OT1 cells (8M cells/mL) are added in the beads during fabrication. The size distribution is also larger. We calculated that 59% of beads with OT-I and 82% of beads without OT-I under 514μm in diameter were smaller than the 21G needle used for injection. However, in terms of cell percentage (correlated with the microbead volume), this corresponds to 18% of beads with OT-I compared to 42% of beads without OT-I. This again means that in terms of bead volume, a significant proportion of gel volume in larger beads may be damaged or deformed during injection.

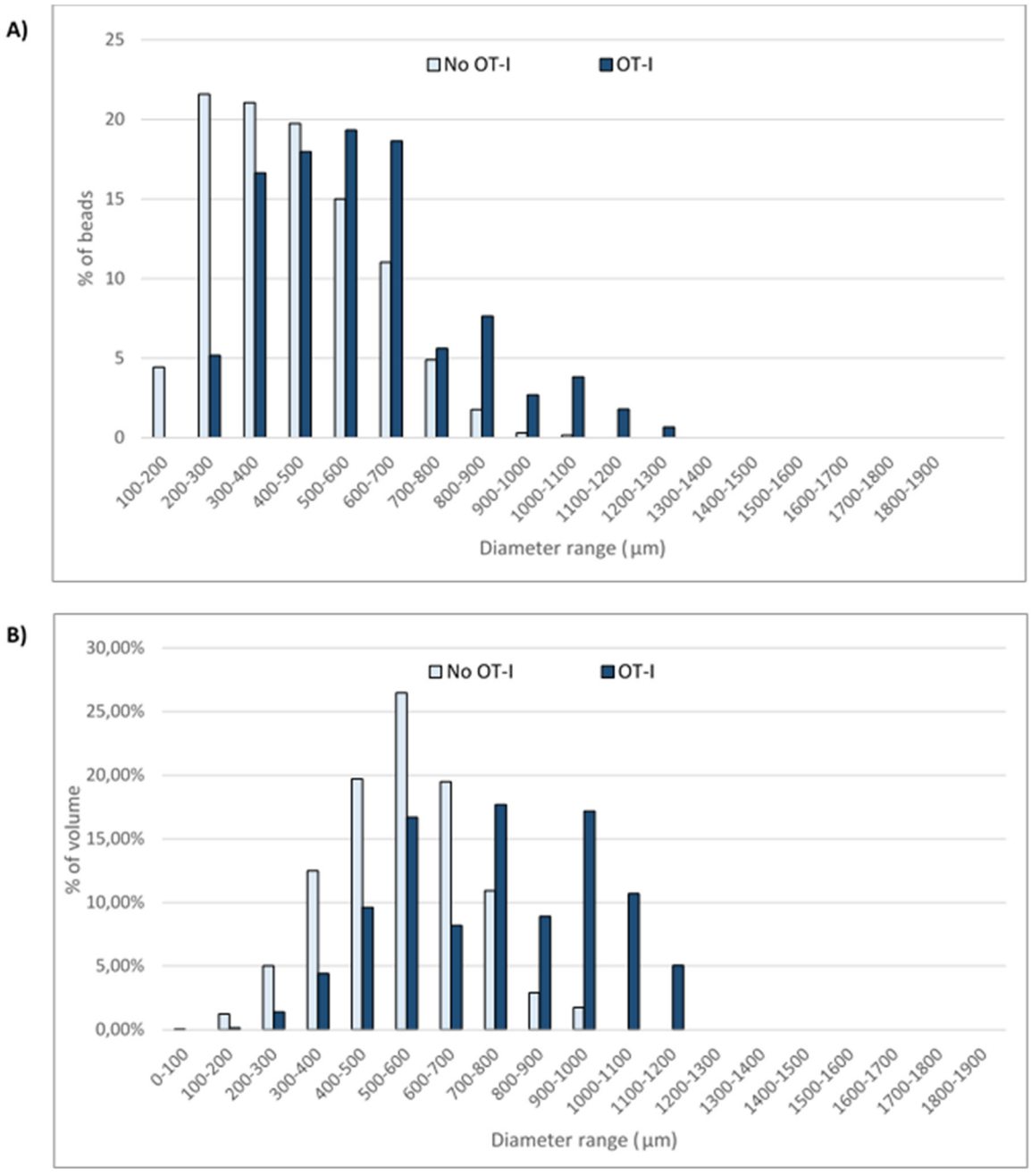

Figure 4-19 Cell presence effect on microbead size and volume distribution
Diameter distribution of P18 microbeads when fabricated with and without 8M/ml encapsulated OT-I cells (2% final FBS concentration, N = 4, n number of beads analysed > 444 per condition; diameter determined using Cell Profiler software

4.4.3 Cell viability in microbeads

4.4.3.1 PBMC

To counter-verify the compatibility of the microbeads for T cell encapsulation, human PBMC (as used in our previously published work) were used as alternative, theoretically more durable immune cells. Despite some variability, both cell survival at D0 and proliferation over 2 weeks was observed (Figure A I-5 and Figure A I-6 in APPENDIX I).

4.4.3.2 OT-I

Having demonstrated the possibility of OT-I encapsulation in microbeads in terms of microbead size, it was then important to assess their survival. The viability of OT-I encapsulated in microbeads was tested using Live-Dead assays over 3 days, in comparison with the macrovolumic gel format (200µl gel in a bottom of a well). Both scaffolds were made with 10% FBS in the cell suspension media to match previous experiments and maximise chances of cell survival. Representative Live/dead images at day 1 and 3 (Figure 4.20) show much greater mortality compared to the macrovolumic gel. This calls for optimisation of the encapsulation process. Despite this limited viability, we decided to test these scaffolds in vivo and compared to the macrogel.

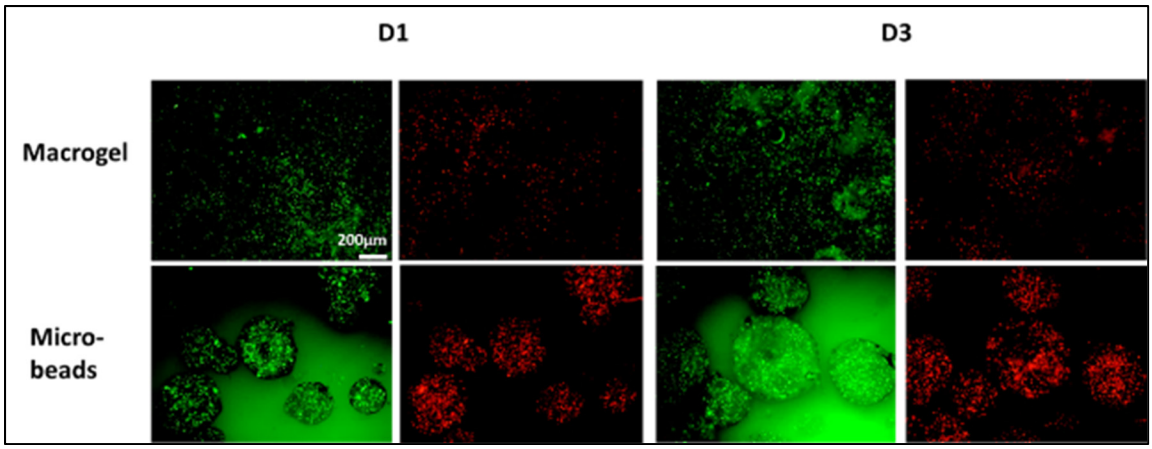

Figure 4-20 OT-I viability in microbeads
Representative images of three independent experiments with one well/condition, showing viability of encapsulated OT-I at D1 and D3 in P18 microbead and macrovolumic hydrogel, assessed by LIVE/DEAD assay (green = live, red = dead; N = 3 n = 3)

4.4.4 MC38 tumour model in vivo – microbead treatment

Having demonstrated that OT-I can be encapsulated in microbeads, we included a microbead + OT-I treated mice as a group to investigate the possible added benefit to the treatment of using the gel in the form of microbeads. This group contained the same number of cells as the Gel group, in the same volume of gel only this time in the form of microbeads of around 500µm in diameter. As with the Gel group, these were injected adjacent to the tumour, suspended in 200µl of PBS to allow for bead suspension and manipulation for loading in the syringe.

Interestingly, the response to the microbead treatment is the same as the macrogel treatment with significantly reduced growth from day 4 to day 9 (Figure 4-21a). Contrary to pooled data using these results, gel and microbead treatment reduce tumour growth compared to untreated mice for a longer period than IV or saline treatment. IV and saline-treated mice showed significantly reduced tumour growth from just Day 4 to Day 7 after treatment (D7: untreated: 186 ± 25%; IV: 109 ± 33%; Saline: 111 ± 19%, $p < 0.01$). Gel and microbead-treated mice showed significantly reduced tumour growth from Day 4 to Day 9 after treatment (D9: untreated: 209 ± 25%; Gel: 88 ± 24%; Microbeads: 115 ± 60%, $p < 0.01$ & 0.05 respectively)

(Figure 4-21b). It is unclear why in this experiment the IV treatment was less effective than in previous experiments. In addition, an outlier can be seen with rapid tumour growth. In this case, the tumour had an elongated form with multiple outgrowths, possibly as an artefact of tumour cell injection. There was also some distance between the injected cells and tumour shown via histology. The combination of these factors may have affected treatment efficacy in this case. Based on this data, there is seemingly little observed benefit of using microbeads vs macrogel in vivo for tumour treatment, though this is only one experiment so we cannot conclude definitively.

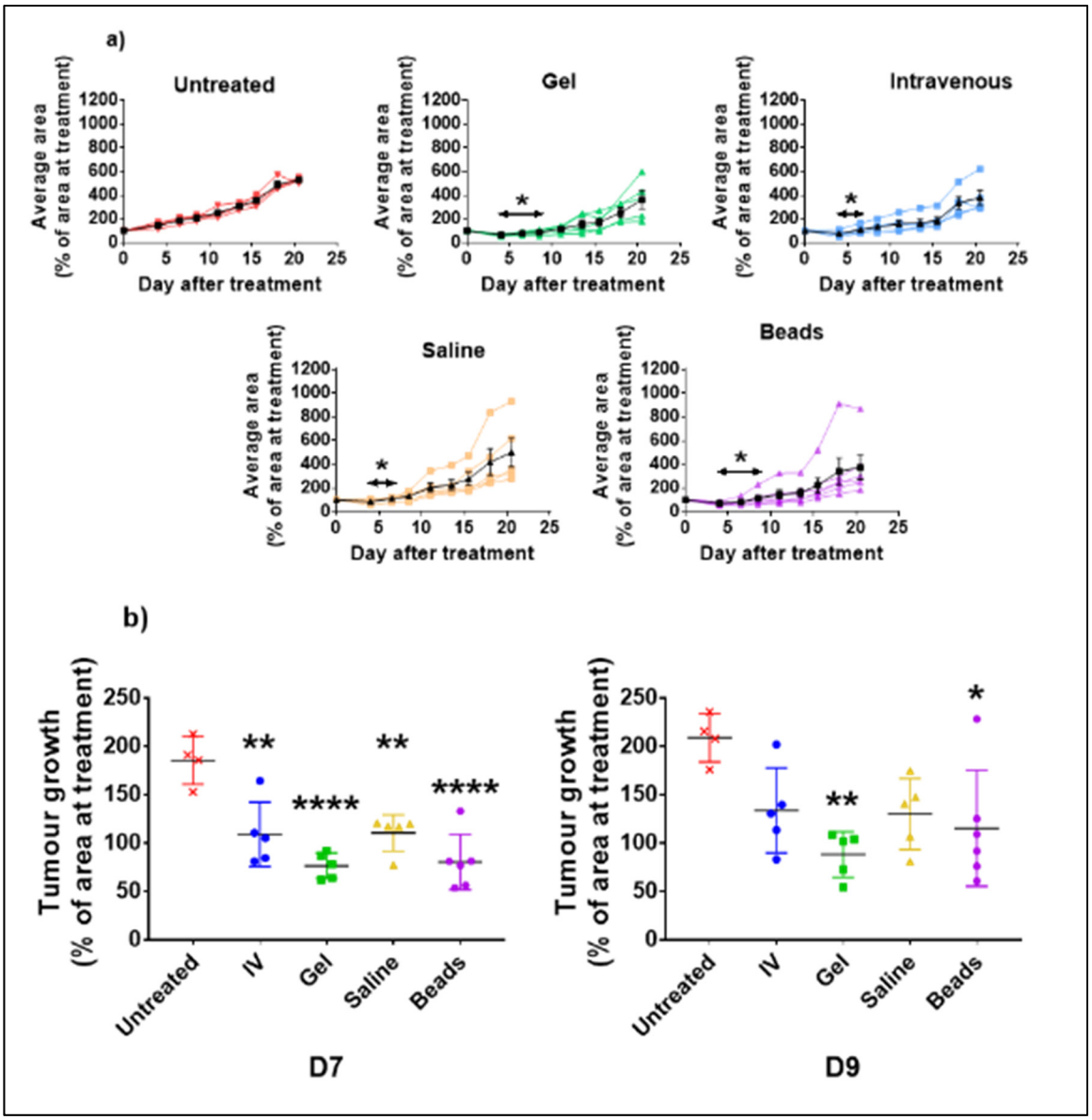

Figure 4-21 Tumour growth curves in MC38-OVA model – microbeads
a) Tumour growth curves are shown up to 21 days after treatment in subcutaneous MC38-OVA tumours (mean ± SEM in black, individual curves). Red = untreated mice, blue = IV-treated mice, green = P18 gel-treated mice, yellow = saline-treated mice, purple = microbead-treated mice. * $p < 0.05$ based on two-way ANOVA with Tukey's post-test, arrows indicate duration of significantly different growth compared to untreated mice. b) Normalised tumour growth scatter graphs are shown at days 7 and 9, timepoints with reduced tumour growth compared to untreated mice (mean ± SD) * $p < 0.05$, ** $p < 0.01$, **** $p < 0.0001$ based on one-way ANOVA with Tukey's post-test, compared to untreated mice (n = 4-6) OT-I stimulated for 72h

When removing the outlier among the microbead-treated mice, the trend was the same, but the time during which tumour growth was significantly reduced increased for all groups (Figure 4-22a), most likely due to a change in the statistical calculations when removing the outlier. IV and saline-treated mice now showed significantly reduced tumour growth from Day 4 to Day 9 after treatment (D9: untreated: 209 ± 25%; IV: 134 ± 44%; Saline: 130 ± 37%, $p < 0.05$). Gel and microbead-treated mice now showed significantly reduced tumour growth from Day 4 to Day 14 after treatment (D14: untreated: 306 ± 27%; Gel: 156 ± 80%; Microbeads: 127 ± 42%, $p < 0.05$ & 0.01 respectively) (Figure 4-22b). This impressive efficacy is promising for the use of gel and microbeads versus IV treatment but would need to be repeated to confirm their efficacy, given this contradicts the trend of experiments 1, 2 and 3 where IV treatment resulted in a longer duration of reduced tumour growth compared to gel treatment.

The Optix signal in the microbead group is similar to that of the gel, with these results shown in APPENDIX V.

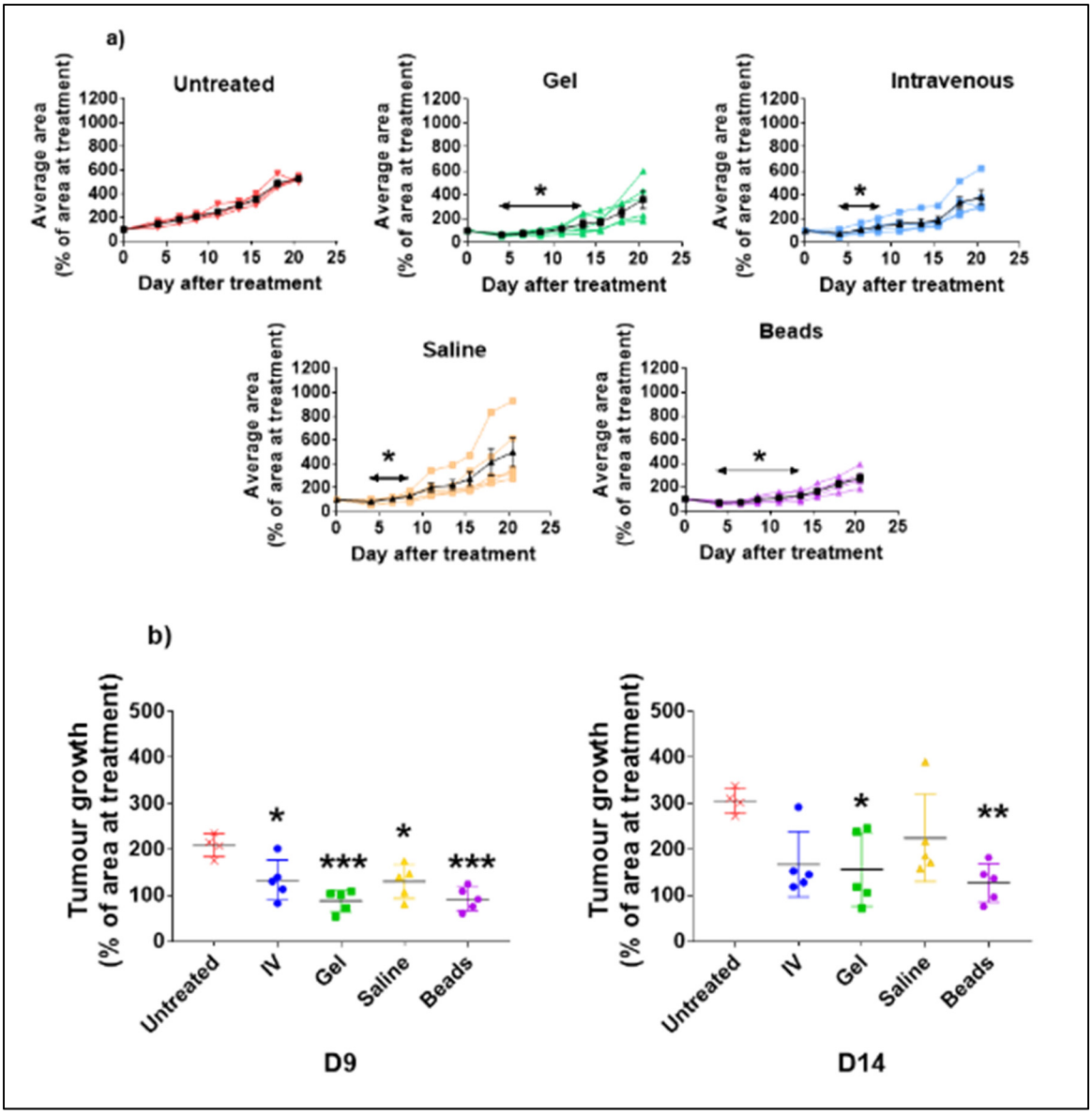

Figure 4-22 Tumour growth curves – microbead group without outlier
a) Tumour growth curves are shown up to 21 days after treatment in subcutaneous MC38-OVA tumours (mean ± SEM in black, individual curves shown). Red = untreated mice, blue = IV-treated mice, green = P18 gel-treated mice, yellow = saline-treated mice, purple = microbead-treated mice. * $p < 0.05$ based on one-way ANOVA with Tukey's post-test, arrows indicate duration of significantly different growth compared to untreated mice. b) Normalised tumour growth scatter graphs are shown at days 7 and 9, timepoints with reduced tumour growth compared to untreated mice (mean ± SD) * $p < 0.05$, ** $p < 0.01$, *** $p < 0.001$ based on one-way ANOVA with Tukey's post-test, compared to untreated mice (n = 4-5) OT-I stimulated for 72h

4.5 Histological analysis

4.5.1 Rationale

After mice sacrifice, histology and immunohistology was performed on the collected tumours and gels. The main questions to be answered were:

- Is the gel visible and cohesive?
- Are OT-I still present in the gel? In the tumour? Can we observe T cell growth and migration with time?
- What is the location of the gel compared to the tumour?
- What is the inflammatory response to the gel and could it play a role in the antitumour response?
- Is there visible tumoral necrosis?

Inflammation and necrosis were both scored by a pathologist blinded to experimental conditions where possible. The scale ranged from 0 to +++ (0-3) with +, ++, and +++ indicating low, moderate, and high inflammation or necrosis respectively.

The next section presents histological results obtained on mice sacrificed at the end of the tumour growth experiments. Due to limited possible conclusions at such a long timepoint, we also performed short term experiments where mice were sacrificed at days 1 and 7 to observe cells earlier during the experiment when there was a greater chance that they would still be present.

4.5.2 Tumour growth experiments (approx. D21)

In multiple cases, the tumour seems to grow and slowly replace the vacant space left by the degrading gel, although these regions are also characterized by increased mixed cell inflammation (lymphocytes and neutrophils) and tumour necrosis (Figure 4-23a, b). Infiltration of immune cells is seen, with predominantly polymorphonuclear cells such as neutrophils

identified. No clear lymphocytic infiltration was observed at the periphery of the gel. In others, the gel and tumour are separated by a thin fibrous capsule with rare signs of a foreign body reaction observed (giant cells), related to gel degradation with time Figure 4-23c. Granulomas begin to form around some samples of the microbeads, which start to be sequestered from the surrounding environment in a classic foreign body response. A mild to moderate, chronic, granulomatous inflammation with multinucleated giant cells (foreign body types) is consistently visible around the gel, while generally absent in all other groups. No significant lymphocytic infiltration was observed at the periphery of the gel nor inside the tumour regions located at the margin of the gel.

Microbeads were recovered in all samples, though with few beads in 2/6 samples. This is probably representative of the greater difficulty in recovering microbeads and their greater dispersal around the tumour. Beads are adjacent to the tumour as with the gels, with beads still adjacent but slightly further from the tumours in samples where few beads were recovered. The microbeads had a slightly higher incidence of fibrous encapsulation compared to the macrogels, with two cases at D21 (2/6 samples). One of these is shown in Figure 4-23f. There also seem to be fewer infiltrating cells in the beads than in the gel, though with some cells present between the beads.

The gel has a porous structure, with some heterogeneity. No vascularisation was observed throughout the scaffold or between the microbeads. Immunostaining of CD31 could more precisely identify any neovessels present. Only few cells are visible in the middle of the gel, indicating that most encapsulated T cells escaped or died before 3 weeks after injection.

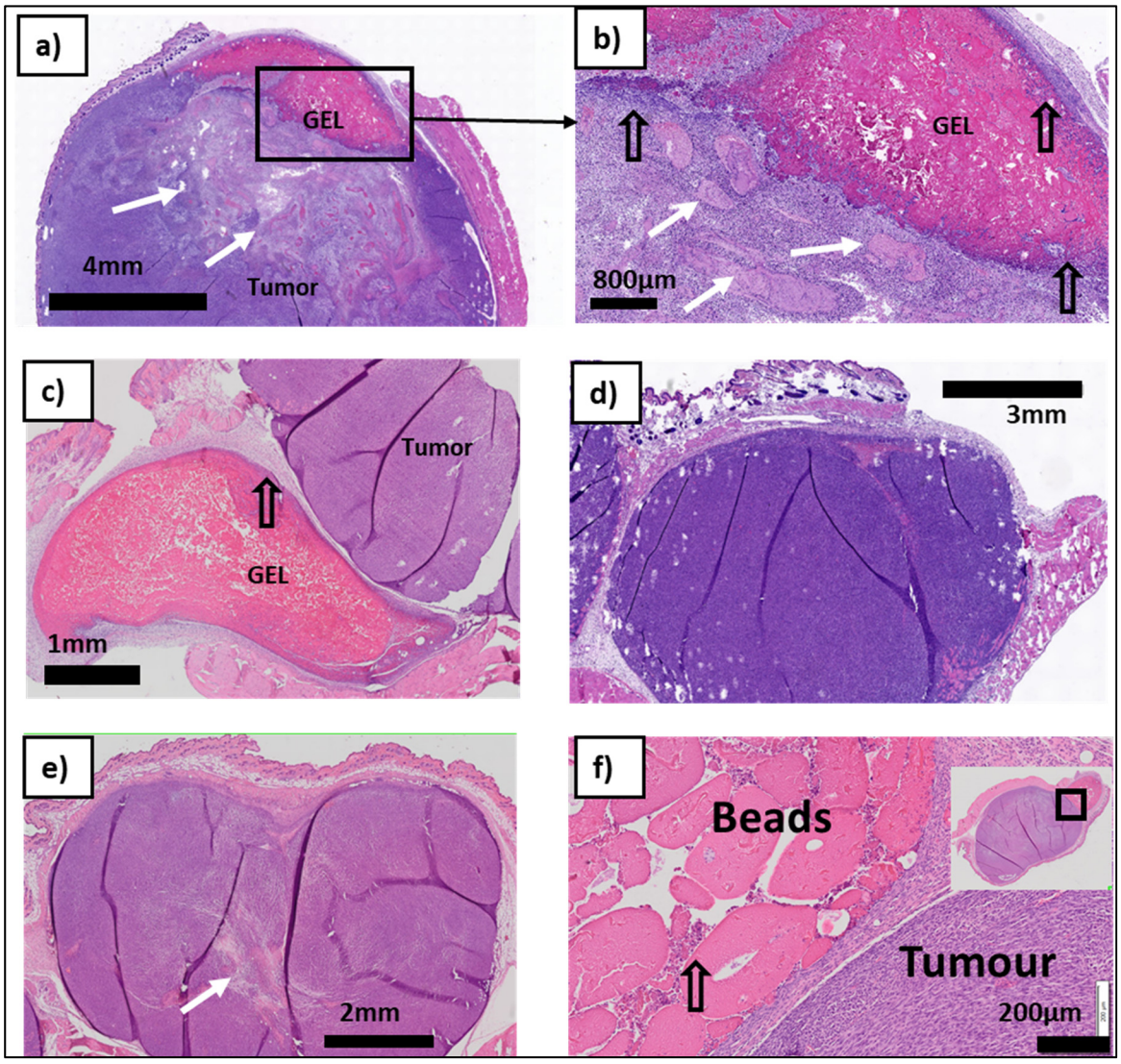

Figure 4-23 D21 histology – H&E
Images of a-c) gel-treated; d) IV treated; e) saline-treated & f) microbead-treated tumours at day 21 after treatment (H&E staining); white arrows show necrotic regions; empty arrows show presence of slight chronic inflammation (mostly macrophages, along with fibrosis)

4.5.3 Gel inflammation and necrosis in vivo at day 21

Inflammation around the gel and beads was minimal at day 21. The score was slightly higher for Gel-only treated mice, but this difference is not significant (Figure 4-24a). The inflammatory response to microbeads and gel with and without encapsulated OT-I is, however,

significantly higher than that against untreated, IV-treated, and OT-I in saline-treated mice ($P<0.0001$). A second experiment would have to be performed to verify the Gel-only results. Intratumoral necrosis is visible in all groups (Figure 4-24b), with no difference between the various treatment groups. As expected, the extent of necrosis tend to increase with the tumour size.

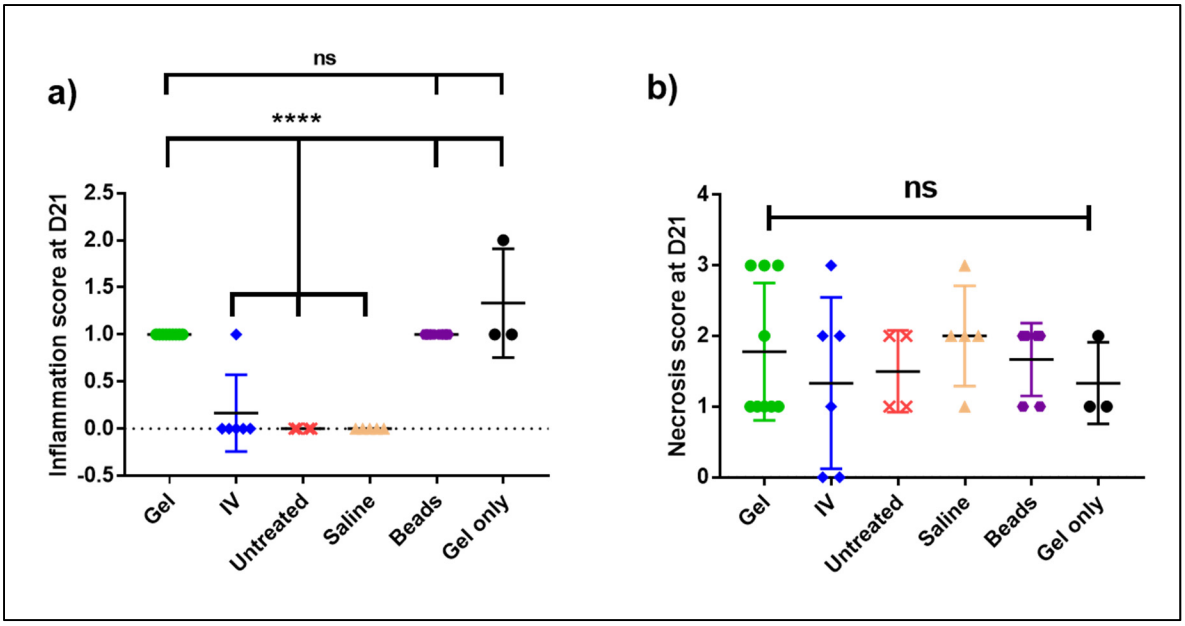

Figure 4-24 Inflammation and necrosis at D21
a) Mean inflammation scores and b) necrosis scores ± SD for gel, IV, untreated, saline, microbead and gel only-treated mice at D21 after treatment in MC38 model. **** Microbead, gel and gel only-treated mice show significantly higher inflammation than IV-treated, untreated, and OT-I in saline-treated mice ($p<0.0001$), $N = 2$, $n \geq 3$

4.5.4 Short term experiments (D0, D1 and D7)

Histology performed on day 0 after injection confirmed the encapsulation and homogenous cell distribution within the scaffold, as also confirmed by immunohistochemistry (IHC) staining ($CD8^+$) as shown in Figure 4-25. Cell number however rapidly decreased after day 0, suggesting their rapid escape or death. We believe this is due to their rapid escape, rather than cell death as no significant signs of apoptotic cells were observed in H&E staining. Unfortunately, we were not able to differentiate endogenous from exogenous lymphocytes

(using CD45.1/CD45.2 immunostaining, our attempts of which are summarised in APPENDIX VI).

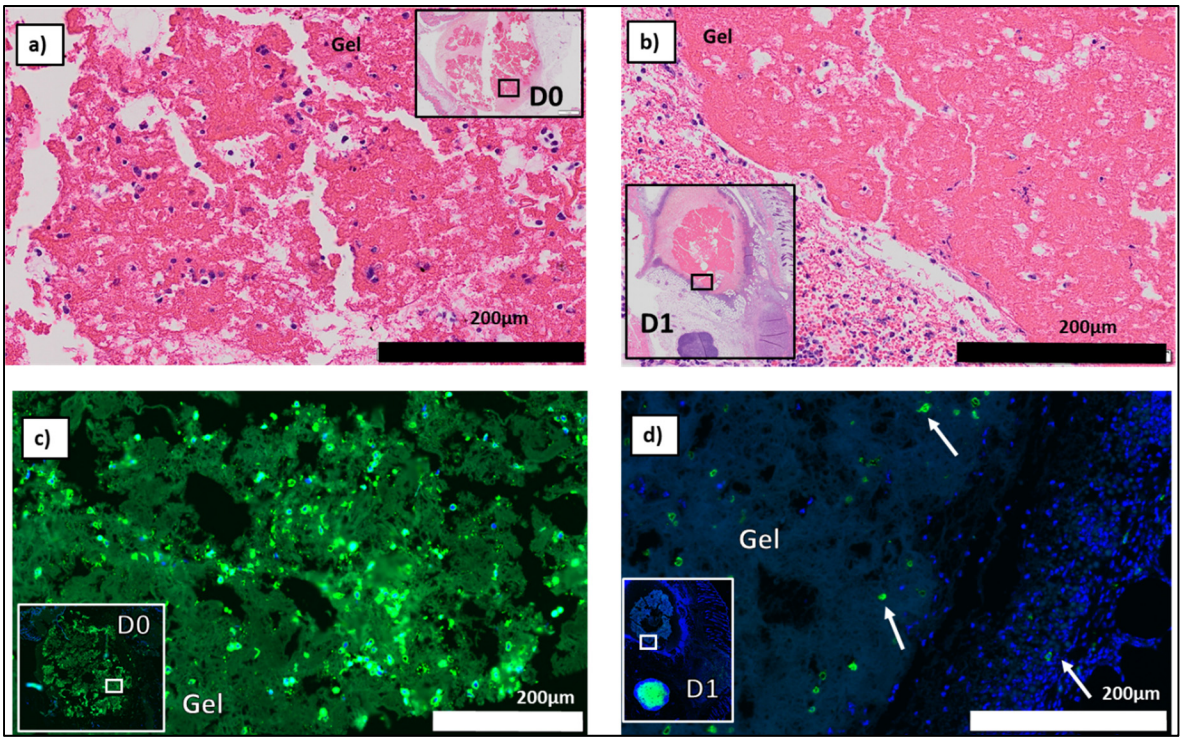

Figure 4-25 OT-I presence in gel at D0 and D1
H&E staining (a, b) and immunofluorescence (c, d; CD8 in green, DAPI in blue) of the gel-encapsulated cells at D0 and D1. White arrows highlight $CD8^+$ cells in d)

In microbeads, a lower number of cells was observed at both timepoints, with a homogenous but lower density cell population at D0 (Figure 4-26a). CD8 IHC staining was not performed on microbead samples at D0, but we can assume at such a short timepoint that the visible cells are $CD8^+$. At D1, cells are visible in the microbead (Figure 4-26b), but IHC in Figure 4-26c shows that these do not correspond to CD8 cells and are likely infiltrating immune cells such as neutrophils. The lower cell number probably reflects the higher OT-I mortality in microbeads as seen in vitro.

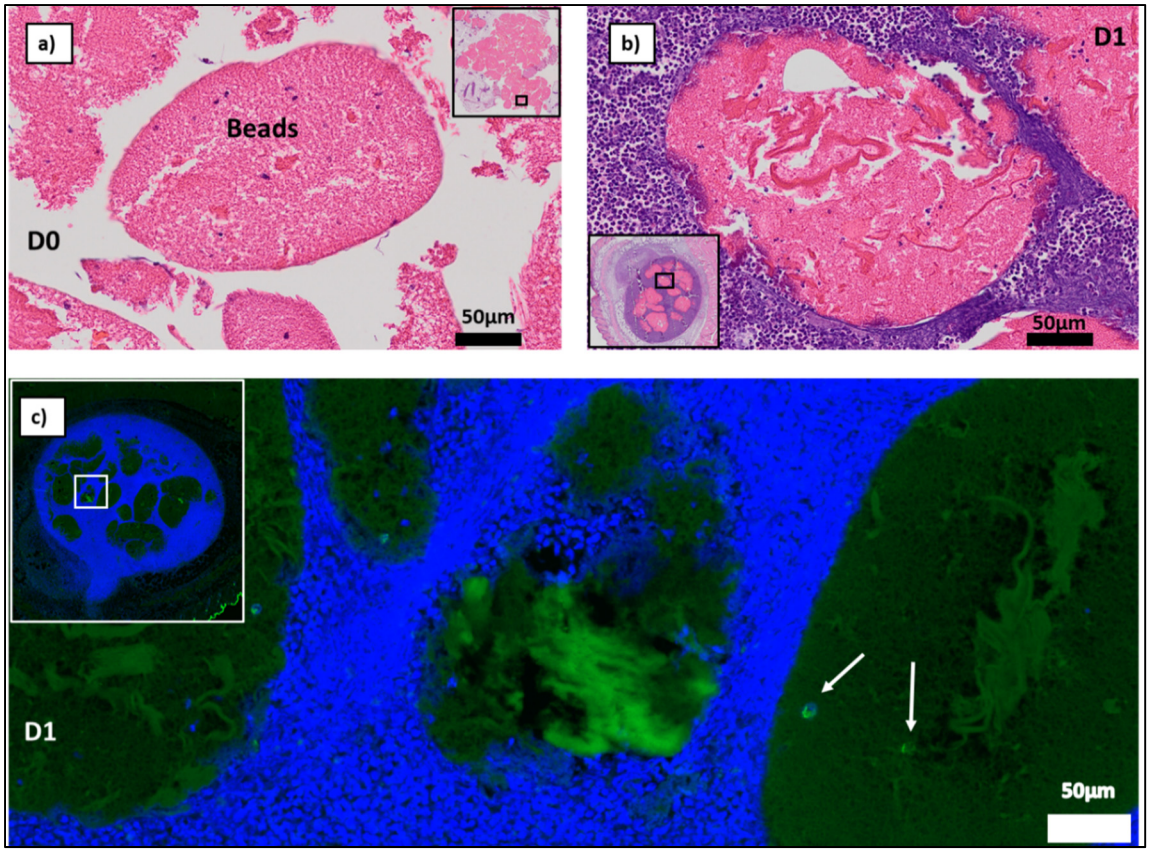

Figure 4-26 OT-I presence in beads at D0 and D1
H&E staining (a, b) and immunofluorescence (c; CD8 in green, DAPI in blue) of the microbead-encapsulated cells at D0 and D1. White arrows highlight CD8+ cells in c)

We also quantified intratumoral CD8 cell numbers, though our preliminary results did not indicate any significant differences between groups as described in APPENDIX IX, where further histological images are also shown.

4.5.5 Inflammation and necrosis at D1 and D7

At day 1, acute inflammation can be observed in the gel group, mainly composed of polymorphonuclear cells (predominantly neutrophils) and mainly concentrated around the gels (Figure 4-27a, c & d). In contrast, only some mild peritumoral inflammation is observed in single cases at day 1 in the saline (Figure 4-27b) and untreated groups (Figure A VIII-4 in

APPENDIX VIII), with no significant inflammation observed at day 7 when no gel is present. Inflammation around the gel is still present at day 7 but tends to decrease (however with high variability between samples) and be replaced by mild chronic inflammation.

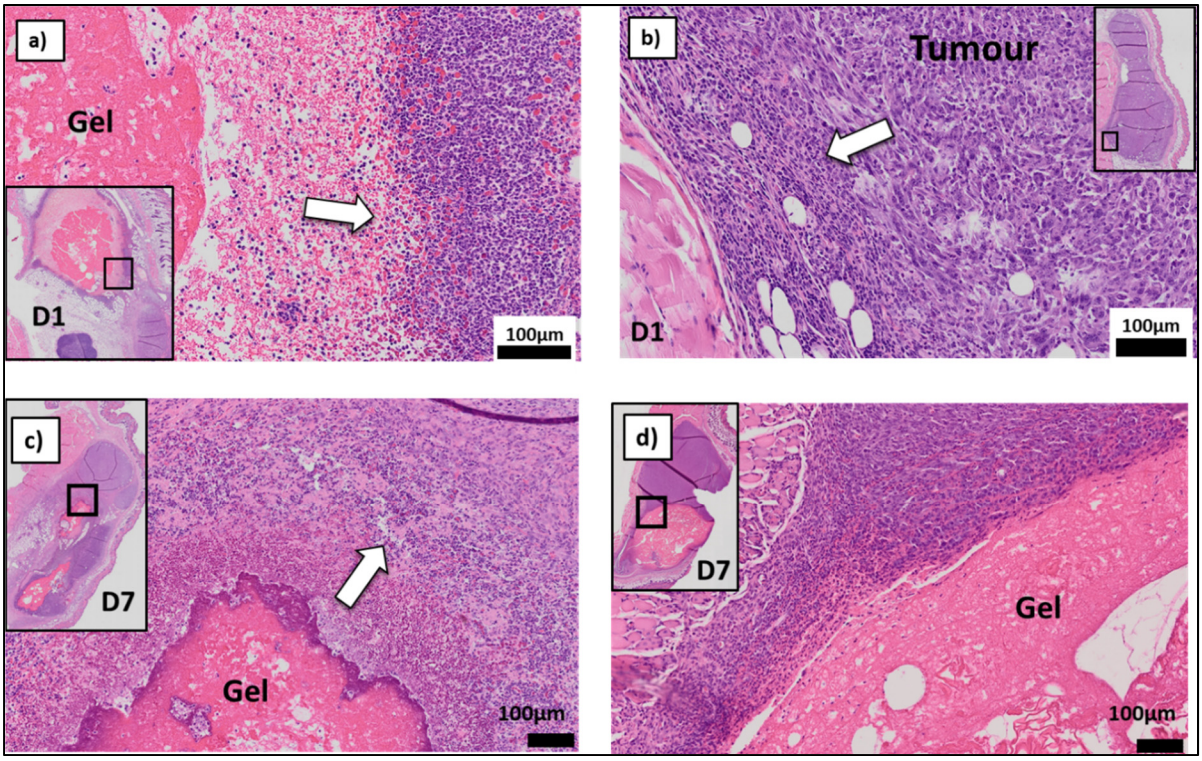

Figure 4-27 Inflammation at D1 and D7
H&E staining showing inflammatory response at a) D1 and c) D7 around the gel, where perigel necrosis is also present at D7; b) Some peritumoral inflammation was observed after treatment with OTI in PBS at D1. d) an example of a gel without significant perigel inflammation at D7. White arrows indicate inflammation

Short-term data for the microbeads is limited, as only one experiment was performed (only one sample recovered with visible microbeads), showing either poor control of bead location at injection or the difficulty of successfully recovering the beads after *in vivo* injection. When recovered, the beads are cohesive, with a strong immune reaction around the beads (Figure 4-28a & b).

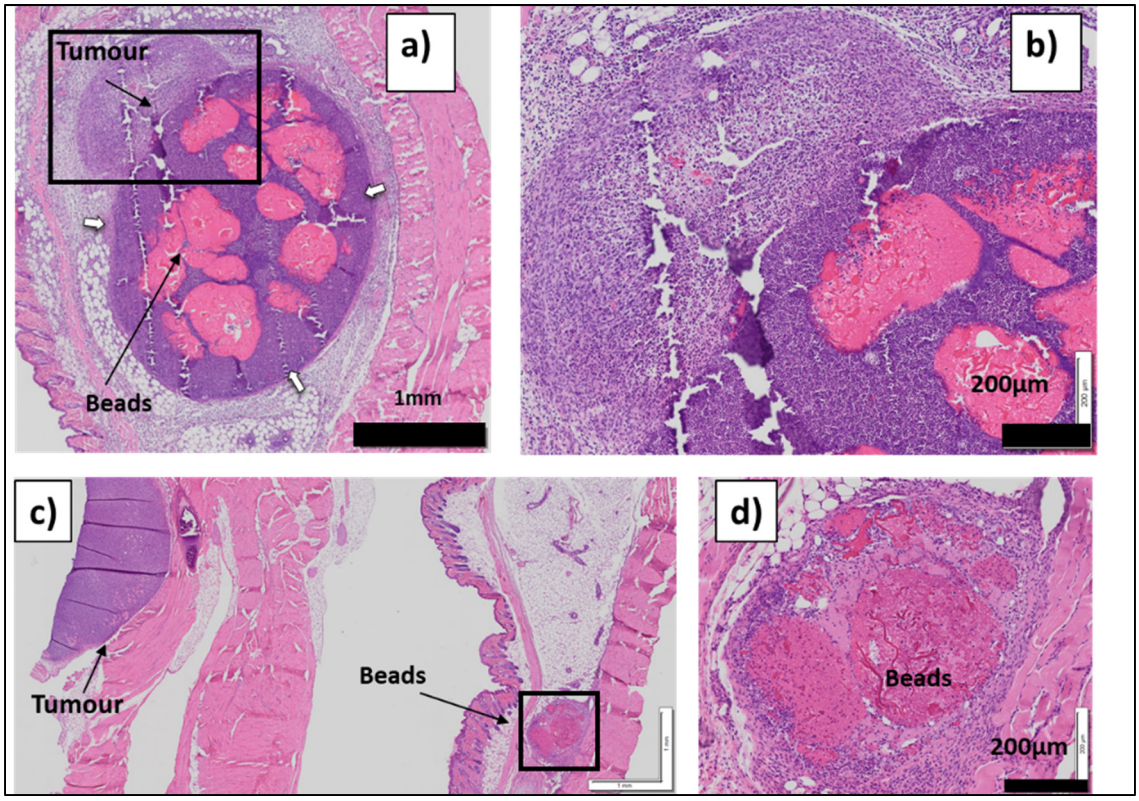

Figure 4-28 Microbead histology at D0 and D1
H&E staining of microbead-treated MC38-OVA tumours in CD45.1 mice at day 1 (a & b) and day 7 (c & d) after treatment (P18 chitosan). White arrows show strong inflammation at the gel and microbead surface

As expected, at D1 after treatment, both gel and microbead-treated mice showed significantly higher inflammation than the IV, untreated and saline groups ($p<0.01$) as shown in Figure 4-29a. At 7 days (Figure 4-29b), only gel-treated conditions show any significant inflammation – though there are not enough microbead samples at 7 days to conclude for this group. Due to the small sample number, the difference with the other groups is no longer significant. The location of inflammation is similar to day 1, with inflammation concentrated around the gels.

At D7 after treatment, gel-treated mice showed significantly higher tumoral necrosis than the IV, microbead and saline groups ($p<0.05$) as shown in Figure 4-29c. It was not significantly higher than in untreated mice but was in a different location. In the untreated group the observed necrosis is intratumoral, due to a necrotic core in response to rapid growth and a

hostile microenvironment at the heart of the tumour. In contrast, in the gel group, inflammation and necrosis are found in the periphery of the tumour (Figure 4-27c). This could suggest that in the first week after treatment we see perigel necrosis due to OT-I activity and/or the inflammatory response to the gel in gel-treated mice, whereas this timescale is sufficient for untreated mouse tumours to grow such that necrotic cores are formed. However, a gel-only control at 7 days would be necessary to confirm that this effect is related to the OT-I escaping the gel and not only to the inflammation induced by the vehicle (the gel).

Interestingly, a strong inverse correlation was observed between the extent of inflammation at day 7 and the tumour growth at day 4 (Figure 4-29d). This suggests that the inflammatory response in gel-treated mice may be beneficial in the anti-tumour response, at least in the short-term. Figure 4-27 shows examples of both a smaller tumour where strong inflammation is present (c), and a larger tumour with a limited inflammatory response to the gel (d).

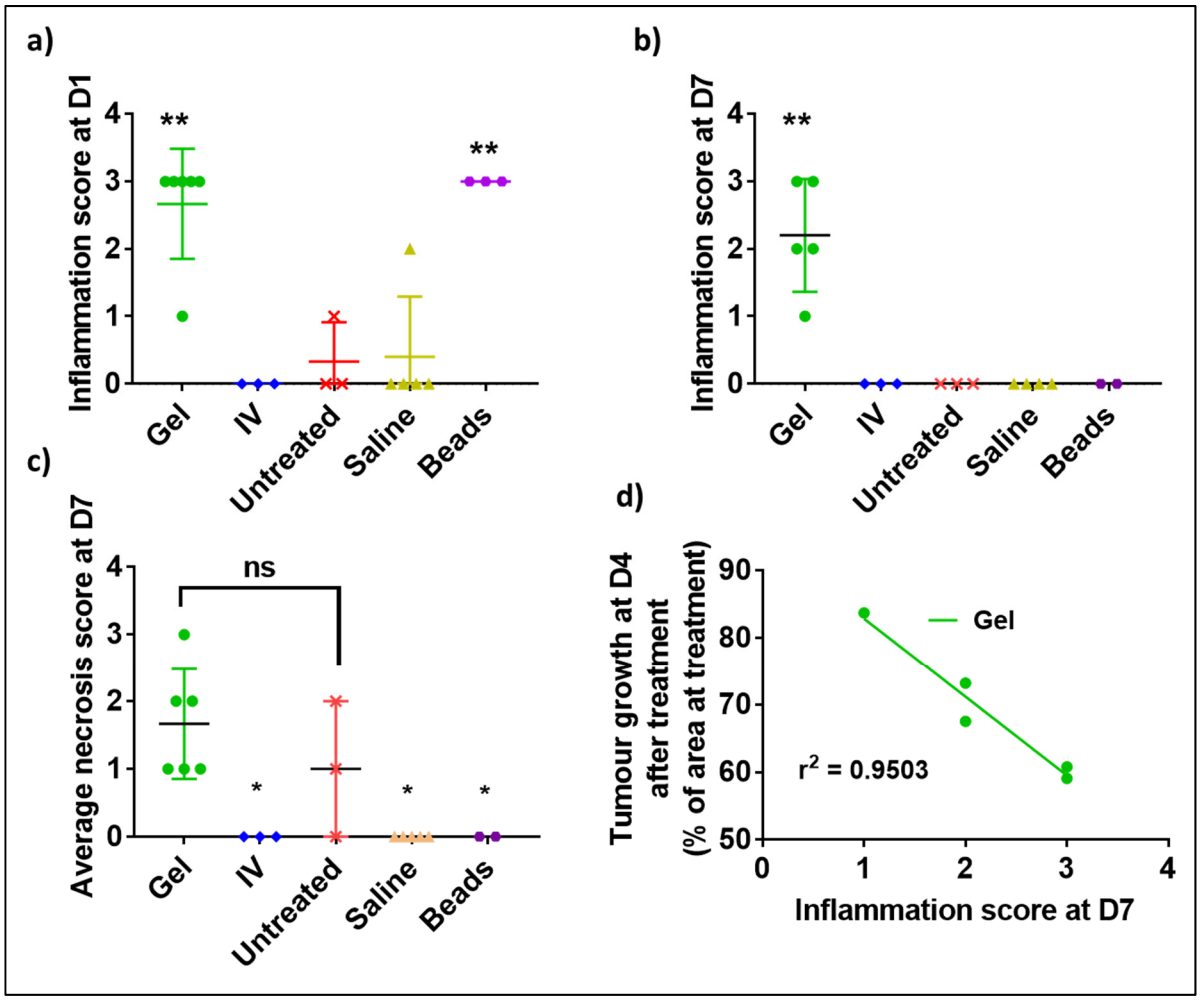

Figure 4-29 Analysis of inflammation and necrosis
Average inflammation scores for gel, IV, untreated, saline and microbead-treated mice after treatment in MC38 model at a) D1 and b) D7 gel and bead-treated mice show significantly higher inflammation than IV-treated, saline-treated and untreated mice (** $p<0.01$); c) Average necrosis scores for gel, IV, untreated, saline and microbead-treated mice at D7 after treatment in MC38 model. * gel-treated mice show significantly higher necrosis than IV-treated, saline-treated and microbead-treated mice ($p<0.01$); d) Correlation of inflammation score and tumour size 4 days after treatment for gel-treated mice. Stronger inflammation is correlated with smaller tumour size at D4 in the gel-treated group

Overall the histology analysis raises many questions as well as offering some potential answers. Clearly there is inflammation induced by the gel, though its benefit or drawback is unclear. Some observations of necrosis and inflammation could show the anti-tumour effect of the gel but more controls would be necessary to confirm that this is truly due to the OT-I. Both

the gel and microbeads are also shown to be capable of persisting up to the 21-day timepoint alongside tumours and in all likelihood beyond as well.

4.6 Reproducibility of in vivo tumour models

Due to the large variability of tumour growth and treatment effect, the reproducibility of in vivo models was studied, based on the size of the tumour at D0 (7 days after tumour cell injection) and at D10 (17 days after tumour cell injection, unless otherwise stated). Reproducibility of the EG7 model is shown in the appendix, and led to the conclusion that the EG7 was not a suitable model due to high variability of the results and spontaneous tumour rejections.

Reproducibility of untreated tumour growth

The reproducibility of untreated tumours was investigated to verify the quality and consistent growth of the tumour cell line, as well as counter-verify tumour growth curves based on initial tumour size. Figure 4-30 shows a comparison of tumour sizes at treatment for mice in all MC38 experiments. Experiments 1 and 4 are quite similar, while tumours are slightly (but significantly) smaller in experiments 2 and 3. It should be noted, however, that these differences are small – with average tumour areas (as the product of perpendicular diameters) ranging between 20 and 25mm^2, these differences would correspond to tumours of around 4.5-5mm in diameter respectively, a small difference when measuring accuracy is considered. As such we can conclude that tumour size at treatment is relatively reproducible in the MC38 model.

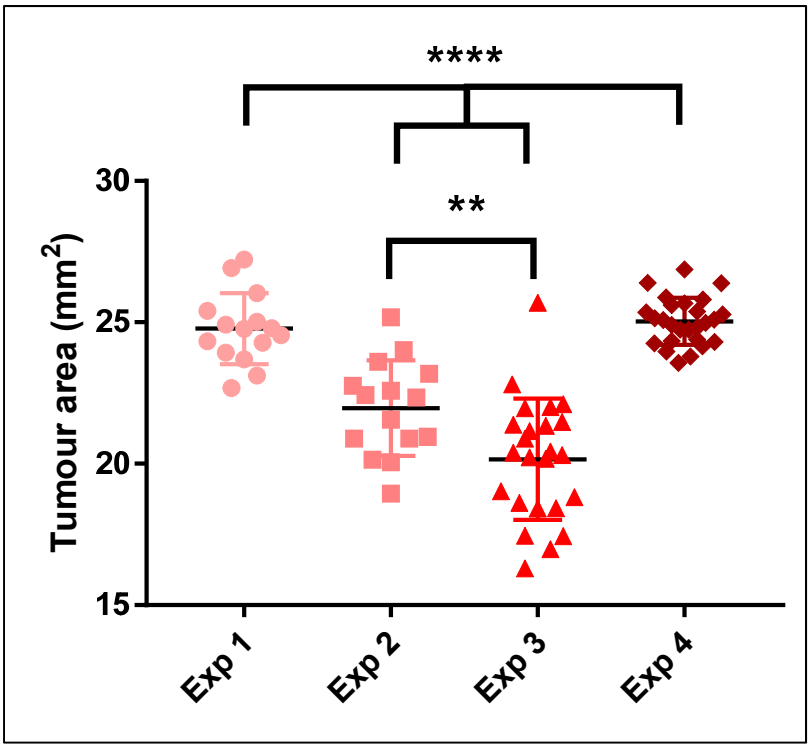

Figure 4-30 Untreated MC38 tumour reproducibility at treatment
Individual values and mean ± SD are compared for 4 experiments at treatment, ** $p < 0.01$, **** $p < 0.0001$ n = 5 mice per experiment

When experiments were compared for later tumour growth (after treatment time in the untreated group only), 1 of 3 experiments has different normalised growth (Figure 4-31). This indicates a moderate level of reproducibility for the untreated groups in the MC38 model, with some variability.

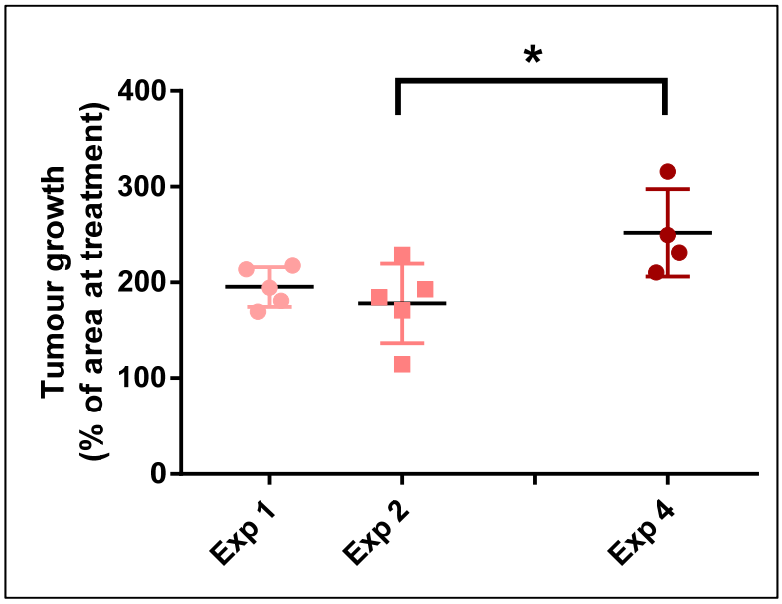

Figure 4-31 Untreated reproducibility 10D after treatment
Individual values and mean ± SD are compared for 3 experiments (1, 2 and 4) * $p < 0.05$, n = 4-5 mice per experiment

Reproducibility of IV treatment and OT-stimulation

Another important aspect to consider is the reproducibility of the bioactivity of the injected cells. It can be assessed by the efficacy of the IV treatment (Figure 4-32) but also by direct assessment using flow cytometry (Figure 4.33 and Figure 4.34). Flow cytometry initially showed that OT-I stimulation over 3 days lead to greater CD25 expression than 4 day stimulation (Figure 4-33). We were therefore particularly interested to compare Exp 1-2 (3-day stimulation) to Exp3-4 (4 day stimulation). Surprisingly, we didn't observe reduced tumour growth with experiments 3 and 4, in fact no statistically significant differences were observed. Experiment 2 was the only one that visibly differed (only 76 ± 30% of their original size at day 10 after IV treatment, compared to about 150% for the 3 others). We have no explanation for this difference. Unfortunately errors in the flow cytometry analysis of the cells used for the 4 experiments mean we cannot compare CD25, a marker of T cell activation, between the two stimulation protocols for cells used in vivo. However, the difference between CD25 expression in Figure 4-33b and

Figure 4-34 shows that shortened stimulation can result in T cells with higher activation. These results suggest that the bioactivity and survival of OT1 after stimulation was highly variable and the process requires improvement. It also shows the importance of testing the bioactivity of the cells in parallel to each animal experiment.

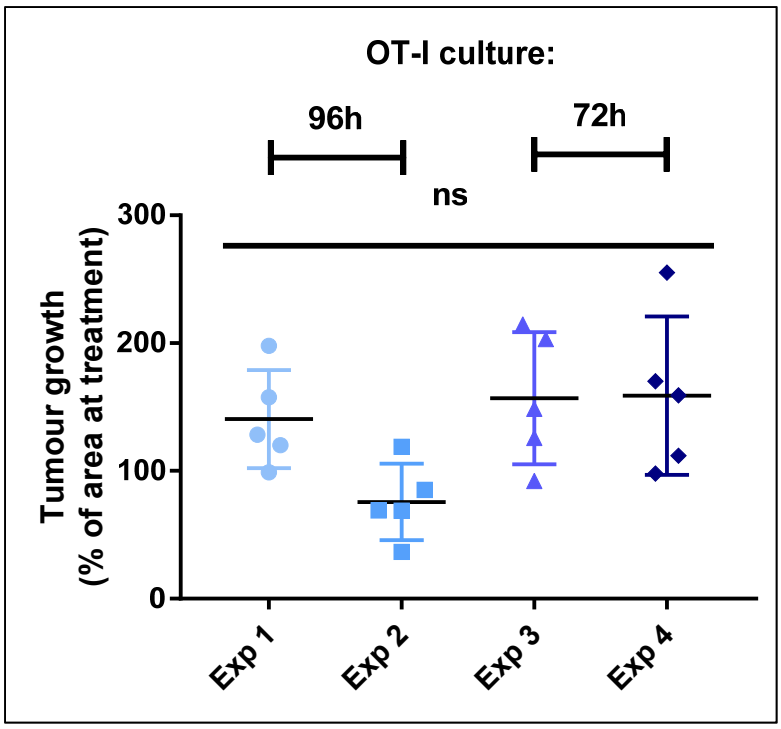

Figure 4-32 IV-treated MC38 tumour reproducibility
All experiments. Individual values and mean ± SD are compared for normalised tumour growth 10D after treatment n = 5 mice per experiment

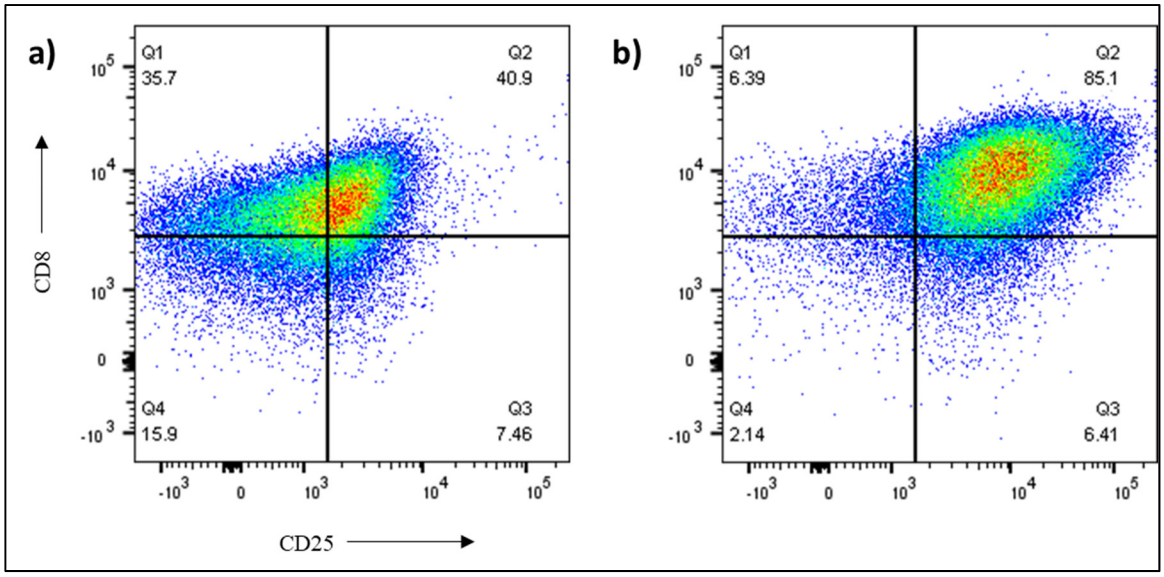

Figure 4-33 FACS plots of stimulated OT-I
Representative flow cytometry plots showing CD8 and CD25 expression of OT-I stimulated in vitro over a) 96h or b) 72h (N = 2 n = 2)

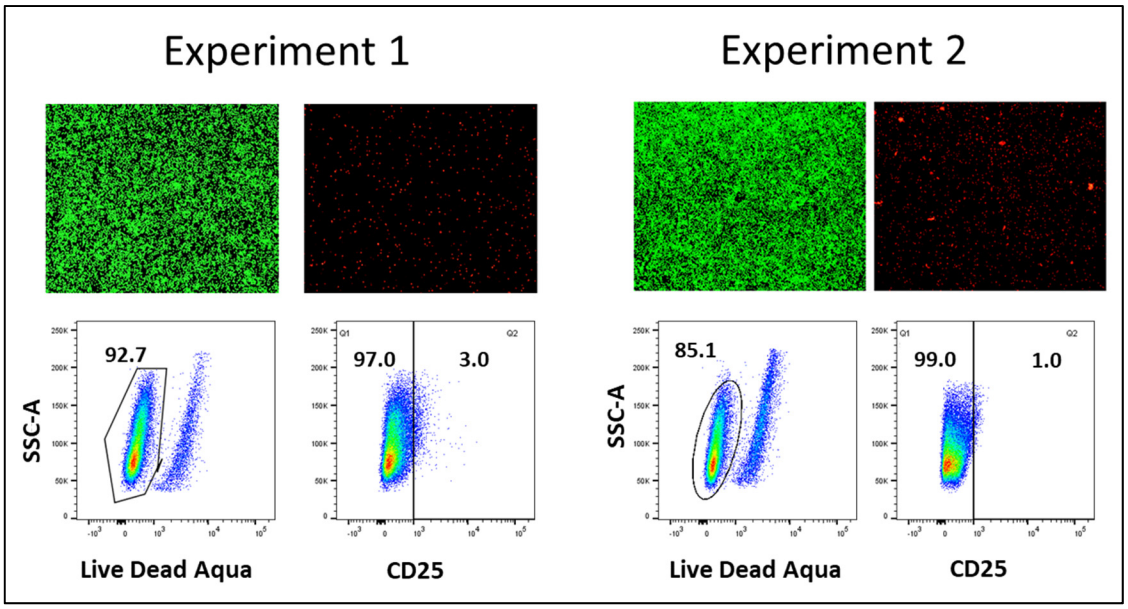

Figure 4-34 FACS plots of OT-I used in vivo
Cell viability and activation of OT-I used in first and second MC38 tumour growth experiments. Live dead assay images are shown of 1M OT-I used in vivo, showing live (green) and dead (red) cells. Also shown are FACS plots of cell viability (Live-Dead Aqua) and cell activation (CD25) for both experiments

4.7 In vitro cell migration and bioactivity

4.7.1 Transwell model

To further understand the limitations and mechanisms of T cell delivery scaffold, in vitro assays were performed. For successful local delivery of T lymphocytes as a cancer immunotherapy, the cells must not only survive within the gel, but they must also be capable of migration out of the gel, towards the tumour. We therefore tested the ability of encapsulated OT-I (in the upper chambers of the transwells) to escape and reach the lower portion of the transwell where either MC38-OVA or MC38 (not expressing OVA) cancer cells were previously seeded.

Figure 4-35 presents the analysis by flow cytometry of the cell population in the lower transwells. In macrogel, many more OT-I cells (identified by positive CD8 and CD25

labelling) escape the macrogel and migrate into the lower transwell portion in response to the presence of MC38-OVA cells (66±17% of the recovered cells were $CD8^+CD25^+$), as opposed to MC38 without OVA where migration is much reduced (24±19% $CD8^+CD25^+$). This was expected since OT-I specifically recognize and are activated by OVA-expressing cells. This data demonstrates the ability of the encapsulated cells to escape the macrogel. Migration from the microbeads seems greatly diminished, virtually negligible compared to the macrogel, at 3±3% and 4±7% of total cell number respectively for MC38 and MC38-OVA transwells respectively. We can however see that cell escape is possible since some cells were observed in the transwell in the condition without cancer cells ($CD8^+$ cells are then more visible, since they are not hidden by the large proportion of cancer cells).

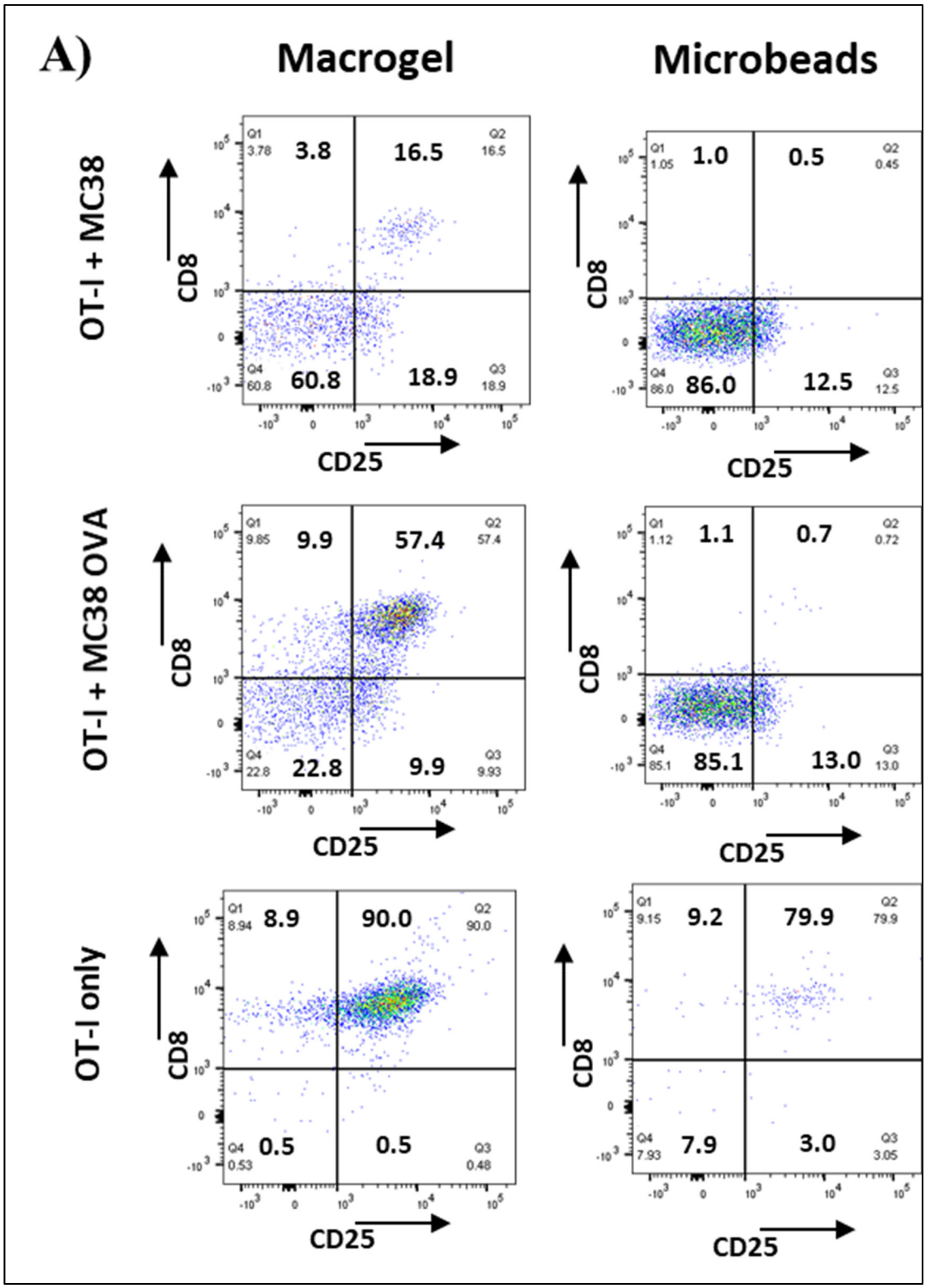
A)
Macrogel
Microbeads
OT-I + MC38
OT-I + MC38 OVA
OT-I only
CD8
CD25
Q1 3.78
3.8
Q2 16.5
16.5
Q4 60.8
60.8
18.9
Q3 18.9
Q1 1.05
1.0
0.5
Q2 0.45
Q4 86.0
86.0
12.5
Q3 12.5
Q1 9.85
9.9
57.4
Q2 57.4
Q4 22.8
22.8
9.9
Q3 9.93
Q1 1.12
1.1
0.7
Q2 0.72
Q4 85.1
85.1
13.0
Q3 13.0
Q1 8.94
8.9
90.0
Q2 90.0
Q4 0.53
0.5
0.5
Q3 0.48
Q1 9.15
9.2
79.9
Q2 79.9
Q4 7.93
7.9
3.0
Q3 3.05

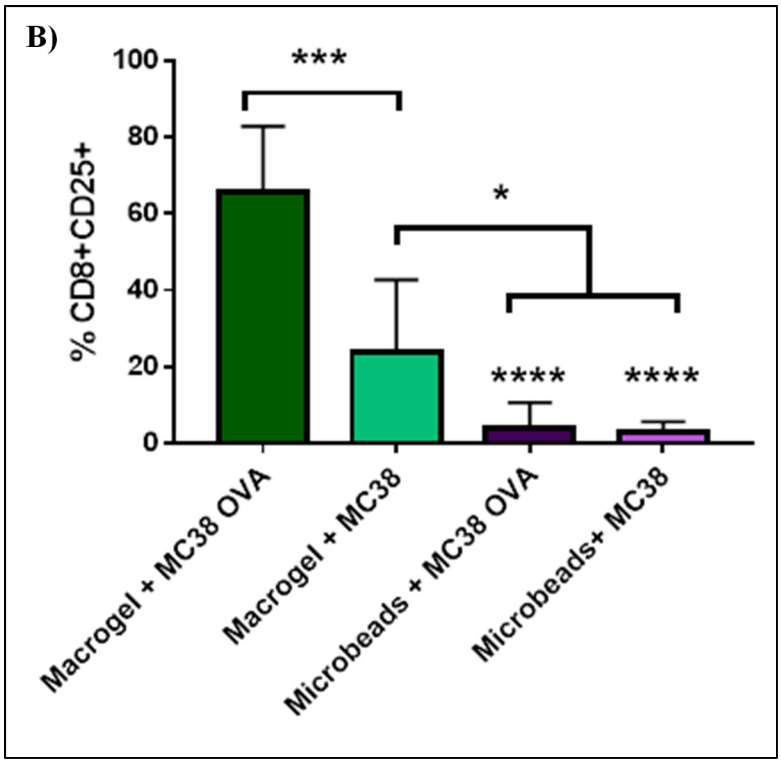

Figure 4-35 OT-I migration out of macrogel and microbead scaffolds
A) Representative flow cytometry of OT-I in lower transwells at D3 for P18 macrogel and microbead encapsulated OT-I, displaying CD8 and CD25 expression. OT-I cells are CD8+ and CD25 expression indicates cell activation. Results for conditions with MC38 without (top) and with (middle) the OVA antigen are shown, demonstrating the attractive effect of MC38-OVA. Conditions without cancer cells in the lower transwell are shown on the bottom row B) percentage of CD8+CD25+ cells among the recovered cells in lower transwells at D3 (mean ± SD; N = 3, n = 4 ; *$p < 0.05$, ***$p < 0.0005$ and ****$p < 0.0001$ compared to Macrogel + MC38 OVA

4.7.2 3D model

Alongside the transwell assays, a 3D in vitro tumour model was developed as an alternative, to investigate the effect of changing various parameters on OT-I migration and function. 3D models, as opposed to 2D models with a layer of cancerous cells representing the tumour – as in the transwell model – better represent the morphology and tissue structure of a tumour in vivo, which can in turn affect processes such as cell signalling to further mimic in vivo behaviour.

In this model a ‘core’, containing cancerous cells (MC38 or MC38-OVA) supported on matrigel and collagen is surrounded by the OT-I-containing hydrogel. Both cancerous cells and OT-I are fluorescently marked, and the interaction between OT-I and cancer cells was observed over time via confocal microscopy and cell tracking. As well as the chitosan hydrogel, matrix combinations were also investigated such as chitosan-gelatin to test any effect of these matrix addition on migration or function.

Figure 4-36 shows the interactions between encapsulated OT-I in different macrogel formats, with different cancerous cells (MC38 & MC38-OVA) and at different sites in the 3D model: the inner gel (Figure 4-36A), the intersection of the two gels (Figure 4-36B, left columns), and the outer gel (Figure 4-36B, right columns). The calculated density of OT1 cells within the gel at Day 0, 1 and 3as a function of time is presented in Figure 4-37.

For the macrogel with MC38 cells, the number of OT-I at the gel intersection and in the outer gel increases over time from days 1 to 3. Furthermore, the OT-I escape the macrogel (seen at day 3) but do not interact with the MC38. For the chitosan macrogels with MC38-OVA cells, the number of OT-I in the gel tend to increase slightly at Day 1 but did not increase further at Day 3, probably because many cells escaped the gel to reach the tumour. Indeed, more OT1 were seen in the inner gel where cancer cells had been clearly attacked, as seen by their lower number and different morphology. This confirms that the encapsulated cells can grow and escape from the macrogel and attack the MC38-OVA cells.

Preliminary results were also obtained for other gel formulations and formats (chitosan-gelatin and microbeads). In CH-gelatin gels, the number of cells tend to increase more with time compared to pure chitosan gels, but the difference was not significant due to high variability. Since cell density is the result of cell growth (increasing cell number) and cell escape (decreasing cell number), this data does not allow us to compare cell growth within the two formulations.

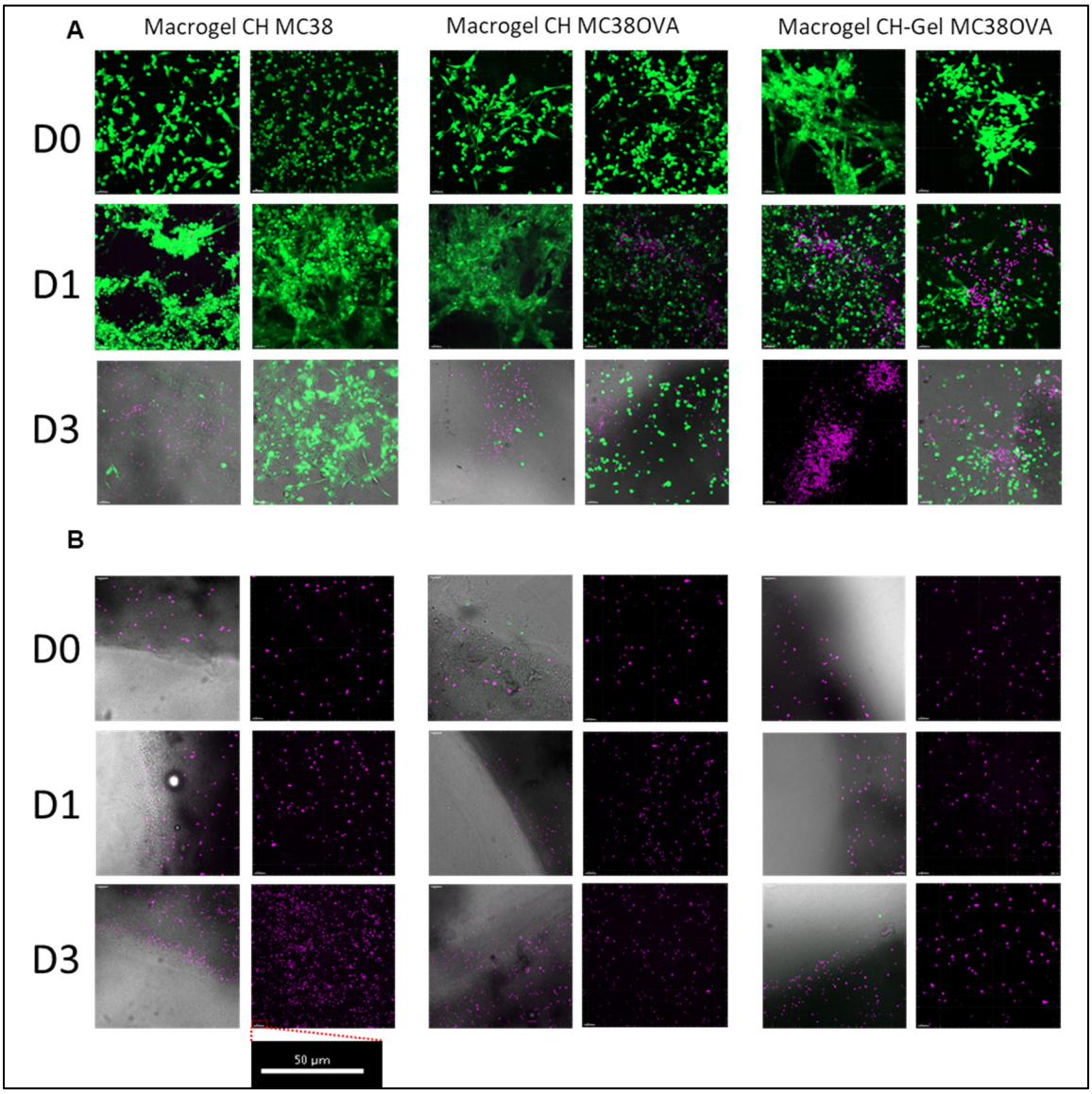

Figure 4-36 Interaction between encapsulated OT-I and cancer cells
(A, B) In vitro imaging of OT-I, MC38 and MC38-OVA in the 3D tumour model at multiple timepoints via confocal microscopy. Images were captured at days 1 and 3 in (A) the inner part of the model ('tumour-like gel'), (B) at the gel intersection (left images) and in the outer part (gel loaded with OT-I; (right images). For the gel intersection, the grey portion indicates the inner gel, whereas the black portion indicates the outer gel. MC38 and MC38-OVA are stained in green, OT-I in purple (scale bar = 50µm) N = 3; n = 3

Data from microencapsulated OT1 cells (Figure 4-37B) shows a clear difference in the number of encapsulated and retained OT-I between hydrogel formats. Macrogels (Figure 4-37A),

particularly the CH-Gel macrogel, contain significantly more living OT-I than the microbeads (Figure 4-37B) at day 0 ($p < 0.05$ for CH, $p < 0.01$ for CH-Gel). There are also significantly more OT-I present in the CH macrogel at day 1 than at any timepoint in the CH microbeads ($P < 0.05$).

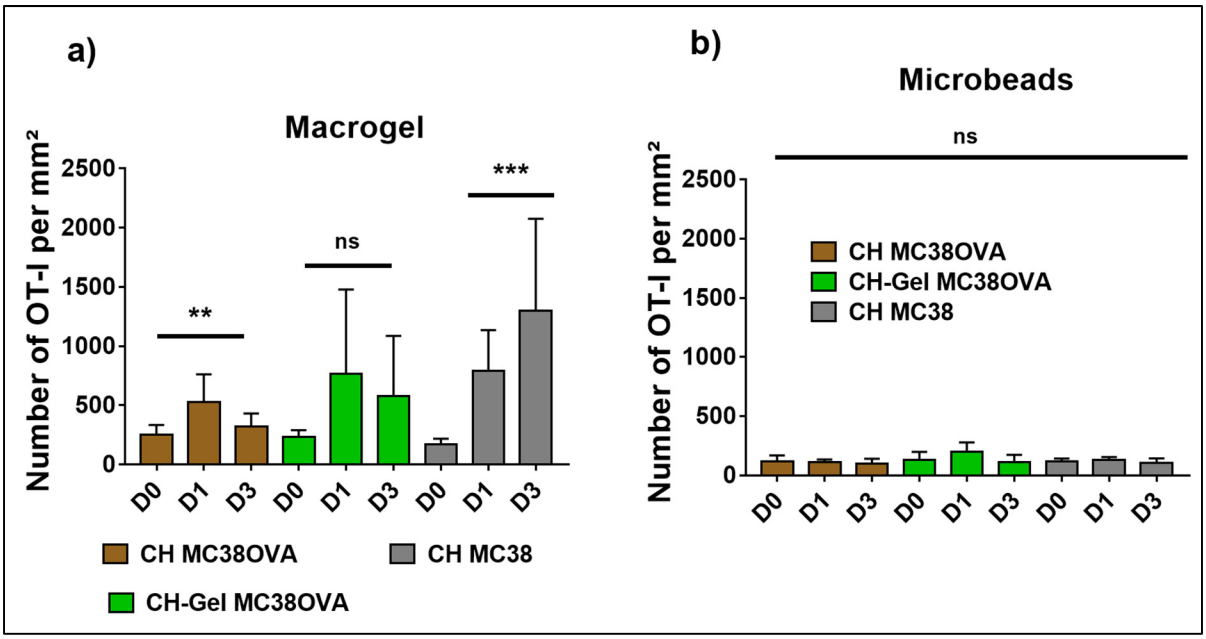

Figure 4-37 OT-I density as a function of time
OT-I density is shown (Days 0, 1 and 3) in the different hydrogels. a) In macrogels (mean ± SD, n=3; N=3); b) in microbeads (mean ± SD, n=2; N=2) (**p<0.002, (***p<0.0001)

The average speed of OT-I in chitosan (CH) and chitosan-gelatin (CH-Gel) macrogels was measured at day 1 by a 30 min Live Imaging sequence, to determine if the gel composition could influence cell migration within the gel. Figure 4-38a shows the average OT-I speed in each group at each timepoint, during the 30-minute evaluation period.

OT-I migrate more slowly in the chitosan gel compared to chitosan-gelatin. Average cell speed is 0.044 µm/s ± 0.003 (min= 0.039; max =0.056) in the CH gel and 0.052 µm/s ± 0.003 (min=0.044; max= 0.063) for the CH-Gel (****p<0.0001, Figure 4-38b).

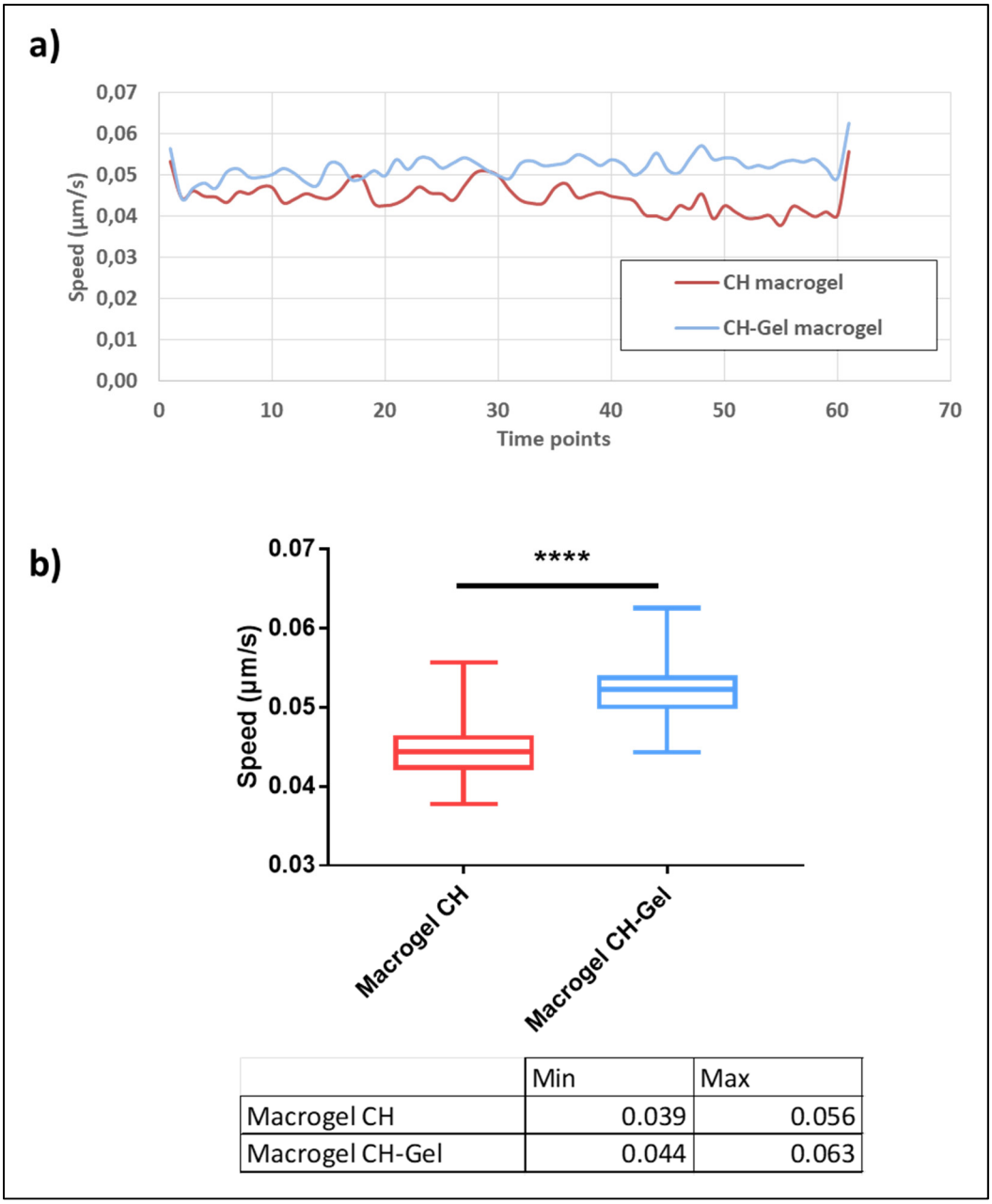

	Min	Max
Macrogel CH	0.039	0.056
Macrogel CH-Gel	0.044	0.063

Figure 4-38 Average speed of encapsulated OT-I
Average speed of OT-I encapsulated in chitosan and chitosan-gelatin macrogels. a) Average of measures taken from confocal microscopy photos captured every 30s over 30 minutes. b) A box plot of the results showing the median, upper and lower quartiles and the minimum and maximum values, also shown in the table. An unpaired t test confirmed the significant difference between the two groups (****$p<0.0001$), $n \geq 67$; N=3

Finally, flow cytometry was performed on the inner gel after digestion, to obtain further information about the activation status of the OT-I and apoptosis in the cancer cells, using markers such as CD25 as an OT-I activation marker and annexin V to as a marker of cancer cell apoptosis.

Unfortunately, current data is unconvincing due to the very low cell numbers acquired and the high variability of the results so no conclusion was drawn from these results. The protocol needs to be optimized for future use.

4.7.3 Improvement of OT-I viability in microbeads

As described above, while the feasibility of microbead encapsulation has been demonstrated, OT-I survival in microbeads is lower than in the macrogel. Further improvement of the microencapsulation technique or microbead composition is required to improve cell survival. Several factors might explain the higher mortality rate in microbeads. Some are related to the microencapsulation process 1) mechanical stress during microencapsulation process, which uses a high stirring rate (>1000rpm); 2) potentially cytotoxic components of the emulsion process such as mineral oil. These are related to the fabrication process and could not easily be modified. Others possible factors are 3) the high cell density (in the macrovolumic gel of 8M cells/ml may be too high for optimum cell viability in the microbeads; 4) the lack of peptide binding sites or bioactive factors as found in the native ECM.

Several attempts were made to improve cell survival, including a reduction in cell density, an alternative alginate microbead composition, and addition of bioactive components such as gelatin to the chitosan microbeads. Here again gels were made with 10% FBS in the cell suspension media to match previous experiments and maximise chances of cell survival.

4.7.3.1 Microbead encapsulation as a factor in OT-I mortality

If mortality is present immediately following encapsulation, then regardless of the scaffold composition or culture conditions, many cells have already been lost. Live/Dead imaging in showed that, indeed, significant OT-I mortality is observed immediately after encapsulation in chitosan microbeads (Figure 4-39). Not only is this mortality observed, but it is not present in non-encapsulated OT-I, clearly demonstrating that the encapsulation process contributes to this mortality. Clearly the violent stress applied to cells under vigorous mixing conditions is an important factor.

4.7.3.2 Survival in alginate microbeads

While acceptable chitosan beads could not be formed at stirring rates much lower than 1100 rpm, alginate microbeads fabrication only requires stirring at 300 rpm, thanks to the lower viscosity of the pre-gel solution. For this reason, investigation of OT-I viability at D0 in alginate beads may answer the question of if the high rotation speed of the spinner flask contributes to OT-I cell death in microbeads. Figure 4-39 presents live/dead images of OT1 cells in alginate microbeads at D0 (immediately following microbead formation) and Day 3. OT-I survival is markedly improved in alginate beads compared to chitosan beads. This suggests that the rotation speed in the flask during emulsification has a significant effect on OT-I survival and 1100rpm is too fast, resulting in a stress that damages and kills the OT-I cells.

However, very few live cells are observed at D3 in alginate microbeads. The greater number of dead cells visible at D3 vs D1 also supports the conclusion that cells die in the gel rather than escape. This highlights the further issue that alginate alone is a suboptimal biomaterial due to its limited bioactivity and porosity and would almost certainly require further additions – gelatin for example as other groups have shown as well as stimulatory molecules for OT-I such as CD3 and CD28 – to allow OT-I survival over an extended period.

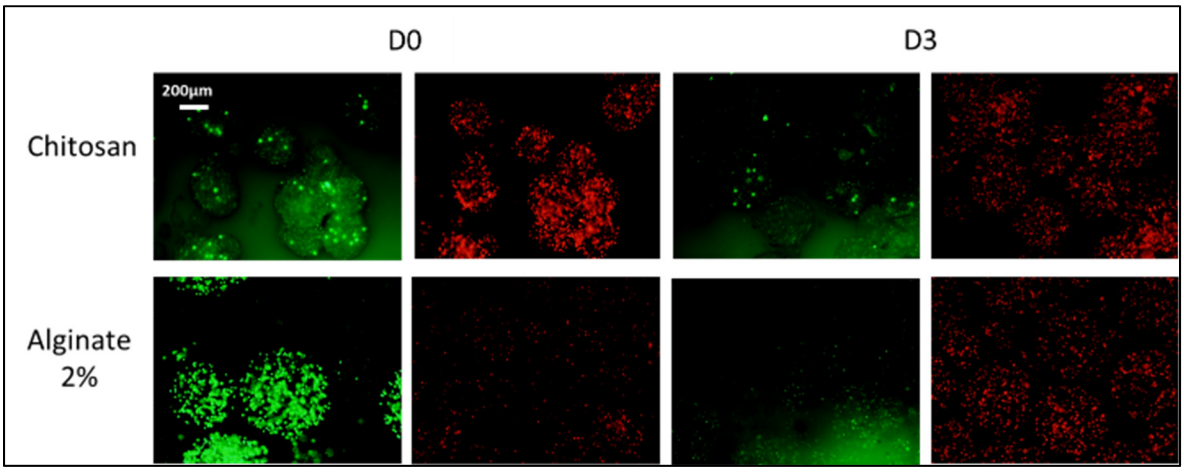

Figure 4-39 OT-I viability in alginate microbeads
Representative images of OT-I survival in alginate microbeads, compared to P18 chitosan, assessed with Live Dead assay, immediately after encapsulation and at D3 (N = 2, n =2 two independent experiments with one well/condition)

4.7.3.3 Cell concentration¸

One hypothesis for the observed cell mortality was the high concentration of cells within the gel. High cell concentration was necessary to deliver enough cells locally in a gel volume suitable for mice, but this required a concentration (8M/ml) significantly higher than the concentrations at which OT-I are expanded, for example (1M/ml). Cell viability 24h after encapsulation was tested with a Live/Dead assay, with various cell concentrations (2, 4 and 8 m/mL. Figure 4-40 shows that high mortality is present regardless of cell concentration. Reducing cell concentration does not reduce this mortality so is probably not a factor, and in fact a reduced cell concentration will probably only limit further the number of viable OT-I encapsulated in the beads.

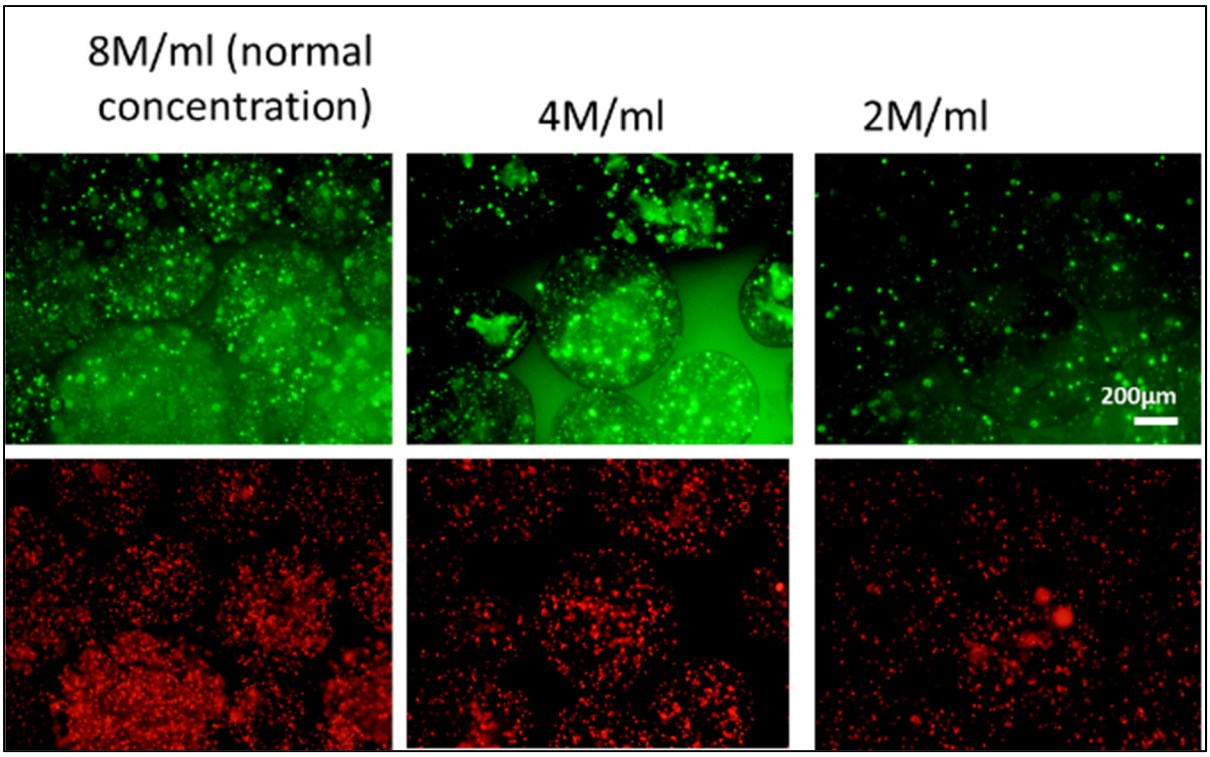

Figure 4-40 Cell concentration effect on OT-I microbead survival
Representative images of OT-I survival at 24h in P18 gel microbeads with decreasing OT-I concentration from 8M/ml to 4M/ml and 2M/ml, assessed by LIVE/DEAD assay (green = live, red = dead; (N=2, n = 2, two independent experiments with one well/condition

4.7.3.4 Effect of collagen or gelatin addition on OT-I survival in microbeads

As with the macrovolumic gels, modifications to the gel matrix were briefly investigated such as the addition of collagen and gelatin. A proportion of 25% of the gel was replaced by PureCol® EZ Gel, giving a final concentration of 0.125% w/v of type I bovine collagen in the gel and the inclusion of type A gelatin during chitosan solubilisation, for a final concentration in the gel of 1%, was investigated. The hypothesis was that collagen or gelatin could add cell-binding motifs and hence improve cell viability. Live/Dead assays at days 1 and 3 investigated any effect on cell survival or proliferation of the inclusion of collagen, though the live/dead imaging shows that no clear benefit is obtained from the addition of collagen in terms of cell survival or proliferation (Figure 4-41). With the short-term mortality observed in microbeads,

as well as limited proliferation expected in only once-stimulated OT-I, it is perhaps to be expected that collagen offers little benefit. Perhaps its benefits would be more clearly seen in a system where stimulated OT-I proliferate long-term, but currently little benefit of collagen is observed.

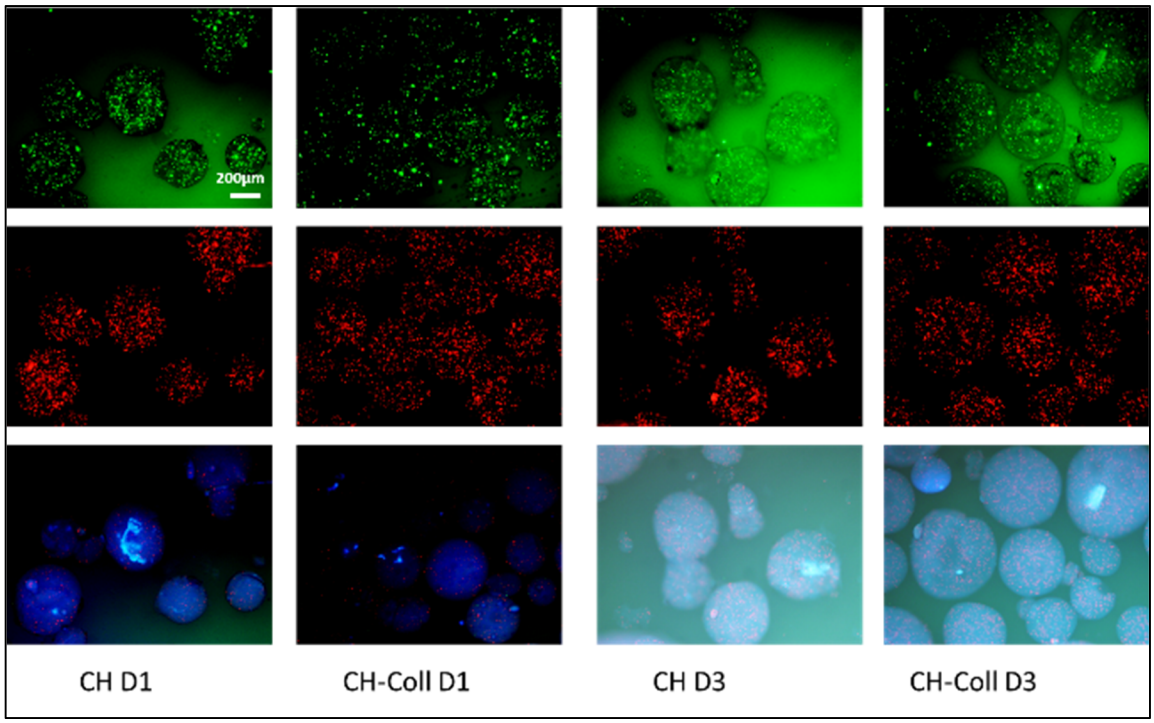

Figure 4-41 OT-I viability in chitosan-collagen microbeads
Representative images of OT-I survival in chitosan microbeads made with 10% FBS, with chitosan alone or 0.125% collagen (25% gel volume), demonstrated over 3 days, assessed by LIVE/DEAD assay (green = live, red = dead; (N=2, n = 2, two independent experiments with one well/condition)

Chitosan-gelatin microbeads like collagen do not show a significant improvement in OT-I cell viability over 3 days of culture at days 1 and 3 based on live/dead images (Figure 4-42). Again, without evidence that OT-I can proliferate in our system under any conditions, it may be that the benefit of gelatin addition is only seen with cells that are already capable of proliferation, such as human T cells.

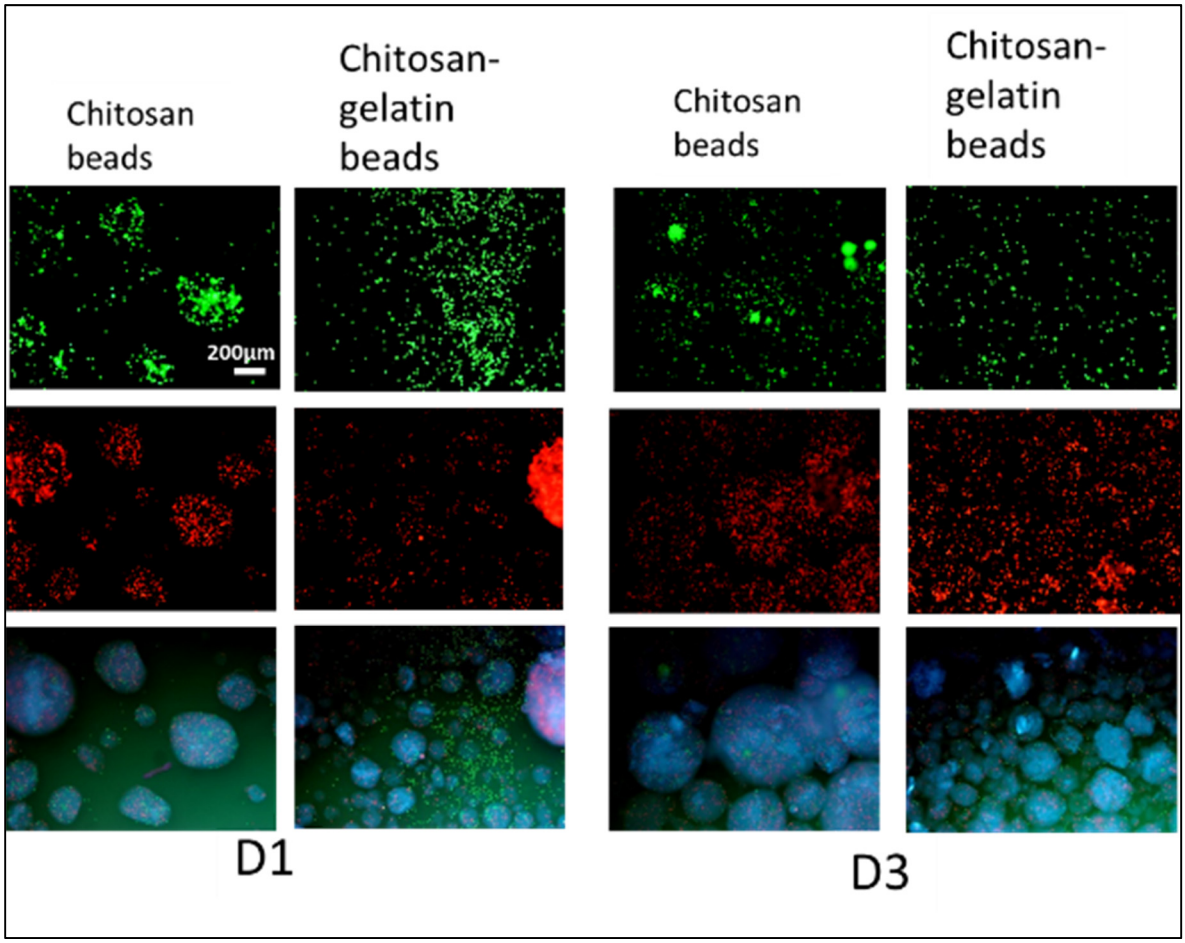

Figure 4-42 OT-I viability in chitosan-gelatin microbeads
Representative images of OT-I survival in P18 chitosan microbeads with chitosan alone or chitosan + 1% gelatin type A, demonstrated over 3 days with Live Dead assay in microbeads. (N=2, n = 2, two independent experiments with one well/condition)

CHAPTER 5

DISCUSSION

As described in the literature review section, current immunotherapy treatments including ACT suffer from limitations associated with their systemic delivery, such as the high number of cells required and dose-related toxicity of administered therapeutics. Biomaterials offer potential avenues to address these limitations by localising treatments and therefore potentially reducing dosages improving efficacy (Koshy & Mooney, 2016).

In this PhD project, our goal was to evaluate the feasibility, safety and efficacy of an injectable, thermosensitive chitosan hydrogel as a scaffold for the localised delivery of immune cells as an anti-cancer treatment. With our group having previously established survival and functionality of human immune cells within the chitosan hydrogel (Monette et al., 2016), our main objective was to demonstrate its degradability and biocompatibility, but most importantly its efficacy as an anti-cancer treatment. In this chapter we will discuss the obtained results and how they relate to our hypothesis that localised treatment would result in similar efficacy to IV treatment – immediately based on the current results we can say that our localised treatment did not show similar efficacy compared to systemic intravenous treatment, though its efficacy was only slightly shorter than IV treatment. Moreover, we will summarize what has been learned about the mechanisms behind its potential anti-cancer effect and both the potential and limitations of the technology. We will also discuss the limitations of our in vivo model and some experimental techniques such as intravital microscopy and immunohistochemistry and make recommendations for future work and what future developments could further improve the system.

5.1 Treatment efficacy

5.1.1 Macrogel efficacy

In the MC38-OVA in vivo tumour model gel and IV-treated mice demonstrated slowed tumour growth compared to untreated mice, confirming the effect of the positive IV control and our localised gel treatment.

Gel-treated mice showed significantly reduced tumour growth for almost as long as IV-treated mice (11 vs 14 days), particularly impressive given that over 3 times fewer OT-I were administered (1.6M locally vs 5M intravenously). However, both treatments had a time-limited effect.

The interaction between OT-I and MC38-OVA cells is also confirmed in the transwell and 3D models, where OT-I escape and elimination of cancer cells is shown, as is the lack of interaction between OT-I and MC38 cells. This is evidence of the specific cytotoxic action of OT-I on MC38-OVA, though further controls could be added in future experiments either in vivo or in the in vitro models to definitively confirm this specificity, such as non-OT-I T cells in vivo or in vitro or MC38 in vivo.

5.1.2 Increased IV efficacy vs gel

Numerous factors could explain the greater efficacy of IV treatment compared to the macrogel, including the differing numbers of OT-I administered between treatments, rapid cell death in the scaffold, as well as access to the bloodstream and lymphatic systems before reaching the tumour.

The dose of OT-I administered intravenously was fixed based on other publications (Klebanoff et al., 2011; Visioni et al., 2018), and is one variable that could be adjusted to optimise treatment efficacy, with these groups showing a dose-dependent anti-tumour response and

almost complete tumour elimination with the administration of 10-100M OT-I, though in B16-OVA models.

Another reason why IV treatment can be more efficient may be some immunological priming that is undertaken by the intravenously injected OT-I during their passage through the bloodstream and potentially lymphatic system on the way to the tumour. Though the administered OT-I are activated prior to injection, classical antigen presentation and T-cell activation generally occurs in lymphoid tissue such as lymph nodes and involves other immune cells such as B cells (Waldman et al., 2020). In addition, this is the same mechanism through which tertiary lymphoid structures, the immune tissues that ultimately we attempt to replicate, ameliorate cancer immunotherapies through these immune cell interactions and antigen presentation (Aoyama, Nakagawa, Mulé, & Mailloux, 2021). It may be that this additional immune stimulation is only experienced by the OT-I cells in IV-treated mice. Optix imaging could support this theory, given the passage of OT-I through the vascular and lymphatic system via the lungs and spleen is visible, which is not the case for gel-treated mice.

A further difference in IV and locally-treated mice is the access to nutrients and oxygen, which are likely to be limited in the subcutaneous tumour environment experienced by locally-injected OT-I, particularly compared to intravenous OT-I. Intravital microscopy showed that IV-injected OT-I reach the tumour via the bloodstream, potentially also passing though lymphoid organs such as the spleen. Passage through the bloodstream or lymphatic system by gel or locally-injected OT-I was not observed, either as it was not present or it was obscured by the much greater local Optix signal concentration. No vascularisation was observed throughout the scaffold and so this could be an important difference between the IV and Gel-treated mice. This could explain the shorter duration of reduced tumour growth in the Gel-treated mice compared to the IV-treated mice.

Vascularisation and hence sufficient oxygen and nutrient delivery remains a challenge for all tissue engineering applications (Rademakers, Horvath, van Blitterswijk, & LaPointe, 2019), and lymphoid tissue engineering is no different. Vascularisation is also important in this

application to allow easier migration of T cells towards the tumour through blood vessels, rather than having to migrate through tissues.

This was our rationale for the creation of chitosan microbeads for T cell delivery, though as previously discussed the limitations of the microbead encapsulation process currently negate any potential benefit of the improved surface area/volume ration in microbeads.

Histological data suggests that limited OT-I persistence in all treated conditions plays a part in the time-limited anti-tumour response, where OT-I are clearly visible in H&E staining immediately following injection within the gel and microbeads but seem to disappear, either rapidly escaping or dying within the gel, after just 24h. We believe this is due to their rapid escape, rather than cell death as no significant signs of apoptotic cells were observed in H&E staining. The gelation speed of the current gel formulation may not be sufficient for cell retention, and it is possible that many OT-I escape in the first 24h while gelation occurs. Furthermore, CD8 immunofluorescence did not show obviously increased numbers of intratumoral or intra-gel CD8 in any treated group. If poor vascularisation or nutrient supply plays a role in this limited persistence, this could again explain why IV-treated mice show greater efficacy.

Indeed, other groups working in this area recently switched their focus from an alginate macrostructure to a thin nitinol film due to challenges in nutrient diffusion and cell survival (Coon et al., 2019) or included oxygen-rich scaffold components to combat the hypoxic environment in vivo (Zuyuan Luo et al., 2020). Therefore, both our results and the literature support the necessity and benefit of close nutrient and oxygen supply and this may explain any difference between IV and gel treatment.

As had been previously demonstrated (Monette et al., 2016), transwell models demonstrated the ability of OT-I to escape from the gel towards MC38 and MC38-OVA in vitro. Passive cell escape from the gel is also shown in macrogel models, indicating that OT-I can escape from the gel. OT-I migration towards tumour cells was observed as early as 24h in the 3D in vitro

model, indicating that rapid cell escape may therefore also contribute to the limited cell persistence in vivo, as an alternative explanation to rapid cell death. The relative contributions of cell death compared to cell escape remain difficult to assess in vivo without alternative methods of cell tracking.

Limited OT-I cell survival could also have contributed to the limited efficacy of the gel treatment. Having successfully re-optimised the hydrogel formulations to obtain gels with suitable gelation properties and JURKAT/PBMC proliferation, it was necessary to demonstrate successful OT-I encapsulation and survival in the gel. OT-I survival up to 72h after encapsulation was demonstrated, though with limited survival past this timepoint. This is not unexpected based on results reported elsewhere, with other groups following similar stimulation methods to our own (CD3 and CD28 stimulation) when using OT-I for in vivo ACT models, with MHC-peptide complexes (pMHC) occasionally used as an alternative (Visioni et al., 2018; J. Zhou et al., 2018). OT-I for intravenous transfer are generally used as soon as possible after sufficient stimulation, and as such limited survival in vitro is not problematic. In the literature data, when characterised in vitro, OT-I are rarely used more than several days after isolation, indirectly indicating their limited utility long-term in vitro. Due to this limited survival, OT-I may not be the optimum immune cell model for biomaterial-delivered ACT. Human CAR T cells seem to be more commonly used and may be more successful due to their more simple and successful culture in vitro (Coon et al., 2019; Zuyuan Luo et al., 2020).

Another striking result is the increased migration of OT-I cells towards the MC38-OVA cells vs MC38 cells. Interesting recent work has shown that CD8 effector cells can themselves secrete the chemokines CCL3 and CCL4 upon interaction with their cognate antigen (Galeano Niño et al., 2020). This creates a positive feedback loop that invokes a “swarming” behaviour attracting further CD8 cells, which we can suppose is what we observe in these results. There seems to be some contradiction in the difference between macrogel and microbeads in our transwell model and in vivo results, where when compared (though admittedly only in a single experiment) the macrogel and microbeads showed equivalent efficacy in slowing tumour

growth. OT-I mortality in the microbeads, combined with these results, raises the possibility that a factor other than the OT-I in the microbeads is responsible for their treatment effect.

Finally, intuitively it would seem that the thin fibrous encapsulation observed after 4 weeks or more in vivo would inhibit T cell activity and hence treatment efficacy, although our treatment effect was not durable enough for this long-term process to clearly have a significant impact. Despite this concern, the nitinol biomaterial of Stephan's group also reported thin fibrous encapsulation of the biomaterial, without obvious detrimental effects on the treatment. It may be that with sufficient survival and proliferation of delivered T lymphocytes, they either bypass this encapsulation or they can establish their presence in the body and lymphatic system before being trapped within the fibrotic tissue. Vascularisation of the scaffold or its surroundings may be key to addressing this fibrotic response.

The above limitations and challenges highlighted the need to improve the gel to obtain efficacy equal to or ideally greater than the IV treatment, for example in the microbead format.

5.1.3 Gel improvement with microbeads

Chitosan microbeads developed in our lab were explored as an alternative to the chitosan macrogel, to improve nutrient and oxygen diffusion and hence potentially enhance OT-I survival within and escape from the gel to the tumour, and subsequently improve treatment efficacy. Microbeads with reduced concentrations of both FBS and BSA (acting as a surfactant) were successfully developed, minimising the potential inflammatory reaction to exogenous FBS in vivo and allowing the possibility of microbeads as an in vivo T cell scaffold. Despite this, microbeads appeared to provoke a greater inflammatory reaction in vivo than the macrogel, possibly indicating that even small amounts of FBS provoke strong inflammation.

In vitro, OT-I successfully escape the macrogel and migrate towards tumour cells. However, a much more limited cell number observed escaping from microbeads is apparent in FACS data, as well as in the preliminary data with the 3D tumour model. It can be at least partly explained

by the high cell mortality in these experiments. This prevents definitive conclusions on whether microbead encapsulation can augment OT-I migration and escape or in contrast decrease cell escape due to lower porosity or surface tension. An alternative to OT-I that is more robust during microencapsulation may be necessary to show the potential benefit of microbeads in terms of T cell migration from the gel to the tumour.

One clear limitation of the microbead-encapsulated OT-I is the high mortality seen immediately after encapsulation. As was previously highlighted in the results section, vigorous mixing at 1100rpm in the spinner flask during microbead encapsulation is clearly one of the biggest factors in this mortality. This is most apparent in the comparison of OT-I cell viability in LIVE/DEAD assays of alginate versus chitosan microbeads immediately after encapsulation, where far greater cell survival is observed in alginate microbeads. High mortality in microbead-encapsulated OT-I is also probably responsible for the low numbers of migrating OT-I in the transwell model. To reduce this problem, the microencapsulation process could be modified by changes to the gel formulation to reduce viscosity or alternative microencapsulation methods such as the use of microfluidics could allow a reduction in the stress applied to cells during the microencapsulation process and hence improved viability.

However, despite this improvement in immediate survival, microbeads made with alginate alone are not a viable alternative to chitosan microbeads due to the high OT-I cell death observed in alginate microbeads at D3 after encapsulation. Here the benefits or drawbacks of microbead encapsulation may start to be hidden by intrinsic difficulty of the OT-I model. As encapsulated OT-I do not proliferate under our culture and stimulation conditions, it can be difficult to differentiate if cell death is due to general limited survival of OT-I in vitro or the unsuitability of alginate beads alone as a scaffold. Owing to the bioinert nature of alginate, the answer is probably a combination of both. Furthermore, the limits of the OT-I model may hide the potential benefits of microbead encapsulation such as oxygen and nutrient transfer, known to be relevant in scaffold for ACT as this was the rationale for the use of the nitinol mesh by Stephan's group. Again, further work using more resilient immune cells such as PBMC or human CAR T cells could be performed to better assess the benefit of microbeads.

5.1.4 Role of inflammation in the efficacy of the scaffolds

The significant inflammation observed around hydrogel and microbeads could play a role in its anti-tumour efficacy as cells involved in the inflammatory response to the chitosan gel can possess anti-tumour functions.

The inherent immunoreactive properties of chitosan itself may affect the anti-cancer immune response. The interactions between chitosan and the immune system are a subject of debate, with chitosan seemingly provoking both pro-inflammatory and anti-inflammatory immune responses (Cai, Li, Akinade, Zhu, & Leong, 2021). In one study, both high and low molecular weight chitosan increased levels of the anti-inflammatory cytokine IL-10 (Davydova et al., 2016), whereas another showed that chitosan induced DC maturation and hence T cell activation via the STING pathway (Carroll et al., 2016). Further research has also shown that chitosan DDA and molecular weight, as well as dosage, affects the immune response (Fong et al., 2017). In our case, molecular weight and dosage are further affected by degradation in vivo, making conclusions on the specific immune response to chitosan difficult. However, from the inflammation observed in histology we can conclude that our chitosan gel induces a pro-inflammatory response, which may augment its anti-cancer effects.

In terms of the inflammatory response to the chitosan gel, a typical foreign body response to the gel is observed whereby there is an accumulation of polymorphonuclear cells, predominantly neutrophils, during the first two weeks after injection. Theoretically, activated neutrophils will release proteolytic enzymes, as well as the chemokines CCL2 and CCL4 that will attract other immune cells such as classically activated M1 macrophages, DC, and lymphocytes, all of which should be beneficial in terms of mounting an anti-tumour response (Mariani, Lisignoli, Borzì, & Pulsatelli, 2019). M1 can lyse tumour cells, present antigens to T cells, and release stimulatory cytokines to enhance the anti-tumour effect of CD8+ T cells and NK cells (J. Liu, Geng, Hou, & Wu, 2021). Infiltration of myeloperoxidase+ tumour-infiltrating neutrophils has also been associated with favourable prognosis of colorectal cancer

in patients (Berry et al., 2017). These potential benefits should be taken with caution however, as without phenotypic marking to identify these immune cell subtypes, as well as proven correlation between their presence and improved anti-tumour efficacy in our model, the potential benefit of this response remains simple conjecture.

As already mentioned, the cell-free gel induced a strong inflammatory reaction in vivo. This was particularly seen in short-term experiments with both gel and microbeads, where moderate inflammation is seen at the surface of the gels and a granulomatous reaction is seen at the microbead surface, possibly provoked by the presence of FBS in the microbeads. Interestingly, stronger inflammation at day 7 in gel-treated mice correlates with smaller tumour size, adding further weight to the hypothesis that induced inflammation contributes to the anti-tumour effect. However, unfortunately again we are missing controls using cell-free gels at days 1 and 7 in these experiments which would allow us to make conclusions about the role and importance of inflammation in the anti-tumour response.

FBS has been shown to be capable of provoking an immune reaction in vivo in both mice and humans (Haase et al., 2005; Mackensen, Dräger, Schlesier, Mertelsmann, & Lindemann, 2000) and clinical developments of this technology would be obliged to use FBS-free microbeads. The low concentration of FBS in our microbeads is, however, acceptable (though undesirable) for in vivo mouse models. It is also important to note that BSA is one of the main protein components of FBS and is itself responsible for the immune reactions in humans and mice exposed to FBS, meaning that BSA itself is not a solution as a replacement for FBS in microbeads. However, as mentioned in the results section, BSA can be a precursor to the use of recombinant human albumin for clinically relevant microbeads, or mouse-derived albumin for tumour models. These species-relevant albumin sources are, however, far higher in cost than BSA and as such possibly unsuitable for scaled-up use. An alternative would be to use the patient platelet poor plasma. Otherwise, another surfactant such as Tween 80 could be investigated as a non-immunogenic alternative to FBS or BSA.

Limited samples were recovered of microbeads but at day 1 the difference to the macrogel is quite striking, indicating some fundamental difference between gel and microbead encapsulated OT-I that affects the associated inflammatory response. While the FBS in microbeads is one possibility, residual mineral oil from the fabrication process is another factor that could provoke this inflammation, with evidence to support this claim in a recent paper showing intraperitoneal mineral oil causes chronic inflammation in mice (Alsina-Sanchis et al., 2020). The format of the microbeads itself may play a role (increased surface area in contact with the tissues). It is also possible that proinflammatory factors released from dead OT-I in the microbeads after stress from the microencapsulation process provoke a STING inflammatory response (Rock & Kono, 2008).

5.2 Comparison of our model to other groups

In the case of IV treatment, our results show in fact greater efficacy to work from another group (Lai, Zhu, Ruan, Chen, & Zhang, 2019a). Furthermore, another study where 20M OT-I were administered over 4 days consecutively showed a similar and again slightly weaker anti-tumour effect, with MC38-OVA tumours treated with intravenous OT-I progressing from 100mm^2 to 250mm^2 in area (using the same calculation as ourselves of the product of perpendicular diameters) between days 6 and 20 after treatment (Katlinski et al., 2017). Admittedly this was performed in Rag-/- mice that lack endogenous T cells, but overall, these other studies indicate that our IV efficacy is within the range we can reasonably expect. The addition of anti-PD-1 improved the anti-tumour effect in Katlinski's work, as well as T cells from mice with resistance to IFN downregulation by the tumour microenvironment. Other groups performing ACT in mice, though with other models such as the B16-OVA melanoma cell line, have administered IL-2, whole-body radiation and increased cell doses up to 10M T cells to improve treatment efficacy (Fernandez-Poma et al., 2017; Visioni et al., 2018).

By way of explanation, the OT-I concentration of 8M cells/ml was chosen as it was the same as our prior in vitro biocompatibility tests with PBMC and OT-I and the was compatible with

the appropriate gel volume for injection in mice (<0.5ml), though only one cell concentration was tested.

5.3 Limitations of the study

5.3.1 Control groups

One clear limitation of our study however is the lack of certain possible control groups. The clearest is a control of cell-free chitosan gel, which was tested but only in one experiment. In this case tumour growth was greater in the cell-free gel than the group treated with gel + OT-I, though this experiment would need to be repeated to reliably confirm that the effect of the gel treatment is due to the OT-I, particularly if we feel that the inflammatory reaction to the gel itself may also play a role in any anti-tumour response observed. Other possible control groups to confirm that the observed effect is due to OT-I could be mice with MC38 rather than MC38-OVA tumours, or CD8+ cells derived from C57Bl/6 mice rather than OT-I mice, both as negative controls. In addition, for reasons of time and practicality the microbead treatment in vivo was only performed in one experiment to assess tumour growth. This must be repeated, along with a control group of cell-free OT-I to assess the impact of microbeads alone and their comparison to gel only treatment, given their inclusion of FBS and hence potentially greater immunogenicity.

5.3.2 Optix imaging limitations

Intravital imaging was performed to track OT-I, and hence aid conclusions as to their contribution to any observed efficacy. For the localised treatment, however, and its comparison with IV, Optix imaging shows its limitations, one of which is that its ability to analyse and quantify localised treatment i.e., a quantitative assessment of T cell infiltrating the tumour, is compromised by its limited resolution and low image quality, making delimitation of the gel and tumour difficult. Moreover, the large fluorescent signal from the gel may “mask” true signal from surrounding OT-I or other areas on the plane of the gel signal. We seem to see a

halo-around the high Optix signal of comparatively weak signal which is nevertheless stronger than the signal seen in IV-treated mice. This could be classified as noise from the high concentration of OT-I in locally treated mice, obscuring “true” OT-I migration or presence in the tumour at lower concentrations than in the gel. For this reason, it is difficult to conclude as to whether OT-I migrate successfully in vivo and access the blood vessels or lymph nodes.

Intravital imaging provided some interesting data in terms of OT-I localisation with imaging of IV-treated mice showing that a large proportion of OT-I are lost in other sites, but a fraction congregates at the tumour site, demonstrating both that the tumour is vascularised, and that OT-I are capable of homing to the tumour. OT-I localisation and concentration when encapsulated in the gel is also shown. This is similar to previous work by other groups using luciferase-tagged tumour cells and CAR T cells, where CAR T cell signalling is more persistent in groups treated with biomaterial-delivered CAR, whereas intraperitoneal or intravenously-delivered cells have a weaker, less persistent signal that is more varied in terms of localisation (Coon et al., 2019; Q. Hu et al., 2021; Smith et al., 2017; S. B. Stephan et al., 2015).

One interesting feature of other groups’ intravital imaging is that delimitation and quantification is more reliable and useful when both T cells and tumour cells are bioluminescent (Coon et al., 2019; Q. Hu et al., 2021). This allows unbiased quantification of tumour size and T cell localisation and even proliferation over time, with a further benefit that luciferase expressing cells correspond to live cells – this is not necessarily the case with our Vybrant DiD-marked OT-I and hence the high cell retention observed may consist of a significant number of dead cells. Bioluminescence may be a better alternative cell tracking methodology if feasible.

Signal concentrations orders of magnitude higher for localised OT-I, particularly gel-encapsulated OT-I, this did not correlate with improved treatment outcomes. This raises a few possibilities in terms of how to explain this discrepancy: the higher signal concentration does not equate to a higher number of tumour-infiltrating lymphocytes – that is, there is a high number of encapsulated T cells within the gel, but they are unable to migrate into the tumour.

This is well illustrated by the consistency over time generally found in mice, where the signal and images do not greatly vary between days 1 and 7. This contrasts with IV-treated mice where we clearly see the optix signal associated with the tumour. Again with more precise and/or informative imaging with bioluminescence of cancer cells and T cells, these measures would perhaps correlate more strongly with treatment efficacy.

5.3.3 In vivo reproductibility

One key limitation of the in vivo models used is the variability sometimes seen between and within experiments. Some variability is inevitable when performing in vivo experiments, though for one a suitable number of animals are used in each experiment to account for this variability, and in addition control groups should confirm consistent behaviour for key defined groups – untreated and IV-treated mice in our case.

An obvious example in our case was the EG7 model (APPENDIX II), where initial promising results were followed by varied and illogical growth in all conditions, as well as spontaneous tumour rejections. This is where not only control groups, but also expected behaviour such as spontaneous tumour rejection perhaps should have been considered. The EG7 model has been shown to occasionally result in spontaneous rejections (D.-E. Hu, Moore, Thomsen, & Brindle, 2004; D. E. Hu, Beauregard, Bearchell, Thomsen, & Brindle, 2003), even though its use persists today in publications where seemingly no spontaneous rejections have occurred (J. Zhou et al., 2018). With hindsight, and assuming financial and logistical capability, ideally each tumour model used would have been well defined before investigation of our hydrogel, through dose-response testing of tumour injection to confirm repeatability and an absence of spontaneous rejections. Dose-response testing of the IV-control, as well as additions such as IL-2, could also have allowed us to work with a “strong” and more consistent positive control.

Furthermore, some variation (though small relatively speaking and within our accepted tolerance) was still present in tumour size at the start of the experiments and in one of the four experiments after 1 week, delaying treatment by 3 days. This can possibly be attributed to

unobserved variability in the culture and injection of tumour cells, which is itself a learning process that requires experience. Some groups have published work detailing typical ACT protocols to inform other groups of potential pitfalls (Ya, Hailemichael, Overwijk, & Restifo, 2015). For IV treatment, there was some variability observed between experiments when the longer initial OT-I stimulation protocol was used, but no such variability when using the shorter stimulation protocol in later experiments. This could also further justify this shorter protocol as preventing some potential variability.

5.3.4 OT-I suitability

Clearly the lack of OT-I proliferation in our scaffolds in vitro (and in all likelihood in vivo as well) is a limitation that contributes efficacy and time-limited effect of our localised treatment. As well as a lack of proliferation, the fragility of OT-I is a limitation as shown by their high mortality after encapsulation in microbeads. This calls for improvement of the scaffolds. One avenue is the addition of pro-proliferative factors, as performed in other work where the scaffolds have been designed for T cell expansion for recovery and later use in ACT rather than cell delivery itself. A diverse range of materials, ranging from carbon nanotube polymers and red blood cell-based artificial APC to glycidyl-methacrylate hyaluronic acid cryogels, all used surface-linked pMHC and CD28 to stimulate OT-I proliferation in vitro and showed increased OT-I proliferation, with expansion over two weeks demonstrated using CD28-pMHC functionalised carbon nanotubes (Fadel et al., 2014; X. Sun et al., 2017; Weiden, 2019). Two-week expansion of OT-I was also demonstrated using MSR scaffolds incorporating either CD3 and CD28 or pMHC (Cheung, Zhang, Koshy, & Mooney, 2018).

Dynabeads, which are used for T cell expansion and acted as controls in these studies, are polystyrene microbeads with conjugated anti-CD3 and anti-CD28. CD3 initiates antigen-independent signalling of the TCR complex and CD28 provides costimulation, with their combination a potent activator of T cells.

To our knowledge these factors have not been incorporated into scaffolds for OT-I ACT.

However Stephan's group did add CD3 and CD28 in their scaffolds for human T cells, suggesting that inclusion of these antibodies would seem highly desirable.
It may even be essential in the case of OT-I due to their difficult culture, as opposed to more easily cultured human T cells. Human CAR T cells are far common than murine T cells in current literature investigating T cell delivery scaffolds for cancer as shown in Table 1.1 in the literature review, perhaps due to their greater resilience and more established culture in vitro. For this reason, a human T cell-cognate cancer cell for biocompatibility testing in vitro, and eventually possibly even use in tumour models with immunocompromised mice could be a useful alternative to the OT-I model.

5.3.5 Improved cell tracking

To address our limitation in precisely identifying the localisation of OT-I after in vivo transfer, some alternative methodologies can be proposed. Confocal microscopy, with T cells trained using CellTracker Orange was used 72h after T cell transfer to localise transferred T cells via immunofluorescence of frozen tissue sections (Q. Hu et al., 2021). Furthermore, for identification of OT-I or indeed any lymphocyte with an appropriate MHC tetramer, in-situ tetramer staining has been demonstrated – for OT-I in the given example (S. Li, Mwakalundwa, & Skinner, 2017).

5.3.6 Quality control for in vivo reproducibility

Currently, "quality control" is performed on administered OT-I to ensure activation and viability at treatment. However, we did not obtain reliable activation data for cells used in vivo for all experiments, and so this process must be more robust and reliable in the future.

5.3.7 In vitro tumour models

While discussed in more detail in Malaret's thesis, a brief discussion of the advantages and limitations of the in vitro transwell and 3D tumour models bears repeating here.

The transwell model is relatively simple, at least compared to the 3D model, and allows for easier recovery of cells (at least in the lower chamber) for characterisation via FACS. It is also faster to perform and cheaper, though still with significant associated costs.

Despite this, the 3D model brings many advantages. Its morphology, even with 3D but shallow layers of cancer cells and T cells, is more representative of tumour morphology than the 2D cancer cell layer in the transwell model. More data can also be obtained, such as cell localisation and migration, as well as some quantification, which is not possible in the transwell model. Some limitations remain to be addressed, such as the difficulty in recovering cells from the 3D model for FACS analysis. Furthermore, the current construction of the molds used in the 3D model limit the media that can be used with cells and hence potentially their in vitro activity – larger, better adapted molds could address this. Cell tracking is currently over short time periods so longer cell tracking would be desirable, and some data such as image selection for quantification currently remains operator dependent.

Despite the interesting data that it yields and the potential for comparison of numerous gel formulations, the 3D model is relatively complex to manufacture and expensive to implement. Unless specific migration data or live cell tracking is required, the simpler, cheaper, and higher throughput transwell model may generally be more appropriate.

5.3.8 Chitosan variability

Due to multiple changes of chitosan supplier during the project, optimisation of the chitosan solubilisation process and hydrogel formulation had to be performed on multiple occasions. Each change required re-optimisation to obtain acceptable physicochemical characteristics and biocompatibility before use in further experiments or in vivo models, which slowed progress in completing the project objectives. Apart from project delays, this is a concern as our own group showed that even small variations in gel formulation can affect PBMC viability within the gel (Monette et al., 2016).

Upon re-optimisation of our chitosan hydrogel, the chosen formulations showed acceptable cell viability and proliferation with encapsulated JURKAT and PBMC, mitigating the concern of reduced biocompatibility upon change of formulation. Despite this, vigilance is required as the observed change of properties – slower gelation in gels using the P17 and especially P18 chitosans where the difference to the previous chitosan was even greater– could negatively affect cell retention as shown in other studies comparing fast and slow-gelling hydrogels (Niu et al., 2019). **Nevertheless, Optix results would seem to contradict a lack of cell retention and the relatively high gelation speed (<15s) of all formulations is likely sufficient for cell delivery despite the differences between them.** The decreased gelation speed may however have an effect on gel morphology, see for example the difference in morphology between the cohesive P17 gels observed for gel degradation and the sometimes two-phased P18 gels recovered in short-term tumour models. We cannot be sure that any inhomogeneity observed is due to gelation speed, but it would be interesting in future to compare the in vivo morphology of gels with different gelation speeds.

The potential variability of chitosan between batches is a known limitation (Younes & Rinaudo, 2015), though one that is generally applicable across many biologically-derived biomaterials and accepted in exchange for their often desirable biological responses or biodegradability, which may be lacking in synthetic biomaterials with more consistent behaviour. Indeed, upon testing in our lab of our own chitosans wide variability was seen in chitosan products with supposedly similar DDA and molecular weights according to manufacturers (see section 3.1.1.1), which can in turn affect biocompatibility where lower DDA for example is associated with reduced cell viability (Foster, Ho, Hook, Basuki, & Marçal, 2015). In terms of practical steps to address chitosan variability, firstly in an ideal scenario any given project would have a sufficient quantity of chitosan to avoid changing batch mid-project. However, this is not always possible as shown in this project, and in any case dependence on a particular (and inevitably limited) batch would be detrimental to scale-up and commercialisation of any given product. For this reason, stringent quality control processes and defined optimisation processes are essential to reproducibility of the product, and already implemented to some extent in our lab. Furthermore, the investigation of alternative chitosan

sources with reduced variability to crustacean waste-derived chitosan (for example fungi-derived chitosan) could offer solutions for obtaining chitosan with more defined and reproducible behaviour (Crognale, Russo, Petruccioli, & D'Annibale, 2022).

5.4 Research contribution and efficacy compared to other research groups

5.4.1 Contributions and originality

This work is the first demonstration of a fast-gelling physical chitosan hydrogel for localised ACT in vivo, where the closest match in literature may be recent work treating retinoblastoma with a chitosan-PEG hydrogel, though this gel is much weaker and slower gelling than our own (K. Wang et al., 2020). We have progressed from an in vitro demonstration at the start of the project to the development of our gel which shows acceptable biocompatibility and potential for use for localised immunotherapy in vivo. The reduced tumour growth in the gel-treated group shows its potential for localised ACT, with our imaging and analysis shedding some light on possible limitations of the treatment and how they may be addressed.

After discussion of these results and the limitations thereof, a key question for this project and technology is where are we situated in terms of treatment efficacy versus the work of other scientific groups? Comparison is not always straightforward, due to the wide variability in terms of treatments, experimental models and conditions and methodologies. However, some general similarities can be observed between certain groups. In our case, we show slowed tumour growth up to 11 days after treatment in gel-treated mice, with a slightly shorter treatment effect in saline-treated mice and slightly longer for IV treatment. Firstly, we can be reassured that this behaviour of slowed growth followed by regrowth is consistent among virtually all groups, with regrowth at a timescale of roughly 10-30 days post-treatment the norm, and highly successful and often complex treatments the exception where tumours are sometimes eliminated.

The fibrin gel for CAR T cell delivery, alginate “microchips”, Wang’s chitosan-PEG hydrogel and Stephan’s work are all examples where particularly successful treatments were obtained, often with common factors such as the fibrin hydrogel and fibrin coating on the nitinol mesh and IL-15 agonists. All these groups used human CAR T cells with corresponding tumour cells in their in vivo models with immunodeficient mice, and their success may indicate to us that these models are better for the demonstration of biomaterial-delivered immunotherapies than the OT-I/OVA tumour models. For the fibrin gel, alginate microchips and nitinol mesh, CAR T cell proliferation in vitro was demonstrated via methods such as the dilution of CFSE signal in stained CAR T cells or the CCK-8 cell counting kit. Porosity was not always assessed, though the nitinol mesh had defined pores of roughly 150x20μm, and the fibrin gel showed pores of 10s of microns after cryo-SEM. These would seem to be desirable porosities for CAR T cell inclusion and migration. Cell dosages also varied, from 1-2M CAR T cells administered in the fibrin and chitosan-PEG gels, and 10M cells delivered in the alginate microchips and nitinol mesh. While our treatment efficacy is not yet as good as some of these groups, the positive side of this comparison is our observed efficacy despite our lack of immunostimulatory molecules, coatings and combination therapies as used by other groups as well as a sometimes-lower T cell dosage. From a simple starting point, these additions confer great potential for improvement of our scaffold to obtain the efficacy seen in other work in the field.

Over 8 weeks of subcutaneous injection in mice, hydrogels were found to be non-toxic due to the lack of observed weight loss or otherwise concerning behaviour from treat mice. This is an accepted method of assessing biocompatibility in vivo, and so as expected given that chitosan is a widely used biomaterial (Zichao Luo et al., 2017), this offers some evidence that the hydrogel is biocompatible in vivo. Further tests could be required however, for formal designation as a biocompatible material. In terms of its biodegradability, the most likely mechanism is enzymatic hydrolysis by lysozyme (Jennings, 2017), contributing to progressive degradation over 8 weeks. No ideal timescale of degradation for a T cell delivery scaffold has been proposed, and indeed some groups have used non-degradable biomaterials in such systems, though we can propose that scaffold biodegradation should occur over the course of

tumour treatment. It is of course disadvantageous and undesirable to have an implant for life as a result of these treatments, though this is with the caveat that these treatments are for serious cancers where a long-term implant may be of lower concern. Other groups have followed tumour growth for 50 days and beyond (Coon et al., 2019), and as such the progressive degradation of our gel over 8 weeks (56 days) without elimination would seem appropriate.

5.5 Perspectives to improve the scaffold

Many developments and additions are possible to build on our work, with the following potentially among the most promising and worthy of consideration to improve the scaffold efficacy:

Improvements to the gel, such as optimising its porosity and fabrication, may improve the observed efficacy. Preliminary work has been done with the addition of gelatin in the chitosan gel, where increased migration was observed in live cell tracking. Two factors may explain the benefit of gelatin inclusion in the hydrogel on OT-I migration: firstly, the action of gelatin as a porogen, leaching from the gel at 37°C and creating pores through which OT-I can move (Babaei, Mohammadian, & Madadlou, 2019). Secondly, gelatin contains the RGD cell binding motif that acts as a ligand for several integrins (Davidenko et al., 2016), which themselves are involved in T cell migration (Denucci, Mitchell, & Shimizu, 2009). However, gelatin addition alone in the hydrogel failed to improve cell survival, and other groups have shown little benefit on T cell migration of RGD motifs (Weiden et al., 2018). Its benefit therefore remains unclear. However, if gelatin can improve porosity and migration in a suitable model (possible CAR T cells as an alternative to OT-I) then its use could be beneficial.

The gel volume and/or OT-I concentration in the gel could be changed to potentially augment treatment efficacy, with other groups using much higher cell densities of 1M CAR T cells in 1µl of hydrogel (K. Wang et al., 2020) or 10M CAR T cells as in the case of the nitinol mesh. As mentioned previously, the use of scaffolds to augment lymphocyte proliferation could be necessary to maximise the T-cell payload at the tumour site while minimising initial cell

concentration and scaffold volume, for example as with the microporous silica rod scaffolds for T cell expansion (Cheung et al., 2018) or various group's T cell delivery scaffolds incorporating factors such as IL-15 (Q. Hu et al., 2021; Zuyuan Luo et al., 2020). If these modifications allow OT-I proliferation in vivo (or in vitro first to demonstrate) then the OT-I model may still be relevant. If not, then we may wish to switch to a CAR T cell model where T cell growth in vivo has been demonstrated by other groups as described above.

Many of the high-efficacy scaffold treatments incorporate biological binding motifs, either throughout their structure or as a grafting or coating on the material surface, such as collagen-like peptide and fibrin. We attempted similar modifications with the inclusion of gelatin and collagen in our hydrogel but with limited success, at least in part due to the limitations of the OT-I model. As described gelatin has potential to improve the gel porosity and T cell migration, though its transformation to a liquid state and hence potential leaching at 37°C could provoke an overly rapid release of cells in vivo and hence limit cell persistence. It may also affect the gelation kinetic or secant modulus negatively, making gelation slower and limiting cell retention or resulting in more fragile gels. Still, an ideal scaffold would likely incorporate bioactive surface components to support immune cell migration and proliferation.

IL-15 is an increasingly common adjuvant to T cell scaffolds for cancer immunotherapy, acting as a supporting cytokine to mare classically used but less well tolerated cytokines for T cell activation such as IL-2. IL-15 favours the growth and persistence of CD8 effector memory cells (Y. Yang & Lundqvist, 2020), which could explain is success in treatments where the anti-tumour response is durable. CD3 and CD28 as used for our OT-I stimulation are also interesting potential additions to the scaffold, as would be STING agonists.

The benefit of combination therapies is a key component of clinical and pre-clinical immunotherapy, and as such the inclusion of ICB such as anti-PD-1 would almost certainly be beneficial for treatment efficacy, while following the likely trend of clinical treatments where multiple immunotherapies will be combined for optimal results.

Finally, we should remember that our treatment system is not limited to ACT. Recent work using a chitosan-BGP hydrogel to deliver immune-priming viruses as a cancer vaccine (Nkanga & Steinmetz, 2022), could inspire work with our own gel as a delivery system for cancer vaccine components as well as ACT.

CONCLUSION

The objective of this PhD was to evaluate the feasibility, safety and efficacy of an injectable chitosan hydrogel for T cell delivery in ACT as local immunotherapy treatment. Firstly, we have demonstrated the feasibility and safety of the product. The gel was injectable through small needles, allowed the survival, escape and functionality of relevant T cells and was proven to be biocompatible and biodegradable in vivo, with a moderate inflammatory reaction. The in vivo inflammatory response to the gel may even augment its anti-tumour effect, and this would be an interesting area of future investigation.

In vivo tests using gel-encapsulated OT-I in the MC38-OVA cancer model demonstrate partial efficacy of chitosan gel as a delivery scaffold for localised ACT, with reduced tumour growth compared to untreated mice and saline controls. Significantly improved cell retention and localisation at the tumour site was demonstrated in gel-encapsulated cells, compared to intravenous treatment where many cells were lost to non-tumour sites such as the lungs and spleen. However, the quantity of cells that truly reach the tumour could not be determined due to the limitation of our cell imaging technique and the difficulty to differentiate exogenous from endogenous cells in histology. Improvements in cell imaging and tracking methodologies may increase the accuracy and utility of in vivo cell imaging. The efficacy of the cell loaded gel, both in the form of an injectable in situ gelling gel and as microbeads, was however lower than intravenous systemic delivery and the efficacy of both treatments was limited to short term (less than 2 weeks), calling for further improvement.

The role of the inflammatory reaction around the gel in its efficacy remains to be fully determined. Complete data for supplementary and control groups such as macrogel without cells and microbeads with and without cells would allow more authoritative conclusions on the specific effect of gel-delivered OT-I, as mentioned in the discussion. Despite this incomplete picture, an interesting observation is the inflammatory effect of the hydrogel and microbeads and its potential role in the overall anti-tumour response. While currently this may cloud the individual contribution of encapsulated OT-I, it also highlights a parallel immune

mechanism that future work may be able to exploit to enhance anti-cancer efficacy. In addition, while the OT-I/MC38-OVA model represented a relatively simple cancer immunotherapy model, difficulties in the culture and in vitro survival of OT-I as well as the artificial nature of the OT-I model call into question its suitability. Alternatives such as CAR T cell models using human xenograft tumours in mice could be considered, having shown success in research from other groups.

To our knowledge, this PhD represents the first use of a fast-gelling physical chitosan hydrogel as a T cell scaffold for localised adoptive cell therapy in the treatment of cancer. Its injectability and simple composition the degradable biomaterial chitosan – commonly used in FDA-approved devices – set it apart from other work in the area often using non-injectable or non-biodegradable materials. Its efficacy is currently limited to very short timescales, due at least in part to limited T cell survival and growth in the scaffold, both with macrogel and the microbeads. The addition of cell binding motifs, pro-proliferative molecules and immune checkpoints inhibitors such as anti-PD-1 could address these limitations. Overall, the gel shows clear promise as an additional candidate alongside the range of biomaterials explored as scaffolds for ACT, with numerous possible improvements that could follow this work.

APPENDIX I

IN VITRO DATA WITH P18 CHITOSAN HYDROGELS

Figure A I-1a shows the evolution of the storage modulus G' over time for P18 gels with SHC 0.075 and increasing PB concentrations. While the gelation kinetic again increases with the PB concentration, differences were observed compared to P17 gels, with a similar gelation kinetic being obtained at a lower PB concentration. The PB 0.02M formulation is closest to previous chitosan formulations in terms of gelation kinetic but its mechanical properties were poor (Figure A I-1b). The PB 0.01M formulation has the closet secant modulus to Kitomer chitosan (108 ± 3kPa vs 100 ± 22 kPa respectively at 50% strain). It presents **slower gelation compared to the P17 chitosan, but gelation was still considered rapid enough (G' greater than G'' after >15s), PB0.01M was therefore chosen as a compromise for P18 chitosan.**

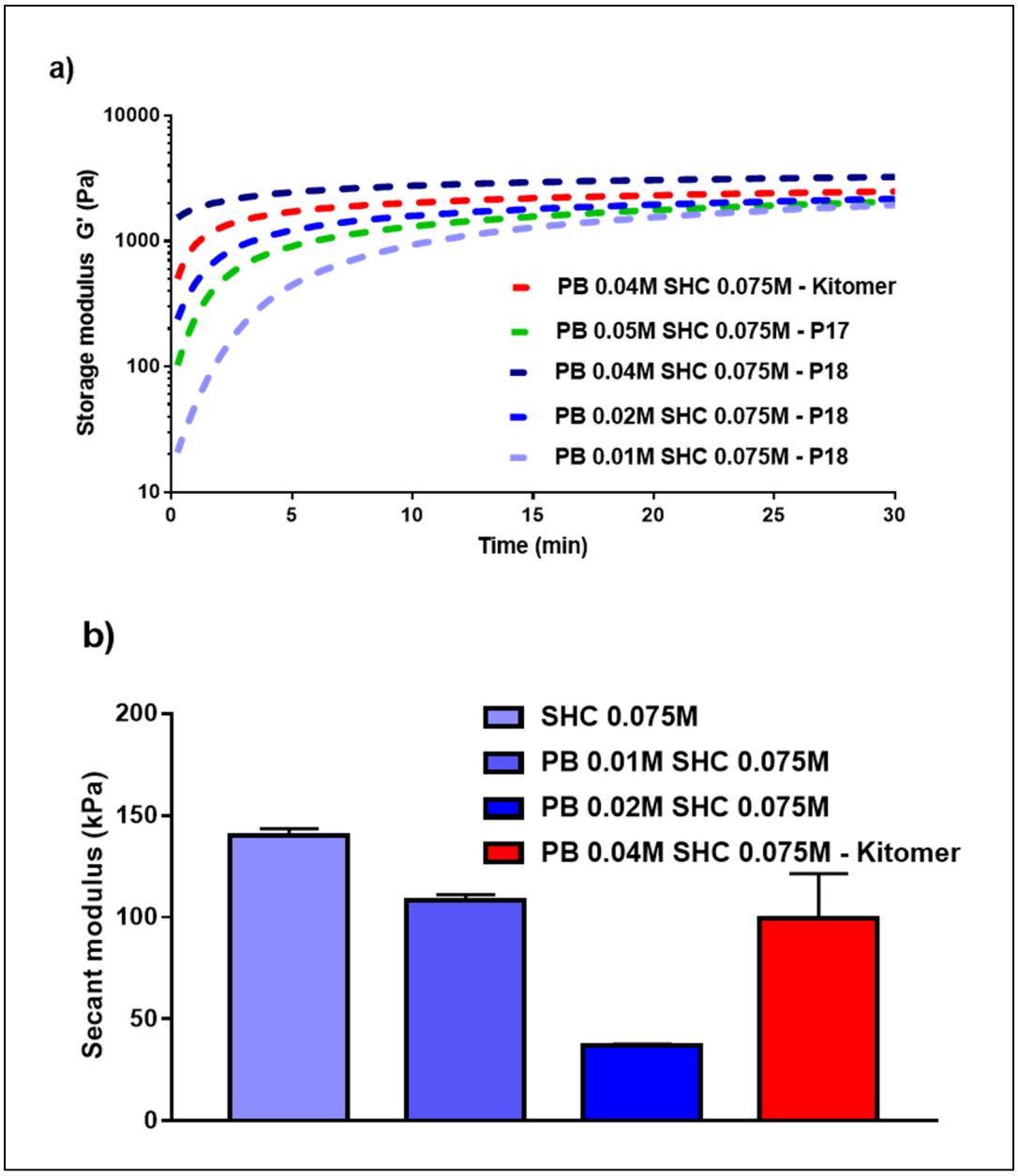

Figure A I-1 a) Evolution of the storage modulus G' for P18 chitosan gels with varying PB concentrations, compared to P17 and Kitomer chitosan. Time sweep experiments were performed at 37°C, 5% strain, 1Hz, using the coaxial cylinder CC10/T200 geometry of a Physica MCR 301 Anton Parr rheometer. Data shown is the average of three independent experiments N = 3 n = 3. b) Secant moduli of P18 gels and kitomer reference value as measured via unconfined compression at 50% strain using the Bose Mach I system (P18) or the Physica MCR 301 Anton Parr rheometer (Kitomer). Data is the mean ±SD of three independent experiments (N = 3, n = 3)

LIVE/DEAD assays were later repeated with the new batch of chitosan (P18), to make sure that the change of chitosan did not negatively impact the cytocompatibility of the hydrogel. In addition, cell encapsulation in Kitomer hydrogels was added as a control. Figure A I-2 to Figure A I-4 show these LIVE/DEAD assays for JURKAT, PBMC and OT-I respectively, where the P18 gel performs equally well as the Kitomer or P17 chitosan.

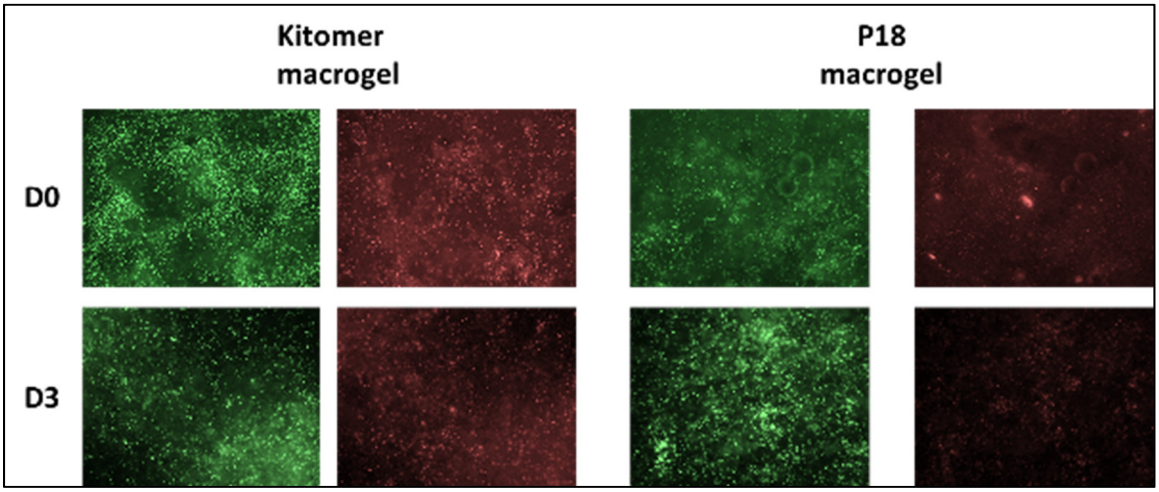

Figure A I-2 Representative Live Dead images of JURKAT cells (live cells in green, dead cells in red) at days 1 and 7 of culture in Kitomer chitosan hydrogel and P18 chitosan hydrogel (N = 1, n = 1). Note that a scale bar was not available with the microscope used for these images

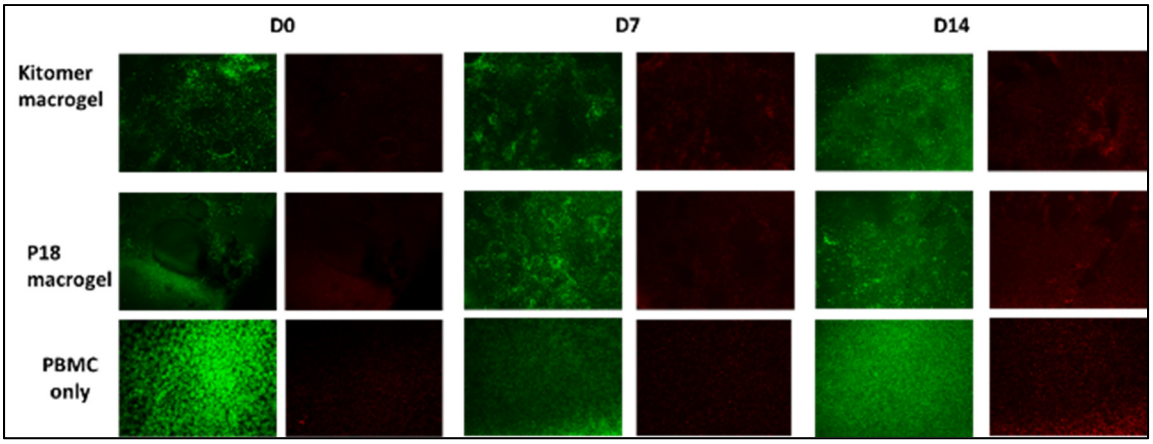

Figure A I-3 Representative Live Dead images of human PBMC from healthy donors (live cells in green, dead cells in red) at days 1, 7 and 14 of culture at 8M cells/ml in Kitomer chitosan, P18 chitosan and non-encapsulated (N = 1, n = 1). Note that a scale bar was not available with the microscope used for these images

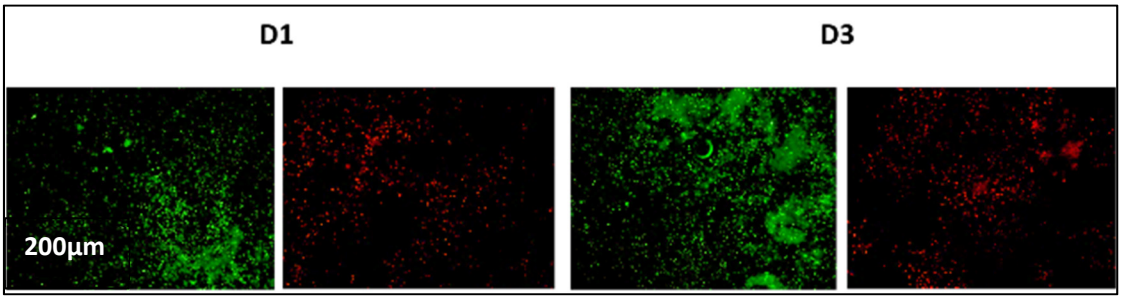

Figure A I-4 Representative images of OT-I survival in chitosan macrogel (8M/ml) demonstrated over 3 days with Live Dead assay in macrogel (N>3, results with unpurified P18 chitosan, PB0.01 SHC0.075)

PBMC survival in microbeads is shown in Figure A I-5 and Figure A I-6. Interestingly, higher cell survival at D0 compared to OT-I is observed in one of two experiments, possibly indicating greater resistance to the microbead protocol of PBMC compared to OT-I (here chitosan beads made at 1100rpm stirring speed). It is unclear why the higher viability at D0 is not observed in

Figure A I-5. Cells do, however, proliferate over 2 weeks, populating the beads and forming cell clusters.

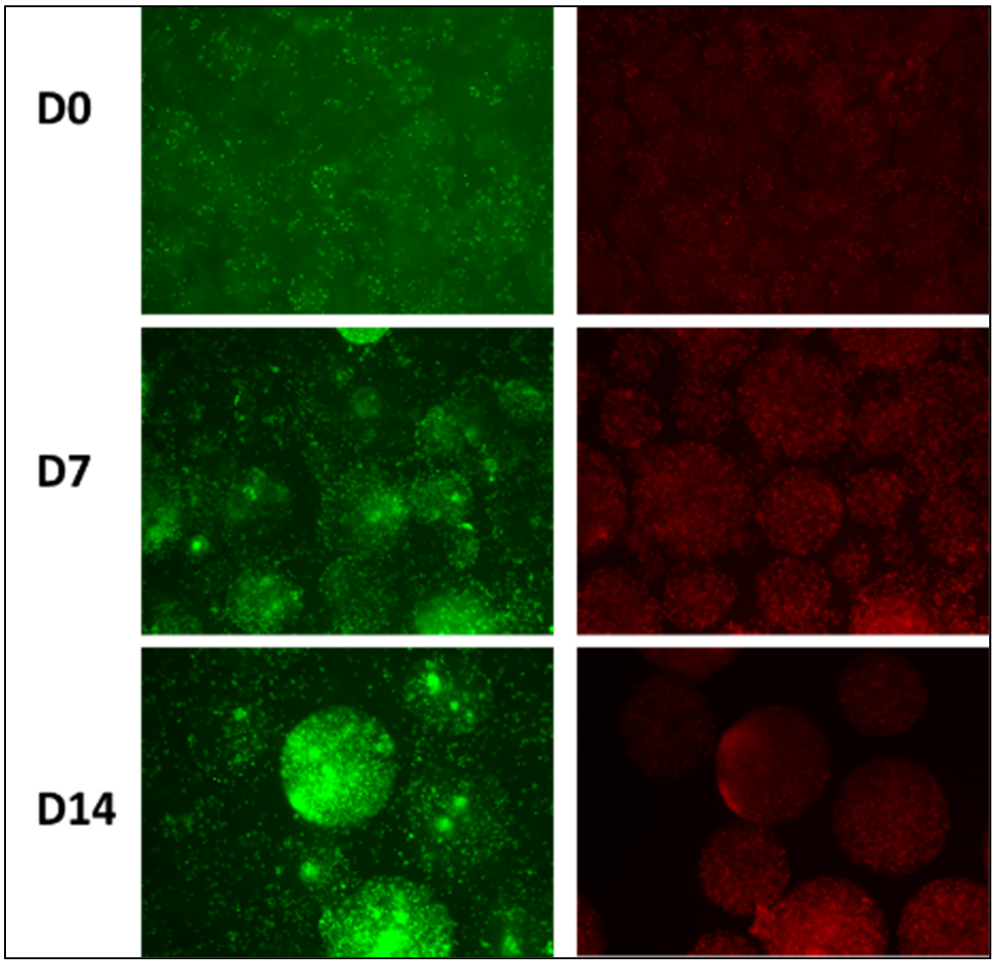

Figure A I-5 Representative Live Dead images of human PBMC from healthy donors (live cells in green, dead cells in red) at days 0, 7 and 14 of culture in PB 0.01 SHC 0.075 P18 chitosan microbeads (N = 1, N = 2 for D0). Note that a scale bar was not available with the microscope used for these images

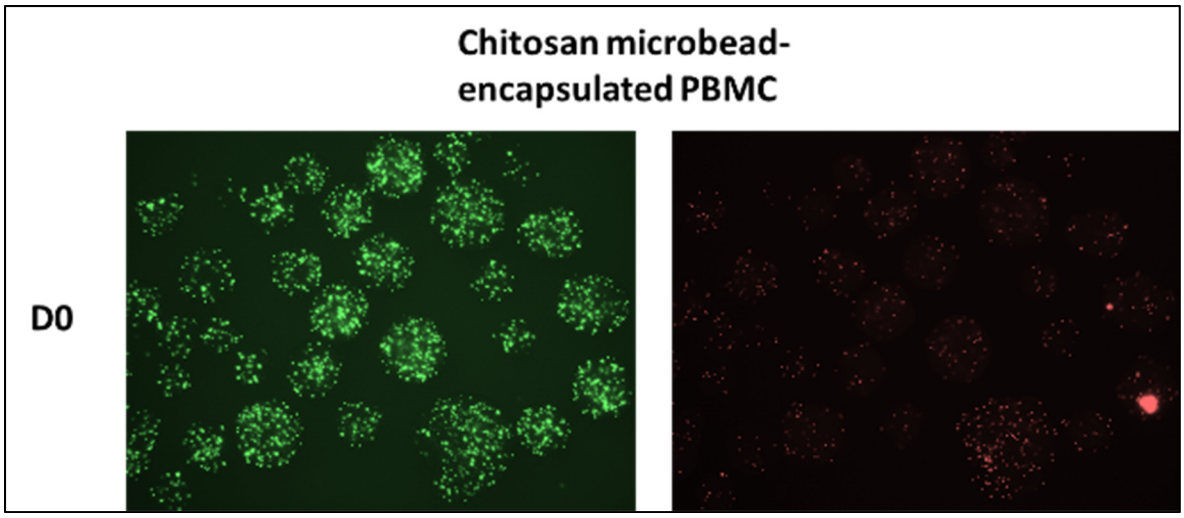

Figure A I-6 Representative Live Dead images of human PBMC from healthy donors (live cells in green, dead cells in red) at 8M cells/ml at day 0 of culture in PB 0.01 SHC 0.075 P18 chitosan microbeads (N = 2). Note that a scale bar was not available with the microscope used for these images

APPENDIX II

IN VIVO RESULTS WITH THE EG7 MODEL

Efficacy of the treatment was first tested in vivo with EG7-OVA tumour cells. Results of two experiments are presented in Figure A II-1a and b respectively, showing the tumour in each mouse as a function of time for each group, with each individual tumour shown, as well as the mean per group. **In the first experiment (Figure A II-1a) strong tumour growth was observed in untreated mice while growth was significantly reduced in both IV-treated and gel-treated mice, up to 30 days in all but one IV-treated tumour and all but two gel-treated tumours.**

Statistical difference was confirmed compared to untreated mice, from days 9 to 12 ($p < 0.05$, after which the death of untreated mice did not allow further statistical analysis, but the effect would likely continue based on later timepoint data in the IV and Gel groups, indicating a clear effect of the treatments. Note that the EG7 tumour model has a higher immunogenicity than the MC38 model and so is easier to treat with greater success (Lai, Zhu, Ruan, Chen, & Zhang, 2019b). No significant difference was observed between the IV and Gel treatments.

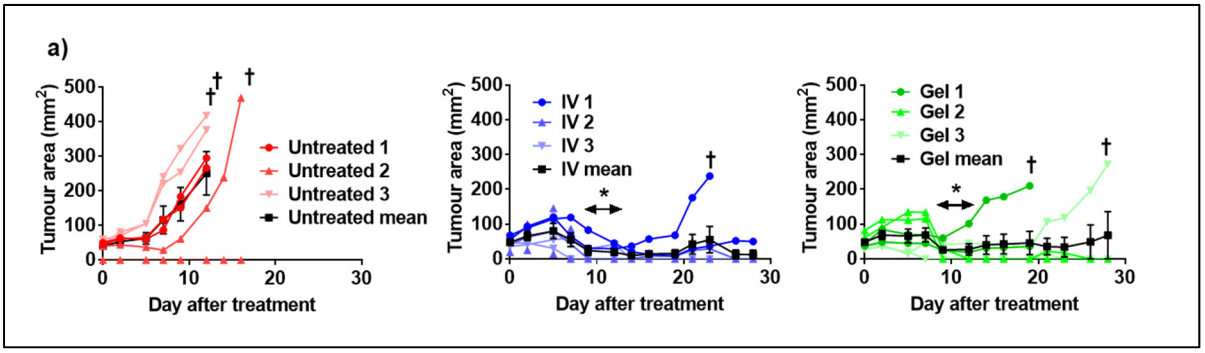

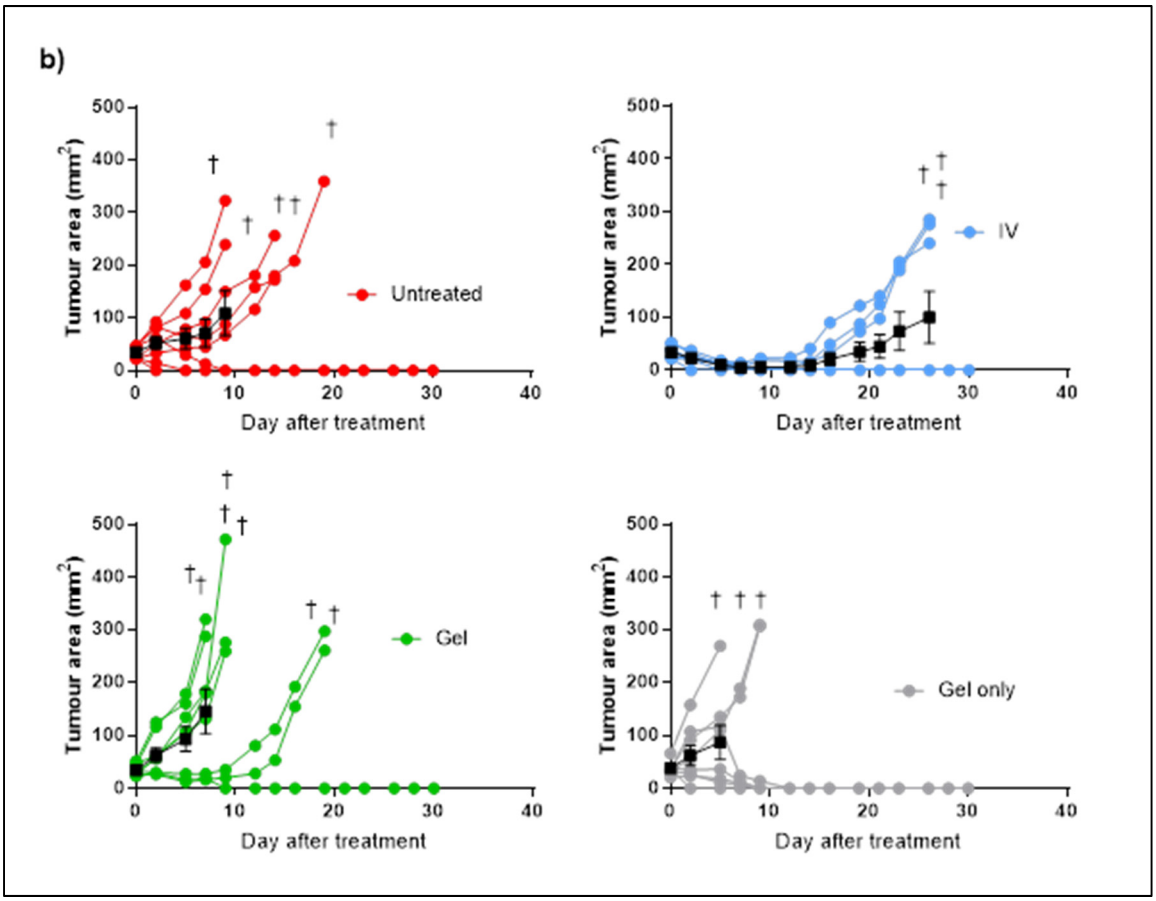

Figure A II-1 Tumour growth curves in EG7 mouse tumour model. Individual tumour growth curves up to 30 days after treatment in subcutaneous EG7-OVA tumours. Each individual tumour (2 per mouse) as well as the mean ± SEM (black curves) is shown. Red = untreated mice, blue = IV-treated mice, green = P17 gel-treated mice. **a)** Experiment 1: (n = 3). (two curves per animal since tumours were created in both flanks) b**)** Experiment 3. (n = 8). † indicates mouse sacrifice. * $p < 0.05$, arrows indicate duration of significantly different growth compared to untreated mice

At the repetition of the experiment, however, for unknown reasons, tumour growth in some mice was minimal, with only 13 of 18 tumours successfully developing at the time of treatment Mice where tumours did not develop were assigned to the untreated group. This was a mistake since it led to IV group (positive control) showing greater tumour growth than the untreated group (negative control) (data not shown). Results of this experiment were thus invalid. **The large number of cases without tumour growth suggested a problem of the reproducibility and hence validity of the model.**

The experiment was reproduced a third time, (Figure A II-1b) with a greater number of mice (8 per group) to clearly determine the extent of reproducibility issues and hence the viability of EG7 as a tumour model to test our gel delivery scaffold. From this experiment onwards, in vivo tumour models were performed while injecting tumour cells in one flank only, to avoid the complications and variability inherent in two-tumour mice. Moreover, mice were randomly assigned to treatment groups and tumour measurements were performed blind where possible. Furthermore, another treatment group was included: gel only, consisting of 200µl of gel injected adjacent to the tumour but without containing OT-I. This was included to investigate the benefit, if any, of the gel itself e.g. by stimulating an immune response, and ensure that any anti-tumour benefit from treatment is principally due to the administered OT-I.

In the untreated group, 3/8 mice showed rapid tumour suppression (non-developed tumours are surely the result of spontaneous rejection), while strong growth in other mice resulted in early sacrifice. IV treated mice showed a stabilisation or decrease of tumour size during the 10 days after treatment and tumour elimination in 5/8 cases, with tumour regrowth in 3/8 cases, indicative of only temporary effect, as expected from the literature (J. Zhou et al., 2018). A similar effect is seen only in 3/8 mice of the T cell loaded hydrogel with only one tumour eliminated in this group. Surprisingly, complete tumour disappearance is obtained in 5/8 cases in the gel-only group. The only significant difference observed up to day 7 (the limit for comparison as mice began to be sacrificed) was significantly smaller tumours in IV-treated mice vs Gel-treated mice ($p < 0.01$). However, **the large variability of tumour growth in the untreated group, including as well as the tumour rejections in all groups, treated or otherwise, indicated the variable growth of EG7 tumours and as such in unsuitability as a valid model to assess our cancer immunotherapy**. Furthermore, 12 mice – equivalent to 3 per group, never developed tumours and as such were excluded before groups were created, adding further evidence of the variability and unsuitability of the EG7 model.

These results could be explained by the high immunogenicity of EG7 tumour, as already reported in the literature ((D. E. Hu et al., 2003). The strong immune response generated by

these cells can result in spontaneous tumour rejection due to endogenous immune cells – hence the observed treatment response is difficult to separate from the endogenous immune response. Without a consistent negative control from the untreated group, it is impossible to draw strong conclusions about the efficacy of the OT-I treatments and hence the gel as a delivery system, so this auto-rejection of the tumours posed a problem for the use of the EG7 model.

Two out of three experiments performed with the EG7 model showed a similar tumour size both at treatment and 10 days after in untreated mice (Figure A II-2), which in some ways indicates relatively good reproducibility. However, these are two examples with weak tumour growth and tumour rejections, and as such simply confirm that this model shows undesirable behaviour.

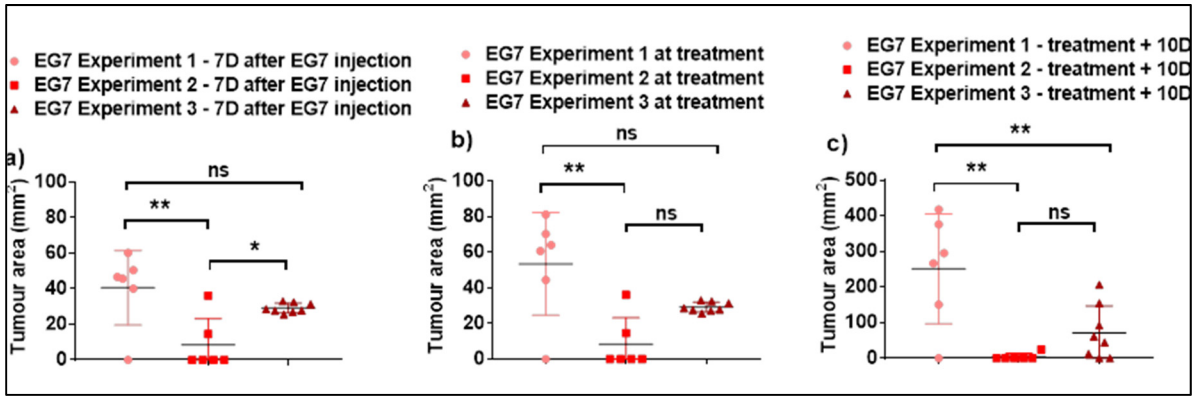

Figure A II-2 Untreated EG7 tumour reproducibility. Individual values and mean ± SD are compared for 3 experiments at: a) 7 days after EG7 injection; b) at treatment; c) 10D after treatment. * $p < 0.05$, ** $p < 0.01$. n = 3-8 mice per experiment

For IV-treated mice, again two out of three experiments performed with the EG7 model showed a similar tumour size at treatment (Figure A II-3) – perhaps also indicating consistency between in the differences between groups within each experiment at treatment. However, in this case no difference is observed 10 days between any of the experiments, indicating at least reproducibility of the treatment. It could be the case that despite (or possibly because of) the high EG7 immunogenicity, IV treatment is so potent that it overcomes other sources of variability in the model.

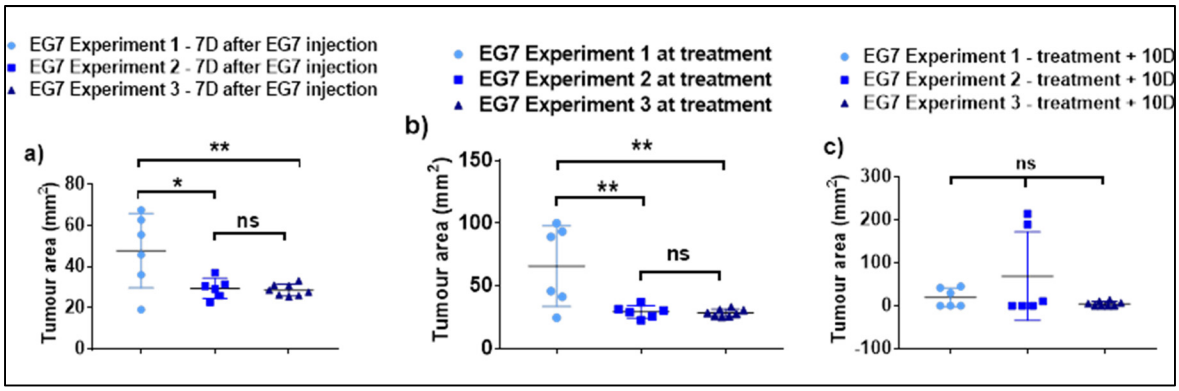

Figure A II-3 IV-treated EG7 tumour reproducibility. Individual values and mean ± SD are compared for 3 experiments at: a) 7 days after EG7 injection; b) at treatment; c) 10D after treatment. * $p < 0.05$, ** $p < 0.01$. n = 3-8 mice per experiment

The large variation in untreated growth is indicative of spontaneous rejection and further supports our previous conclusion as to why the EG7 model is unsuitable.

APPENDIX III

MC38 TUMOUR GROWTH – GEL AND IV TREATMENT AND REPRODUCIBILITY IN INITIAL EXPERIMENTS

Separate results of the first and second experiment and pooled data are presented in Figure A III-1a) and b). The mean average tumour area as a function of time after treatment is shown normalised as a % of tumour area at treatment, with each individual replicate also shown.

The first experiment, shown in Figure A III-1**a showed no significant difference between treatment groups after statistical analysis.** The absence of an effect of the IV treatment compared to untreated mice (the positive vs negative control) indicates a possible problem with the experiment. Thus, we cannot conclude a treatment effect based on these results.

In the second experiment (Figure A III-1b), tumour growth remained constant compared to the first experiment, with no significant difference in normalised untreated tumour growth between the two experiments. **Treated mice showed significantly reduced tumour growth up to 14 days in IV-treated mice (untreated: 338 ± 35%; IV: 143 ± 47%) and 11 days in gel-treated mice (untreated: 245 ± 21%; Gel: 138 ± 36%).**

The effect of the treatment was clear in the second experiment and demonstrated the potential of the local treatment in reducing tumour growth, despite using over 3 times fewer cells than the IV treatment. **However, the variability of treatment response between the two experiments raises questions of the treatment's reproducibility.**

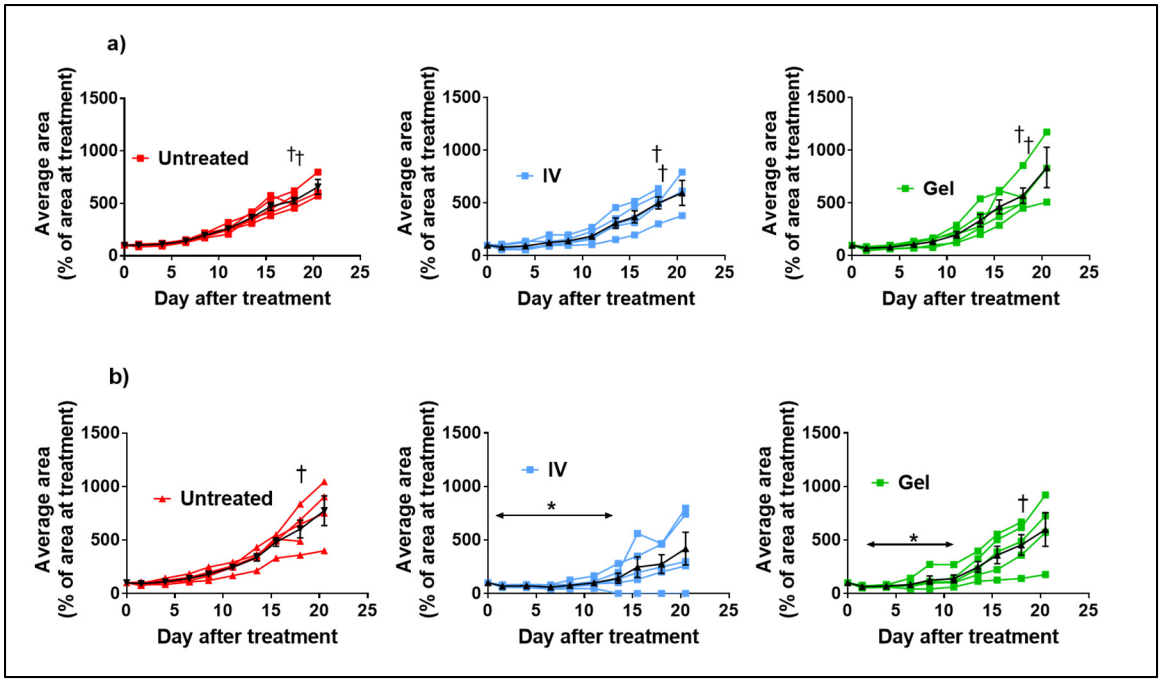

Figure A III-1 Tumour growth curves in MC38-OVA mouse tumour model. Individual tumour growth curves up to 21 days after treatment in subcutaneous MC38-OVA tumours. Each individual tumour as well as the mean ± SEM (black curves) is shown. Red = untreated mice, blue = IV-treated mice, green = P17 gel-treated mice (n = 5 mice per group in each experiment). a) Experiment 1; b) Experiment 2. † indicates mouse sacrifice. * $p < 0.05$ based on two-way ANOVA with Tukey's post-test, arrows indicate duration of significantly different growth compared to untreated mice OT-I stimulated for 96h

APPENDIX IV

EFFECT OF BSA CONCENTRATION IN MICROBEADS

This section contains the results of microbead characterization when prepared with BSA instead of FBS, which complete the results shown in section 4.4.2.1.

Figure A IV-1 presents typical images of the beads as a function of BSA concentration in the cell culture media from 10 to 0% v/v (2 to 0% final concentration in the microbeads). As for FBS concentration, bead size increases when decreasing BSA concentration: from 387 ± 139 µm with 2% final BSA concentration to 466 ± 163, 527 ± 183 and 619 ± 196 µm with 1%, 0.4% and 0% BSA respectively. Each group is again significantly different to each other group ($P < 0.0001$ using one way ANOVA).

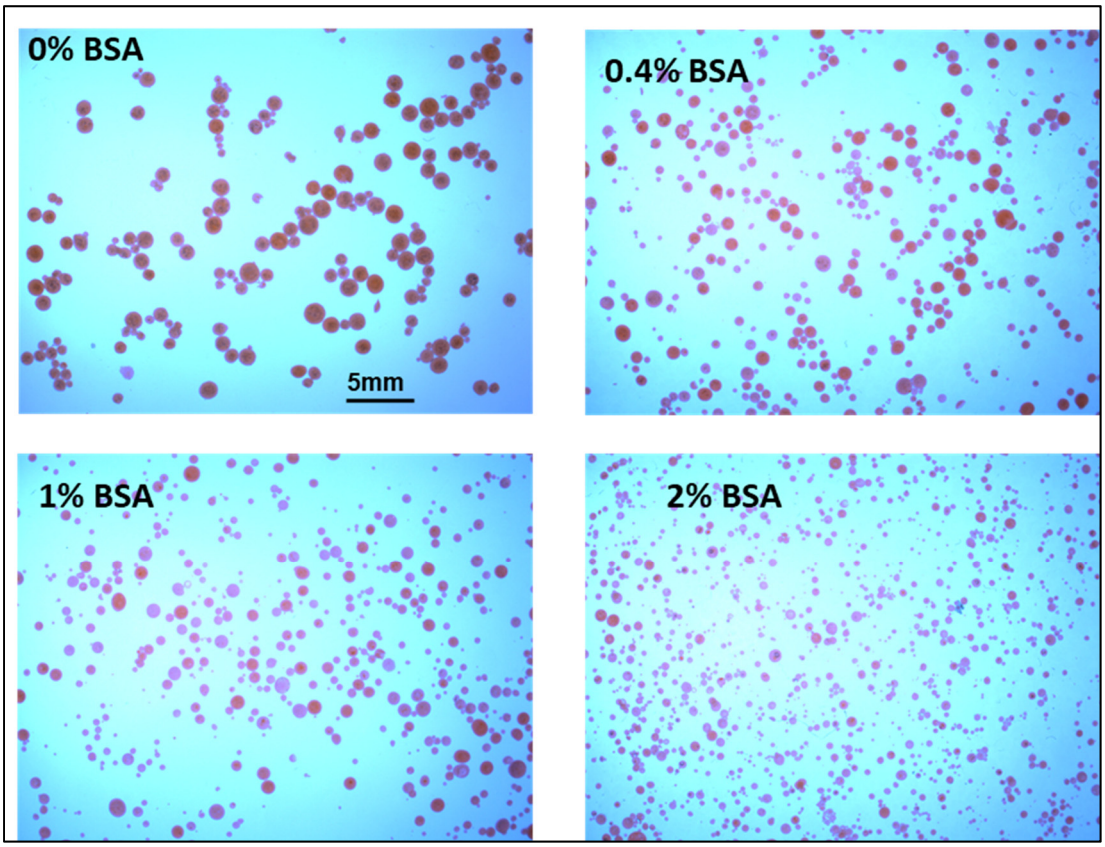

Figure A IV-1 Microbead appearance – eosin staining. Pictures of microbeads fabricated with media containing 0, 2, 5 and 10% BSA (0, 0.4, 1 and 2% final BSA concentration in the microbeads)

Figure A IV-2 shows the size and volume distribution of the microbeads. Decreasing BSA concentration tends to increase the coefficient of variation. The percentage of beads with a diameter smaller than the 21G needle inner diameter (514µm) used for injection in mice with decreasing BSA% was respectively 32%, 48%, 62% and 81% when containing 0, 0.4, 1 and 2% of BSA.

The volume of beads smaller than 514 µm is 8%, 17%, 26% and 47% for 0, 0.4, 1 and 2% BSA respectively as a percentage of total bead volume. All together, these data show that FBS could be easily replaced by albumin in in vivo and clinical studies, to avoid immunogenic reactions.

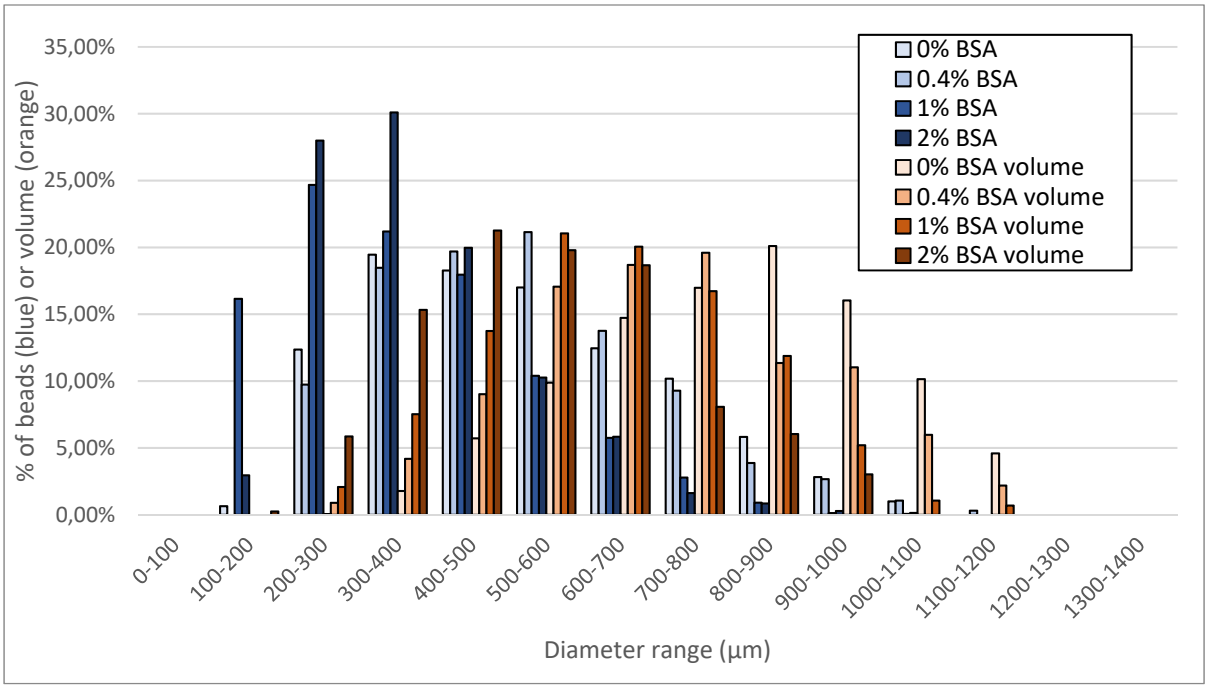

Figure A IV-2 Effect of final BSA concentration on chitosan microbead diameter with size distribution of chitosan microbeads (blue) and volume distribution (orange) shown, as calculated using Cell Profiler software (chitosan P18 SHC0.075M PB0.01MN = 2, n number of beads analyzed > 1099 per condition)

APPENDIX V

INTRAVITAL MICROSCOPY FOR OT-I LOCALISATION IN MICROBEADS

In terms of the Optix signal in the microbead group is similar to that of the gel but slightly reduced, at 4372 ± 1147 NC at day 1 and 4060 ± 4449 NC at day 7, though the difference is not significant (Figure A V-1b). It appears the microbead format does not have a strong effect on the observed Optix signal. Furthermore, in Optix imaging the gel form is similar to the macrogel – the Optix resolution is not great enough to identify individual microbeads (Figure A V-1a). As with the other treatment groups, no trend is observed correlating Optix signal with treatment efficacy (Figure A V-1c).

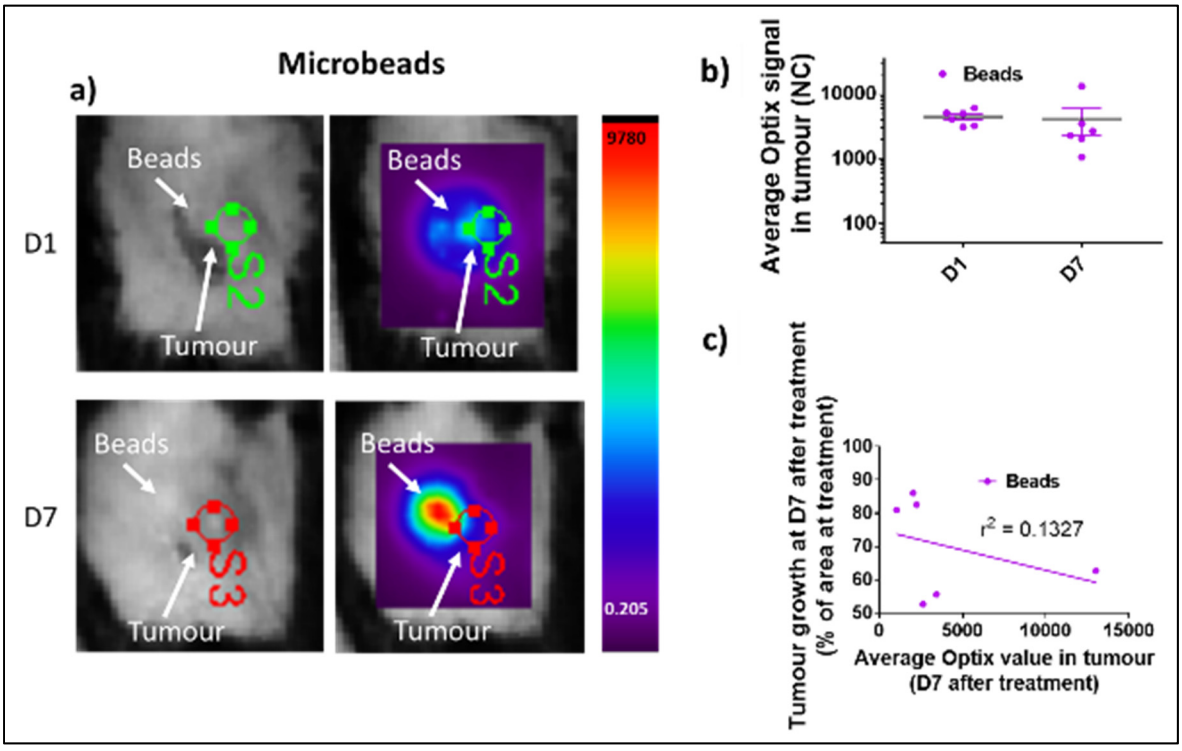

Figure A V-1 Localisation of OT-I cells by intravital microscopy – microbead group. a) Region of interest (ROI) for standardised Optix quantification. Images of a microbead-treated tumour, followed by the placement of a standardised 9mm^2 ROI are shown. Images with the standardised ROI are shown both with and without signal. b) Average Optix signal intensity of a 9mm^2 region of the tumour (indicated with red/green circles on the images) for microbead-treated mice (mean ± SD, n = 6); c) Correlation between Optix signal in the tumour and tumour growth at Day 7 after treatment in MC38-OVA/OT-I model for microbead treatment (n = 6)

APPENDIX VI

CD45.2 IMMUNOFLUORESCENCE

In short term in vivo experiments using CD45.1 mice, our chosen method to differentiate administered OT-I from endogenous CD8 T cells was via the phenotypic cell markers CD45.1 and CD45.2. CD45 is a leukocyte marker, with standard Bl6 mice expressing the CD45.2 phenotype, and the B6 SJL mice used in these experiments expressing the CD45.1 phenotype. Therefore, markers such as CD8 and CD45 should identify all corresponding lymphocytes, whereas through immunofluorescence and an antibody against CD45.2, for example. OT-I could be identified.

For immunohistochemistry, mouse anti-rabbit CD8 (D4W2Z, Cell signalling) and primary anti-mouse CD45.2 monoclonal antibodies (Thermofisher Scientific, Canada) were used to identify cytotoxic lymphocytes and OT-I respectively (where OT-I were CD45.2 cells injected in mice whose CD8+ T cells were of the CD45.1 phenotype. For deparaffinisation, antigen retrieval and primary blockage of slide-mounted sections of tumour and gels, the BenchMark Ultra (Ventana, IGR) automated immunostainer was used. Slides were subsequently rinsed with PBS, then incubated with Dako blocking reagent for 20 minutes at room temperature. For CD45.2 staining, slides were then incubated with Mouse-on-mouse blocking reagent for 1 hour at room temperature. Slides were incubated with primary antibodies for 1 hour at room temperature, rinsed twice with PBS, then incubated for 1 hour with the secondary antibodies and DAPI. Slides were rinsed again twice with PBS, quenched with 0.1% Sudan Black solution for 15 minutes at room temperature, rinsed twice with PBS then mounted with fluoromount mounting solution and conserved at 4°C before scanning.

However, despite numerous attempts to optimise our protocol, and having tried multiple secondary antibodies and conjugated forms of CD45.1 and CD45.2 to mark cells (where the principle of CD45.1 cells would be all endogenous lymphocytes are marked, and CD8+CD45.1- cells correspond to OT-I), OT-I could not be clearly identified against

background fluorescence (Figure A VI-1). We recommend that changing the histological staining protocol to work with frozen tissue sections could solve our problems, as other groups have performed with some success (Hérault et al., 2017; Klein et al., 2007).

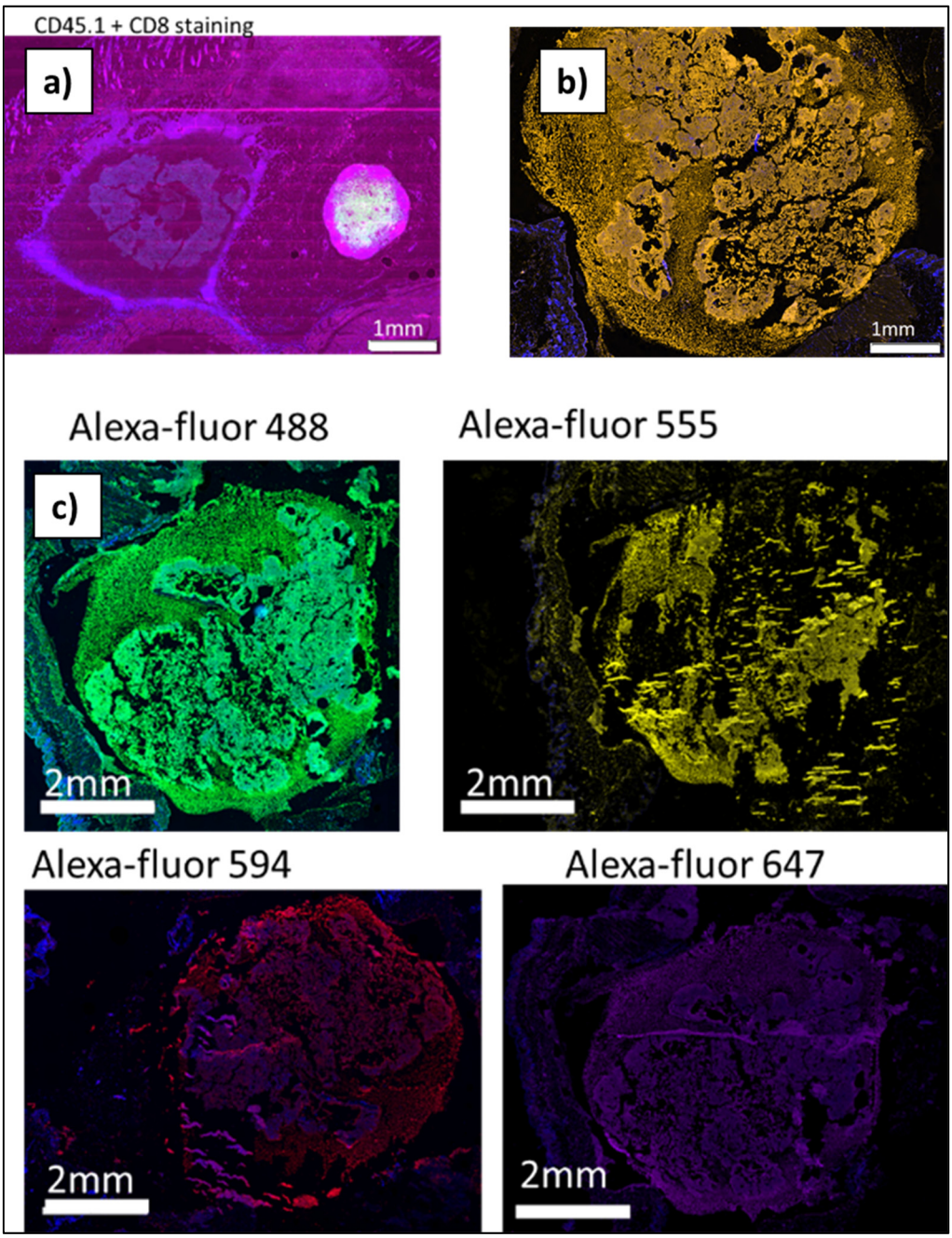

Figure A VI-1 Immunofluorescence of CD45.2 with a) APC-Cy7-linked CD45.1, CD8 and negative control in a sample of macrogel + OT-I with a tumour, 24h after gel injection; gel + OT-I sample recovered 1h after injection. b) a Trit-C 594 antibody and c) various secondary antibodies

APPENDIX VII

SHORTER OT-I ACTIVATION EFFECT ON IV TREATMENT EFFICACY

The shorter OT-I stimulation, while seemingly improving cell activation and being cheaper and less time consuming, was compared in terms of treatment efficacy as well against the previous experiment with longer OT-I stimulation. No significant difference in tumour growth with 3 vs 4 days OT-I stimulation at 11, 16 & 21 days based on IV results as shown in Figure A VII-1.

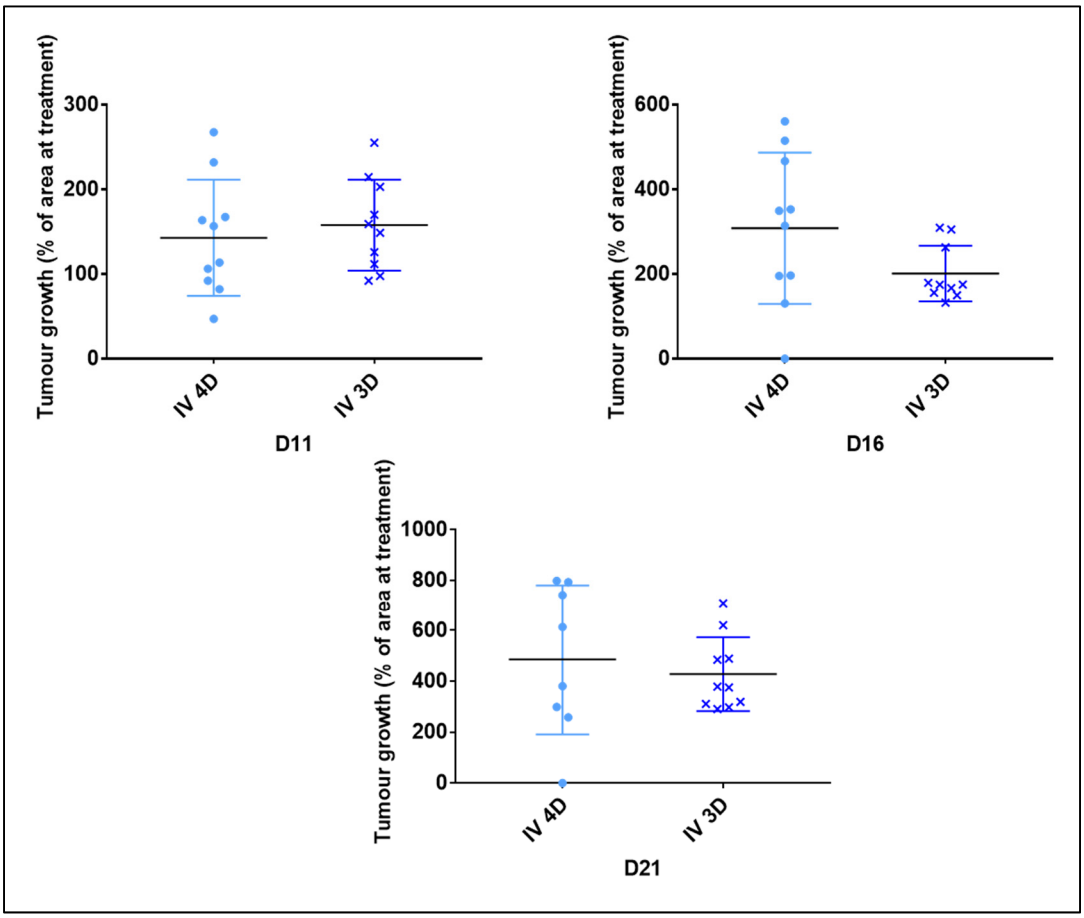

Figure A VII-1 Comparison of tumour growth 11, 16 and 21 days after treatment, as a % of initial area, between IV-treated mice with either 3- or 4-day stimulation of OT-I. While 3D stimulation seems to have reduced tumour growth partly at D16, at none of these timepoints is the difference between these two groups significant

APPENDIX VIII

SUPPLEMENTARY HISTOLOGY IMAGES

This section shows histological images of certain conditions, timepoints, or images of interest such as the ulceration seen below, that are not shown in the main body of the thesis.

Ulceration occurred in mice and caused early sacrifice in some cases and seems to be visible in Figure A VIII-1a. This occurred in all groups however, and was particularly prevalent, at least proportionally, in the untreated group, visible in 75% (3/4) slides at sacrifice, compared to 50% (3/6) for saline-treated mice, 30% for gel-treated mice (3/10), 20% for IV and gel only mice (1/5) and none in the microbead group. Firstly, this seems to indicate that ulceration is the natural response to unchecked growth and will eventually occur in all cases. An example of an untreated tumour with mild inflammation present is shown in Figure A VIII-1b.

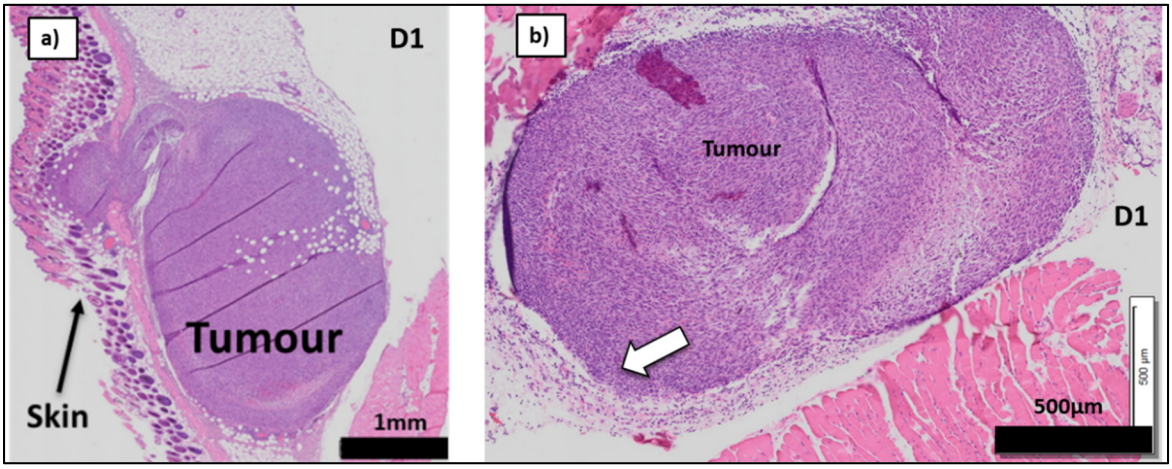

Figure A VIII-1 H&E staining of an untreated tumours at D1, a) in the process of breaking the skin during ulceration; b) where mild peritumoral inflammation is present. White arrows show mild inflammation

Figure A VIII-2 shows an example where the injected gel was distant from the tumour, with the gel also showing more infiltration by immune cells than in other examples as seen in the main body of the thesis. This distance was an exception, most likely related to greater distance

between the gel and tumour at injection. It could be the case that the immunosuppressive environment of the tumour was less effective at a greater distance, hence the greater immune cell infiltration of the gel. The gel does, however, seem more degraded than some samples in the biodegradation experiment, so the TME may not be the only factor at play.

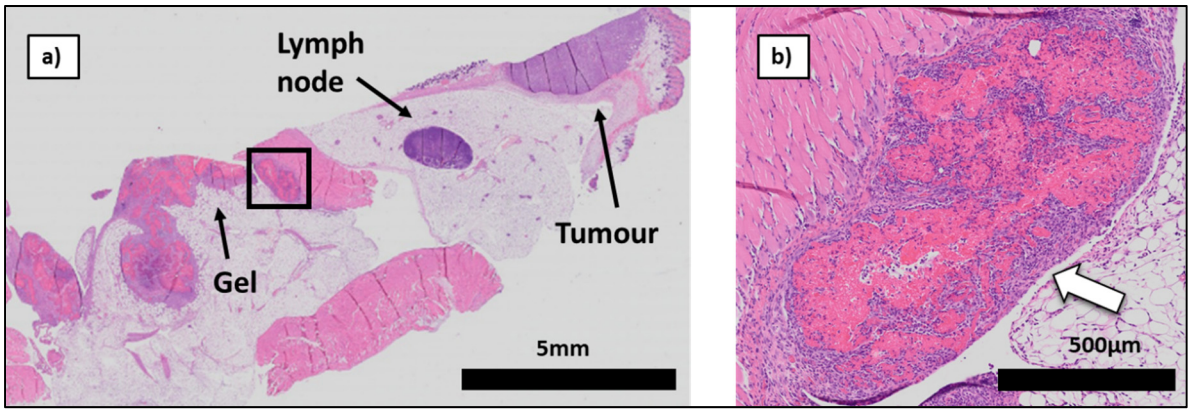

Figure A VIII-2 a) H&E staining of a Gel-treated mouse at D7 where the gel is distant from the tumour; b) a close-up image of the gel. White arrow shows immune cell infiltration into the gel

Figure A VIII-3 shows examples of IV, untreated and saline-treated tumours at either day 1 or day 7. There is little of note in these images, apart from the intratumoral necrosis visible in the untreated sample

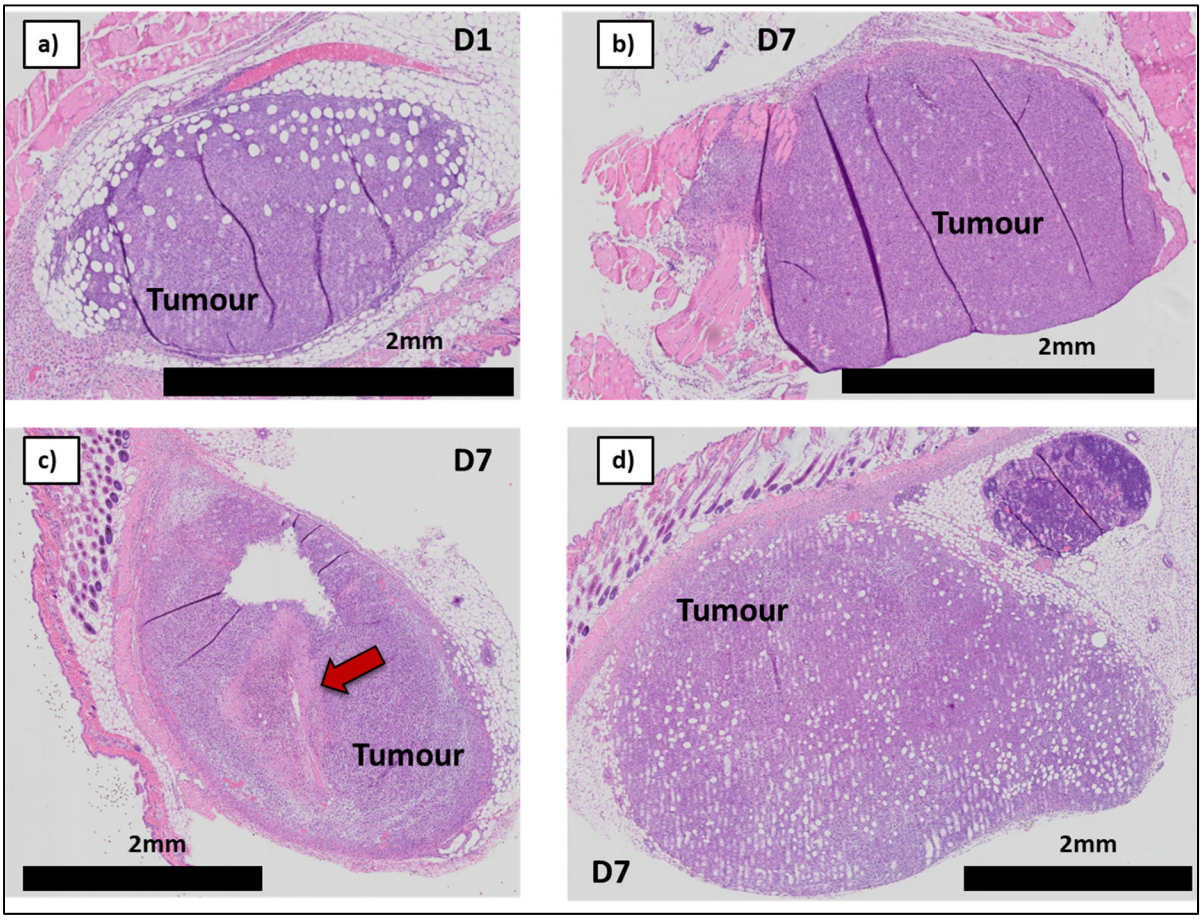

Figure A VIII-3 Images of a, b) IV-treated; c) untreated and d) saline-treated tumours (H&E staining); red arrow shows necrosis

Figure A VIII-4 shows H&E staining of an untreated tumour 21 days after other groups were treated. Intratumoral necrosis can be seen in Figure A VIII-4b, which was extensively observed at this timepoint.

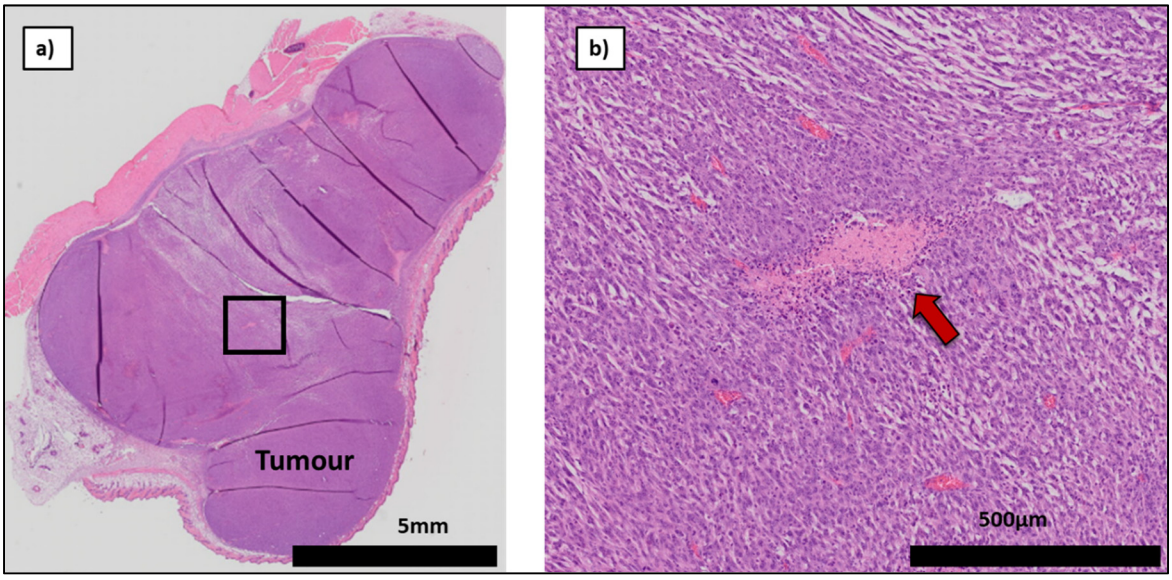

Figure A VIII-4 H&E staining of an untreated mouse at D21 after treatment of other groups, red arrow shows necrosis. a) The whole tumour; b) zoomed view of the inner tumour

Figure A VIII-5 shows H&E staining of a Gel-only-treated tumour 21 days after treatment. Some infiltration of immune cells into the gel can be seen in Figure A VIII-5b.

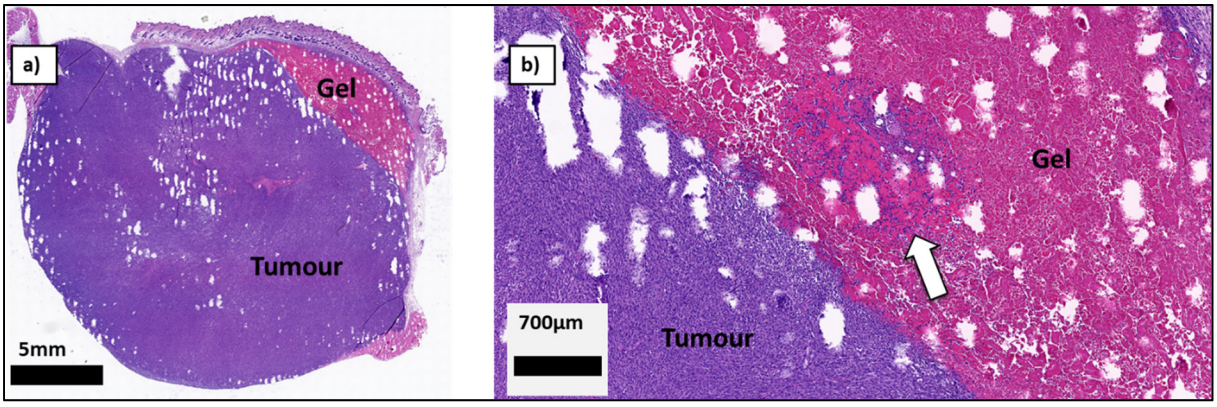

Figure A VIII-5 H&E staining of a Gel-only-treated mouse at D21 after treatment, white arrow shows immune cell infiltration into the gel. a) The whole tumour and gel; b) zoomed view of the tumour-gel interface

APPENDIX IX

PRELIMINARY CD8 QUANTIFICATION IN IMMUNOFLUORESCENCE

To quantify the CD8 IHC staining, a Matlab image processing script was developed to analyse histological images and approximatively count the number of CD8-stained cells by area. This was developed by the PhD student Baptiste Morin in our lab and tested in preliminary results on samples of tumours and in mice at days 1 and 7, shown in Figure A IX-1. Not enough data was obtained to quantify the CD8 cells in tumours in microbead-treated mice. Currently there is high variability between the samples, with no significant difference observed between groups or timepoints. It is currently unclear if this because of the non-specific nature of the CD8 staining (which stains endogenous lymphocytes as well as OT-I), non-optimised parameters in image analysis, or both. These results would seem to indicate that CD8 staining is not specific enough to differentiate between groups under the conditions tested, and that the chosen marker, staining efficacy or image analysis (or a combination thereof) will need to be optimised to quantitatively assess lymphocyte presence in the tumours in vivo.

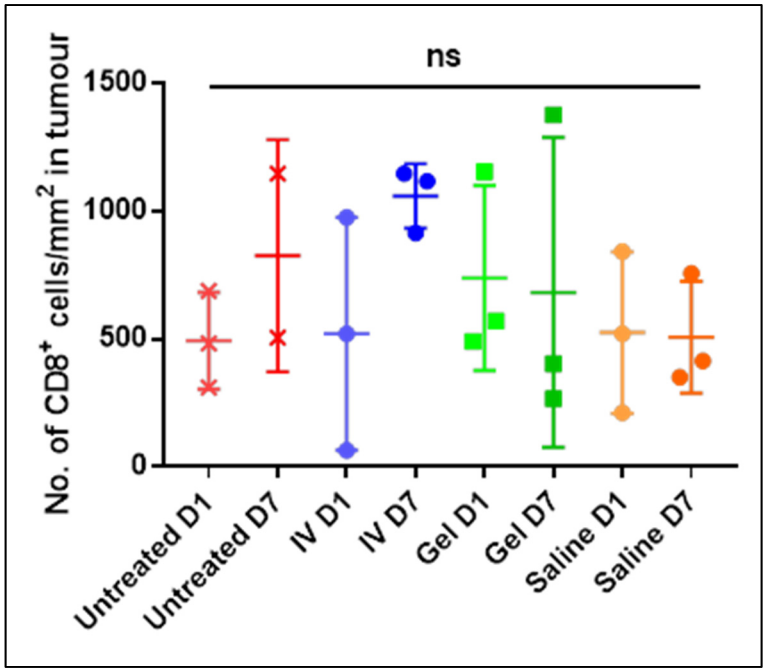

Figure A IX-1 Mean ± SD of CD8 cell counts in tumours for untreated, IV, Gel and Saline groups after Matlab image analysis of IHC slides N = 2, n ≥ 2

Intratumoral CD8+ cells

Figure A IX-2 to Figure A IX-5 present immunofluorescence images of tumours and gels with T lymphocytes (CD8+, shown in green). Interestingly, CD8 cells infiltrate into tumours in all groups, regardless of treatment. Furthermore, the number of CD8+ cells in the tumours in general is potentially only weakly linked to the anti-tumour response, given the high number of CD8+ cells identified in untreated tumours at day 7 for example. Unfortunately, without further markers such as CD45.2 to confirm this, it is not possible to conclude which CD8+ cells are exogenous OT-I cells administration during IV injection versus endogenous CD8+ cells from the mice immune system.

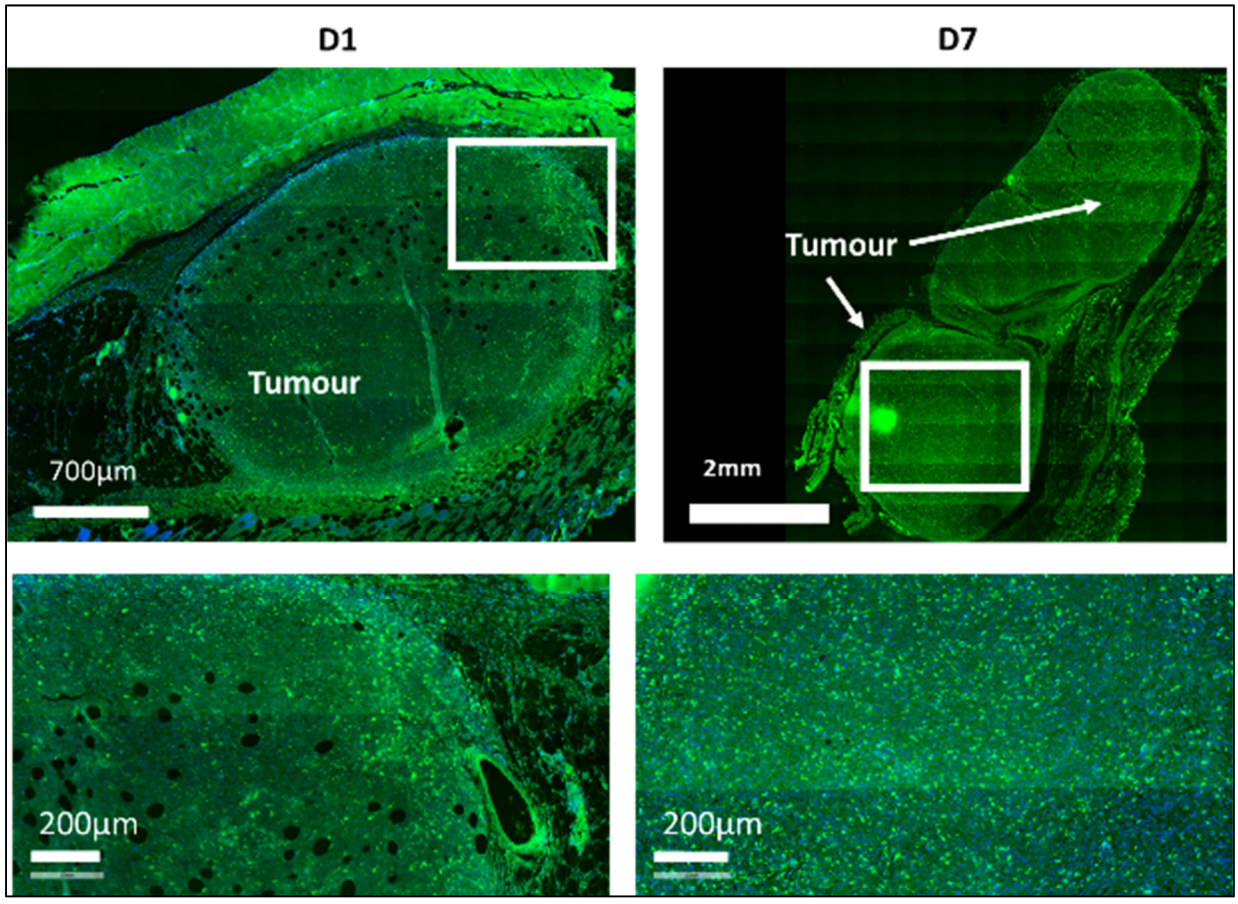

Figure A IX-2 Representative images showing CD8 positive cells in immunofluorescence samples of untreated mouse tumours recovered 24h and 7 days after injection in mouse flank, N = 2 n = 4

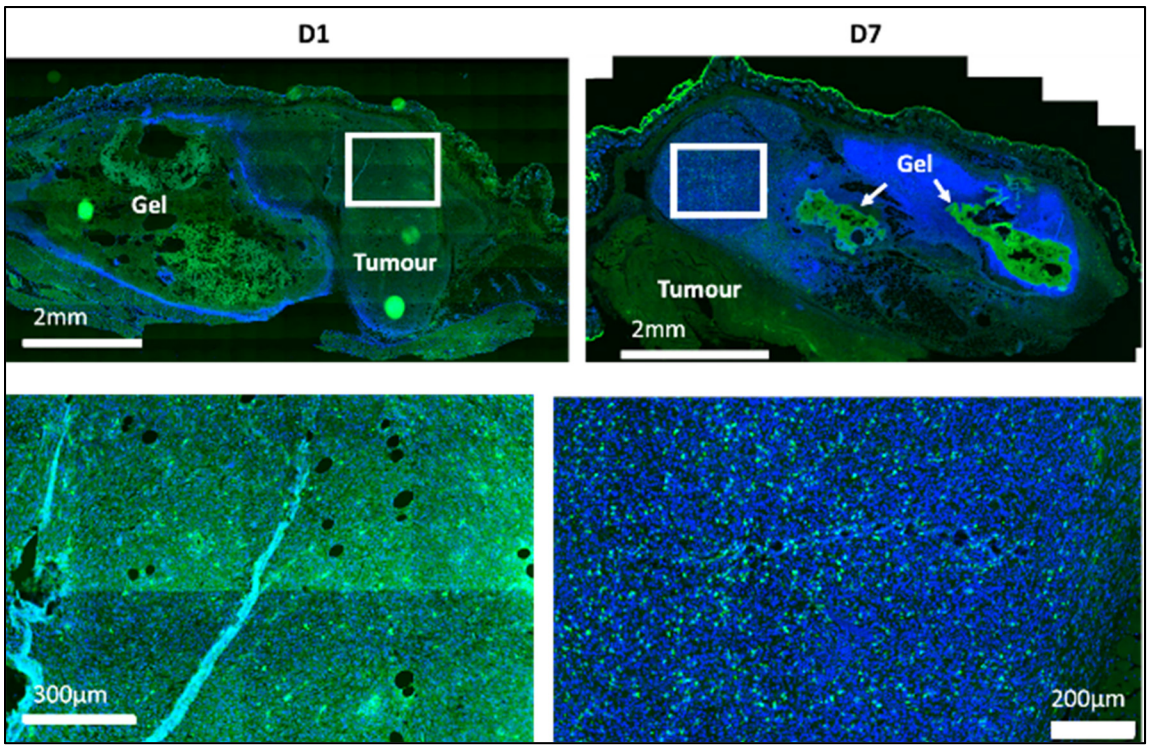

Figure A IX-3 Representative images showing CD8 positive cells in immunofluorescence samples of gel-treated mouse tumours recovered 24h and 7 days after injection in mouse flank, N = 2 n = 6

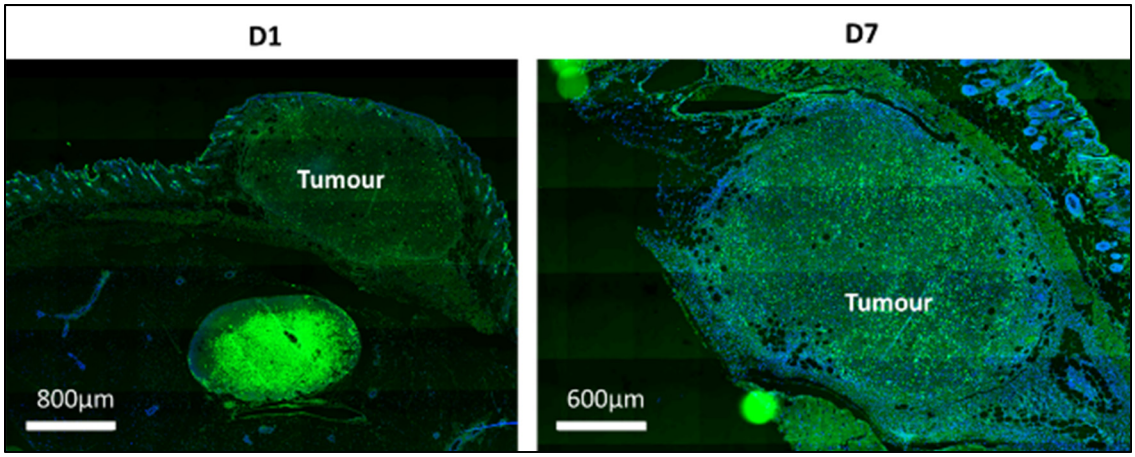

Figure A IX-4 Representative images showing CD8 positive cells in immunofluorescence samples of saline-treated mouse tumours recovered 24h and 7 days after injection in mouse flank N = 2 n = 4

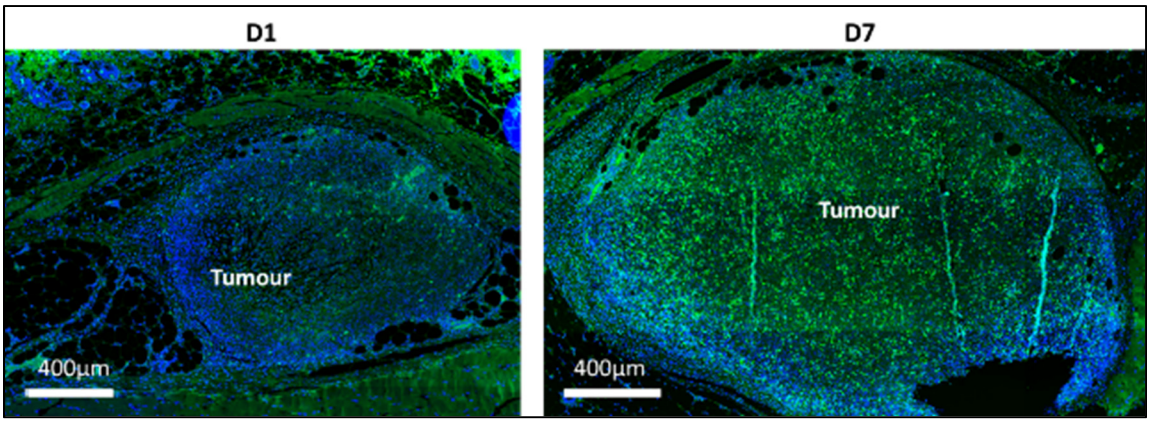

Figure A IX-5 Representative images showing CD8 positive cells in immunofluorescence samples of IV-treated mouse tumours recovered 24h and 7 days after injection in mouse flank N = 2 n = 4

Encapsulated CD8+ cells

Immunofluorescence was also performed on the gel scaffolds (Figure A IX-6 and Figure A IX-7). Relatively few CD8+ cells are observed, with overall numbers comparable to the number of CD8+ cells observed after 24h in tumours, and certainly fewer than are visible at D7 in tumours. Probably the CD8+ cells observed within the gels correspond to the OT-I, as it would be unlikely for infiltrating CD8 T cells to infiltrate and populate the gel in a homogeneous and consistent manner across multiple samples and timepoints. How these results relate to treatment response and observations in the tumour, however, remains somewhat unclear. There is no clear link between CD8 cells in the gel and in the tumour – for example if a significant number of OT-I migrate from the gel towards the tumour, we would expect to see a large initial number of OT-I in the gel that is decreased at day 7, but this is not the case. One possibility is that even these short timepoints are after a rapid escape of encapsulated OT-I which could occur in the first 24h after injection, so gel recovery at even shorter timescales of e.g. 1h could explain the relatively small number of cells observed in the gel compared to the tumours.

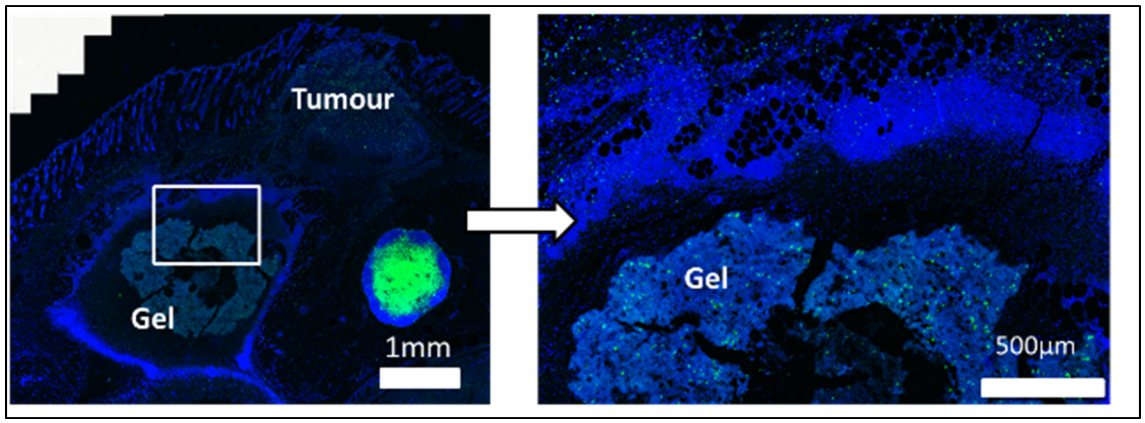

Figure A IX-6 Representative images showing CD8 positive cells in immunofluorescence samples of gels in gel-treated mice, 24h after tumour cell injection in mouse flank N = 2 n = 6

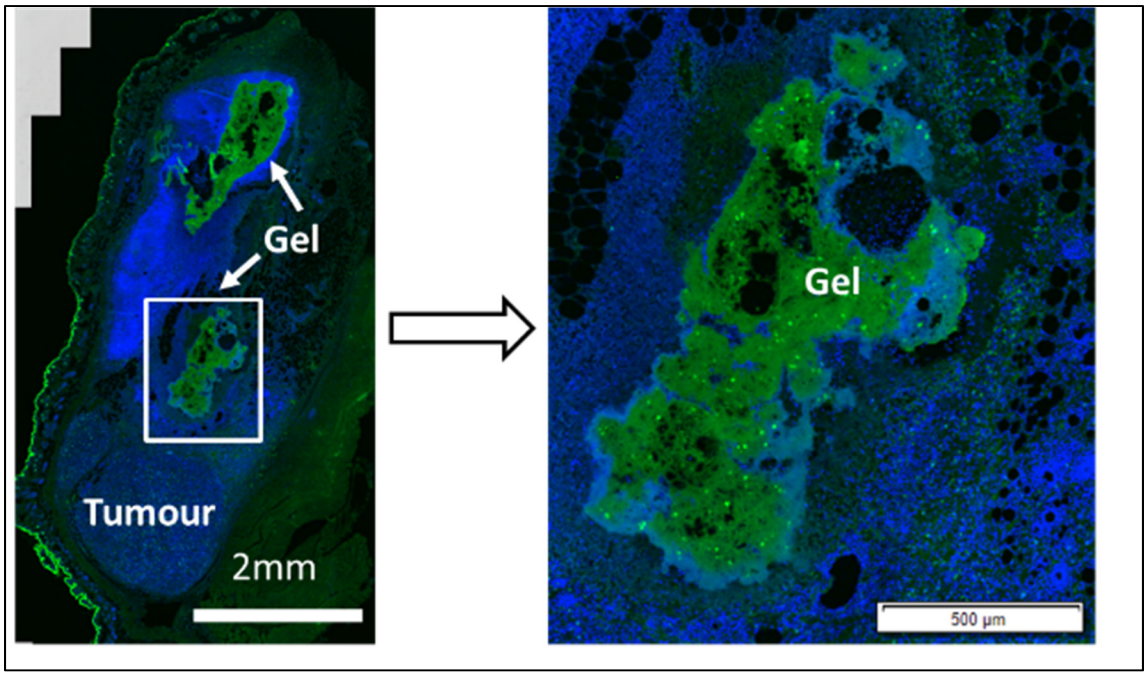

Figure A IX-7 Representative images showing CD8 positive cells in immunofluorescence samples of gels in gel-treated mice, 7 days after tumour cell injection in mouse flank

LIST OF BIBLIOGRAPHICAL REFERENCES

Ahmed, E. M. (2015). Hydrogel: Preparation, characterization, and applications: A review. *Journal of Advanced Research, 6*(2), 105-121. doi: http://dx.doi.org/10.1016/j.jare.2013.07.006. Repéré à http://www.sciencedirect.com/science/article/pii/S2090123213000969

Ahn, Y. H., Ren, L., Kim, S. M., Seo, S.-H., Jung, C.-R., Kim, D. S., . . . Kim, T.-D. (2020). A three-dimensional hyaluronic acid-based niche enhances the therapeutic efficacy of human natural killer cell-based cancer immunotherapy. *Biomaterials, 247*, 119960. doi: https://doi.org/10.1016/j.biomaterials.2020.119960. Repéré à https://www.sciencedirect.com/science/article/pii/S0142961220302064

Ahsan, S. M., Thomas, M., Reddy, K. K., Sooraparaju, S. G., Asthana, A., & Bhatnagar, I. (2018). Chitosan as biomaterial in drug delivery and tissue engineering. *International Journal of Biological Macromolecules, 110*, 97-109. doi: https://doi.org/10.1016/j.ijbiomac.2017.08.140. Repéré à https://www.sciencedirect.com/science/article/pii/S0141813017318846

Akther, F., Little, P., Li, Z., Nguyen, N.-T., & Ta, H. T. (2020). Hydrogels as artificial matrices for cell seeding in microfluidic devices. *RSC Advances, 10*(71), 43682-43703. doi: 10.1039/D0RA08566A. Repéré à http://dx.doi.org/10.1039/D0RA08566A

Ali, O. A., Huebsch, N., Cao, L., Dranoff, G., & Mooney, D. J. (2009). Infection-mimicking materials to program dendritic cells in situ. *Nature Materials, 8*(2), 151-158. doi: 10.1038/nmat2357. Repéré à https://doi.org/10.1038/nmat2357

Ali, O. A., Lewin, S. A., Dranoff, G., & Mooney, D. J. (2016). Vaccines Combined with Immune Checkpoint Antibodies Promote Cytotoxic T-cell Activity and Tumor Eradication. *Cancer Immunology Research, 4*(2), 95. doi: 10.1158/2326-6066.CIR-14-0126. Repéré à http://cancerimmunolres.aacrjournals.org/content/4/2/95.abstract

Ali, O. A., Verbeke, C., Johnson, C., Sands, R. W., Lewin, S. A., White, D., . . . Mooney, D. J. (2014). Identification of Immune Factors Regulating Antitumor Immunity Using Polymeric Vaccines with Multiple Adjuvants. *Cancer Research, 74*(6), 1670. doi: 10.1158/0008-5472.CAN-13-0777. Repéré à http://cancerres.aacrjournals.org/content/74/6/1670.abstract

Aliaghaie, M., Mirzadeh, H., Dashtimoghadam, E., & Taranejoo, S. (2012). Investigation of gelation mechanism of an injectable hydrogel based on chitosan by rheological measurements for a drug delivery application. *Soft Matter, 8*(27), 7128-7137. doi: 10.1039/C2SM25254F. Repéré à http://dx.doi.org/10.1039/C2SM25254F

Alinejad, Y., Bitar, C. M. E., Martinez Villegas, K., Perignon, S., Hoesli, C. A., & Lerouge, S. (2020). Chitosan Microbeads Produced by One-Step Scalable Stirred Emulsification: A Promising Process for Cell Therapy Applications. *ACS Biomaterials Science & Engineering, 6*(1), 288-297. doi: 10.1021/acsbiomaterials.9b01638. Repéré à https://doi.org/10.1021/acsbiomaterials.9b01638

Alsina-Sanchis, E., Mülfarth, R., Moll, I., Mogler, C., Rodriguez-Vita, J., & Fischer, A. (2020). Intraperitoneal oil application causes local inflammation with depletion of resident peritoneal macrophages. *bioRxiv*, 2020.2007.2015.203885. doi: 10.1101/2020.07.15.203885. Repéré à http://biorxiv.org/content/early/2020/07/29/2020.07.15.203885.abstract

Anguille, S., Smits, E. L., Bryant, C., Van Acker, H. H., Goossens, H., Lion, E., . . . Berneman, Z. N. (2015). Dendritic Cells as Pharmacological Tools for Cancer Immunotherapy. *Pharmacological Reviews, 67*(4), 731-753. doi: 10.1124/pr.114.009456

Anton Paar. (2021). Physica MCR. In A. Paar (Éd.).

Antonarakis, E. S., Small, E. J., Petrylak, D. P., Quinn, D. I., Kibel, A. S., Chang, N. N., . . . Drake, C. G. (2018). Antigen-Specific CD8 Lytic Phenotype Induced by Sipuleucel-T in Hormone-Sensitive or Castration-Resistant Prostate Cancer and Association with Overall Survival. *Clinical cancer research : an official journal of the American Association for Cancer Research, 24*(19), 4662-4671. doi: 10.1158/1078-0432.CCR-18-0638. Repéré à https://pubmed.ncbi.nlm.nih.gov/29858218 https://www.ncbi.nlm.nih.gov/pmc/articles/PMC6481607/

Antonarelli, G., Corti, C., Tarantino, P., Ascione, L., Cortes, J., Romero, P., . . . Curigliano, G. (2021). Therapeutic cancer vaccines revamping: technology advancements and pitfalls. *Annals of Oncology, 32*(12), 1537-1551. doi: https://doi.org/10.1016/j.annonc.2021.08.2153. Repéré à https://www.sciencedirect.com/science/article/pii/S0923753421044574

Aoyama, S., Nakagawa, R., Mulé, J. J., & Mailloux, A. W. (2021). Inducible Tertiary Lymphoid Structures: Promise and Challenges for Translating a New Class of Immunotherapy. *Frontiers in Immunology, 12*. Repéré à https://www.frontiersin.org/article/10.3389/fimmu.2021.675538

Argiris, A., Harrington, K. J., Tahara, M., Schulten, J., Chomette, P., Castro, A. F., & Licitra, L. (2017). Evidence-Based Treatment Options in Recurrent and/or Metastatic Squamous Cell Carcinoma of the Head and Neck. *Frontiers in Oncology, 7*. doi: 10.3389/fonc.2017.00072

Assaad, E., Maire, M., & Lerouge, S. (2015). Injectable thermosensitive chitosan hydrogels with controlled gelation kinetics and enhanced mechanical resistance. *Carbohydrate Polymers, 130*, 87-96. doi: https://doi.org/10.1016/j.carbpol.2015.04.063. Repéré à http://www.sciencedirect.com/science/article/pii/S0144861715003896

Atik, A. F., Suryadevara, C. M., Schweller, R. M., West, J. L., Healy, P., Herndon Ii, J. E., . . . Sampson, J. H. (2018). Hyaluronic acid based low viscosity hydrogel as a novel carrier for Convection Enhanced Delivery of CAR T cells. *Journal of clinical neuroscience : official journal of the Neurosurgical Society of Australasia, 56*, 163-168. doi: 10.1016/j.jocn.2018.06.005. Repéré à https://www.ncbi.nlm.nih.gov/pubmed/30041899 https://www.ncbi.nlm.nih.gov/pmc/articles/PMC6185757/

Atkins, M. B., Lotze, M. T., Dutcher, J. P., Fisher, R. I., Weiss, G., Margolin, K., . . . Rosenberg, S. A. (1999). High-Dose Recombinant Interleukin 2 Therapy for Patients With Metastatic Melanoma: Analysis of 270 Patients Treated Between 1985 and 1993. *Journal of Clinical Oncology, 17*(7), 2105-2105. doi: 10.1200/JCO.1999.17.7.2105. Repéré à http://dx.doi.org/10.1200/JCO.1999.17.7.2105

Aulisa, L., Dong, H., & Hartgerink, J. D. (2009). Self-Assembly of Multidomain Peptides: Sequence Variation Allows Control over Cross-Linking and Viscoelasticity. *Biomacromolecules, 10*(9), 2694-2698. doi: 10.1021/bm900634x. Repéré à https://doi.org/10.1021/bm900634x

Babaei, J., Mohammadian, M., & Madadlou, A. (2019). Gelatin as texture modifier and porogen in egg white hydrogel. *Food Chemistry, 270*, 189-195. doi: https://doi.org/10.1016/j.foodchem.2018.07.109. Repéré à https://www.sciencedirect.com/science/article/pii/S0308814618312561

Badrinath, N., Jeong, Y. I., Woo, H. Y., Bang, S. Y., Kim, C., Heo, J., . . . Yoo, S. Y. (2018). Local delivery of a cancer-favoring oncolytic vaccinia virus via poly (lactic-co-glycolic acid) nanofiber for theranostic purposes. *International Journal of Pharmaceutics, 552*(1), 437-442. doi: https://doi.org/10.1016/j.ijpharm.2018.10.020. Repéré à https://www.sciencedirect.com/science/article/pii/S0378517318307555

Bencherif, S. A., Sands, R. W., Ali, O. A., Li, W. A., Lewin, S. A., Braschler, T. M., . . . Dranoff, G. (2015). Injectable cryogel-based whole-cell cancer vaccines. *Nature communications, 6*.

Berger, J., Reist, M., Mayer, J. M., Felt, O., & Gurny, R. (2004). Structure and interactions in chitosan hydrogels formed by complexation or aggregation for biomedical applications. *European Journal of Pharmaceutics and Biopharmaceutics, 57*(1), 35-52. doi: http://dx.doi.org/10.1016/S0939-6411(03)00160-7. Repéré à http://www.sciencedirect.com/science/article/pii/S0939641103001607

Berger, J., Reist, M., Mayer, J. M., Felt, O., Peppas, N. A., & Gurny, R. (2004). Structure and interactions in covalently and ionically crosslinked chitosan hydrogels for biomedical applications. *European Journal of Pharmaceutics and Biopharmaceutics, 57*(1), 19-34. doi: http://dx.doi.org/10.1016/S0939-6411(03)00161-9. Repéré à http://www.sciencedirect.com/science/article/pii/S0939641103001619

Berry, R. S., Xiong, M.-J., Greenbaum, A., Mortaji, P., Nofchissey, R. A., Schultz, F., . . . Hanson, J. A. (2017). High levels of tumor-associated neutrophils are associated with improved overall survival in patients with stage II colorectal cancer. *PLOS ONE, 12*(12), e0188799-e0188799. doi: 10.1371/journal.pone.0188799. Repéré à https://pubmed.ncbi.nlm.nih.gov/29211768 https://www.ncbi.nlm.nih.gov/pmc/articles/PMC5718511/

Bhattarai, N., Gunn, J., & Zhang, M. (2010). Chitosan-based hydrogels for controlled, localized drug delivery. *Advanced Drug Delivery Reviews, 62*(1), 83-99. doi: http://dx.doi.org/10.1016/j.addr.2009.07.019. Repéré à http://www.sciencedirect.com/science/article/pii/S0169409X09002828

Bidarra, S. J., Barrias, C. C., & Granja, P. L. (2014). Injectable alginate hydrogels for cell delivery in tissue engineering. *Acta Biomaterialia, 10*(4), 1646-1662. doi: http://dx.doi.org/10.1016/j.actbio.2013.12.006. Repéré à http://www.sciencedirect.com/science/article/pii/S1742706113006028

Bozec, L., & Odlyha, M. (2011). Thermal Denaturation Studies of Collagen by Microthermal Analysis and Atomic Force Microscopy. *Biophysical Journal, 101*(1), 228-236. doi: http://dx.doi.org/10.1016/j.bpj.2011.04.033. Repéré à http://www.sciencedirect.com/science/article/pii/S0006349511004796

Bradley, C. J. (2019). Economic Burden Associated with Cancer Caregiving. *Seminars in Oncology Nursing, 35*(4), 333-336. doi: https://doi.org/10.1016/j.soncn.2019.06.003. Repéré à https://www.sciencedirect.com/science/article/pii/S0749208119300786

Brewer, K., Gundsambuu, B., Facal Marina, P., Barry, S. C., & Blencowe, A. (2020). Thermoresponsive Poly(ε-Caprolactone)-Poly(Ethylene/Propylene Glycol) Copolymers as Injectable Hydrogels for Cell Therapies. *Polymers, 12*(2), 367. doi: 10.3390/polym12020367. Repéré à https://pubmed.ncbi.nlm.nih.gov/32046029 https://www.ncbi.nlm.nih.gov/pmc/articles/PMC7077385/

Brugada-Vilà, P., Cascante, A., Lázaro, M. Á., Castells-Sala, C., Fornaguera, C., Rovira-Rigau, M., . . . Fillat, C. (2020). Oligopeptide-modified poly(beta-amino ester)s-coated AdNuPARmE1A: Boosting the efficacy of intravenously administered therapeutic adenoviruses. *Theranostics, 10*(6), 2744-2758. doi: 10.7150/thno.40902. Repéré à https://www.thno.org/v10p2744.htm

Cai, S. S., Li, T., Akinade, T., Zhu, Y., & Leong, K. W. (2021). Drug delivery carriers with therapeutic functions. *Advanced Drug Delivery Reviews, 176*, 113884. doi: https://doi.org/10.1016/j.addr.2021.113884. Repéré à https://www.sciencedirect.com/science/article/pii/S0169409X21002763

Calafiore, R. (2018). Microencapsulation for cell therapy of type 1 diabetes mellitus: The interplay between common beliefs, prejudices and real progress. *Journal of diabetes investigation, 9*(2), 231-233. doi: 10.1111/jdi.12788. Repéré à https://pubmed.ncbi.nlm.nih.gov/29215800 https://www.ncbi.nlm.nih.gov/pmc/articles/PMC5835460/

Canaple, L., Rehor, A., & Hunkeler, D. (2002). Improving cell encapsulation through size control. *Journal of Biomaterials Science, Polymer Edition, 13*(7), 783-796. doi: 10.1163/156856202760197410. Repéré à https://doi.org/10.1163/156856202760197410

Cancer Research Institute. (2022). FDA Approval Timeline of Active Immunotherapies - Cancer Research Institute. Repéré le 27 October à https://www.cancerresearch.org/fda-approval-timeline-of-active-immunotherapies

Carroll, E. C., Jin, L., Mori, A., Muñoz-Wolf, N., Oleszycka, E., Moran, H. B. T., . . . Lavelle, E. C. (2016). The Vaccine Adjuvant Chitosan Promotes Cellular Immunity via DNA Sensor cGAS-STING-Dependent Induction of Type I Interferons. *Immunity, 44*(3), 597-608. doi: https://doi.org/10.1016/j.immuni.2016.02.004. Repéré à https://www.sciencedirect.com/science/article/pii/S107476131630019X

Ceccaldi, C., Assaad, E., Hui, E., Buccionyte, M., Adoungotchodo, A., & Lerouge, S. (2017). Optimization of Injectable Thermosensitive Scaffolds with Enhanced Mechanical Properties for Cell Therapy. *Macromolecular Bioscience*, 1600435-n/a. doi: 10.1002/mabi.201600435. Repéré à http://dx.doi.org/10.1002/mabi.201600435

Chacon, J. A., Pilon-Thomas, S., Sarnaik, A. A., & Radvanyi, L. G. (2013). Continuous 4–1BB co-stimulatory signals for the optimal expansion of tumor-infiltrating lymphocytes for adoptive T-cell therapy. *Oncoimmunology, 2*(9), e25581. doi: 10.4161/onci.25581. Repéré à http://www.ncbi.nlm.nih.gov/pmc/articles/PMC3850170/

Chen, Daniel S., & Mellman, I. (2013). Oncology Meets Immunology: The Cancer-Immunity Cycle. *Immunity, 39*(1), 1-10. doi: https://doi.org/10.1016/j.immuni.2013.07.012. Repéré à https://www.sciencedirect.com/science/article/pii/S1074761313002963

Chenite, A., Buschmann, M., Wang, D., Chaput, C., & Kandani, N. (2001). Rheological characterisation of thermogelling chitosan/glycerol-phosphate solutions. *Carbohydrate Polymers, 46*(1), 39-47. doi: http://dx.doi.org/10.1016/S0144-8617(00)00281-2. Repéré à http://www.sciencedirect.com/science/article/pii/S0144861700002812

Chenite, A., Chaput, C., Wang, D., Combes, C., Buschmann, M. D., Hoemann, C. D., . . . Selmani, A. (2000). Novel injectable neutral solutions of chitosan form biodegradable gels in situ. *Biomaterials, 21*(21), 2155-2161. doi: 10.1016/s0142-9612(00)00116-2. Repéré à <Go to ISI>://WOS:000088972500006

Cheung, A. S., Zhang, D. K. Y., Koshy, S. T., & Mooney, D. J. (2018). Scaffolds that mimic antigen-presenting cells enable ex vivo expansion of primary T cells. *Nature biotechnology, 36*(2), 160-169. doi: 10.1038/nbt.4047. Repéré à https://doi.org/10.1038/nbt.4047

Chin, A. L., Jiang, S., Jang, E., Niu, L., Li, L., Jia, X., & Tong, R. (2021). Implantable optical fibers for immunotherapeutics delivery and tumor impedance measurement. *Nature communications, 12*(1), 5138. doi: 10.1038/s41467-021-25391-z. Repéré à https://doi.org/10.1038/s41467-021-25391-z

Choi, A. H., O'Leary, M. P., Fong, Y., & Chen, N. G. (2016). From Benchtop to Bedside: A Review of Oncolytic Virotherapy. *Biomedicines, 4*(3). doi: 10.3390/biomedicines4030018. Repéré à https://www.ncbi.nlm.nih.gov/pubmed/28536385

Choi, J. W., Kang, E., Kwon, O. J., Yun, T. J., Park, H. K., Kim, P. H., . . . Yun, C. O. (2013). Local sustained delivery of oncolytic adenovirus with injectable alginate gel for cancer virotherapy. *Gene Therapy, 20*(9), 880-892. doi: 10.1038/gt.2013.10. Repéré à https://doi.org/10.1038/gt.2013.10

Coon, M. E., Stephan, S. B., Gupta, V., Kealey, C. P., & Stephan, M. T. (2019). Nitinol thin films functionalized with CAR-T cells for the treatment of solid tumours. *Nature Biomedical Engineering*. doi: 10.1038/s41551-019-0486-0. Repéré à https://doi.org/10.1038/s41551-019-0486-0

Cormier, A. R., Ruiz-Orta, C., Alamo, R. G., & Paravastu, A. K. (2012). Solid State Self-Assembly Mechanism of RADA16-I Designer Peptide. *Biomacromolecules, 13*(6), 1794-1804. doi: 10.1021/bm300313h. Repéré à https://doi.org/10.1021/bm300313h

Corrales, L., Glickman, L. H., McWhirter, S. M., Kanne, D. B., Sivick, K. E., Katibah, G. E., . . . Gajewski, T. F. (2015). Direct Activation of STING in the Tumor Microenvironment Leads to Potent and Systemic Tumor Regression and Immunity. *Cell reports, 11*(7), 1018-1030. doi: 10.1016/j.celrep.2015.04.031. Repéré à https://pubmed.ncbi.nlm.nih.gov/25959818
https://www.ncbi.nlm.nih.gov/pmc/articles/PMC4440852/

Correa, S., Grosskopf, A. K., Lopez Hernandez, H., Chan, D., Yu, A. C., Stapleton, L. M., & Appel, E. A. (2021). Translational Applications of Hydrogels. *Chemical Reviews, 121*(18), 11385-11457. doi: 10.1021/acs.chemrev.0c01177. Repéré à https://doi.org/10.1021/acs.chemrev.0c01177

Crews, D. W., Dombroski, J. A., & King, M. R. (2021). Prophylactic Cancer Vaccines Engineered to Elicit Specific Adaptive Immune Response. *Frontiers in Oncology, 11*. Repéré à https://www.frontiersin.org/article/10.3389/fonc.2021.626463

Crognale, S., Russo, C., Petruccioli, M., & D'Annibale, A. (2022). Chitosan Production by Fungi: Current State of Knowledge, Future Opportunities and Constraints. *Fermentation, 8*(2). doi: 10.3390/fermentation8020076

Das, R. K., Gocheva, V., Hammink, R., Zouani, O. F., & Rowan, A. E. (2016). Stress-stiffening-mediated stem-cell commitment switch in soft responsive hydrogels. *Nature Materials, 15*(3), 318-325. doi: 10.1038/nmat4483. Repéré à https://doi.org/10.1038/nmat4483

Davidenko, N., Schuster, C. F., Bax, D. V., Farndale, R. W., Hamaia, S., Best, S. M., & Cameron, R. E. (2016). Evaluation of cell binding to collagen and gelatin: a study of the effect of 2D and 3D architecture and surface chemistry. *Journal of materials science. Materials in medicine, 27*(10), 148-148. doi: 10.1007/s10856-016-5763-9. Repéré à https://pubmed.ncbi.nlm.nih.gov/27582068 https://www.ncbi.nlm.nih.gov/pmc/articles/PMC5007264/

Davydova, V. N., Kalitnik, A. A., Markov, P. A., Volod'ko, A. V., Popov, S. V., & Ermak, I. M. (2016). Cytokine-inducing and anti-inflammatory activity of chitosan and its low-molecular derivative. *Applied Biochemistry and Microbiology, 52*(5), 476-482. doi: 10.1134/S0003683816050070. Repéré à https://doi.org/10.1134/S0003683816050070

Dellacherie, M. O., Li, A., Lu, B. Y., Verbeke, C. S., Gu, L., Stafford, A. G., . . . Mooney, D. J. (2020). Single-Shot Mesoporous Silica Rods Scaffold for Induction of Humoral Responses Against Small Antigens. *Advanced Functional Materials, 30*(38), 2002448. doi: https://doi.org/10.1002/adfm.202002448. Repéré à https://doi.org/10.1002/adfm.202002448

. Dendritic Cell Activating Scaffold in Melanoma. https://ClinicalTrials.gov/show/NCT01753089.

Denucci, C. C., Mitchell, J. S., & Shimizu, Y. (2009). Integrin function in T-cell homing to lymphoid and nonlymphoid sites: getting there and staying there. *Critical reviews in immunology, 29*(2), 87-109. doi: 10.1615/critrevimmunol.v29.i2.10. Repéré à https://pubmed.ncbi.nlm.nih.gov/19496742 https://www.ncbi.nlm.nih.gov/pmc/articles/PMC2744463/

Domingues, B., Lopes, J. M., Soares, P., & Populo, H. (2018). Melanoma treatment in review. *IMMUNOTARGETS AND THERAPY, 7*, 35-49. doi: 10.2147/ITT.S134842

Duma, N., Santana-Davila, R., & Molina, J. R. (2019). Non-Small Cell Lung Cancer: Epidemiology, Screening, Diagnosis, and Treatment. *MAYO CLINIC PROCEEDINGS, 94*(8), 1623-1640. doi: 10.1016/j.mayocp.2019.01.013

Eskandari, S., Guerin, T., Toth, I., & Stephenson, R. J. (2017). Recent advances in self-assembled peptides: Implications for targeted drug delivery and vaccine engineering. *Advanced Drug Delivery Reviews, 110-111*, 169-187. doi: https://doi.org/10.1016/j.addr.2016.06.013. Repéré à https://www.sciencedirect.com/science/article/pii/S0169409X1630206X

Fadel, T. R., Sharp, F. A., Vudattu, N., Ragheb, R., Garyu, J., Kim, D., . . . Fahmy, T. M. (2014). A carbon nanotube–polymer composite for T-cell therapy. *Nature Nanotechnology, 9*(8), 639-647. doi: 10.1038/nnano.2014.154. Repéré à https://doi.org/10.1038/nnano.2014.154

Farkona, S., Diamandis, E. P., & Blasutig, I. M. (2016). Cancer immunotherapy: the beginning of the end of cancer? *BMC Medicine, 14*, 73. doi: 10.1186/s12916-016-0623-5. Repéré à http://www.ncbi.nlm.nih.gov/pmc/articles/PMC4858828/

Fenton, O. S., Olafson, K. N., Pillai, P. S., Mitchell, M. J., & Langer, R. (2018). Advances in Biomaterials for Drug Delivery. *Advanced Materials, 30*(29), 1705328. doi: https://doi.org/10.1002/adma.201705328. Repéré à https://doi.org/10.1002/adma.201705328

Fernandez-Poma, S. M., Salas-Benito, D., Lozano, T., Casares, N., Riezu-Boj, J.-I., Mancheño, U., . . . Hervas-Stubbs, S. (2017). Expansion of Tumor-Infiltrating CD8+ T cells Expressing PD-1 Improves the Efficacy of Adoptive T-cell Therapy. *Cancer Research, 77*(13), 3672-3684. doi: 10.1158/0008-5472.CAN-17-0236. Repéré à https://doi.org/10.1158/0008-5472.CAN-17-0236

Filion, D., & Buschmann, M. D. (2013). Chitosan–glycerol-phosphate (GP) gels release freely diffusible GP and possess titratable fixed charge. *Carbohydrate Polymers, 98*(1), 813-819. doi: https://doi.org/10.1016/j.carbpol.2013.06.055. Repéré à https://www.sciencedirect.com/science/article/pii/S0144861713006516

Flanagan, K., Moroziewicz, D., Kwak, H., Hörig, H., & Kaufman, H. L. (2004). The lymphoid chemokine CCL21 costimulates naïve T cell expansion and Th1 polarization of non-regulatory CD4+ T cells. *Cellular Immunology, 231*(1), 75-84. doi: https://doi.org/10.1016/j.cellimm.2004.12.006. Repéré à https://www.sciencedirect.com/science/article/pii/S000887490400200X

Fong, D., Grégoire-Gélinas, P., Cheng, A. P., Mezheritsky, T., Lavertu, M., Sato, S., & Hoemann, C. D. (2017). Lysosomal rupture induced by structurally distinct chitosans either promotes a type 1 IFN response or activates the inflammasome in macrophages. *Biomaterials, 129*, 127-138. doi: https://doi.org/10.1016/j.biomaterials.2017.03.022. Repéré à https://www.sciencedirect.com/science/article/pii/S0142961217301667

Foster, L. J. R., Ho, S., Hook, J., Basuki, M., & Marçal, H. (2015). Chitosan as a Biomaterial: Influence of Degree of Deacetylation on Its Physiochemical, Material and Biological Properties. *PLOS ONE, 10*(8), e0135153. doi: 10.1371/journal.pone.0135153. Repéré à https://doi.org/10.1371/journal.pone.0135153

Galeano Niño, J. L., Pageon, S. V., Tay, S. S., Colakoglu, F., Kempe, D., Hywood, J., . . . Biro, M. (2020). Cytotoxic T cells swarm by homotypic chemokine signalling. *eLife, 9*, e56554. doi: 10.7554/eLife.56554. Repéré à https://doi.org/10.7554/eLife.56554

Ganji, F., & Abdekhodaie, M. J. (2008). Synthesis and characterization of a new thermosensitive chitosan–PEG diblock copolymer. *Carbohydrate Polymers, 74*(3), 435-441. doi: http://dx.doi.org/10.1016/j.carbpol.2008.03.017. Repéré à http://www.sciencedirect.com/science/article/pii/S0144861708001537

Garcia, L., Aguilar, M. R., & San Roman, J. (2010). Biodegradable Hydrogels for Controlled Drug Release. Dans *Biomedical Applications of Hydrogels Handbook* (pp. 147-155). Springer New York. Repéré à https://books.google.ca/books?id=PRvZdNXoO-MC

Ghasemi-Mobarakeh, L., Kolahreez, D., Ramakrishna, S., & Williams, D. (2019). Key terminology in biomaterials and biocompatibility. *Current Opinion in Biomedical Engineering, 10*, 45-50. doi: https://doi.org/10.1016/j.cobme.2019.02.004. Repéré à https://www.sciencedirect.com/science/article/pii/S2468451118300746

Giang Phan, V. H., Duong, H. T. T., Thambi, T., Nguyen, T. L., Turabee, M. H., Yin, Y., . . . Lee, D. S. (2019). Modularly engineered injectable hybrid hydrogels based on protein-polymer network as potent immunologic adjuvant in vivo. *Biomaterials, 195*, 100-110. doi: https://doi.org/10.1016/j.biomaterials.2018.12.034. Repéré à https://www.sciencedirect.com/science/article/pii/S014296121830869X

Goff, S. L., Smith, F. O., Klapper, J. A., Sherry, R., Wunderlich, J. R., Steinberg, S. M., . . . Yang, J. C. (2010). Tumor Infiltrating Lymphocyte Therapy for Metastatic Melanoma: Analysis of Tumors Resected for TIL. *Journal of immunotherapy, 33*(8). Repéré à https://journals.lww.com/immunotherapy-journal/Fulltext/2010/10000/Tumor_Infiltrating_Lymphocyte_Therapy_for.11.aspx

Goff, S. L., Smith, F. O., Klapper, J. A., Sherry, R., Wunderlich, J. R., Steinberg, S. M., . . . Yang, J. C. (2010). Tumor infiltrating lymphocyte therapy for metastatic melanoma: analysis of tumors resected for TIL. *J Immunother, 33*(8), 840-847. doi: 10.1097/CJI.0b013e3181f05b91. Repéré à https://www.ncbi.nlm.nih.gov/pubmed/20842052

Gonzalez-Pujana, A., Santos, E., Orive, G., Pedraz, J. L., & Hernandez, R. M. (2017). Cell microencapsulation technology: Current vision of its therapeutic potential through the administration routes. *Journal of Drug Delivery Science and Technology, 42*, 49-62. doi: https://doi.org/10.1016/j.jddst.2017.03.028. Repéré à https://www.sciencedirect.com/science/article/pii/S177322471630630X

Guyot, C., & Lerouge, S. (2018). Can we achieve the perfect injectable scaffold for cell therapy? *Future Science OA, 4*(4), FSO284. doi: 10.4155/fsoa-2017-0153. Repéré à https://doi.org/10.4155/fsoa-2017-0153

Haanen, J. B. A. G., Thienen, H. v., & Blank, C. U. (2015). Toxicity Patterns With Immunomodulating Antibodies and Their Combinations. *Seminars in Oncology, 42*(3), 423-428. doi: https://doi.org/10.1053/j.seminoncol.2015.02.011. Repéré à https://www.sciencedirect.com/science/article/pii/S0093775415000275

Haase, C., Ejrnaes, M., Juedes, A. E., Wolfe, T., Markholst, H., & von Herrath, M. G. (2005). Immunomodulatory dendritic cells require autologous serum to circumvent nonspecific immunosuppressive activity in vivo. *Blood, 106*(13), 4225-4233. doi: 10.1182/blood-2005-03-0975. Repéré à https://pubmed.ncbi.nlm.nih.gov/16118326 https://www.ncbi.nlm.nih.gov/pmc/articles/PMC1895252/

Hérault, A., Binnewies, M., Leong, S., Calero-Nieto, F. J., Zhang, S. Y., Kang, Y.-A., . . . Passegué, E. (2017). Myeloid progenitor cluster formation drives emergency and leukaemic myelopoiesis. *Nature, 544*(7648), 53-58. doi: 10.1038/nature21693. Repéré à https://doi.org/10.1038/nature21693

Hodi , F. S., O'Day , S. J., McDermott , D. F., Weber , R. W., Sosman , J. A., Haanen , J. B., . . . Urba , W. J. (2010). Improved Survival with Ipilimumab in Patients with Metastatic Melanoma. *New England Journal of Medicine, 363*(8), 711-723. doi: doi:10.1056/NEJMoa1003466. Repéré à http://www.nejm.org/doi/full/10.1056/NEJMoa1003466

Hoesli, C. A., Kiang, R. L. J., Raghuram, K., Pedroza, R. G., Markwick, K. E., Colantuoni, A. M. R., & Piret, J. M. (2017). Mammalian Cell Encapsulation in Alginate Beads Using a Simple Stirred Vessel. *Journal of Visualized Experiments : JoVE,* (124), 55280. doi: 10.3791/55280. Repéré à https://pubmed.ncbi.nlm.nih.gov/28715390 https://www.ncbi.nlm.nih.gov/pmc/articles/PMC5608521/

Hoesli, C. A., Raghuram, K., Kiang, R. L. J., Mocinecová, D., Hu, X., Johnson, J. D., . . . Piret, J. M. (2011). Pancreatic cell immobilization in alginate beads produced by emulsion and internal gelation. *Biotechnology and Bioengineering, 108*(2), 424-434. doi: https://doi.org/10.1002/bit.22959. Repéré à https://doi.org/10.1002/bit.22959

Hoffman, A. S. (2002). Hydrogels for biomedical applications. *Advanced Drug Delivery Reviews, 54*(1), 3-12. doi: http://dx.doi.org/10.1016/S0169-409X(01)00239-3. Repéré à http://www.sciencedirect.com/science/article/pii/S0169409X01002393

Hu, D.-E., Moore, A. M., Thomsen, L. L., & Brindle, K. M. (2004). Uric Acid Promotes Tumor Immune Rejection. *Cancer Research, 64*(15), 5059-5062. doi: 10.1158/0008-5472.CAN-04-1586. Repéré à https://doi.org/10.1158/0008-5472.CAN-04-1586

Hu, D. E., Beauregard, D. A., Bearchell, M. C., Thomsen, L. L., & Brindle, K. M. (2003). Early detection of tumour immune-rejection using magnetic resonance imaging. *British Journal of Cancer, 88*(7), 1135-1142. doi: 10.1038/sj.bjc.6600814. Repéré à https://doi.org/10.1038/sj.bjc.6600814

Hu, Q., Li, H., Archibong, E., Chen, Q., Ruan, H., Ahn, S., . . . Gu, Z. (2021). Inhibition of post-surgery tumour recurrence via a hydrogel releasing CAR-T cells and anti-PDL1-conjugated platelets. *Nature Biomedical Engineering, 5*(9), 1038-1047. doi: 10.1038/s41551-021-00712-1. Repéré à https://doi.org/10.1038/s41551-021-00712-1

Itzhaki, O., Hovav, E., Ziporen, Y., Levy, D., Kubi, A., Zikich, D., . . . Zippel, D. (2011). Establishment and large-scale expansion of minimally cultured "young" tumor infiltrating lymphocytes for adoptive transfer therapy. *Journal of immunotherapy, 34*(2), 212-220.

Jennings, J. A. (2017). 7 - Controlling chitosan degradation properties in vitro and in vivo. Dans J. A. Jennings & J. D. Bumgardner (Éds.), *Chitosan Based Biomaterials Volume 1* (pp. 159-182). Woodhead Publishing. doi: https://doi.org/10.1016/B978-0-08-100230-8.00007-8. Repéré à https://www.sciencedirect.com/science/article/pii/B9780081002308000078

Jin, Q., Zhu, W., Zhu, J., Zhu, J., Shen, J., Liu, Z., . . . Chen, Q. (2021). Nanoparticle-Mediated Delivery of Inhaled Immunotherapeutics for Treating Lung Metastasis. *Advanced Materials, 33*(7), 2007557. doi: https://doi.org/10.1002/adma.202007557. Repéré à https://doi.org/10.1002/adma.202007557

Jung, B.-K., Oh, E., Hong, J., Lee, Y., Park, K. D., & Yun, C.-O. (2017). A hydrogel matrix prolongs persistence and promotes specific localization of an oncolytic adenovirus in a tumor by restricting nonspecific shedding and an antiviral immune response. *Biomaterials, 147*, 26-38. doi: https://doi.org/10.1016/j.biomaterials.2017.09.009. Repéré à https://www.sciencedirect.com/science/article/pii/S0142961217305720

Jung, S.-H., Choi, J.-W., Yun, C.-O., Yhee, J. Y., Price, R., Kim, S. H., . . . Ghandehari, H. (2014). Sustained local delivery of oncolytic short hairpin RNA adenoviruses for treatment of head and neck cancer. *The Journal of Gene Medicine, 16*(5-6), 143-152. doi: https://doi.org/10.1002/jgm.2770. Repéré à https://doi.org/10.1002/jgm.2770

Kasala, D., Lee, S.-H., Hong, J. W., Choi, J.-W., Nam, K., Chung, Y. H., . . . Yun, C.-O. (2017). Synergistic antitumor effect mediated by a paclitaxel-conjugated polymeric micelle-coated oncolytic adenovirus. *Biomaterials, 145*, 207-222. doi: https://doi.org/10.1016/j.biomaterials.2017.08.035. Repéré à https://www.sciencedirect.com/science/article/pii/S0142961217305458

Katlinski, K. V., Gui, J., Katlinskaya, Y. V., Ortiz, A., Chakraborty, R., Bhattacharya, S., . . . Fuchs, S. Y. (2017). Inactivation of Interferon Receptor Promotes the Establishment of Immune Privileged Tumor Microenvironment. *Cancer Cell, 31*(2), 194-207. doi: https://doi.org/10.1016/j.ccell.2017.01.004. Repéré à https://www.sciencedirect.com/science/article/pii/S1535610817300041

Kennedy, R., & Celis, E. (2008). Multiple roles for CD4+ T cells in anti-tumor immune responses. *Immunological Reviews, 222*(1), 129-144. doi: 10.1111/j.1600-065X.2008.00616.x. Repéré à http://dx.doi.org/10.1111/j.1600-065X.2008.00616.x

Kesavadev, J., Saboo, B., Krishna, M. B., & Krishnan, G. (2020). Evolution of Insulin Delivery Devices: From Syringes, Pens, and Pumps to DIY Artificial Pancreas. *Diabetes Therapy, 11*(6), 1251-1269. doi: 10.1007/s13300-020-00831-z. Repéré à https://doi.org/10.1007/s13300-020-00831-z

Kim, J., Li, W. A., Choi, Y., Lewin, S. A., Verbeke, C. S., Dranoff, G., & Mooney, D. J. (2015). Injectable, spontaneously assembling, inorganic scaffolds modulate immune cells in vivo and increase vaccine efficacy. *Nature biotechnology, 33*(1), 64-72. doi: 10.1038/nbt.3071. Repéré à https://pubmed.ncbi.nlm.nih.gov/25485616 https://www.ncbi.nlm.nih.gov/pmc/articles/PMC4318563/

Kim, J., Li, Y., Kim, S. W., Lee, D. S., & Yun, C.-O. (2013). Therapeutic efficacy of a systemically delivered oncolytic adenovirus – Biodegradable polymer complex. *Biomaterials, 34*(19), 4622-4631. doi: https://doi.org/10.1016/j.biomaterials.2013.03.004. Repéré à https://www.sciencedirect.com/science/article/pii/S014296121300286X

Kim, M., Kim, T.-J., Kim, H. M., Doh, J., & Lee, K.-M. (2017). Multi-cellular natural killer (NK) cell clusters enhance NK cell activation through localizing IL-2 within the cluster. *Scientific Reports, 7*(1), 40623. doi: 10.1038/srep40623. Repéré à https://doi.org/10.1038/srep40623

Klebanoff, C. A., Gattinoni, L., Palmer, D. C., Muranski, P., Ji, Y., Hinrichs, C. S., . . . Restifo, N. P. (2011). Determinants of successful CD8+ T-cell adoptive immunotherapy for large established tumors in mice. *Clinical cancer research : an official journal of the American Association for Cancer Research, 17*(16), 5343-5352. doi: 10.1158/1078-0432.CCR-11-0503. Repéré à https://pubmed.ncbi.nlm.nih.gov/21737507 https://www.ncbi.nlm.nih.gov/pmc/articles/PMC3176721/

Klein, I., Cornejo, J. C., Polakos, N. K., John, B., Wuensch, S. A., Topham, D. J., . . . Crispe, I. N. (2007). Kupffer cell heterogeneity: functional properties of bone marrow–derived and sessile hepatic macrophages. *Blood, 110*(12), 4077-4085. doi: 10.1182/blood-2007-02-073841. Repéré à https://doi.org/10.1182/blood-2007-02-073841

Koshy, S. T., & Mooney, D. J. (2016). Biomaterials for enhancing anti-cancer immunity. *Current Opinion in Biotechnology, 40*, 1-8. doi: https://doi.org/10.1016/j.copbio.2016.02.001. Repéré à https://www.sciencedirect.com/science/article/pii/S0958166916300246

Kranz, L. M., Diken, M., Haas, H., Kreiter, S., Loquai, C., Reuter, K. C., . . . Sahin, U. (2016). Systemic RNA delivery to dendritic cells exploits antiviral defence for cancer immunotherapy. *Nature, 534*(7607), 396-401. doi: 10.1038/nature18300. Repéré à https://doi.org/10.1038/nature18300

Kumar, M. N. V. R., Muzzarelli, R. A. A., Muzzarelli, C., Sashiwa, H., & Domb, A. J. (2004). Chitosan Chemistry and Pharmaceutical Perspectives. *Chemical Reviews, 104*(12), 6017-6084. doi: 10.1021/cr030441b. Repéré à http://dx.doi.org/10.1021/cr030441b

Kverneland, A. H., Pedersen, M., Westergaard, M. C. W., Nielsen, M., Borch, T. H., Olsen, L. R., . . . Svane, I. M. (2020). Adoptive cell therapy in combination with checkpoint inhibitors in ovarian cancer. *Oncotarget, 11*(22), 2092-2105. doi: 10.18632/oncotarget.27604. Repéré à https://pubmed.ncbi.nlm.nih.gov/32547707 https://www.ncbi.nlm.nih.gov/pmc/articles/PMC7275789/

Kwon, O.-J., Kang, E., Choi, J.-W., Kim, S. W., & Yun, C.-O. (2013). Therapeutic targeting of chitosan–PEG–folate-complexed oncolytic adenovirus for active and systemic cancer gene therapy. *Journal of Controlled Release, 169*(3), 257-265. doi: https://doi.org/10.1016/j.jconrel.2013.03.030. Repéré à https://www.sciencedirect.com/science/article/pii/S0168365913001739

Lai, J.-Z., Zhu, Y.-Y., Ruan, M., Chen, L., & Zhang, Q.-Y. (2019a). Local Irradiation Sensitized Tumors to Adoptive T Cell Therapy via Enhancing the Cross-Priming, Homing, and Cytotoxicity of Antigen-Specific CD8 T Cells. *Frontiers in Immunology, 10*. Repéré à https://www.frontiersin.org/article/10.3389/fimmu.2019.02857

Lai, J.-Z., Zhu, Y.-Y., Ruan, M., Chen, L., & Zhang, Q.-Y. (2019b). Local Irradiation Sensitized Tumors to Adoptive T Cell Therapy via Enhancing the Cross-Priming, Homing, and Cytotoxicity of Antigen-Specific CD8 T Cells. *Frontiers in Immunology, 10*, 2857. Repéré à https://www.frontiersin.org/article/10.3389/fimmu.2019.02857

Larkin, J., Chiarion-Sileni, V., Gonzalez, R., Grob, J. J., Cowey, C. L., Lao, C. D., . . . Wolchok, J. D. (2015). Combined Nivolumab and Ipilimumab or Monotherapy in Untreated Melanoma. *The New England journal of medicine, 373*(1), 23-34. doi: 10.1056/NEJMoa1504030. Repéré à https://pubmed.ncbi.nlm.nih.gov/26027431 https://www.ncbi.nlm.nih.gov/pmc/articles/PMC5698905/

Lavertu, M., Filion, D., & Buschmann, M. D. (2008). Heat-Induced Transfer of Protons from Chitosan to Glycerol Phosphate Produces Chitosan Precipitation and Gelation. *Biomacromolecules, 9*(2), 640-650. doi: 10.1021/bm700745d. Repéré à http://dx.doi.org/10.1021/bm700745d

Le, T. M. D., Jung, B.-K., Li, Y., Duong, H. T. T., Nguyen, T. L., Hong, J. W., . . . Lee, D. S. (2019). Physically crosslinked injectable hydrogels for long-term delivery of oncolytic adenoviruses for cancer treatment. *Biomaterials Science, 7*(10), 4195-4207. doi: 10.1039/C9BM00992B. Repéré à http://dx.doi.org/10.1039/C9BM00992B

Leach, D. G., Dharmaraj, N., Lopez-Silva, T. L., Venzor, J. R., Pogostin, B. H., Sikora, A. G., . . . Young, S. (2021). Biomaterial-Facilitated Immunotherapy for Established Oral Cancers. *ACS Biomaterials Science & Engineering, 7*(2), 415-421. doi: 10.1021/acsbiomaterials.0c01575. Repéré à https://doi.org/10.1021/acsbiomaterials.0c01575

Lee, J.-j., Kang, J. A., Ryu, Y., Han, S.-S., Nam, Y. R., Rho, J. K., . . . Kim, H.-S. (2017). Genetically engineered and self-assembled oncolytic protein nanoparticles for targeted cancer therapy. *Biomaterials, 120*, 22-31. doi: https://doi.org/10.1016/j.biomaterials.2016.12.014. Repéré à https://www.sciencedirect.com/science/article/pii/S0142961216307323

Lee, S.-Y., Ma, J., Khoo, T. S., Abdullah, N., Nik Md Noordin Kahar, N. N. F., Abdul Hamid, Z. A., & Mustapha, M. (2021). Polysaccharide-Based Hydrogels for Microencapsulation of Stem Cells in Regenerative Medicine. *Frontiers in Bioengineering and Biotechnology, 9*. doi: 10.3389/fbioe.2021.735090. Repéré à https://www.frontiersin.org/article/10.3389/fbioe.2021.735090

Li, A. W., Sobral, M. C., Badrinath, S., Choi, Y., Graveline, A., Stafford, A. G., . . . Mooney, D. J. (2018). A facile approach to enhance antigen response for personalized cancer vaccination. *Nature Materials, 17*(6), 528-534. doi: 10.1038/s41563-018-0028-2. Repéré à https://doi.org/10.1038/s41563-018-0028-2

Li, J., Luo, Y., Li, B., Xia, Y., Wang, H., & Fu, C. (2020). Implantable and Injectable Biomaterial Scaffolds for Cancer Immunotherapy. *Frontiers in Bioengineering and Biotechnology, 8*, 612950-612950. doi: 10.3389/fbioe.2020.612950. Repéré à https://pubmed.ncbi.nlm.nih.gov/33330440 https://www.ncbi.nlm.nih.gov/pmc/articles/PMC7734317/

Li, J., & Mooney, D. J. (2016). Designing hydrogels for controlled drug delivery. *Nature Reviews Materials, 1*(12), 16071. doi: 10.1038/natrevmats.2016.71. Repéré à https://doi.org/10.1038/natrevmats.2016.71

Li, S., Mwakalundwa, G., & Skinner, P. J. (2017). In Situ MHC-tetramer Staining and Quantitative Analysis to Determine the Location, Abundance, and Phenotype of Antigen-specific CD8 T Cells in Tissues. *Journal of Visualized Experiments : JoVE,* (127), 56130. doi: 10.3791/56130. Repéré à https://pubmed.ncbi.nlm.nih.gov/28994787 https://www.ncbi.nlm.nih.gov/pmc/articles/PMC5752327/

Li, X., Kong, X., Zhang, J., Wang, Y., Wang, Y., Shi, S., . . . Qian, Z. (2011). PHARMACEUTICAL NANOTECHNOLOGY: A Novel Composite Hydrogel Based on Chitosan and Inorganic Phosphate for Local Drug Delivery of Camptothecin Nanocolloids. *Journal of Pharmaceutical Sciences, 100*(1), 232-241. doi: http://dx.doi.org/10.1002/jps.22256. Repéré à http://www.sciencedirect.com/science/article/pii/S0022354915323364

Li, Y., Fang, M., Zhang, J., Wang, J., Song, Y., Shi, J., . . . Wang, L. (2015). Hydrogel dual delivered celecoxib and anti-PD-1 synergistically improve antitumor immunity. *Oncoimmunology, 5*(2), e1074374-e1074374. doi: 10.1080/2162402X.2015.1074374. Repéré à https://pubmed.ncbi.nlm.nih.gov/27057439 https://www.ncbi.nlm.nih.gov/pmc/articles/PMC4801446/

Liang, X., Li, L., Li, X., He, T., Gong, S., Zhu, S., . . . Gong, C. (2021). A spontaneous multifunctional hydrogel vaccine amplifies the innate immune response to launch a powerful antitumor adaptive immune response. *Theranostics, 11*(14), 6936-6949. doi: 10.7150/thno.58173. Repéré à https://pubmed.ncbi.nlm.nih.gov/34093863 https://www.ncbi.nlm.nih.gov/pmc/articles/PMC8171104/

Liu, J., Geng, X., Hou, J., & Wu, G. (2021). New insights into M1/M2 macrophages: key modulators in cancer progression. *Cancer Cell International, 21*(1), 389. doi: 10.1186/s12935-021-02089-2. Repéré à https://doi.org/10.1186/s12935-021-02089-2

Liu, L., Tang, X., Wang, Y., & Guo, S. (2011). Smart gelation of chitosan solution in the presence of NaHCO3 for injectable drug delivery system. *International Journal of Pharmaceutics, 414*(1–2), 6-15. doi: http://dx.doi.org/10.1016/j.ijpharm.2011.04.052. Repéré à http://www.sciencedirect.com/science/article/pii/S0378517311003796

Liu, S., Etto, T., Rodríguez-Cruz, T., Li, Y., Wu, C., Fulbright, O. J., . . . Lizée, G. (2010). TGF-β1 Induces Preferential Rapid Expansion and Persistence of Tumor Antigen-specific CD8+ T Cells for Adoptive Immunotherapy. *Journal of immunotherapy, 33*(4), 371-381. doi: 10.1097/CJI.0b013e3181cd1180. Repéré à http://journals.lww.com/immunotherapy-journal/Fulltext/2010/05000/TGF__1_Induces_Preferential_Rapid_Expansion_and.4.aspx

Lu, Y.-C., Zheng, Z., Robbins, P. F., Tran, E., Prickett, T. D., Gartner, J. J., . . . Rosenberg, S. A. (2018). An Efficient Single-Cell RNA-Seq Approach to Identify Neoantigen-Specific T Cell Receptors. *Molecular Therapy, 26*(2), 379-389. doi: https://doi.org/10.1016/j.ymthe.2017.10.018. Repéré à https://www.sciencedirect.com/science/article/pii/S1525001617305555

Lu, Y., Wu, C., Yang, Y., Chen, X., Ge, F., Wang, J., & Deng, J. (2022). Inhibition of tumor recurrence and metastasis via a surgical tumor-derived personalized hydrogel vaccine. *Biomaterials Science, 10*(5), 1352-1363. doi: 10.1039/D1BM01596F. Repéré à http://dx.doi.org/10.1039/D1BM01596F

Luo, Z., Liu, Z., Liang, Z., Pan, J., Xu, J., Dong, J., . . . Wei, S. (2020). Injectable Porous Microchips with Oxygen Reservoirs and an Immune-Niche Enhance the Efficacy of CAR T Cell Therapy in Solid Tumors. *ACS Applied Materials & Interfaces, 12*(51), 56712-56722. doi: 10.1021/acsami.0c15239. Repéré à https://doi.org/10.1021/acsami.0c15239

Luo, Z., Wu, Q., Yang, C., Wang, H., He, T., Wang, Y., . . . Yang, Z. (2017). A Powerful CD8+ T-Cell Stimulating D-Tetra-Peptide Hydrogel as a Very Promising Vaccine Adjuvant. *Advanced Materials, 29*(5), 1601776. doi: https://doi.org/10.1002/adma.201601776. Repéré à https://doi.org/10.1002/adma.201601776

Mackensen, A., Dräger, R., Schlesier, M., Mertelsmann, R., & Lindemann, A. (2000). Presence of IgE antibodies to bovine serum albumin in a patient developing anaphylaxis after vaccination with human peptide-pulsed dendritic cells. *Cancer Immunology, Immunotherapy, 49*(3), 152-156. doi: 10.1007/s002620050614. Repéré à https://doi.org/10.1007/s002620050614

Madan, R. A., Antonarakis, E. S., Drake, C. G., Fong, L., Yu, E. Y., McNeel, D. G., . . . Gulley, J. L. (2020). Putting the Pieces Together: Completing the Mechanism of Action Jigsaw for Sipuleucel-T. *JNCI: Journal of the National Cancer Institute, 112*(6), 562-573. doi: 10.1093/jnci/djaa021. Repéré à https://doi.org/10.1093/jnci/djaa021

Malaret, T. (2022). *Conception et validation d'un modèle 3D de tumeur avec immunothérapie*.

Mariani, E., Lisignoli, G., Borzì, R. M., & Pulsatelli, L. (2019). Biomaterials: Foreign Bodies or Tuners for the Immune Response? *International journal of molecular sciences, 20*(3), 636. doi: 10.3390/ijms20030636. Repéré à https://pubmed.ncbi.nlm.nih.gov/30717232 https://www.ncbi.nlm.nih.gov/pmc/articles/PMC6386828/

Martínez-Lostao, L., Anel, A., & Pardo, J. (2015). How Do Cytotoxic Lymphocytes Kill Cancer Cells? *Clinical Cancer Research, 21*(22), 5047-5056. doi: 10.1158/1078-0432.ccr-15-0685

Mi, Y., Smith, C. C., Yang, F., Qi, Y., Roche, K. C., Serody, J. S., . . . Wang, A. Z. (2018). A Dual Immunotherapy Nanoparticle Improves T-Cell Activation and Cancer Immunotherapy. *Advanced Materials, 30*(25), 1706098. doi: https://doi.org/10.1002/adma.201706098. Repéré à https://doi.org/10.1002/adma.201706098

Monette, A., Ceccaldi, C., Assaad, E., Lerouge, S., & Lapointe, R. (2016). Chitosan thermogels for local expansion and delivery of tumor-specific T lymphocytes towards enhanced cancer immunotherapies. *Biomaterials, 75*, 237-249. doi: https://doi.org/10.1016/j.biomaterials.2015.10.021. Repéré à https://www.sciencedirect.com/science/article/pii/S014296121500825X

Mullinax, J. E., Hall, M., Prabhakaran, S., Weber, J., Khushalani, N., Eroglu, Z., . . . Sarnaik, A. A. (2018). Combination of Ipilimumab and Adoptive Cell Therapy with Tumor-Infiltrating Lymphocytes for Patients with Metastatic Melanoma. *Frontiers in Oncology, 8*, 44. Repéré à https://www.frontiersin.org/article/10.3389/fonc.2018.00044

Nair, L. S., Starnes, T., Ko, J.-W. K., & Laurencin, C. T. (2007). Development of Injectable Thermogelling Chitosan–Inorganic Phosphate Solutions for Biomedical Applications. *Biomacromolecules, 8*(12), 3779-3785. doi: 10.1021/bm7006967. Repéré à http://dx.doi.org/10.1021/bm7006967

Najibi, A. J., Shih, T.-Y., & Mooney, D. J. (2022). Cryogel vaccines effectively induce immune responses independent of proximity to the draining lymph nodes. *Biomaterials, 281*, 121329. doi: https://doi.org/10.1016/j.biomaterials.2021.121329. Repéré à https://www.sciencedirect.com/science/article/pii/S0142961221006852

Neelapu, S. S., Tummala, S., Kebriaei, P., Wierda, W., Gutierrez, C., Locke, F. L., . . . Shpall, E. J. (2018). Chimeric antigen receptor T-cell therapy - assessment and management of toxicities. *Nature reviews. Clinical oncology, 15*(1), 47-62. doi: 10.1038/nrclinonc.2017.148. Repéré à https://pubmed.ncbi.nlm.nih.gov/28925994 https://www.ncbi.nlm.nih.gov/pmc/articles/PMC6733403/

Niu, H., Li, X., Li, H., Fan, Z., Ma, J., & Guan, J. (2019). Thermosensitive, fast gelling, photoluminescent, highly flexible, and degradable hydrogels for stem cell delivery. *Acta Biomaterialia, 83*, 96-108. doi: https://doi.org/10.1016/j.actbio.2018.10.038. Repéré à https://www.sciencedirect.com/science/article/pii/S1742706118306378

Nkanga, C. I., & Steinmetz, N. F. (2022). Injectable Hydrogel Containing Cowpea Mosaic Virus Nanoparticles Prevents Colon Cancer Growth. *ACS Biomaterials Science & Engineering, 8*(6), 2518-2525. doi: 10.1021/acsbiomaterials.2c00284. Repéré à https://doi.org/10.1021/acsbiomaterials.2c00284

O'Brien, F. J. (2011). Biomaterials & scaffolds for tissue engineering. *Materials Today, 14*(3), 88-95. doi: http://dx.doi.org/10.1016/S1369-7021(11)70058-X. Repéré à http://www.sciencedirect.com/science/article/pii/S136970211170058X

Ogunnaike Edikan, A., Valdivia, A., Yazdimamaghani, M., Leon, E., Nandi, S., Hudson, H., . . . Dotti, G. Fibrin gel enhances the antitumor effects of chimeric antigen receptor T cells in glioblastoma. *Science Advances, 7*(41), eabg5841. doi: 10.1126/sciadv.abg5841. Repéré à https://doi.org/10.1126/sciadv.abg5841

Oh, E., Oh, J.-E., Hong, J., Chung, Y., Lee, Y., Park, K. D., . . . Yun, C.-O. (2017). Optimized biodegradable polymeric reservoir-mediated local and sustained co-delivery of dendritic cells and oncolytic adenovirus co-expressing IL-12 and GM-CSF for cancer immunotherapy. *Journal of Controlled Release, 259*, 115-127. doi: https://doi.org/10.1016/j.jconrel.2017.03.028. Repéré à https://www.sciencedirect.com/science/article/pii/S0168365917301396

Palladini, A., Thrane, S., Janitzek, C. M., Pihl, J., Clemmensen, S. B., de Jongh, W. A., . . . Sander, A. F. (2018). Virus-like particle display of HER2 induces potent anti-cancer responses. *Oncoimmunology, 7*(3), e1408749-e1408749. doi: 10.1080/2162402X.2017.1408749. Repéré à https://pubmed.ncbi.nlm.nih.gov/29399414 https://www.ncbi.nlm.nih.gov/pmc/articles/PMC5790387/

Patel, R., Kaki, M., Potluri, V. S., Kahar, P., & Khanna, D. (2022). A comprehensive review of SARS-CoV-2 vaccines: Pfizer, Moderna & Johnson & Johnson. *Human Vaccines & Immunotherapeutics, 18*(1), 2002083. doi: 10.1080/21645515.2021.2002083. Repéré à https://doi.org/10.1080/21645515.2021.2002083

Pei, M., Liang, J., Zhang, C., Wang, X., Zhang, C., Ma, G., & Sun, H. (2019). Chitosan/calcium phosphates nanosheet as a vaccine carrier for effective cross-presentation of exogenous antigens. *Carbohydrate Polymers, 224*, 115172. doi: https://doi.org/10.1016/j.carbpol.2019.115172. Repéré à https://www.sciencedirect.com/science/article/pii/S0144861719308392

Pérez del Río, E., Santos, F., Rodriguez Rodriguez, X., Martínez-Miguel, M., Roca-Pinilla, R., Arís, A., . . . Guasch, J. (2020). CCL21-loaded 3D hydrogels for T cell expansion and differentiation. *Biomaterials, 259*, 120313. doi: https://doi.org/10.1016/j.biomaterials.2020.120313. Repéré à https://www.sciencedirect.com/science/article/pii/S0142961220305597

Perica, K., De León Medero, A., Durai, M., Chiu, Y. L., Bieler, J. G., Sibener, L., . . . Schneck, J. (2014). Nanoscale artificial antigen presenting cells for T cell immunotherapy. *Nanomedicine : nanotechnology, biology, and medicine, 10*(1), 119-129. doi: 10.1016/j.nano.2013.06.015. Repéré à https://pubmed.ncbi.nlm.nih.gov/23891987 https://www.ncbi.nlm.nih.gov/pmc/articles/PMC4114774/

Pillai, C. K. S., Paul, W., & Sharma, C. P. (2009). Chitin and chitosan polymers: Chemistry, solubility and fiber formation. *Progress in Polymer Science, 34*(7), 641-678. doi: http://dx.doi.org/10.1016/j.progpolymsci.2009.04.001. Repéré à http://www.sciencedirect.com/science/article/pii/S0079670009000318

Rademakers, T., Horvath, J. M., van Blitterswijk, C. A., & LaPointe, V. L. S. (2019). Oxygen and nutrient delivery in tissue engineering: Approaches to graft vascularization. *Journal of Tissue Engineering and Regenerative Medicine, 13*(10), 1815-1829. doi: https://doi.org/10.1002/term.2932. Repéré à https://doi.org/10.1002/term.2932

Raman, S. S., Hecht, J. R., & Chan, E. (2019). Talimogene laherparepvec: review of its mechanism of action and clinical efficacy and safety. *Immunotherapy, 11*(8), 705-723. doi: 10.2217/imt-2019-0033. Repéré à https://doi.org/10.2217/imt-2019-0033

Recillas, M., Silva, L. L., Peniche, C., Goycoolea, F. M., Rinaudo, M., & Argüelles-Monal, W. M. (2009). Thermoresponsive Behavior of Chitosan-g-N-isopropylacrylamide Copolymer Solutions. *Biomacromolecules, 10*(6), 1633-1641. doi: 10.1021/bm9002317. Repéré à http://dx.doi.org/10.1021/bm9002317

Riley, R. S., June, C. H., Langer, R., & Mitchell, M. J. (2019). Delivery technologies for cancer immunotherapy. *Nature Reviews Drug Discovery, 18*(3), 175-196. doi: 10.1038/s41573-018-0006-z. Repéré à https://doi.org/10.1038/s41573-018-0006-z

Roche, E. T., Hastings, C. L., Lewin, S. A., Shvartsman, D. E., Brudno, Y., Vasilyev, N. V., . . . Mooney, D. J. (2014). Comparison of biomaterial delivery vehicles for improving acute retention of stem cells in the infarcted heart. *Biomaterials, 35*(25), 6850-6858. doi: https://doi.org/10.1016/j.biomaterials.2014.04.114. Repéré à https://www.sciencedirect.com/science/article/pii/S0142961214005274

Rock, K. L., & Kono, H. (2008). The inflammatory response to cell death. *Annual review of pathology, 3*, 99-126. doi: 10.1146/annurev.pathmechdis.3.121806.151456. Repéré à https://pubmed.ncbi.nlm.nih.gov/18039143 https://www.ncbi.nlm.nih.gov/pmc/articles/PMC3094097/

Ruel-Gariépy, E., & Leroux, J.-C. (2004). In situ-forming hydrogels—review of temperature-sensitive systems. *European Journal of Pharmaceutics and Biopharmaceutics, 58*(2), 409-426. doi: http://dx.doi.org/10.1016/j.ejpb.2004.03.019. Repéré à http://www.sciencedirect.com/science/article/pii/S0939641104000876

Shah, N. J., Najibi, A. J., Shih, T.-Y., Mao, A. S., Sharda, A., Scadden, D. T., & Mooney, D. J. (2020). A biomaterial-based vaccine eliciting durable tumour-specific responses against acute myeloid leukaemia. *Nature Biomedical Engineering, 4*(1), 40-51. doi: 10.1038/s41551-019-0503-3. Repéré à https://doi.org/10.1038/s41551-019-0503-3

Shapira-Frommer, R., & Schachter, J. (2012). Adoptive immunotherapy of advanced melanoma. *Current treatment options in oncology, 13*(3), 340-353. doi: 10.1007/s11864-012-0203-7. Repéré à http://europepmc.org/abstract/MED/22864561 https://doi.org/10.1007/s11864-012-0203-7

Shapira-Frommer, R., & Schachter, J. (2012). Adoptive immunotherapy of advanced melanoma. *Curr Treat Options Oncol, 13*(3), 340-353. doi: 10.1007/s11864-012-0203-7. Repéré à https://www.ncbi.nlm.nih.gov/pubmed/22864561

Sharonov, G. V., Serebrovskaya, E. O., Yuzhakova, D. V., Britanova, O. V., & Chudakov, D. M. (2020). B cells, plasma cells and antibody repertoires in the tumour microenvironment. *Nature Reviews Immunology, 20*(5), 294-307. doi: 10.1038/s41577-019-0257-x. Repéré à https://doi.org/10.1038/s41577-019-0257-x

Shemesh, C. S., Hsu, J. C., Hosseini, I., Shen, B.-Q., Rotte, A., Twomey, P., . . . Wu, B. (2021). Personalized Cancer Vaccines: Clinical Landscape, Challenges, and Opportunities. *Molecular therapy : the journal of the American Society of Gene Therapy, 29*(2), 555-570. doi: 10.1016/j.ymthe.2020.09.038. Repéré à https://pubmed.ncbi.nlm.nih.gov/33038322 https://www.ncbi.nlm.nih.gov/pmc/articles/PMC7854282/

Shi, Y., Xie, T.-x., Leach, D. G., Wang, B., Young, S., Osman, A. A., . . . Rangel, R. (2021). Local Anti–PD-1 Delivery Prevents Progression of Premalignant Lesions in a 4NQO-Oral Carcinogenesis Mouse Model. *Cancer Prevention Research, 14*(8), 767-778. doi: 10.1158/1940-6207.CAPR-20-0607. Repéré à https://doi.org/10.1158/1940-6207.CAPR-20-0607

Shimasaki, N., Jain, A., & Campana, D. (2020). NK cells for cancer immunotherapy. *Nature Reviews Drug Discovery, 19*(3), 200-218. doi: 10.1038/s41573-019-0052-1. Repéré à https://doi.org/10.1038/s41573-019-0052-1

Sitarz, R., Skierucha, M., Mielko, J., Offerhaus, G. J. A., Maciejewski, R., & Polkowski, W. P. (2018). Gastric cancer: epidemiology, prevention, classification, and treatment. *CANCER MANAGEMENT AND RESEARCH, 10*, 239-248. doi: 10.2147/CMAR.S149619

Smith, T. T., Moffett, H. F., Stephan, S. B., Opel, C. F., Dumigan, A. G., Jiang, X., . . . Stephan, M. T. (2017). Biopolymers codelivering engineered T cells and STING agonists can eliminate heterogeneous tumors. *The Journal of Clinical Investigation, 127*(6), 2176-2191. doi: 10.1172/JCI87624. Repéré à http://www.ncbi.nlm.nih.gov/pmc/articles/PMC5451231/

Sponchioni, M., Capasso Palmiero, U., & Moscatelli, D. (2019). Thermo-responsive polymers: Applications of smart materials in drug delivery and tissue engineering. *Materials Science and Engineering: C, 102*, 589-605. doi: https://doi.org/10.1016/j.msec.2019.04.069. Repéré à https://www.sciencedirect.com/science/article/pii/S0928493119307775

Stagg, J., Divisekera, U., Duret, H., Sparwasser, T., Teng, M. W. L., Darcy, P. K., & Smyth, M. J. (2011). CD73-Deficient Mice Have Increased Antitumor Immunity and Are Resistant to Experimental Metastasis. *Cancer Research, 71*(8), 2892-2900. doi: 10.1158/0008-5472.can-10-4246

Stephan, M. T., Moon, J. J., Um, S. H., Bershteyn, A., & Irvine, D. J. (2010). Therapeutic cell engineering with surface-conjugated synthetic nanoparticles. *Nature Medicine, 16*(9), 1035-1041. doi: 10.1038/nm.2198. Repéré à https://doi.org/10.1038/nm.2198

Stephan, S. B., Taber, A. M., Jileaeva, I., Pegues, E. P., Sentman, C. L., & Stephan, M. T. (2015). Biopolymer implants enhance the efficacy of adoptive T cell therapy. *Nature biotechnology, 33*(1), 97-101. doi: 10.1038/nbt.3104. Repéré à http://www.ncbi.nlm.nih.gov/pmc/articles/PMC4289408/

Strand, B. L., Coron, A. E., & Skjak-Braek, G. (2017). Current and Future Perspectives on Alginate Encapsulated Pancreatic Islet. *Stem Cells Translational Medicine, 6*(4), 1053-1058. doi: 10.1002/sctm.16-0116. Repéré à https://doi.org/10.1002/sctm.16-0116

Sun, X., Han, X., Xu, L., Gao, M., Xu, J., Yang, R., & Liu, Z. (2017). Surface-Engineering of Red Blood Cells as Artificial Antigen Presenting Cells Promising for Cancer Immunotherapy. *Small, 13*(40), 1701864. doi: https://doi.org/10.1002/smll.201701864. Repéré à https://doi.org/10.1002/smll.201701864

Sun, Z., Liang, J., Dong, X., Wang, C., Kong, D., & Lv, F. (2018). Injectable Hydrogels Coencapsulating Granulocyte-Macrophage Colony-Stimulating Factor and Ovalbumin Nanoparticles to Enhance Antigen Uptake Efficiency. *ACS Applied Materials & Interfaces, 10*(24), 20315-20325. doi: 10.1021/acsami.8b04312. Repéré à https://doi.org/10.1021/acsami.8b04312

Sung, H., Ferlay, J., Siegel, R. L., Laversanne, M., Soerjomataram, I., Jemal, A., & Bray, F. (2021). Global Cancer Statistics 2020: GLOBOCAN Estimates of Incidence and Mortality Worldwide for 36 Cancers in 185 Countries. *CA: A Cancer Journal for Clinicians, 71*(3), 209-249. doi: https://doi.org/10.3322/caac.21660. Repéré à https://doi.org/10.3322/caac.21660

Sung Lee, D., & He, C. (2010). In-Situ Gelling Stimuli-Sensitive PEG-Based Amphiphilic Copolymer Hydrogels. Dans *Biomedical Applications of Hydrogels Handbook* (pp. 123-144). Springer New York. Repéré à https://books.google.ca/books?id=PRvZdNXoO-MC

Supper, S., Anton, N., Seidel, N., Riemenschnitter, M., Schoch, C., & Vandamme, T. (2013). Rheological Study of Chitosan/Polyol-phosphate Systems: Influence of the Polyol Part on the Thermo-Induced Gelation Mechanism. *Langmuir, 29*(32), 10229-10237. doi: 10.1021/la401993q. Repéré à http://dx.doi.org/10.1021/la401993q

TA Instruments. (2016). Fundamentals of Polymer Rheology. Repéré le 27 October à https://www.tainstruments.com/wp-content/uploads/TA-Instruments-CUICAR-presentation-201609-Polymer-Rheology.pdf

Tawbi, H. A., Schadendorf, D., Lipson, E. J., Ascierto, P. A., Matamala, L., Castillo Gutiérrez, E., . . . Long, G. V. (2022). Relatlimab and Nivolumab versus Nivolumab in Untreated Advanced Melanoma. *New England Journal of Medicine, 386*(1), 24-34. doi: 10.1056/NEJMoa2109970. Repéré à https://doi.org/10.1056/NEJMoa2109970

Tian, Y., Xu, C., Feng, J., Huangfu, Y., Wang, K., & Zhang, Z.-L. (2021). Personalized gel-droplet monocyte vaccines for cancer immunotherapy. *Lab on a Chip, 21*(22), 4414-4426. doi: 10.1039/D1LC00646K. Repéré à http://dx.doi.org/10.1039/D1LC00646K

Torre, L. A., Siegel, R. L., Ward, E. M., & Jemal, A. (2016). Global Cancer Incidence and Mortality Rates and Trends—An Update. *Cancer Epidemiology, Biomarkers & Prevention, 25*(1), 16-27. doi: 10.1158/1055-9965.EPI-15-0578. Repéré à https://doi.org/10.1158/1055-9965.EPI-15-0578

Tsao, C.-T., Kievit, F. M., Ravanpay, A., Erickson, A. E., Jensen, M. C., Ellenbogen, R. G., & Zhang, M. (2014). Thermoreversible Poly(ethylene glycol)-g-Chitosan Hydrogel as a Therapeutic T Lymphocyte Depot for Localized Glioblastoma Immunotherapy. *Biomacromolecules, 15*(7), 2656-2662. doi: 10.1021/bm500502n. Repéré à http://dx.doi.org/10.1021/bm500502n

Van Vlierberghe, S., Dubruel, P., & Schacht, E. (2011). Biopolymer-Based Hydrogels As Scaffolds for Tissue Engineering Applications: A Review. *Biomacromolecules, 12*(5), 1387-1408. doi: 10.1021/bm200083n. Repéré à http://dx.doi.org/10.1021/bm200083n

Verma, V., Kim, Y., Lee, M.-C., Lee, J.-T., Cho, S., Park, I.-K., . . . Rhee, J. H. (2016). Activated dendritic cells delivered in tissue compatible biomatrices induce in-situ anti-tumor CTL responses leading to tumor regression. *Oncotarget, 7*(26), 39894-39906. doi: 10.18632/oncotarget.9529. Repéré à http://www.ncbi.nlm.nih.gov/pmc/articles/PMC5129979/

Visioni, A., Kim, M., Wilfong, C., Blum, A., Powers, C., Fisher, D., . . . Skitzki, J. (2018). Intra-arterial Versus Intravenous Adoptive Cell Therapy in a Mouse Tumor Model. *Journal of immunotherapy (Hagerstown, Md. : 1997), 41*(7), 313-318. doi: 10.1097/CJI.0000000000000235. Repéré à https://pubmed.ncbi.nlm.nih.gov/29985207 https://www.ncbi.nlm.nih.gov/pmc/articles/PMC6092084/

Waghule, T., Singhvi, G., Dubey, S. K., Pandey, M. M., Gupta, G., Singh, M., & Dua, K. (2019). Microneedles: A smart approach and increasing potential for transdermal drug delivery system. *Biomedicine & Pharmacotherapy, 109*, 1249-1258. doi: https://doi.org/10.1016/j.biopha.2018.10.078. Repéré à https://www.sciencedirect.com/science/article/pii/S0753332218348091

Waldman, A. D., Fritz, J. M., & Lenardo, M. J. (2020). A guide to cancer immunotherapy: from T cell basic science to clinical practice. *Nature reviews. Immunology, 20*(11), 651-668. doi: 10.1038/s41577-020-0306-5. Repéré à https://pubmed.ncbi.nlm.nih.gov/32433532 https://www.ncbi.nlm.nih.gov/pmc/articles/PMC7238960/

Wang, C., Wang, J., Zhang, X., Yu, S., Wen, D., Hu, Q., . . . Gu, Z. (2018). In situ formed reactive oxygen species–responsive scaffold with gemcitabine and checkpoint inhibitor for combination therapy. *Science Translational Medicine, 10*(429), eaan3682. doi: 10.1126/scitranslmed.aan3682. Repéré à https://doi.org/10.1126/scitranslmed.aan3682

Wang, K., Chen, Y., Ahn, S., Zheng, M., Landoni, E., Dotti, G., . . . Han, Z. (2020). GD2-specific CAR T cells encapsulated in an injectable hydrogel control retinoblastoma and preserve vision. *Nature Cancer, 1*(10), 990-997. doi: 10.1038/s43018-020-00119-y. Repéré à https://doi.org/10.1038/s43018-020-00119-y

Weiden, J. (2019). *Synthetic immune niches for localized cancer therapy* (PhD, Radboud University Nijmegen). Repéré à https://repository.ubn.ru.nl/bitstream/handle/2066/213928/213928.pdf

Weiden, J., Voerman, D., Dölen, Y., Das, R. K., van Duffelen, A., Hammink, R., . . . Figdor, C. G. (2018). Injectable Biomimetic Hydrogels as Tools for Efficient T Cell Expansion and Delivery. *Frontiers in Immunology, 9*, 2798-2798. doi: 10.3389/fimmu.2018.02798. Repéré à https://www.ncbi.nlm.nih.gov/pubmed/30546367 https://www.ncbi.nlm.nih.gov/pmc/articles/PMC6279891/

Wilky, B. A. (2019). Immune checkpoint inhibitors: The linchpins of modern immunotherapy. *Immunological Reviews, 290*(1), 6-23. doi: https://doi.org/10.1111/imr.12766. Repéré à https://doi.org/10.1111/imr.12766

Winter, H. (1986). Analysis of Linear Viscoelasticity of a Cross-Linking Polymer at the Gel Point. *Journal of Rheology - J RHEOL, 30*. doi: 10.1122/1.549853

Wissinger, E., Griebsch, I., Lungershausen, J., Foster, T., & Pashos, C. L. (2014). The Economic Burden of Head and Neck Cancer: A Systematic Literature Review. *PharmacoEconomics, 32*(9), 865-882. doi: 10.1007/s40273-014-0169-3. Repéré à https://doi.org/10.1007/s40273-014-0169-3

Workman, C. J., & Vignali, D. A. A. (2005). Negative Regulation of T Cell Homeostasis by Lymphocyte Activation Gene-3 (CD223). *The Journal of Immunology, 174*(2), 688. doi: 10.4049/jimmunol.174.2.688. Repéré à http://www.jimmunol.org/content/174/2/688.abstract

Wu, R., Forget, M.-A., Chacon, J., Bernatchez, C., Haymaker, C., Chen, J. Q., . . . Radvanyi, L. G. (2012). Adoptive T-Cell Therapy Using Autologous Tumor-Infiltrating Lymphocytes for Metastatic Melanoma: Current Status and Future Outlook. *The Cancer Journal, 18*(2). Repéré à https://journals.lww.com/journalppo/Fulltext/2012/03000/Adoptive_T_Cell_Therapy_Using_Autologous.9.aspx

Wu, R., Forget, M. A., Chacon, J., Bernatchez, C., Haymaker, C., Chen, J. Q., . . . Radvanyi, L. G. (2012). Adoptive T-cell therapy using autologous tumor-infiltrating lymphocytes for metastatic melanoma: current status and future outlook. *Cancer J, 18*(2), 160-175. doi: 10.1097/PPO.0b013e31824d4465. Repéré à https://www.ncbi.nlm.nih.gov/pubmed/22453018

Ya, Z., Hailemichael, Y., Overwijk, W., & Restifo, N. P. (2015). Mouse model for pre-clinical study of human cancer immunotherapy. *Current protocols in immunology, 108*, 20.21.21-20.21.43. doi: 10.1002/0471142735.im2001s108. Repéré à https://pubmed.ncbi.nlm.nih.gov/25640991 https://www.ncbi.nlm.nih.gov/pmc/articles/PMC4361407/

Yadav, S. (2018). Correlation analysis in biological studies. *Journal of the Practice of Cardiovascular Sciences, 4*(2), 116-121. doi: 10.4103/jpcs.jpcs_31_18. Repéré à https://www.j-pcs.org/article.asp?issn=2395-5414;year=2018;volume=4;issue=2;spage=116;epage=121;aulast=Yadav

Yan, J., Gundsambuu, B., Krasowska, M., Platts, K., Facal Marina, P., Gerber, C., . . . Blencowe, A. (2022). Injectable Diels–Alder cycloaddition hydrogels with tuneable gelation, stiffness and degradation for the sustained release of T-lymphocytes. *Journal of Materials Chemistry B*. doi: 10.1039/D2TB00274D. Repéré à http://dx.doi.org/10.1039/D2TB00274D

Yang, A., Bai, Y., Dong, X., Ma, T., Zhu, D., Mei, L., & Lv, F. (2021). Hydrogel/nanoadjuvant-mediated combined cell vaccines for cancer immunotherapy. *Acta Biomaterialia, 133*, 257-267. doi: https://doi.org/10.1016/j.actbio.2021.08.014. Repéré à https://www.sciencedirect.com/science/article/pii/S1742706121005407

Yang, A., Dong, X., Bai, Y., Sheng, S., Zhang, Y., Liu, T., . . . Lv, F. (2021). Doxorubicin/CpG self-assembled nanoparticles prodrug and dendritic cells co-laden hydrogel for cancer chemo-assisted immunotherapy. *Chemical Engineering Journal, 416*, 129192. doi: https://doi.org/10.1016/j.cej.2021.129192. Repéré à https://www.sciencedirect.com/science/article/pii/S138589472100783X

Yang, J. C. (2015). Toxicities Associated With Adoptive T-Cell Transfer for Cancer. *Cancer journal (Sudbury, Mass.), 21*(6), 506-509. doi: 10.1097/PPO.0000000000000157. Repéré à https://pubmed.ncbi.nlm.nih.gov/26588684 https://www.ncbi.nlm.nih.gov/pmc/articles/PMC4656113/

Yang, P., Chen, M., Qin, W., Shi, C., Bai, X., Quan, G., . . . Wu, C. (2021). Effective Photothermal Therapy Mediated by Indocyanine Green Nanoparticle Tip-Loaded Microneedles to Enhance Checkpoint Inhibitor Immunotherapy for Melanoma Treatment. *ACS Applied Nano Materials, 4*(6), 5921-5931. doi: 10.1021/acsanm.1c00832. Repéré à https://doi.org/10.1021/acsanm.1c00832

Yang, P., Lu, C., Qin, W., Chen, M., Quan, G., Liu, H., . . . Wu, C. (2020). Construction of a core-shell microneedle system to achieve targeted co-delivery of checkpoint inhibitors for melanoma immunotherapy. *Acta Biomaterialia, 104*, 147-157. doi: https://doi.org/10.1016/j.actbio.2019.12.037. Repéré à https://www.sciencedirect.com/science/article/pii/S1742706119308803

Yang, P., Song, H., Qin, Y., Huang, P., Zhang, C., Kong, D., & Wang, W. (2018). Engineering Dendritic-Cell-Based Vaccines and PD-1 Blockade in Self-Assembled Peptide Nanofibrous Hydrogel to Amplify Antitumor T-Cell Immunity. *Nano Letters, 18*(7), 4377-4385. doi: 10.1021/acs.nanolett.8b01406. Repéré à https://doi.org/10.1021/acs.nanolett.8b01406

Yang, Y., & Lundqvist, A. (2020). Immunomodulatory Effects of IL-2 and IL-15; Implications for Cancer Immunotherapy. *Cancers, 12*(12). doi: 10.3390/cancers12123586

Younes, I., & Rinaudo, M. (2015). Chitin and Chitosan Preparation from Marine Sources. Structure, Properties and Applications. *Marine Drugs, 13*(3). doi: 10.3390/md13031133

Zeng, J., Li, X., Sander, M., Zhang, H., Yan, G., & Lin, Y. (2021). Oncolytic Viro-Immunotherapy: An Emerging Option in the Treatment of Gliomas. *Frontiers in Immunology, 12*. doi: 10.3389/fimmu.2021.721830. Repéré à https://www.frontiersin.org/article/10.3389/fimmu.2021.721830

Zhao, J., Ye, H., Lu, Q., Wang, K., Chen, X., Song, J., . . . Sun, J. (2022). Inhibition of post-surgery tumour recurrence via a sprayable chemo-immunotherapy gel releasing PD-L1 antibody and platelet-derived small EVs. *Journal of Nanobiotechnology, 20*(1), 62. doi: 10.1186/s12951-022-01270-7. Repéré à https://doi.org/10.1186/s12951-022-01270-7

Zhou, H. Y., Jiang, L. J., Cao, P. P., Li, J. B., & Chen, X. G. (2015). Glycerophosphate-based chitosan thermosensitive hydrogels and their biomedical applications. *Carbohydrate Polymers, 117*, 524-536. doi: http://dx.doi.org/10.1016/j.carbpol.2014.09.094. Repéré à http://www.sciencedirect.com/science/article/pii/S0144861714010121

Zhou, J., Bethune, M. T., Malkova, N., Sutherland, A. M., Comin-Anduix, B., Su, Y., . . . Heath, J. R. (2018). A kinetic investigation of interacting, stimulated T cells identifies conditions for rapid functional enhancement, minimal phenotype differentiation, and improved adoptive cell transfer tumor eradication. *PLOS ONE, 13*(1), e0191634. doi: 10.1371/journal.pone.0191634. Repéré à https://doi.org/10.1371/journal.pone.0191634

Zimoch, J., Padial, J. S., Klar, A. S., Vallmajo-Martin, Q., Meuli, M., Biedermann, T., . . . Reichmann, E. (2018). Polyisocyanopeptide hydrogels: A novel thermo-responsive hydrogel supporting pre-vascularization and the development of organotypic structures. *Acta Biomaterialia, 70*, 129-139. doi: https://doi.org/10.1016/j.actbio.2018.01.042. Repéré à https://www.sciencedirect.com/science/article/pii/S1742706118300539

Zuidema, J. M., Rivet, C. J., Gilbert, R. J., & Morrison, F. A. (2014). A protocol for rheological characterization of hydrogels for tissue engineering strategies. *Journal of Biomedical Materials Research Part B: Applied Biomaterials, 102*(5), 1063-1073.